A Journey into Reciprocal Space

A crystallographer's perspective

Anthony Michael Glazer

SECOND EDITION

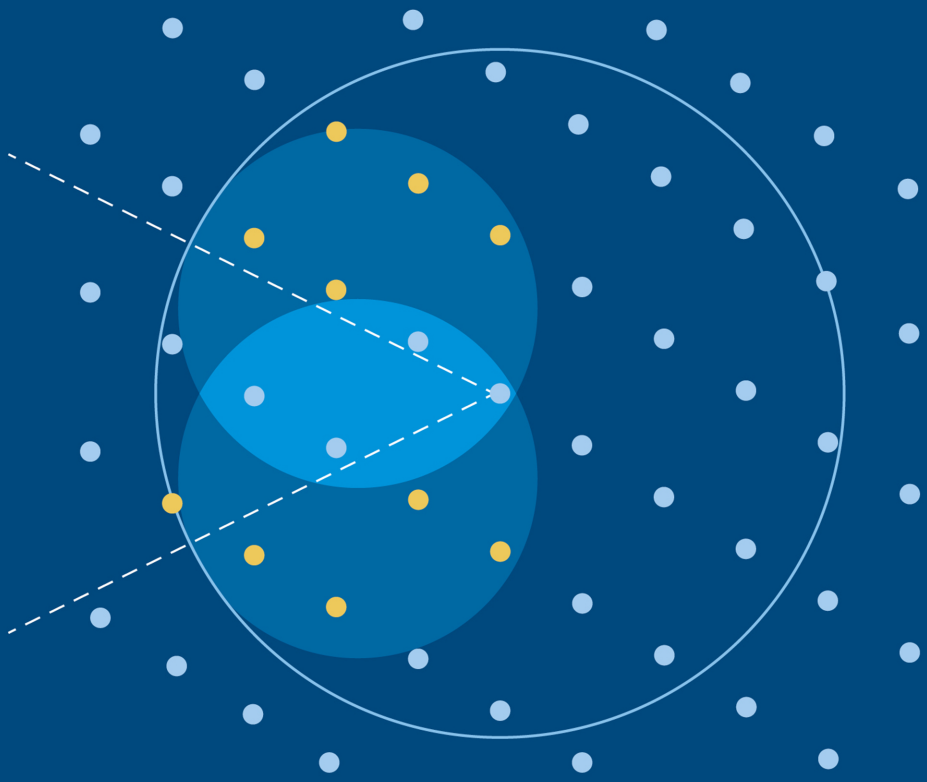

IOP | ebooks

A Journey into Reciprocal Space (Second Edition)

A crystallographer's perspective

A Journey into Reciprocal Space (Second Edition)

A crystallographer's perspective

Anthony Michael Glazer
Physics Department, Oxford University, Oxford, UK
and
Jesus College, Oxford, UK

IOP Publishing, Bristol, UK

ISBN 978-0-7503-3875-2 (ebook)
ISBN 978-0-7503-3873-8 (print)
ISBN 978-0-7503-3876-9 (myPrint)
ISBN 978-0-7503-3874-5 (mobi)

DOI 10.1088/978-0-7503-3875-2

Version: 20210701

IOP ebooks

British Library Cataloguing-in-Publication Data: A catalogue record for this book is available from the British Library.

Published by IOP Publishing, wholly owned by The Institute of Physics, London

IOP Publishing, Temple Circus, Temple Way, Bristol, BS1 6HG, UK

US Office: IOP Publishing, Inc., 190 North Independence Mall West, Suite 601, Philadelphia, PA 19106, USA

Contents

Preface ix

Acknowledgments x

Author biography xi

1 Direct space 1-1

1.1 What are crystals? 1-1
1.2 Miller indices 1-2
1.3 Symmetry operations and elements 1-4
1.4 Point-group symmetry 1-5
1.4.1 Symmetry operations of the first kind 1-5
1.4.2 Symmetry operations of the second kind 1-8
1.4.3 Point groups 1-12
1.5 Translational symmetry 1-14
1.5.1 Lattices 1-15
1.5.2 Unit cells 1-17
1.5.3 Planes and directions 1-19
1.5.4 Crystal systems 1-20
1.5.5 Crystallographic restriction theorem 1-21
1.5.6 Bravais lattices 1-22
1.6 Crystal structures 1-26
1.6.1 Convolution 1-27
1.6.2 Convolution applied to crystals 1-27
1.6.3 Examples of simple crystal structures 1-28
1.7 Space groups 1-34
1.7.1 Symmorphic space groups 1-35
1.7.2 Non-symmorphic space groups 1-38
1.7.3 Types 1-41
1.7.4 Subgroups and supergroups 1-43
References 1-44

2 The reciprocal lattice 2-1

2.1 A brief history 2-1
2.2 Definition of the reciprocal lattice 2-2
2.3 Construction 2-4

2.4 Geometrical calculations 2-8
2.4.1 Metric tensors 2-8
2.4.2 Interplanar distances 2-8
2.4.3 Example calculations 2-10
References 2-11

3 Diffraction 3-1
3.1 Introduction 3-1
3.2 Laue equations 3-1
3.3 Bragg's Law 3-3
3.4 The Ewald sphere 3-7
3.5 Lost in reciprocal space? 3-7
3.5.1 Stationary crystal 3-8
3.5.2 Oscillating and rotating crystal 3-10
3.5.3 Polycrystalline powder 3-12
3.5.4 Laue diffraction 3-14
3.5.5 Energy-dispersive diffraction 3-17
3.5.6 Confusion over sub and super? 3-19
3.6 Imaging 3-21
3.6.1 Fourier transformation 3-24
3.6.2 A simple view of crystal diffraction 3-26
3.6.3 Lattice diffraction 3-30
3.7 Form factors 3-32
3.7.1 X-rays 3-32
3.7.2 Neutrons 3-35
3.7.3 Electrons 3-36
3.8 Structure factors 3-38
3.9 Thermal scattering 3-41
3.10 Intensities of reflections 3-45
3.11 Laue classes 3-50
3.12 Anomalous dispersion 3-51
3.13 Solution of crystal structures 3-54
3.13.1 The phase problem 3-54
3.13.2 Fourier synthesis 3-56
3.13.3 The Patterson method 3-59
3.13.4 Charge flipping 3-61
3.13.5 Rietveld refinement 3-62

3.13.6 Total scattering analysis 3-64
3.13.7 What's new? 3-67
3.14 Aperiodic crystals 3-69
3.15 Disordered and partially-ordered crystals 3-74
References 3-78

4 Dynamical diffraction 4-1
4.1 Multiple scattering 4-1
4.2 Renninger effect 4-3
4.3 Darwin's dynamical theory 4-4
4.4 Bloch's theorem 4-7
4.5 Two-beam approximation in electron diffraction 4-10
4.6 Pendellösung or thickness fringes 4-15
References 4-17

5 Waves in a periodic medium 5-1
5.1 Waves in space 5-1
5.2 Periodic boundary conditions 5-2
5.3 Brillouin zones 5-4
5.4 Wigner–Seitz cell 5-5
5.5 Higher-order Brillouin zones 5-10
5.6 Density of states 5-12
References 5-15

6 Thermal and electronic properties 6-1
6.1 Heat capacity of solids 6-1
6.1.1 Einstein model 6-2
6.1.2 Debye model 6-3
6.2 Vibrations of atoms 6-7
6.2.1 One-dimensional monatomic chain 6-8
6.2.2 One-dimensional diatomic chain 6-12
6.2.3 Lattice dynamics 6-19
6.3 Heat conduction 6-22
6.3.1 Normal processes 6-22
6.3.2 Umklapp processes 6-23
6.4 Measurement of phonon dispersion 6-24
6.4.1 Absorption spectroscopy 6-25

6.4.2 Inelastic scattering of light 6-26
6.4.3 Inelastic scattering of neutrons 6-29
6.5 Free electrons in a metal 6-30
6.6 Tight-binding and nearly-free electrons 6-32
6.6.1 Tight-binding 6-33
6.6.2 Nearly-free electron 6-34
6.7 Metal or insulator? 6-37
6.7.1 Sodium 6-39
6.7.2 Calcium 6-39
6.7.3 Diamond, silicon, germanium 6-40
References 6-40

7 Distortion modes 7-1
7.1 Introduction 7-1
7.2 Atomic displacements 7-2
7.3 Octahedral tilting 7-5
7.4 Group representations 7-7
7.5 Distortion modes 7-10
References 7-17

Appendices

Appendix A A-1

Appendix B B-1

Appendix C C-1

Appendix D D-1

Appendix E E-1

Appendix F F-1

Appendix G G-1

Appendix H H-1

Index: With reference to Section Headings I-1

Preface

The concept of reciprocal space is over 100 years old and has been of particular use for crystallographers to understand the patterns of spots seen on a detector when x-rays are diffracted by crystals. However, it has a much more general use, especially in the physics of the solid state. In order to understand what it is, how to construct it, and how to make use of it, it is first necessary to start with the so-called real or direct space and then show how reciprocal space is related to it. Direct space describes the objects we see around us, especially regarding crystals, their physical shapes and symmetries, and the arrangements of atoms within: the so-called crystal structure. Reciprocal space, on the other hand, deals with the crystals as seen through their diffraction images. Indeed, crystallographers are accustomed to working backward from the diffraction images to the crystal structures, which we call crystal-structure solution. In solid-state physics, one usually works the other way, starting with reciprocal space to explain various solid-state properties, such as thermal and electrical phenomena.

In this book, I begin with the crystallographer's point of view of direct and reciprocal space and then develop this in a form suitable for solid-state physics applications. Note that, while for the crystallographer, reciprocal space is a handy means of dealing with diffraction, for the solid-state physicist, it is thought of as a way to describe the formation and motion of waves, in which case the physicist thinks of reciprocal space in terms of momentum or wave-vector **k**-space. This is because, for periodic structures, a characteristic of normal crystals, elementary quantum excitations, e.g., phonons and electrons, can be described both as particles and waves. The treatment given here will be, by necessity, brief, but I would hope that this will suffice to lead the reader to build upon the concepts described. I have tried to write this book in a suitable form for both undergraduate and graduate students of what today we call 'condensed matter physics'.

Acknowledgments

I am grateful to Berthold Stoeger for pointing out errors in the previous edition, and to Uwe Grimm for his help with my understanding of aperiodic crystals. I thank Stephen Blundell for an interesting discussion on the meaning of ‘degrees of freedom’ and ‘normal modes’. I am especially indebted to the International Union of Crystallography for permitting me to include so many useful figures.

Author biography

Anthony Michael Glazer

Mike Glazer is Emeritus Professor of Physics at the University of Oxford and Emeritus fellow of Jesus College, Oxford, having officially retired in 2010. Despite this, he continues to teach undergraduates, mainly in Condensed Matter Physics. His PhD research between 1965 and 1968 was under the supervision of Professor Dame Kathleen Lonsdale in the Crystallography Department, University College London, working on the crystallography of organic mixed crystals. In 1968–1969, he was a Fellow at Harvard University, and then from 1969 to 1976, he was at the Cavendish Laboratory, Cambridge. From 1972, he was one of the earliest investigators to use synchrotron radiation for crystallographic applications. In 1976, he was appointed Lecturer in Physics at the Clarendon Laboratory, Oxford, and as an Official Fellow and Tutor in Physics at Jesus College, Oxford. Mike Glazer's research has mainly been in understanding the relationship between the physical properties of crystals and their structures. He is perhaps best known for his classification system for tilted octahedra in perovskites, and the crystallography of piezoelectrics, especially the important lead-zirconate system. He was also one of the co-founders of Oxford Cryosystems Ltd, which supplies the world market in low-temperature apparatus for crystallographers. Its most well-known product is the Cryostream, which can be found in almost every crystallography laboratory throughout the world. From 1992 to 1996, Mike Glazer was President of the British Crystallographic Association. He was elected Vice-President of the International Union of Crystallography from 2014 to 2017.

IOP Publishing

A Journey into Reciprocal Space (Second Edition)
A crystallographer's perspective
Anthony Michael Glazer

Chapter 1

Direct space

Je ne te parlerai que cristaux

(Louis Pasteur, in a letter to Charles Chappuis from Strasbourg, July, 1850)

In order to set out on our journey, we shall follow Louis Pasteur (1822–95) and talk about crystals in terms of *direct* (or *real*) *space*. Once this is understood, we can then advance to the next leg of the journey that takes us into *reciprocal space* itself, the principal aim of this book. This discussion will centre mainly around crystalline materials from the point of view of their symmetries. In this chapter, we shall make a 'whistle-stop' tour through crystallographic symmetry. However, there are many books (e.g. [1–4] and [5]) and web pages, e.g. [6], that explain these ideas more thoroughly than I shall be able to do here. A particularly good book on symmetry and crystal structures is by Müller [7].

1.1 What are crystals?

Crystals (from the Greek κρυσταλλοσ, meaning 'rock crystal' but also 'ice' from κρυσ, 'icy cold, frost') have been known about for centuries as minerals that have naturally-occurring flat faces bearing some sort of relationship to each other. Interest in crystals goes back a long way. Collections of quartz crystals [8] have been found at several ancient sites of *Homo Erectus.* The crystals are too small to be used as tools, and have not been modified, suggesting that these ancient hominins regarded the crystals as precious. One can speculate why, but it is clear that crystals meant something special to them. Perhaps we can say that the first crystallographers lived over one million years ago!

One of the earliest written accounts of crystals was made in China in 135 BC by Han Ying in his book 'Disconnection (韓詩外傳)', where six-sided snow crystals were compared with the pentagonal symmetry of flowers. Then in 1611, Johannes Kepler (1571–1630) wrote a small booklet entitled *De nive sexangula (On the*

doi:10.1088/978-0-7503-3875-2ch1

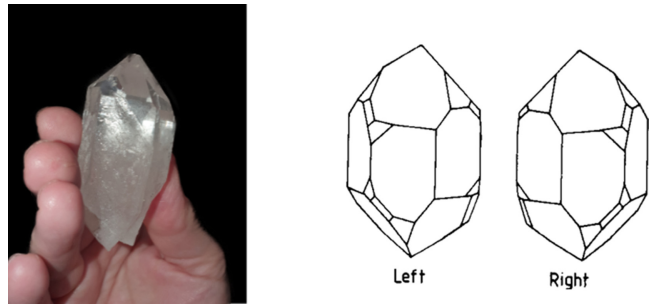

Figure 1.1. On the left, an example of a natural crystal of quartz (rock crystal). On the right, morphological drawings of left and right-handed quartz crystals. Such crystals form enantiomorphic pairs.

Six-Cornered Snowflake) in which he also noted the hexagonal symmetry of snowflakes, and this led him to conjecture that the shapes of crystals could be created by packing together their constituent particles.

The common feature of these, and other observations, is the concept that we call *symmetry*. Symmetry is something that we all have some instinct about, but a formal definition can be elusive. According to Wikipedia, symmetry, as used in physics, has been generalized to mean invariance—that is, a lack of change—under any kind of transformation, for example, arbitrary coordinate transformations. In the study of crystals, this can be formalized in terms of mathematical operations that take a point in space and move it to another position, and which bring the point back to its original position when repeated enough times. This is the approach we shall use shortly.

Probably the most well-known mineral crystal is that of quartz, especially in its clear state called rock crystal (figure 1.1). Quartz, chemical formula SiO_2, grows naturally as elongated prisms with large faces arranged around a 3-fold axis of symmetry, together with inclined faces top and bottom. Crystals of this particular mineral can be found that are mirror images of each other, a symmetry property known as *chirality* (see [9] and [10] for a discussion of the many errors made in the literature in describing quartz). Other terms that are commonly used to describe crystals are *habit* and *morphology*.

Definition. *Crystal **habit** is the formal name for the shape of a crystal. Some examples of crystal habit are acicular (needle-like), prismatic (elongated prisms) and stellate (star-shaped). There are many others.*

Definition. *Crystal **morphology** is a term that describes the crystal in terms of its habit, defect nature and polymorphism (where a substance can crystallize in different states, e.g., diamond and graphite).*

1.2 Miller indices

To characterize the different crystal morphologies, it is necessary to introduce a system whereby each of the crystal faces can be assigned a label. The most commonly used system is that introduced in 1839 by the British mineralogist

William Hallowes Miller (1801–80). To explain this, a convention is first needed for naming axes and angles in a crystal.

Figure 1.2(a) shows the right-hand screw convention for the choice of lengths a, b and c measured along the x, y and z axes and for interaxial angles α, β and γ. Note that a, b and c can be any length, in general, and the angles need not be 90°, depending on the crystal symmetry. To a physicist, who is accustomed to using orthogonal Cartesian axes wherever possible, this may seem to be a perverse choice. But, in fact, it makes the description of symmetry much simpler. In figure 1.2(b), a plane (in grey) intersects the three axes to make intercepts at a/h, b/k and c/l. The plane is then indexed as (h k l). According to the Law of Rational Indices, found by René Just Häuy (1743–1822), the indices should be integers. However, there are, in fact, a few rare cases, such as in the mineral calaverite, $AuTe_2$, where some faces could only be indexed on irrational indices.

Notation. *Miller indices are written in parentheses like this* (h k l).

So in a cube, a face perpendicular to the a-axis and parallel to b and c has the plane symbol (1 0 0), as it cuts off unit intercept along a and makes an infinite intercept along b and c (figure 1.3). Similarly, once the axes have been assigned, the faces of an octahedron have indices (111), (1$\bar{1}$1), (1$\bar{1}\bar{1}$), (11$\bar{1}$), ... as each face cuts off unit intercept on all three axes.

Notation. *Negative indices are marked with a bar above the number. Typically, this is expressed as 'bar* 1*' in the United Kingdom, while Americans usually say '*1 *bar'! I'm not sure what the rest of the world says.*

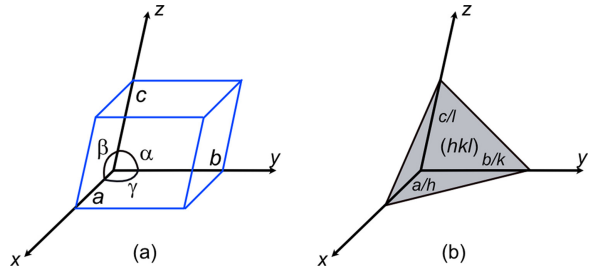

Figure 1.2. Miller indices. (a) Right-hand convention for choice of axes. (b) Definition of a plane.

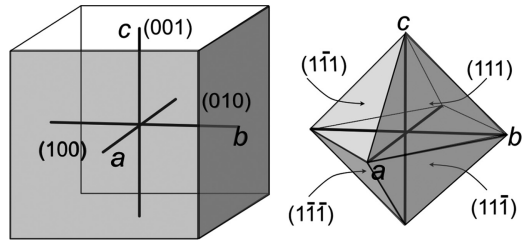

Figure 1.3. Miller indices for the faces of a cube and an octahedron. Only the front faces are marked in this figure.

Definition. *The complete set of indexed faces with a particular set of Miller indices related by symmetry is called a* ***form*** *and is denoted* {h k l}. *Thus, the eight faces of an octahedron belong to the form* {1 1 1}. *Note the curly brackets.*

1.3 Symmetry operations and elements

These terms are often confused in the literature, and so some clarification is needed. In mathematical group theory, the term 'element' is used to denote any member of a group. A *group* contains a set of elements in which an *operator* carries out an *operation*[1] to combine them to produce another element. To qualify as a group, the following conditions must be met:

1. The combination of any two members P and Q is also a member of the set (closure). PQ = R.
2. The set includes an identity, symbolized by 1 or E. One can show that a right identity is also a left identity, i.e., P1 = 1P = P.
3. For each operator R, there is an inverse R^{-1}, such that $RR^{-1} = 1$.
4. The combination of members is associative (this is axiomatic for symmetry operations). (PQ)R = P(QR).

Note that the number of elements in a group is called the *order* of the group. When PQ = QP for all elements, the group is called *Abelian*.

In crystallography, however, and perhaps confusingly, it is essential to distinguish between symmetry elements and symmetry operations. Symmetry elements represent the geometric aspect of a symmetry operation, e.g., a 2-fold rotation has as its symmetry element a line, the 2-fold axis, about which the 2-fold rotation is applied. However, the 2-fold rotation operator (or operation) may be a member of a *point group* where it acts on the coordinates of an object with respect to a chosen origin.

The online dictionary of the International Union of Crystallography (IUCr) [12] defines a symmetry element as follows:

Definition. *A* ***symmetry element*** *(of a given crystal structure or object) is defined as a concept with a double meaning, namely the combination of a* ***geometric element*** *with the set of symmetry operations having this geometric element in common (termed its* ***element set****).*

It is also worth noting that no symmetry element is defined for an identity operation (i.e., one that does nothing to an object). Therefore, it could be argued that the number of symmetry elements does not necessarily equate strictly to the number of symmetry operations in a group. This implies that, while symmetry operations

[1] Generally, the subtle distinction between 'operator' and 'operation' is not made in crystallography (unlike the usage in quantum mechanics), and often, the two terms are used interchangeably. According to [11], an operator is similar to an operation in that it refers to the symbol or the process used to denote the operation; hence their point of view is different. For instance, one often speaks of 'the operation of addition' when focusing on the operands and result, but one switches to 'addition operator' when focusing on the process.

(and their associated operators) are elements of a group in the mathematical sense, symmetry elements are not.

Definition. *A **symmetry operation** is an isometry, i.e., a transformation under which two objects, or two configurations of an object, are brought to coincide. A symmetry operation is a Euclidean mapping, meaning that to each point of the first configuration, there corresponds a point of the second configuration. The distances between the two points are kept by the transformation, as are the angles.*

In other words, a symmetry operation leaves an object looking the same after it has been carried out.

1.4 Point-group symmetry

Tidiness is a virtue; symmetry is often a constituent of beauty.
(Winston Churchill)

The sorts of groups that are used in describing crystal symmetry are *point groups,* whose group elements are point-group symmetry operators (or operations). Sometimes the term *point symmetry* is used for short.

Definition. ***Point-group symmetry** operations are those that act to leave at least one point unchanged.*

In other words, point symmetry can be thought of as being the symmetry seen from a particular point in the crystal [13]. In crystallography, we shall need to discuss two types of point-symmetry operations: proper rotations, known as symmetry operations of the first kind, and reflection, inversion and rotoinversions (or rotoreflections), known as symmetry operations of the second kind.

1.4.1 Symmetry operations of the first kind

A proper rotation rotates a vector, through an angle about an axis that passes through a defined point. Repeated rotation finally brings the position vector back to its starting position. Table 1.1 shows the rotations (here, about the z-axis) used to describe crystallographic symmetry. Notice that the only rotations considered are 2, 3, 4 and 6-fold. The reason for this will become apparent in section 1.5.4. The symbols are given in two standard notations: the International system, described originally by the French mineralogist Charles-Victor Mauguin (1878–1958) and the German crystallographer Carl Hermann (1898–1961), and the Schoenflies system (in parentheses) due to Artur Moritz Schoenflies (1853–1928). It is the International notation that is used in crystallography, while subjects such as chemical spectroscopy tend to use the Schoenflies system. Table 1.1 also gives matrices $\boldsymbol{R}$ that define linear symmetry operators that can be used to carry out the operation

$$\boldsymbol{R}\mathbf{r} = \mathbf{r}' \tag{1.1}$$

Table 1.1. Symmetry operations of the first kind with respect to the z-axis.

Symbol	Operation	Geometric element	Element set	Matrix
$1(E)$	Identity	–	–	$\begin{bmatrix} 1 & 0 & 0 \\ 0 & 1 & 0 \\ 0 & 0 & 1 \end{bmatrix}$
$2(C_2)$	2-fold rotation	Axis or line	Rotation* about z	$\begin{bmatrix} \bar{1} & 0 & 0 \\ 0 & \bar{1} & 0 \\ 0 & 0 & 1 \end{bmatrix}$
$3(C_3)$	3-fold rotation	Axis or line	Rotation* about z	$\begin{bmatrix} 0 & \bar{1} & 0 \\ 1 & \bar{1} & 0 \\ 0 & 0 & 1 \end{bmatrix}$
$4(C_4)$	4-fold rotation	Axis or line	Rotation* about z	$\begin{bmatrix} 0 & \bar{1} & 0 \\ 1 & 0 & 0 \\ 0 & 0 & 1 \end{bmatrix}$
$6(C_6)$	6-fold rotation	Axis or line	Rotation* about z	$\begin{bmatrix} 1 & \bar{1} & 0 \\ 1 & 0 & 0 \\ 0 & 0 & 1 \end{bmatrix}$

* The element set consists of the rotation and all its coaxial equivalents.

where $\mathbf{r}$ and $\mathbf{r}'$ are position vectors for coordinates x, y, z. Strictly speaking, $\boldsymbol{R}$ is the *symmetry operator*, while $\boldsymbol{R}\mathbf{r}$ represents the *symmetry operation*.

Thus, with rotation axes along z, the rotation operations result in the following mappings of coordinates:

$$\begin{aligned} &2\text{: } (x, y, z) \rightarrow (\bar{x}, \bar{y}, z) \\ &3\text{: } (x, y, z) \rightarrow (\bar{y}, x - y, z) \\ &4\text{: } (x, y, z) \rightarrow (\bar{y}, x, z) \\ &6\text{: } (x, y, z) \rightarrow (x - y, x, z) \end{aligned} \tag{1.2}$$

A useful method of illustrating the result of symmetry operations is by making use of the stereographic projection. This represents points on a sphere by projecting onto a plane, much like a map of the world viewed down onto the North Pole. Imagine, figure 1.4(a), that there is a point C on the surface of a sphere. Now draw a line SC: this intersects the horizontal plane perpendicular to NS at the point P. N and S can be thought of as the north and south poles, respectively. Figure 1.4(b) shows the projection plane viewed from above, where the point P is plotted. The distance OP in this projection is a measure of the angle ϕ measured from the north pole (90°– latitude in cartography), and the point P is called a *pole*.

Figure 1.5 shows how the effects of symmetry operations of the first kind are conventionally shown in stereographic projections. The upper four diagrams are for the proper rotations. Consider first the diagram for the rotation operation 2. The small circle with the plus sign next to it represents any object or motif in space (not necessarily a circle!). This could be an atom or a collection of atoms, such as a molecule.

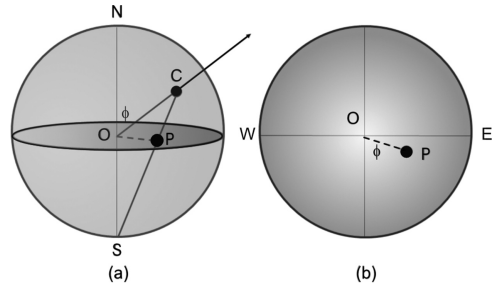

Figure 1.4. The stereographic projection. (a) Construction of a pole, (b) resulting projection onto a plane.

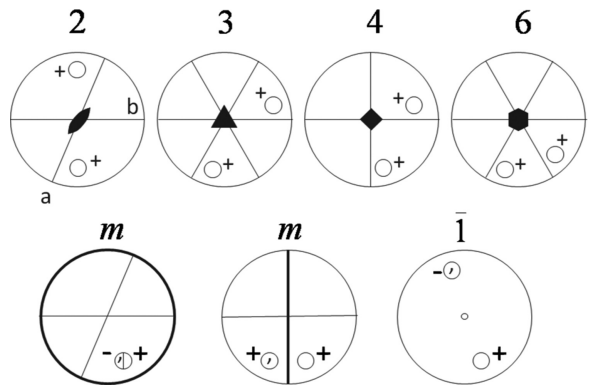

Figure 1.5. Stereographic projections showing rotations, reflection and inversion.

The position in the diagram of this circle is known as a *general position*. The plus sign indicates that it is in the northern hemisphere (you may prefer to think of it as being above the plane of projection, i.e., towards you). In each case, start with the circle near the bottom. The 2-fold operation about the axis perpendicular to the stereographic projection, i.e., along NS, rotates this through 180° to another general position near the top. The resulting circle remains in the northern hemisphere, as marked by the plus sign. The black symbol at the centre of the stereographic projection, looking somewhat like a rugby football, denotes the geometric element, the 2-fold axis.

Note. *It is conventional for rotation operations to turn a position vector anticlockwise about the chosen axis.*

Note also that if the 2-fold rotation is applied again, the object returns to its starting position, i.e.,

$$2^2 = 1 \text{ or } C_2^2 = E \tag{1.3}$$

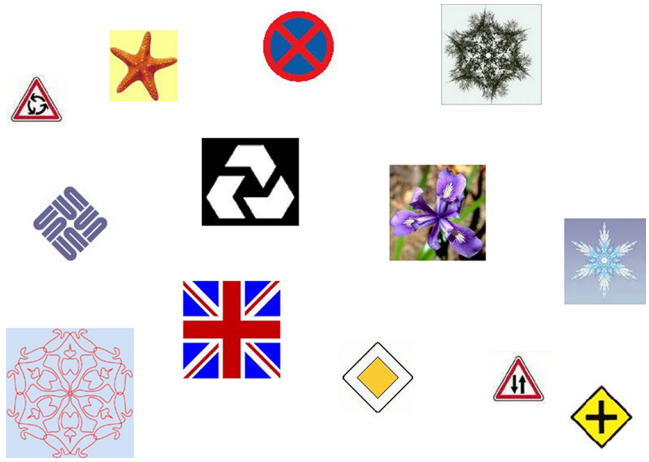

Figure 1.6. Some examples of everyday objects showing rotational symmetry. Reprinted from [17], Copyright (2013), with permission from Elsevier.

The next three diagrams show the effect of rotations 3, 4 and 6. By studying these diagrams (or by multiplying out the matrices in table 1.1), interesting relationships are found, such as the following:

$$\begin{aligned} 6^5 &= 6^{-1} \\ 6^4 &= 3^2 = 3^{-1} \\ 6^3 &= 2 \end{aligned} \tag{1.4}$$

Note that, these days, the International Union of Crystallography denotes the rotations thus:

$$\begin{aligned} 3 &= 3^+ \qquad & 3^2 &= 3^- \\ 4 &= 4^+ \qquad & 4^3 &= 4^- \\ 6 &= 6^+ \qquad & 6^5 &= 6^- \end{aligned} \tag{1.5}$$

Figure 1.6 shows a few examples of rotational symmetry in some everyday objects. It is a good exercise to see how many instances of rotational symmetry you can find during a walk through your neighbourhood.

1.4.2 Symmetry operations of the second kind

These types of symmetry operations are listed in table 1.2.

The reflection or mirror operation reflects every point in an object through a plane, as if through a mirror. For a mirror plane perpendicular to the z-axis

$$m\colon (x, y, z) \rightarrow (x, y, \bar{z}) \tag{1.6}$$

Figure 1.7 shows some examples of reflections. One effect of the reflection operation is to convert left-handed objects into right-handed objects, such as in the relationship between the two quartz crystals in figure 1.1.

Table 1.2. Symmetry operations of the second kind with respect to the z-axis.

Symbol	Operation	Geometric element	Element set	Matrix
$m(\sigma)$	Reflection	Plane	Reflection*	$\begin{bmatrix} 1 & 0 & 0 \\ 0 & 1 & 0 \\ 0 & 0 & \bar{1} \end{bmatrix}$
$\bar{1}(i)$	Inversion	Point	Inversion	$\begin{bmatrix} \bar{1} & 0 & 0 \\ 0 & \bar{1} & 0 \\ 0 & 0 & \bar{1} \end{bmatrix}$
$\bar{2}$	Rotoinversion	Point plus line	Rotation plus inversion†	$\begin{bmatrix} 1 & 0 & 0 \\ 0 & 1 & 0 \\ 0 & 0 & \bar{1} \end{bmatrix}$
S_2	Rotoreflection	Point plus line	Rotation plus reflection†	$\begin{bmatrix} \bar{1} & 0 & 0 \\ 0 & \bar{1} & 0 \\ 0 & 0 & \bar{1} \end{bmatrix}$
$\bar{3}$	Rotoinversion	Point plus line	Rotation plus inversion†	$\begin{bmatrix} 0 & 1 & 0 \\ \bar{1} & 1 & 0 \\ 0 & 0 & \bar{1} \end{bmatrix}$
S_3	Rotoreflection	Point plus line	Rotation plus reflection†	$\begin{bmatrix} 0 & \bar{1} & 0 \\ 1 & \bar{1} & 0 \\ 0 & 0 & \bar{1} \end{bmatrix}$
$\bar{4}$	Rotoinversion	Point plus line	Rotation plus inversion†	$\begin{bmatrix} 0 & 1 & 0 \\ \bar{1} & 0 & 0 \\ 0 & 0 & \bar{1} \end{bmatrix}$
S_4	Rotoreflection	Point plus line	Rotation plus reflection†	$\begin{bmatrix} 0 & \bar{1} & 0 \\ 1 & 0 & 0 \\ 0 & 0 & \bar{1} \end{bmatrix}$
$\bar{6}$	Rotoinversion	Point plus line	Rotation plus inversion†	$\begin{bmatrix} \bar{1} & 1 & 0 \\ \bar{1} & 0 & 0 \\ 0 & 0 & \bar{1} \end{bmatrix}$
S_6	Rotoreflection	Point plus line	Rotation plus reflection†	$\begin{bmatrix} 1 & \bar{1} & 0 \\ 1 & 0 & 0 \\ 0 & 0 & \bar{1} \end{bmatrix}$

* and coplanar equivalents,
† and coaxial equivalents.

It is impossible to transform a left-handed object into a right-handed object by using rotation and *vice versa*. Actually, in mathematical terms, this statement is not entirely true, provided that we are allowed to change dimensionality: we first transform the description of a three-dimensional chiral object into four dimensions, rotate it, and then collapse it back into three dimensions!

The bottom line of figure 1.5 shows the stereographic projections for the reflection and inversion operations. The first two diagrams are different views of the same type of operation, namely the reflection or mirror operation. In the first stereographic projection, a mirror plane is located on the plane perpendicular to the z-axis towards you: this is signified by the thick black line around the perimeter. The effect of this is

Figure 1.7. Examples of reflection (mirror) symmetry in everyday objects. Reprinted from [17], Copyright (2013), with permission from Elsevier.

to reflect the object from the northern to the southern hemisphere (or from above to behind the plane of projection). This is given by the mapping

$$m\colon (x, y, z) \rightarrow (x, y, \bar{z}) \tag{1.7}$$

As this places the reflected object directly beneath the original object in this projection, this is indicated by splitting the circle motif by a vertical line. The minus sign now shows that the reflected motif is below the plane of projection and the comma indicates a change of chirality or hand. The second stereographic projection shows the reflection operation, this time with the mirror plane indicated by the thick line, perpendicular to the y-axis (to the right).

The third diagram shows the inversion operation:

$$\bar{1}\colon (x, y, z) \rightarrow (\bar{x}, \bar{y}, \bar{z}) \tag{1.8}$$

This operation is nicely illustrated in a drawing by Holbein of the hands of Erasmus of Rotterdam (figure 1.8). The relationship between the two hands shows that each point, on one hand, is (more or less) related to an equivalent point on the other hand, as indicated by the added lines. These lines all pass through a point known as the *centre of inversion*, sometimes called the *centre of symmetry*. Any object that contains a centre of symmetry is said to be *centrosymmetric*. Some scientists mistakenly use the terms *centric* and *acentric* to describe this, but these terms are used in crystallography to refer to intensity distributions in diffraction patterns, and not to crystal symmetry. Note that, just like with reflection, inversion also changes the chirality of an object.

The final point-symmetry operations that we need to discuss are slightly more complicated than the others. The complication arises because of the different ways in which the International and Schoenflies systems define these operations. These operations combine a rotation and an inversion (International system) or a rotation

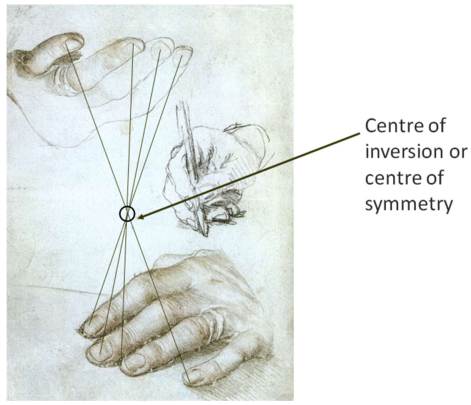

Figure 1.8. Drawing of left and right hands of Erasmus of Rotterdam by Holbein (1523). Lines have been added to indicate the inversion relationship. Reprinted from [17], Copyright (2013), with permission from Elsevier.

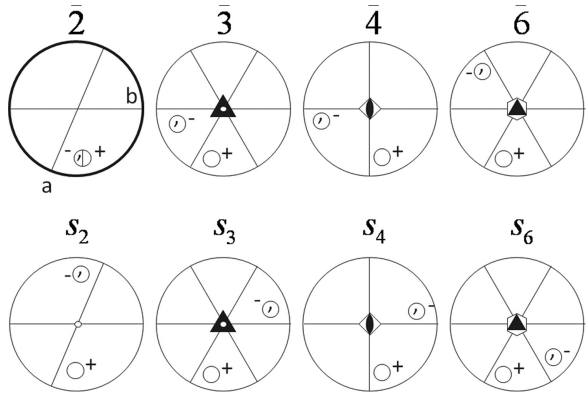

Figure 1.9. Stereographic projections for rotoinversion operations (top) and rotoreflection operations (bottom).

and a reflection (Schoenflies system). Table 1.2 lists these operations and figure 1.9 shows the stereographic projections. The following mappings follow for the International system:

$$\begin{aligned}
&\bar{2}\colon (x, y, z) \rightarrow (x, y, \bar{z}) = m\colon (x, y, z)\\
&\bar{3}\colon (x, y, z) \rightarrow (y, \bar{x} + y, \bar{z})\\
&\bar{4}\colon (x, y, z) \rightarrow (y, \bar{x}, \bar{z})\\
&\bar{6}\colon (x, y, z) \rightarrow (\bar{x} + y, \bar{x}, \bar{z})
\end{aligned} \tag{1.9}$$

We see several relationships. First of all, the International $\bar{2}$ operation is, in fact, equivalent to a reflection m, while the Schoenflies S_2 operation is equivalent to an inversion. More confusingly, perhaps, the following is found:

$$\begin{aligned}
\bar{3} &= S_6^5 = S_6^{-1} \\
\bar{4} &= S_4^3 = S_4^{-1} \\
\bar{6} &= S_3^5 = S_3^{-1} \\
S_3 &= \bar{6}^5 = \bar{6}^{-1} \\
S_6 &= \bar{3}^5 = \bar{3}^{-1}
\end{aligned} \tag{1.10}$$

So, there is a possible confusion between 3-fold and 6-fold roto-operations for these types of operations, depending on which system one uses.

1.4.3 Point groups

Suppose the symmetry of a crystal can be described by a 2-fold rotation, and at the same time, by a reflection perpendicular to the 2-fold axis. Taking the 2-fold axis to lie along the z-axis and using the matrices in tables 1.1 and 1.2, we find the following relationships.

$$\begin{aligned}
2.2 &= 1 \\
m.\ m &= 1 \\
2.\ m &= \bar{1} \\
\bar{1}.\ \bar{1} &= 1
\end{aligned} \tag{1.11}$$

This shows that the combination of the 2-fold and perpendicular reflection operation generates a centre of inversion. Therefore, in this case, we have four symmetry operations $\{1, 2, m, \bar{1}\}$. We now show that these operations form a group, as defined in mathematics by the following four criteria.

1. The following multiplication table of operations can be written as a matrix, thus

	1	**2**	***m***	$\bar{\mathbf{1}}$
1	1	2	m	$\bar{1}$
2	2	1	$\bar{1}$	m
m	m	$\bar{1}$	1	2
$\bar{\mathbf{1}}$	$\bar{1}$	m	2	1

   This shows that the application of each operation on another always generates another that is one of the four, and so these operations form a closed set. Because this particular matrix is symmetric, this is an Abelian group (not all crystallographic groups are Abelian, though)
2. There is an identity operation 1.
3. There is an inverse operation given by $XX^{-1} = 1$. In this case, each operation is its own inverse.

$$\begin{aligned}
1.1 &= 1 \\
2.2 &= 1 \\
m.\ m &= 1 \\
\bar{1}.\ \bar{1} &= 1
\end{aligned} \tag{1.12}$$

4. Associativity is true. For example,

$$2.(m.\ \bar{1}) = (2.m).\ \bar{1} \tag{1.13}$$

Figure 1.10 shows a stereographic projection for this group, including the symmetry elements. This group contains four operations, and generates four general positions, and is, therefore, a group of order 4. This group is given the International symbol 2/*m*, the / indicating that the 2-fold axis is perpendicular to the mirror plane. The Schoenflies symbol is C_{2h}: *C* stands for cyclic, and the subscript 2 is for the 2-fold axis and *h* for a horizontal mirror plane. Another example, point group 4*mm,* is shown in figure 1.10. The 4-fold axis is symbolised by the black square at the centre and the mirror planes by the thick lines. In the 4*mm* symbol, the first *m* refers to the two mirror planes perpendicular to the *x* and *y* axes. Notice that they are orthogonal to one another because of the 4-fold axis (4.*m* = *m*, closure). The second *m* in the symbol refers to the two diagonal mirror planes, each also related by the 4-fold rotation. This is a group of order 8.

Therefore, we can think of a crystallographic point group as a group whose symmetry operations leave at least one point unmoved, i.e., consisting of point-symmetry operations. The point group is a useful concept since it allows us to classify different crystals. Historically, this was done by reference to crystal morphology and the directions normal to the faces. It was established around 1830 that there are just 32 possible ways to do this, and so any crystal could be classified as belonging to one of the 32 so-called crystal classes. Each of these crystal classes corresponds to a point group.

Note. *If all the possible point-symmetry operations describing crystal symmetry are used to form groups, it is found that there are* 32 *distinct point groups in three dimensions, sometimes called the* 32 ***geometric crystal classes****. These are listed in* table 1.3.

Stereographic projections for all 32 geometric crystal classes are shown in appendix A, and all crystallographic symbols are given in appendix B.

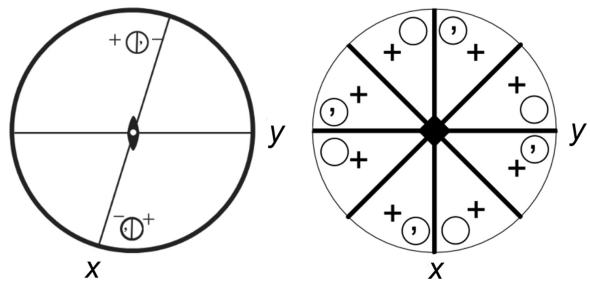

Figure 1.10. Stereographic projections for the point groups 2/*m*(C_{2h}) and 4*mm*(C_{4v}).

Table 1.3. Crystal systems, point groups and restrictions.

Crystal system	Crystallographic point group (Schoenflies)	Crystallographic point group (International)	Restrictions on unit-cell parameters
Triclinic	C_1	1	
	$S_2(C_i)$	$\bar{1}$	
Monoclinic	C_2	2	$\alpha = \gamma = 90°$
	$C_{1h}(C_S)$	m	
	C_{2h}	$2/m$	
Orthorhombic	$D_2(V)$	222	$\alpha = \beta = \gamma = 90°$
	C_{2v}	$mm2$	
	$D_{2h}(V_h)$	mmm	
Tetragonal	C_4	4	$a = b$; $\alpha = \gamma = 90°$
	S_4	$\bar{4}$	
	C_{4h}	$4/m$	
	D_4	422	
	C_{4v}	$4mm$	
	$D_{2d}(V_d)$	$\bar{4}2m$	
	D_{4h}	$4/mmm$	
Trigonal	C_3	3	$a = b$; $\alpha = \beta = 90°$ $\gamma = 120°$
	$S_6(C_{3i})$	$\bar{3}$	
	D_3	32	
	C_{3v}	$3m$	
	D_{3d}	$\bar{3}m$	
Hexagonal	C_6	6	$a = b$; $\alpha = \beta = 90°$ $\gamma = 120°$
	C_{3h}	$\bar{6}$	
	C_{6h}	$6/m$	
	D_6	622	
	C_{6v}	$6mm$	
	D_{3h}	$\bar{6}m2$	
	D_{6h}	$6/mmm$	
Cubic	T	23	$a=b=c$ $\alpha=\beta=\gamma=90°$
	T_h	$m\bar{3}$	
	O	432	
	T_d	$\bar{4}3m$	
	O_h	$m\bar{3}m$	

1.5 Translational symmetry

So far, our discussion on symmetry has been concerned with macroscopic objects, such as the crystals we might encounter in nature. We shall now turn our attention to the internal structure of a crystal and how we can describe the arrangements of atoms that make up this structure. The point symmetries will still be relevant at the

microscopic scale of atoms and molecules in the crystal. However, before looking at atomic arrangements, we shall first introduce a form of symmetry that is characteristic of normal ideal crystalline materials, *periodic* or *translational symmetry*.

Definition. ***Translational symmetry*** *is the symmetry that is exhibited by a collection of identical objects repeated periodically throughout space.*

As an illustration, figure 1.11 shows a picture of a herd of elephants in a regularly repeating pattern, which can be described by translational symmetry. Each elephant is at a fixed distance from its neighbour in each direction in space.

1.5.1 Lattices

> *This is infinity here. It could be infinity. We don't really don't know. But it could be. It has to be something—but it could be infinity, right?*
>
> (Donald J. Trump, July 2017)

In crystallography, the term *lattice* has a particular meaning, and should not be confused by common usage elsewhere, such as in a structure of crossed wooden or metal strips or trellis. To explain the crystallographic concept, suppose now we replace each of the elephants in figure 1.11 by a point, for instance, placed at the tip of each tusk. Now remove the elephants (figure 1.12). The result is a repeating pattern of points. Now I have to emphasize something here that I have seen many students (and working scientists for that matter) become confused about. Do not mistake the points in this figure for atoms. These are mathematical, infinitesimal points, and the only reason they are drawn with a finite diameter is so that you can see them. Mathematically we can treat the points as a series of repeating delta functions. This then leads to an important definition.

Definition. *A* ***lattice*** *is an infinite periodic, repeating array of points (not atoms!).*

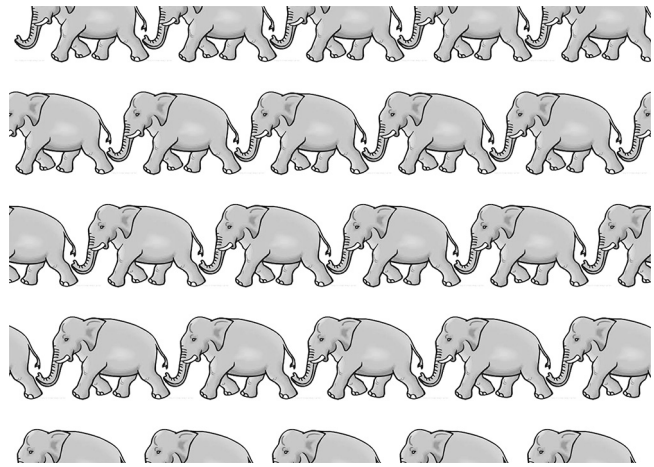

Figure 1.11. A herd of elephants illustrating translational symmetry (www.carlswebgraphics.com).

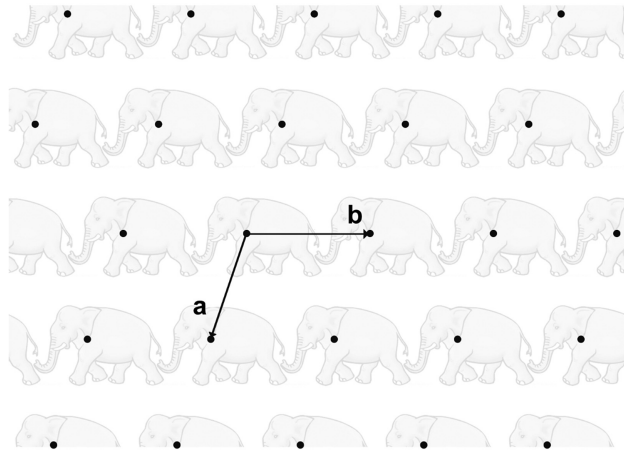

Figure 1.12. Lattice describing the translational symmetry of figure 1.11 (www.carlswebgraphics.com).

Here is my 'Government Health Warning'. Unfortunately, in much of the literature, the word 'lattice' is used when referring to crystal structures, which consist of arrays of atoms, not points. So, for instance, if we had a repeating pattern of single atoms, it would look just like figure 1.12, but in fact, this would not be a lattice but a crystal structure (more of this below). I recommend the excellent articles by Nespolo for discussions on this matter [14, 15]. In the figure, faint traces of the original elephants have been left so that it can be seen where the lattice points have been set. A lattice is a mathematical device that acts as a template to tell us how to position atoms and molecules in space: as such, a lattice has no physical existence. A powerful microscope, such as an electron microscope, would not show a lattice but a crystal structure instead.

Similarly, when someone mentions, for example, the diamond lattice or the copper lattice, they almost certainly should have said the diamond crystal structure and the copper crystal structure. Diamond has pairs of carbon atoms per lattice point, and copper has single copper atoms repeating throughout space, so they look quite different. On the other hand, they have the same lattice type, apart from an overall change in dimensions: all-face-centred cubic. Please resist using the term *lattice structures,* which you will often see in books: it is an old term, and these days it is best avoided as it can create confusion between lattice and structure. You may think that I am a bit 'picky', but misunderstandings of this sort can have practical consequences. I recall, many years ago, a student who wasted a year's computing resources on an erroneous electronic band structure calculation because he had not understood the difference between lattice and structure.

In figure 1.12, the lattice is shown as a two-dimensional array, but of course, in three dimensions, there will be repeating lattice points above and below this plane. Two arbitrarily chosen basis vectors, **a** and **b**, have been marked, with an origin arbitrarily selected on one of the lattice points (it can be assumed that the **c**-axis is

out of the plane of points). Once the axes and origin have been chosen, all lattice points can be reached from a chosen origin on a lattice point by the so-called *primitive* translation vector $\mathbf{t}_n$

$$\mathbf{t}_n = n_1\mathbf{a} + n_2\mathbf{b} + n_3\mathbf{c} \tag{1.14}$$

In this expression, n_1, n_2 and n_3 are integers. Therefore, it is the primitive translation operation that defines the lattice. The set of translation operations defined by $\mathbf{t}_n$ forms an infinite group, the *translation group*.

1.5.2 Unit cells

Having defined the lattice, we can make good use of the periodicity it exhibits. Periodicity lies at the heart of most condensed matter physics theory. Consider figure 1.13, where the same lattice is shown, but this time with two regions outlined in black. These regions are called unit cells.

Definition. *A **unit cell** can be thought of as a region of space which, when repeated by translational vectors, fills all space. It can, in principle, be of any shape, although crystallographers almost always use a parallelepiped shape to describe the unit cell in direct space.*

So, the importance of defining a unit cell is that we need only consider the unit cell alone (as used in describing crystal structures, where we add atoms and molecules into each unit cell) and then allow the primitive translation operations to repeat it. In other words, it is not necessary to write down all the coordinates of the lattice points or atoms in the whole crystal. After all, that is the point of symmetry: it enables one to specify just a few things and then allow symmetry operations to generate everything else.

In this lattice, two examples of unit cells are drawn, but a moment's thought should convince you that we could define an infinite number of different unit cells. Furthermore, these unit cells have the same volume (in three dimensions). How do we know this? Simply count the number of lattice points per unit cell, and we shall find that it is the same for both unit cells drawn. Now here is a little trick. Often you will see in textbooks and on the Internet that to count the number of lattice points

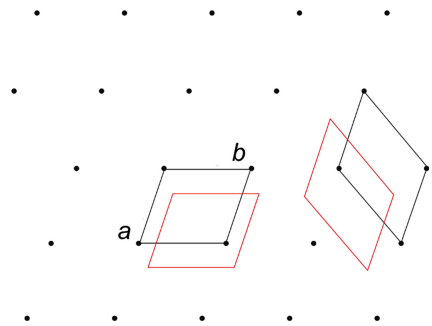

Figure 1.13. A primitive lattice showing primitive unit cells, origin at the top left corner.

per unit cell, partition the lattice points between neighbouring unit cells as if there are fractions of a lattice point (I don't know how to make a fraction of a point!). In the figure, we might take a lattice point at each corner of the unit cell and then say that each point is shared between neighbouring unit cells. But there is a much easier way to do the counting. Simply move the origin of the unit cell, as the origin is, in fact, arbitrary: if we move one unit cell, then all the other equivalent cells must move with it and so still cover all space. Here, the displaced unit cells are in red, and then it is easy to see that each contains just one lattice point. These unit cells must therefore have the same volume, like all other possible unit cells that contain a single lattice point.

Definition. *Unit cells that contain one lattice point are called* ***primitive*** *unit cells, and the lattice described by them is called a primitive lattice. Primitive lattices are designated by the letter P.*

While in any lattice, one can define an infinite variety of primitive unit cells, it is often convenient to define *centred* unit cells. In figure 1.14, the unmarked points form a lattice at height 0, while the points marked ½ are those on the plane above at a distance *c*/2. The next plane repeats the plane at height *c* and so on. Shown in black is an example of a unit cell with a lattice point at the origin, at coordinate position (0, 0, 0), and another point in the unit-cell centre at (½, ½, ½). The coordinates are given as fractions of the unit-cell edges *a, b* and *c*. Note that mathematicians often define the term unit cell to mean the smallest cell, i.e., a primitive cell, but in crystallography, centred cells are still called unit cells.

Displacing the unit cell (marked in red) shows immediately that this centred unit cell contains two lattice points. Because this unit cell has a lattice point at its centre, it is called a *body-centred unit cell,* and the lattice is body-centred. This type of lattice is conventionally given the symbol *I*. Figure 1.15 shows other centrings together with their conventional symbols and fractional coordinates of the lattice points.

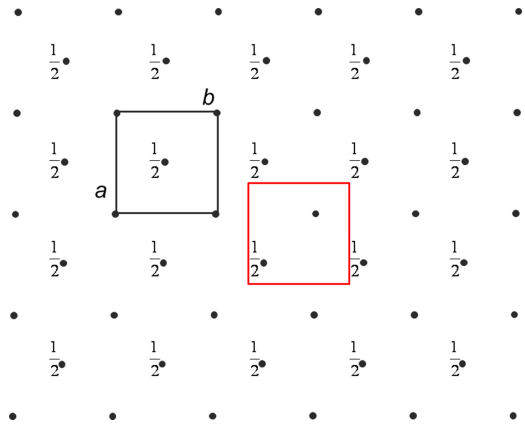

Figure 1.14. Body-centred (*I*) unit cell and corresponding lattice. The points marked ½ lie on a plane through c/2 above the unmarked points.

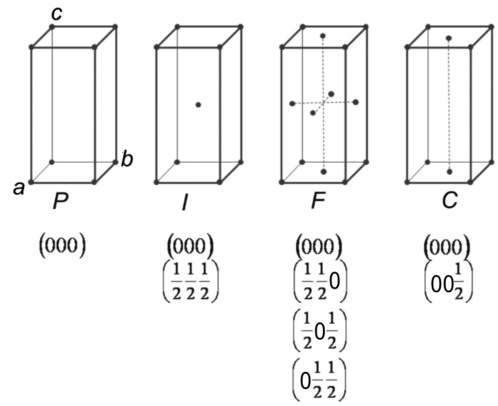

Figure 1.15. Different types of unit cells: *P* primitive, *I* body-centred, *F* all-face-centred, *C* one-face-centred. In each case, the fractional coordinates of the lattice points are tabulated.

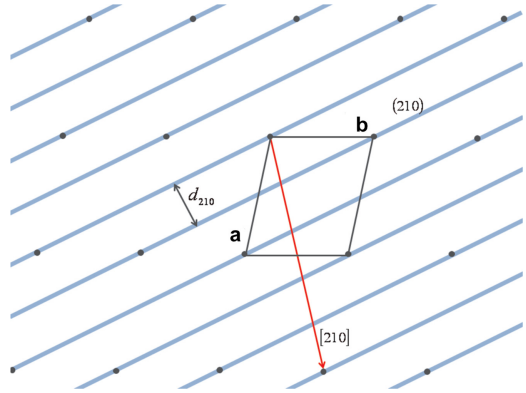

Figure 1.16. Lattice showing (210) planes (blue) and the [210] direction (red). Unit-cell vectors are in bold.

The *C*-face-centred unit cell can equally be described as *A* or *B*-centring by merely changing the labels for the axes.

1.5.3 Planes and directions

We have already seen that Miller indices (*h k l*) are used to denote the faces of a crystal. The same types of indices are used to denote planes within a lattice (or, for that matter, in a crystal structure).

Figure 1.16 shows a plane section of a lattice on which the (2 1 0) planes have been marked in blue: the plane closest to the origin cuts the *a*-axis at *a*/2, the *b*-axis at unit intercept, and is parallel to *c*, out of the plane of the diagram. Because of translational periodicity, we see that this leads to a whole family of planes separated by the interplanar distance d_{210}. Now, suppose we mark off a vector (drawn in red) from the origin of the unit cell to another lattice point 2 units along vector **a**, 1 unit along **b** and 0 units along **c,** i.e., given by the vector 2**a** +**b** +0**c**.

Definition. *A crystal **direction** is given by u***a** + *v***b** + *w***c** *and has the symbol* [*u v w*]. *The set of all directions related by symmetry is denoted by* <*u v w*>.

Thus, in our example, we denote the direction as [2 1 0]. Note that in this case, [2 1 0] is not perpendicular to the (2 1 0) planes: they will be only if $a = b$ and $\gamma = 90°$. A crystallographic direction refers to a vector quantity in direct space: we shall see later, when we get to the reciprocal lattice, that it is possible in the case of planes to define another vector, the reciprocal-lattice vector, corresponding to a direction perpendicular to a plane.

1.5.4 Crystal systems

So far, we have used point-symmetry groups to classify any normal crystal. However, crystals and their corresponding lattices can also be classified into seven so-called *crystal systems*. They each have a name: cubic, tetragonal, orthorhombic, trigonal, hexagonal, monoclinic and triclinic. These are defined in terms of the minimum symmetry operations and elements that they contain. Table 1.3 lists them together with the 32 crystal classes and the restrictive effect the symmetry has on the unit-cell axes and angles. Thus, for example, anything belonging to the cubic system must have four 3-fold axes of symmetry. The effect of this is to permute the *a, b* and *c*-axes and also ensure that they are orthogonal to each other.

In the monoclinic system, there are two common choices for the direction of the 2-fold axis (or direction perpendicular to the mirror plane). The first setting takes this to be along *c*, while the more commonly used second setting used by crystallographers takes it along *b*.

Now, here is another 'Government Health Warning'. Often in textbooks, you will see that the cubic system is *defined* by $a = b = c$; $\alpha = \beta = \gamma = 90°$. Similarly, the other crystal systems are sometimes defined according to their unit-cell geometry. This works in defining the crystal systems for lattices, but it should not be used for crystal structures. The restrictions on the lattice parameters in, say, the cubic system are a *consequence* of the four 3-fold axes and not the other way round. It is entirely possible to measure the unit-cell axes and angles of a crystal and find within the precision of the measurement relationships like $a = b = c$; $\alpha = \beta = \gamma = 90°$. And yet, when one examines the crystal structure, i.e., the atomic arrangements within a unit cell, the four 3-fold axes are missing. In this case, it is an apparent metric relationship that arises accidentally.

An example of this is the material lead zirconate, $PbZrO_3$, where measurements of the unit cell were initially found to suggest $a = b$ $\alpha = \beta = \gamma = 90°$, which is consistent with tetragonal symmetry. However, when the arrangement of atoms in the crystal was examined, it was evident that there is no 4-fold axis of symmetry present. Meticulous measurements carried out later, in fact, showed that the angle γ was not precisely 90°, as would have been required for tetragonal symmetry.

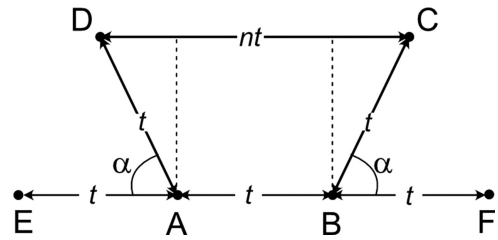

Figure 1.17. Limitations on rotational symmetry for a lattice.

1.5.5 Crystallographic restriction theorem

The limit in the number of crystal systems arises because only 1, 2, 3, 4 and 6-fold operations are possible in a conventional three-dimensional lattice. Figure 1.17 shows a lattice row EABF with period t between the points. Consider an m-fold rotation placed at the lattice points A and B, such that AE is rotated clockwise through an angle α to form AD. Similarly, BF is rotated anticlockwise through α to form BC. Suppose that D and C are the positions of lattice points and let the distance CD equal some multiple number nt of translations. It follows that

$$nt = \mathrm{CD} = t + 2t\cos\alpha \tag{1.15}$$

Therefore,

$$\cos\alpha = \frac{n-1}{2} \tag{1.16}$$

and since $|\cos\alpha| \leqslant 1$, the following values for the rotation angle α are calculated :

$n-1$	$\cos\alpha$	α	m
2	1	360° or 0	1
1	½	60°	6
0	0	90°	4
−1	−½	120°	3
−2	−1	180°	2

It is clear from this that a 5-fold rotation ($\alpha = 72°$) is not possible.

An alternative proof comes from group theory. Any proper rotation through an angle α about the z-axis, say, is given with respect to orthogonal Cartesian axes by the matrix

$$\begin{bmatrix} \cos\alpha & -\sin\alpha & 0 \\ \sin\alpha & \cos\alpha & 0 \\ 0 & 0 & 1 \end{bmatrix} \tag{1.17}$$

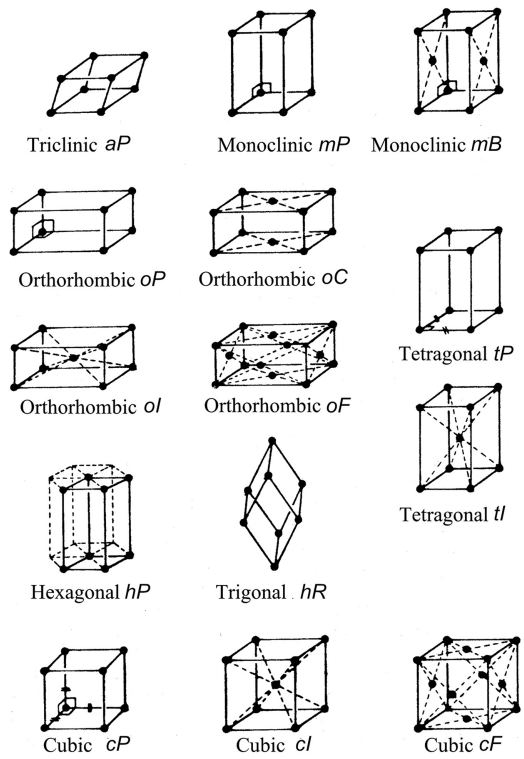

Figure 1.18. The 14 Bravais lattice types. The black spheres indicate lattice points, and should not be mistaken for atoms! The hexagonal unit cell is outlined in black—the dashed prism shown serves to indicate the angles of the unit cell.

It is well-known that the trace of such a matrix (sum of the diagonal elements) must be equal to an integer, provided that we are dealing with a symmetry operation (see, for example, Streitwolf, p. 60) [16]. Since $|\cos\alpha|$ can at most be equal to 1, the trace must lie between +3 and −1, i.e.,

$$\begin{aligned} 1 - 2\cos\alpha \quad &= 3, \quad 2, \quad 1, \quad 0, \quad -1 \\ \therefore \qquad \cos\alpha &= -1, \quad -\frac{1}{2}, \quad 0, \quad \frac{1}{2}, \quad 1 \end{aligned} \tag{1.18}$$

These five solutions give rotations with $n = 2$, 3, 4, 6 and 1, respectively.

Yet another way of thinking about this is in terms of tiling a plane with regular polygons. If you try this with 5-fold or 7-fold polygons, you will find that, however hard you try, stacking them together on a plane will always leave spaces.

1.5.6 Bravais lattices

In the mid-19th century, Auguste Bravais (1811–63) and Moritz Ludwig Frankenheim (1801–69) independently considered whether there was a limit to the number of possible *types* of lattice that could be defined. For three-dimensional lattices (figure 1.18),

Bravais determined that there were 14 in all[2], and any other description could be transformed into one of the 14. Note that each one is symbolized by reference to the crystal system.

Of the 14 Bravais lattice types, there are three that are compatible with cubic symmetry, defined by the presence of four 3-fold axes, namely *P, I* and *F*. A one-face-centred unit cell would not be cubic (even though metrically it might accidentally look like a cube) because the 3-fold axes along the four body-diagonals of the cube would want to make each face equivalent.

One way to derive the 14 Bravais lattice types is to search for the smallest unit cell possible in any lattice that, at the same time, reflects the point-group symmetry of the lattice. Thus, for example, in the tetragonal system, there are two Bravais lattices, labelled here *P* and *I*. So, what about the possibility of *C* and *F*? As can be seen (figure 1.19), by redefining a smaller unit cell through rotation by 45° about the *c*-axis, the 4-fold symmetry necessary for a tetragonal lattice is retained. Then $C \equiv P$ and $F \equiv I$. As a result, tetragonal *C* and *F* lattices are not uniquely different. Which one chooses is a matter of personal preference. Thus, one could choose to specify axes such that in, say, the triclinic system, the unit cell is all-face-centred rather than primitive. This would make a unit cell four times as big as is necessary (containing four lattice points rather than one). Still, there could be reasons why, in a particular case, one would prefer this larger unit cell: for instance, it might make it easier to compare two different phases of a material.

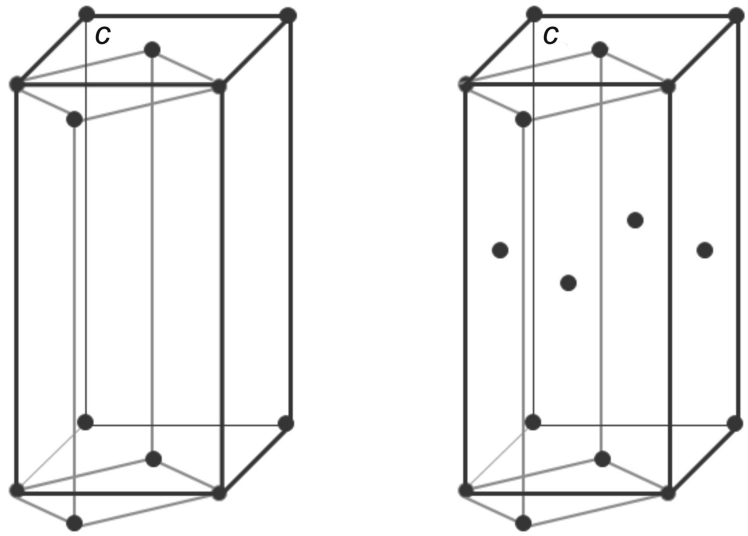

Figure 1.19. Tetragonal system showing equivalence of *C* and *P*, and *I* and *F*.

[2] Frankenheim mistakenly found 15 originally.

The unit cells shown are the conventional choices used in crystallography, but it should be understood that any of these lattices can always be described by primitive unit cells if required (often preferred by theoretical physicists).

Another point to note is our use of the word *type* in the context of Bravais lattices. When we describe a particular lattice, we infer not only its symmetry but also its metric dimensions. This means that there are only 14 Bravais lattice types, but an infinite number of Bravais lattices! The significance of this will be discussed later in section 1.7.3, after discussing space groups.

Finally, consider the symmetry of a lattice, which is always centrosymmetric. In particular, the point group of a lattice is described by the largest number of symmetry operations in any crystal system. For example, in the triclinic system, there are two possible point groups, 1 and $\bar{1}$. The latter has twice the number of symmetry operations describing it, and so the triclinic lattice has the symmetry $\bar{1}$. Again, in the cubic system, there are five point groups and three lattice types (*P*, *I* and *F*). The point groups are

$$23 \qquad m\bar{3} \qquad 432 \qquad \bar{4}3m \qquad m\bar{3}m$$

The number of symmetry operations in each point group is

$$12 \qquad 24 \qquad 24 \qquad 24 \qquad 48$$

Therefore, the point group of the cubic lattices, irrespective of the centring conditions, is $m\bar{3}m$.

Definition. *The point group of a crystal is called* ***holohedral*** *if it is identical to the point group of its lattice. The corresponding geometric crystal class is called a* ***holohedry****.*

In three-dimensional space, as there are seven crystal systems, there are seven holohedries:

$$\bar{1} \qquad 2/m \qquad mmm \qquad \bar{3}m \qquad 4/mmm \qquad 6/mmm \qquad m\bar{3}m$$

Again, note that the point groups of all lattices are centrosymmetric.

1.5.6.1 Hexagonal, trigonal (and rhombohedral)

You will notice in figure 1.18 that, in addition to a hexagonal *hP* lattice type, there is also a trigonal lattice type given the symbol *hR*. The three terms, hexagonal, trigonal and rhombohedral, are often confused and need special attention. Let us, first of all, consider a primitive hexagonal lattice. This is shown in figure 1.20. The figure shows four unit cells, where it can be seen that around each lattice point are six lattice points to form a hexagon[3]. At each lattice point, there is 6-fold rotational symmetry. Suppose now we draw the equivalent diagram using 3-fold rotational symmetry at each lattice point. The strange thing is that when you do

[3] Physicists often call this a triangular lattice, in my view incorrectly. You cannot make a lattice by repeating triangles, without every other triangle pointing in opposite directions, i.e., the triangle on its own does not constitute a unit cell.

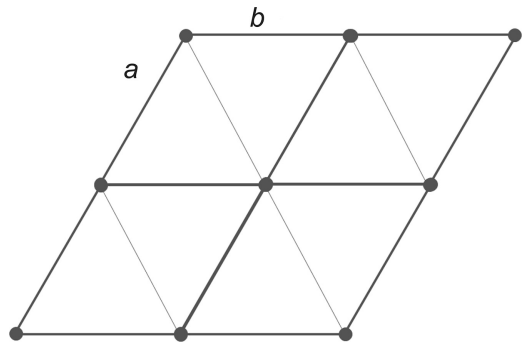

Figure 1.20. A primitive hexagonal lattice viewed on (001).

this, it looks the same as the hexagonal array! So, does this mean that the trigonal and hexagonal systems are in fact equivalent? To deal with this, the *crystal family* has been defined (see appendix C).

Notation. *There are six crystal families: triclinic symbol a (anorthic), monoclinic symbol m, orthorhombic symbol o, tetragonal symbol t, hexagonal symbol h and cubic symbol c.*

However, be aware that, often in the American and Russian literature, the term 'crystal family' corresponds to 'crystal system'. The 14 Bravais lattice types in figure 1.18 are grouped according to the crystal system, and each is denoted by a symbol for the crystal family followed by the symbol for the lattice centring.

Now, recall that there are seven crystal systems, triclinic, monoclinic, orthorhombic, tetragonal, hexagonal, trigonal and cubic. However, when we consider Bravais lattices alone, one can define seven *lattice systems* (originally called Bravais systems in the older literature). These are triclinic, monoclinic, orthorhombic, tetragonal, hexagonal, *rhombohedral* and cubic. Note that the term *trigonal* is replaced by *rhombohedral*: trigonal refers to a crystal system, not to a lattice system. Rhombohedral crystals belong to the trigonal crystal system, but trigonal crystals may belong to the rhombohedral or hexagonal lattice system.

Now consider figure 1.21(a). This time in each unit cell, two extra lattice points have been added at heights 1/3 and 2/3. Notice now that the 6-fold symmetry has been replaced by 3-fold symmetry, for example, relating the lattice points at height 1/3. We can therefore think of each unit cell as hexagonal with extra centring points. By joining up the lattice points, as indicated, a smaller rhombohedron-shaped unit cell with axes a_R, b_R and c_R of equal length and at equal angles can be constructed. This unit cell is primitive (it contains one lattice point) and has a single 3-fold axis, with

$$a_R = b_R = c_R \; \alpha = \beta = \gamma \tag{1.19}$$

When the unit cell is described in this way, it is known as *rhombohedral* and is given the symbol R, and in figure 1.18 it is listed as trigonal-hR (i.e., crystal system—crystal family—lattice system). In the International Tables for Crystallography [5],

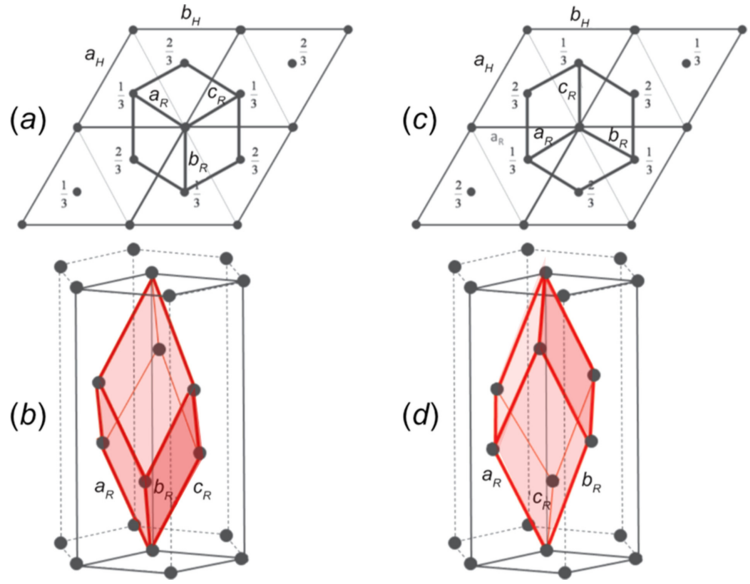

Figure 1.21. Hexagonal centring with a primitive rhombohedral unit cell added. Left is the obverse setting and right is the reverse setting.

where crystal symmetry is carefully defined, the convention is to classify rhombohedral symmetry as a member of the trigonal crystal system, in which case one can choose to specify the unit cell using either hexagonal or rhombohedral axes.

Note another complexity. The drawing in figure 1.21(b) is known as the *obverse* setting, whereas the one in figure 1.21(d) is the so-called *reverse* setting. It is the accepted convention to use the obverse setting in describing rhombohedral crystals, although you may encounter the reverse setting from time to time.

1.6 Crystal structures

> *Some studies pursued by the writer as to the nature of molecules have led him to believe that in the atom-groupings which modern chemistry reveals to us, the several atoms occupy distinct portions of space and do not lose their individuality…*
> (William Barlow, 1883 paper in which he predicted the structure of the alkali halides)

We now put together the ideas discussed hitherto to explain what is meant by the term *crystal*.

Definition. In direct space, *an **ideal** crystal is a solid in which a group of atoms or molecules repeat to form a periodic arrangement*.

Actually, in a real crystal, the atoms are in constant vibration. There may be all sorts of defects and impurities present, in which case our definition refers to the time and

space-averaged positions of the atoms or molecules. Note, also, that the definition relates to atoms and molecules and not to lattice points. One of the simplest ways to define a crystal and its structure is through the use of the mathematical operation of convolution.

It is worth noting here, that while the concept of periodic order in direct space lies at the heart of our understanding of crystals, and in fact of most condensed matter physics, this traditional view has, in recent years, been challenged by the discovery of examples of the so-called aperiodic crystals. This has led the International Union of Crystallography to redefine the meaning of what is meant by a crystal in terms of reciprocal space. We shall return to this question in section 3.14. The traditional view of periodicity, however, is still valid for most crystals.

1.6.1 Convolution

Consider two functions $g(\mathbf{r})$ and $h(\mathbf{r})$ spanning a space given by the vector $\mathbf{r}$. The convolution of these two functions $f(\mathbf{r})$ is given by

$$f(\mathbf{r}) = g(\mathbf{r}) * h(\mathbf{r}) = \int_{-\infty}^{\infty} g(\mathbf{r}')h(\mathbf{r} - \mathbf{r}')d\mathbf{r}' \tag{1.20}$$

The effect of this operation is effectively to slide one function over the other while integrating. Figure 1.22 illustrates this process for two arbitrarily chosen functions. It can be seen that here, where one of the functions, $h(\mathbf{r})$, consists of three sharp lines, the effect is to repeat the first function, $g(\mathbf{r})$, in sympathy.

1.6.2 Convolution applied to crystals

Suppose we have a collection of atoms described by a function $B(\mathbf{r})$: often in physics texts, this is referred to as the 'basis' (this should not be confused with *crystallographic* or *lattice basis*, terms that refer to the set of vectors used in defining the unit-cell axes). To form a crystal structure, we need to repeat the basis according to the

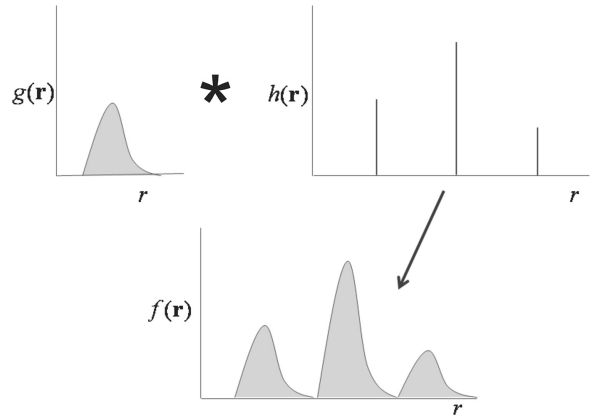

Figure 1.22. An example of the convolution of two functions.

translational symmetry of the lattice. The lattice function $L(\mathbf{r})$ can be defined by a series of δ-functions, thus

$$L(\mathbf{r}) = \sum_{uvw} \delta(\mathbf{r} - \mathbf{r}_{uvw}) \tag{1.21}$$

where

$$\mathbf{r}_{uvw} = u\mathbf{a} + v\mathbf{b} + w\mathbf{c} \tag{1.22}$$

and

$$\begin{aligned} \delta(\mathbf{r} - \mathbf{r}_{uvw}) &= 0 \qquad \mathbf{r} \neq \mathbf{r}_{uvw} \\ &= \infty \qquad \mathbf{r} = \mathbf{r}_{uvw} \end{aligned} \tag{1.23}$$

Then the crystal structure $C(\mathbf{r})$ is given by

$$C(\mathbf{r}) = L(\mathbf{r}) * B(\mathbf{r}) \tag{1.24}$$

In figure 1.11, the function $B(\mathbf{r})$ was represented by an elephant! By convoluting this with the lattice in figure 1.12, the result is the 'crystal' structure, in this case consisting of a regular array of elephants. Of course, this is not a real crystal structure, but it does illustrate how the lattice acts as a template to instruct how the basis is to be repeated.

1.6.3 Examples of simple crystal structures

The concept of a basis convoluted with a lattice is a useful and convenient way to describe relatively simple crystal structures, although to describe more complex cases, one has to resort to the idea of space groups (to be explained in section 1.7) . Here we shall consider a few examples.

1.6.3.1 Copper Cu

The crystal structure of the metal copper is very simple and can be summarised thus (figure 1.23):

Crystal system	Cubic	a = 3.610Å
Lattice type	*cF*	(0, 0, 0) (½, ½, 0) (½, 0, ½) (0, ½, ½)
Basis	Cu	(0, 0, 0)
Number of atoms in the unit cell	Z	4
Fractional coordinates	Cu	(0, 0, 0) (½, ½, 0) (½, 0, ½) (0, ½, ½)

This illustrates why some people become confused between lattices and structures. This structure has a basis consisting of one atom so that when we construct the crystal structure, we see that there is a single atom for each lattice point. The result is a diagram that closely resembles the equivalent drawing for the *cF* lattice, as seen in figure 1.18: but remember in the picture of the structure we have atoms, not points!

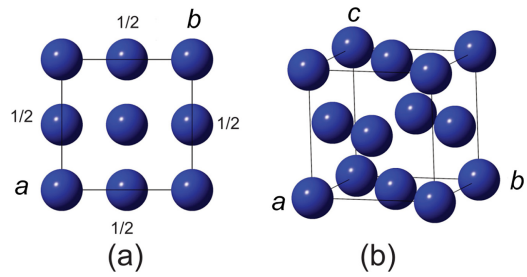

Figure 1.23. Copper crystal structure: (a) (0 0 1) projection, (b) perspective view.

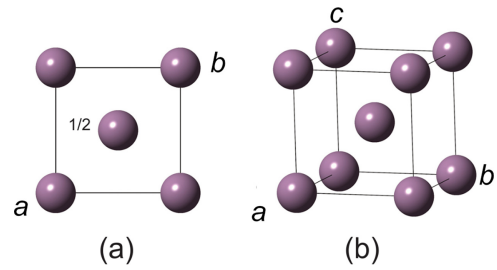

Figure 1.24. Molybdenum crystal structure: (a) (0 0 1) projection, (b) perspective view.

1.6.3.2 Molybdenum Mo

Once again, this structure has a basis consisting of a single atom but with a body-centred cubic lattice, and so too, there is one atom per lattice point (figure 1.24).

Crystal system	Cubic	$a = 3.150$Å
Lattice type	*cI*	(0, 0, 0) (½, ½, ½)
Basis	Mo	(0, 0, 0)
Number of atoms in the unit cell	*Z*	2
Fractional coordinates	Mo	(0, 0, 0) (½, ½, ½)

Note that the crystal structure of iron, Fe, has the same atomic arrangement.

1.6.3.3 Sodium chloride NaCl

The structure of the alkali halides, as exemplified by NaCl, consists of an alternating arrangement of cations and anions, as shown in figure 1.25.

Crystal system	Cubic	$a = 5.628$Å
Lattice type	*cF*	(0, 0, 0) (½, ½, 0) (½, 0, ½) (0, ½, ½)
Basis	Na	(0, 0, 0)
	Cl	(½, 0, 0)
Number of atoms in the unit cell	*Z*	8
Fractional coordinates	Na	(0, 0, 0) (½, ½, 0) (½, 0, ½) (0, ½, ½)
	Cl	(½, 0, 0) (0, ½, 0) (0, 0, ½) (½, ½, ½)

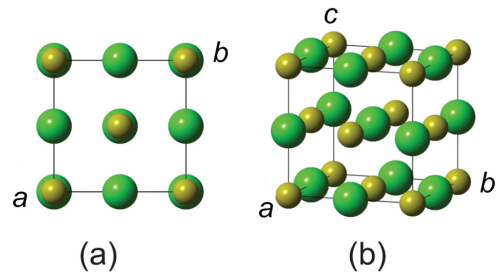

Figure 1.25. The sodium chloride crystal structure: (a) (0 0 1) projection, (b) perspective drawing. Na: yellow, Cl: green.

This structure is an example of a crystal structure with a basis consisting of two atoms. The result of convoluting the four lattice points of the *F* unit cell with the two atoms in the basis is to create eight atoms in the unit cell. This structure has the same Bravais lattice type as copper, but since the lattice parameter and unit-cell contents are different, it has a different Bravais lattice (the lattice must include both symmetry and its metrics: the term lattice type just refers to the lattice symmetry).

1.6.3.4 Cesium chloride CsCl

This structure is what I call 'an old chestnut' as it has been used in countless condensed matter physics examination questions.

Crystal system	Cubic	$a = 4.123$Å
Lattice type	*cP*	(0, 0, 0)
Basis	Cs	(0, 0, 0)
	Cl	(½, ½, ½)
Number of atoms in the unit cell	*Z*	2
Fractional coordinates	Cs	(0, 0, 0)
	Cl	(½, ½, ½)

At first sight (figure 1.26), this structure looks like that of molybdenum, but the difference here is that the atom at the centre of the unit cell is not the same as the one at the corners. Therefore, it is a mistake to say that the lattice is body-centred *I*, as implied misleadingly in some books. It is primitive c*P* with a basis consisting of two atoms.

The crystal structure of β-brass (CuZn) at low temperature is similar. In this structure, as the temperature is increased, the Cu and Zn atoms tend to hop onto each other's sites, until at a specific temperature, each of the two atomic sites has on average ½ (Cu + Zn). The structure, when averaged over all unit cells, is then effectively body-centred cubic, as in molybdenum. This is an example of an order-disorder phase transition.

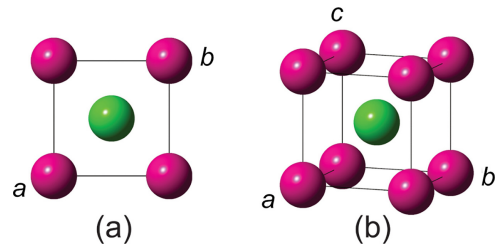

Figure 1.26. Cesium chloride structure: (a) (0 0 1) projection, (b) perspective view. Cs: pink, Cl: green.

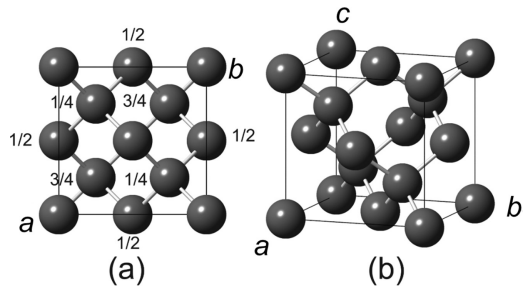

Figure 1.27. Diamond/silicon/germanium structure: (a) (0 0 1) projection, (b) perspective view.

1.6.3.5 Diamond C

Here is another old favourite, and possibly the most important crystal structure for physicists to learn (figure 1.27).

Crystal system	Cubic	$a = 5.646$Å
Lattice type	*cF*	(0, 0, 0) (½, ½, 0) (½, 0, ½) (0, ½, ½)
Basis	C1	(0, 0, 0)
	C2	(¼, ¼, ¼)
Number of atoms in the unit cell	*Z*	8
Fractional coordinates	C1	(0, 0, 0) (½, ½, 0) (½, 0, ½) (0, ½, ½)
	C2	(¼, ¼, ¼) (¾, ¾, ¼) (¾, ¼, ¾) (¼, ¾, ¾)

This is a structure with two carbon atoms in the basis, denoted C1 and C2. Notice how the convolution of the basis with the lattice results in eight atoms in the unit cell, but with a structure that is different from that of NaCl. While these two crystals have the same lattice type, the differences in the basis create different crystal structures. This is why phrases like 'the diamond lattice' are confusing, because the diamond lattice means face-centred cubic: what is meant is 'the diamond crystal structure'. Sorry to labour the point, but it is important to understand this distinction between lattice and structure. The same basic structure type is adopted by silicon and germanium. This structure is centrosymmetric: see if you can work out where the centre of inversion lies (hint: move the unit-cell origin to halfway between C1 and C2 and recalculate the atomic coordinates).

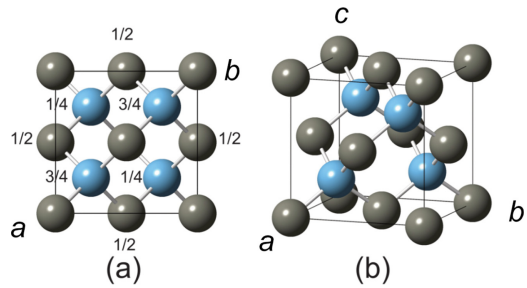

Figure 1.28. Zinc blende structure: (a) (0 0 1) projection, (b) perspective view. Zn: grey, S: blue.

1.6.3.6 Zinc sulfide ZnS

This structure type, otherwise known as the zinc blende or sphalerite structure, and adopted by many compounds such as GaAs, InSb, etc., looks at first sight to be the same as that of diamond. However, the difference here is that the two atoms in the basis are not the same element. This structure type is non-centrosymmetric, and so this material can exhibit a polar property such as piezoelectricity (but not pyroelectricity, as it has no unique polar axis) (figure 1.28).

Crystal system	Cubic	$a = 5.420$Å
Lattice type	*cF*	(0, 0, 0) (½, ½, 0) (½, 0, ½) (0, ½, ½)
Basis	Zn	(0, 0, 0)
	S	(¼, ¼, ¼)
Number of atoms in the unit cell	*Z*	8
Fractional coordinates	Zn	(0, 0, 0) (½, ½, 0) (½, 0, ½) (0, ½, ½)
	S	(¼, ¼, ¼) (¾, ¾, ¼) (¾, ¼, ¾) (¼, ¾, ¾)

1.6.3.7 Perovskites

This structure is one of my favourites since I have spent most of my research life studying these compounds. The perovskite structure is adopted by many compounds of general formula ABX_3, where A and B are cations, and X is an anion, usually oxygen. Recently, there has been an enormous surge of interest in this structure, especially where the A cation is replaced by an organic molecule, as it shows enhanced photovoltaic properties that can compete with the standard silicon photocell applications. An example of such a hybrid perovskite is methylammonium lead chloride. The structure described below is the usual high-temperature structure of many perovskites, such as in $SrTiO_3$.

Figure 1.29(a) and (b) show the usual drawings of the structure. In contrast, figure 1.29(c) shows that when the O–O bonds are drawn in, the result is a framework of corner-linked octahedra (in the figure, the oxygen atoms are not shown but occur at the vertices of the octahedra). Drawings of structures that emphasize polyhedral coordination in this way are often to be found in the literature.

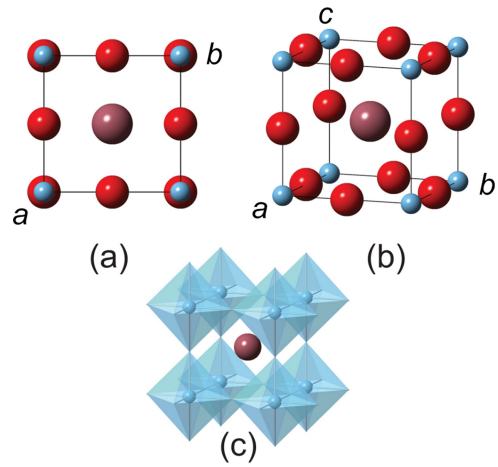

Figure 1.29. The $SrTiO_3$ crystal structure: (a) (0 0 1) projection, (b) perspective drawing, (c) showing oxygen octahedra. Sr: maroon, Ti: blue, O: red.

Crystal system	Cubic	a = 3.91Å
Lattice type	*cP*	(0, 0, 0)
Basis	Sr	(½, ½, ½)
	Ti	(0, 0, 0)
	O	(½, 0, 0) (0, ½, 0) (0, 0, ½)
Number of atoms in the unit cell	Z	5
Fractional coordinates	Sr	(½, ½, ½)
	Ti	(0, 0, 0)
	O	(½, 0, 0) (0, ½, 0) (0, 0, ½)

1.6.3.8 Wurtzite ZnS

Just to show that not everything is cubic, consider the wurtzite structure. This is another form of zinc sulfide. The crystal system, in this case, is hexagonal (figure 1.30).

Crystal system	Hexagonal	a = 3.81Å. c = 6.23Å
Lattice type	*hP*	(0, 0, 0)
Basis	Zn1	(⅓, ⅔, 0)
	Zn2	(⅔, ⅓, ½)
	S1	(⅓, ⅔, 0.375)
	S2	(⅔, ⅓, ½+0.375)
Number of atoms in the unit cell	Z	4
Fractional coordinates	Zn	(⅓, ⅔, 0) (⅔, ⅓, ½)
	S	(⅓, ⅔, 0.375) (⅔, ⅓, ½+0.375)

The lattice is primitive, and there are four atoms in the basis and, therefore, in the unit cell. Notice that in this structure, there is just one freely variable parameter for

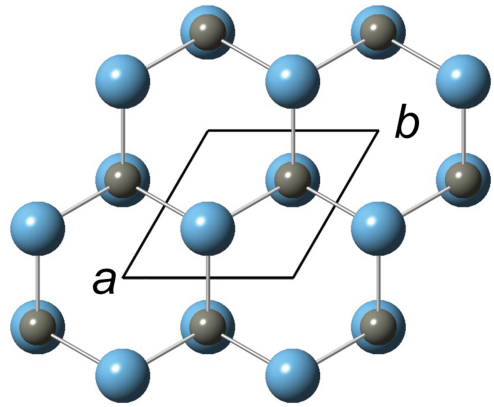

Figure 1.30. The wurtzite crystal structure: (0 0 1) projection. Zn: grey, S: blue.

the S atomic coordinates. Having fixed the Zn positions, the z-coordinate of the S atoms obeys the relationship

$$z(S2) = ½ + z(S1) = 0.875 \tag{1.25}$$

Definition. *The ability for a chemical entity, in this case, ZnS, to exist in different crystal structures is called* ***polymorphism****.*

1.7 Space groups

The concept of a lattice and a basis is used in most condensed matter physics textbooks. While this may be sufficient to describe very simple structures, more complex structures, where there are many atoms in the unit cell, need a different approach. Indeed, no self-respecting crystallographer would talk about a lattice and a basis. Instead, space groups are used to describe crystal structures.

Definition. *A space group of a crystal structure is the set of all symmetry operations that describe the symmetry properties of the crystal structure.*

A full description of space groups lies outside the scope of this book, and the reader should consult the International Tables for Crystallography, Volume A (ITA) [5], or the book by Burns and Glazer [17]. I regard the ITA as one of the most outstanding books produced in the 20th–21st centuries! Note that in appendix B, all the symbols used in the International Notation for the space groups are given. Here I shall only provide a brief explanation of some of the important features.

Definition. *The* ***asymmetric unit*** *is the smallest part of space that generates the whole of space when all the symmetry operations of a space group are applied. In mathematics, it is called the* ***fundamental region*** *or* ***fundamental domain****.*

Thus, in the example above of diamond, the asymmetric unit contains a single atom of carbon, as opposed to the basis consisting of two carbon atoms. A crystallographer would describe the crystal structure of diamond by specifying the space group with the symbol $Fd\bar{3}m$ with a carbon atom at (0, 0, 0). With this designation, we now only have to specify the position of one carbon atom, instead of two, but let the space group with all its symmetry operations automatically generate the remaining seven atoms in the unit cell, a saving of 50% of the information needed. This approach obviates the need to write out the positions of all the atoms in a unit cell. Symmetry allows us to specify fewer parameters than otherwise.

1.7.1 Symmorphic space groups

Many space groups are constructed by combining the 32 point groups with the 14 Bravais lattice types to generate the 73 so-called *symmorphic* space-group types. A useful way to represent their symmetry operations is by use of the Seitz symbol $\{\boldsymbol{R}|\mathbf{t}_n\}$, commonly used in crystallographic group-theory texts.

$$\{\boldsymbol{R}|\mathbf{t}_n\}\mathbf{r} = \boldsymbol{R}\mathbf{r} + \mathbf{t}_n \tag{1.26}$$

$\boldsymbol{R}$ represents a point-group symmetry operator.

The set of translation vectors $\mathbf{t}_n$ is of infinite size, but because of periodicity, we normally need only consider the point-group operations applied to one unit cell. In this case, the Seitz symbol can be written thus

$$\{\boldsymbol{R}|\mathbf{0}\}\mathbf{r} = \boldsymbol{R}\mathbf{r} \tag{1.27}$$

The set of operations defined by Seitz operators forms a so-called *real affine group* of which space groups are subgroups. An affine group is defined by transformations in a vector space that leave straight lines as straight lines and preserve parallelism. The Seitz operators form a group for the following reasons:

1. Combining two Seitz operators $\{\boldsymbol{R}|\mathbf{t}\}$ and $\{\boldsymbol{S}|\mathbf{u}\}$ gives another operator that is a member of the set:

$$\{\boldsymbol{R}|\boldsymbol{t}\}\{\boldsymbol{S}|\boldsymbol{u}\}\boldsymbol{r} = \{\boldsymbol{R}|\boldsymbol{t}\}(\boldsymbol{S}\boldsymbol{r} + \boldsymbol{u}) = \boldsymbol{R}\boldsymbol{S}\boldsymbol{r} + \boldsymbol{R}\boldsymbol{u} + \boldsymbol{t} = \{\boldsymbol{R}\boldsymbol{S}|\boldsymbol{R}\boldsymbol{u} + \boldsymbol{t}\}\boldsymbol{r}$$

2. There is obviously an identity operator $\{1|\mathbf{0}\}$.
3. There is an inverse given by $\{\boldsymbol{R}^{-1}|-\boldsymbol{R}^{-1}\mathbf{t}\}$ since

$$\{\boldsymbol{R}|\mathbf{t}\}\{\boldsymbol{R}^{-1}| - \boldsymbol{R}^{-1}\mathbf{t}\} = \{1|\mathbf{0}\}$$

4. Associativity is obeyed.

The Seitz symbols are listed in appendix D for all space-group operations. To develop a space group, take as an example the point group $2/m$ combined with a C-centred lattice to give the space group $C2/m$. Assuming the monoclinic second setting, one can write the Seitz symbols as $\{2_{010}|\mathbf{0}\}$ for the 2-fold rotation about the b-axis and $\{m_{010}|\mathbf{0}\}$ for the reflection perpendicular to the b-axis, with both symmetry operations acting through the unit-cell origin. This combination produces an inversion operation $\{\bar{1}|\mathbf{0}\}$. To each of these, the C-centring adds

(½, ½, 0). Operating on the point x, y, z therefore gives eight general coordinate positions

$$\begin{array}{llll} \{1|\mathbf{0}\} & \rightarrow x, y, z & \{1|½,½,0\} & \rightarrow ½ + x, ½ + y, z \\ \{2_{010}|\mathbf{0}\} & \rightarrow \overline{x}, y, \overline{z} & \{2_{010}|½,½,0\} & \rightarrow ½ - x, ½ + y, \overline{z} \\ \{m_{010}|\mathbf{0}\} & \rightarrow x, \overline{y}, z & \{m_{010}|½,½,0\} & \rightarrow ½ + x, ½ - y, z \\ \{\bar{1}|\mathbf{0}\} & \rightarrow \overline{x}, \overline{y}, \overline{z} & \{\bar{1}|½,½,0\} & \rightarrow ½ - x, ½ - y, ½ - z \end{array}$$

See how, by just giving the symbol *C*2/*m* plus the coordinates in the unit cell of just one atom, eight atoms are automatically specified!

Consider combining point group 4/*m,* together with a primitive lattice, to give *P*4/*m*. Let's take a 'whistle-stop tour' through some of the features on the page of the ITA for this space group (figure 1.31). Reading from left to right, at the top is the short space-group symbol *P*4/*m*, followed by the Schoenflies symbol C_{4h}^{1}. The Schoenflies symbol is not much used for space groups in practice, because differentiation between space groups with the same point-group symmetry is by a numerical superscript, and the only way to know what this means is to look it up in a book. The International symbol, on the other hand, is sufficient for a competent person to derive all the space group information.

The next entry 4/*m* is the point group followed by the crystal system, tetragonal. On the next line, No. 83 means that this is number 83 in the book. This is followed by the full symbol *P*4/*m*. In this case, it is the same as the short symbol. However, for example, in space group *C*2/*m,* if we take the unique axis to be along *b*, the full symbol is *C*12/*m*1, the numbers 1 in the first and third place indicating no symmetry with respect to the *a* and *c*-axes. The next entry at the right is the Patterson symmetry. This is the symmetry of so-called Patterson maps (see section 3.13.3), which are used in crystal-structure determinations.

Below this, there are two diagrams. The one on the left marks the symmetry elements using standard symbols to denote them. The origin is at the top left corner, with *a* down, *b* to the right and *c* towards you. The right-hand diagram shows how any object, such as an atom or group of atoms, is transformed under the symmetry operations. Then, below this, we see that a centre of symmetry has been placed at the origin. Here, the 4-fold axis meets the perpendicular mirror plane, and the combination of the two automatically creates a centre of inversion.

The next entry is the asymmetric unit showing that any information put into this unit cell within these limits will automatically appear throughout all space after application of the space-group operations. The list of symmetry operations then appears. These are each numbered serially, beginning with the identity operation. In this case, there are eight in total. For example, (3) 4^{+} 0,0, z refers to an anticlockwise 4-fold operation whose axis is along 0, 0, z.

After this, a list of 'Generators Selected' is given. These include the translation operations along *x, y* and *z* plus three of the symmetry operations from the previous list. With these sets of operations, one can generate the whole space group.

Below, under the heading 'Coordinates', is the list of coordinate triplets that specify how any object at *x, y, z* is transformed under the symmetry operations (1)–(8). That is, if we place an atom at some general position, another seven will be

$P4/m$ C_{4h}^1 $4/m$ Tetragonal

No. 83 $P4/m$ Patterson symmetry $P4/m$

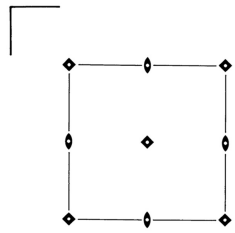

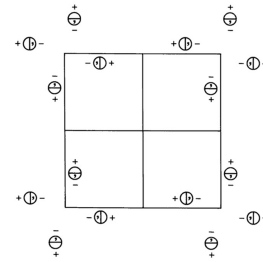

Origin at centre $(4/m)$

Asymmetric unit $0 \le x \le \frac{1}{2}$; $0 \le y \le \frac{1}{2}$; $0 \le z \le \frac{1}{2}$

Symmetry operations

(1) 1 (2) 2 $0,0,z$ (3) 4^+ $0,0,z$ (4) 4^- $0,0,z$
(5) $\bar{1}$ $0,0,0$ (6) m $x,y,0$ (7) $\bar{4}^+$ $0,0,z$; $0,0,0$ (8) $\bar{4}^-$ $0,0,z$; $0,0,0$

Generators selected (1); $t(1,0,0)$; $t(0,1,0)$; $t(0,0,1)$; (2); (3); (5)

Positions

Multiplicity, Wyckoff letter, Site symmetry	Coordinates				Reflection conditions
					General:
8 l 1	(1) x,y,z (5) $\bar{x},\bar{y},\bar{z}$	(2) $\bar{x},\bar{y},z$ (6) $x,y,\bar{z}$	(3) $\bar{y},x,z$ (7) $y,\bar{x},\bar{z}$	(4) $y,\bar{x},z$ (8) $\bar{y},x,\bar{z}$	no conditions
					Special:
4 k m . .	$x,y,\frac{1}{2}$	$\bar{x},\bar{y},\frac{1}{2}$	$\bar{y},x,\frac{1}{2}$	$y,\bar{x},\frac{1}{2}$	no extra conditions
4 j m . .	$x,y,0$	$\bar{x},\bar{y},0$	$\bar{y},x,0$	$y,\bar{x},0$	no extra conditions
4 i 2 . .	$0,\frac{1}{2},z$	$\frac{1}{2},0,z$	$0,\frac{1}{2},\bar{z}$	$\frac{1}{2},0,\bar{z}$	hkl : $h+k=2n$
2 h 4 . .	$\frac{1}{2},\frac{1}{2},z$	$\frac{1}{2},\frac{1}{2},\bar{z}$			no extra conditions
2 g 4 . .	$0,0,z$	$0,0,\bar{z}$			no extra conditions
2 f $2/m$ . .	$0,\frac{1}{2},\frac{1}{2}$	$\frac{1}{2},0,\frac{1}{2}$			hkl : $h+k=2n$
2 e $2/m$ . .	$0,\frac{1}{2},0$	$\frac{1}{2},0,0$			hkl : $h+k=2n$
1 d $4/m$ . .	$\frac{1}{2},\frac{1}{2},\frac{1}{2}$				no extra conditions
1 c $4/m$ . .	$\frac{1}{2},\frac{1}{2},0$				no extra conditions
1 b $4/m$ . .	$0,0,\frac{1}{2}$				no extra conditions
1 a $4/m$ . .	$0,0,0$				no extra conditions

Symmetry of special projections

Along [001] $p4$
$\mathbf{a}' = \mathbf{a}$ $\mathbf{b}' = \mathbf{b}$
Origin at $0,0,z$

Along [100] $p2mm$
$\mathbf{a}' = \mathbf{b}$ $\mathbf{b}' = \mathbf{c}$
Origin at $x,0,0$

Along [110] $p2mm$
$\mathbf{a}' = \frac{1}{2}(-\mathbf{a}+\mathbf{b})$ $\mathbf{b}' = \mathbf{c}$
Origin at $x,x,0$

Figure 1.31. Example from the International Tables for Crystallography, Volume A, of space group *P4/m.* (Reproduced by permission of the International Union of Crystallography, https://it.iucr.org.)

generated according to this list. You can see immediately how powerful space groups are because, instead of writing out all eight atomic positions, we just need to provide one position and let the space group determine the rest.

Below the general positions, lists are given to show what happens if one places an atom at a *special* position. For instance, an atom placed on the mirror plane *x, y,* ½ will appear four times in the unit cell at

$$x,\ y,\ \tfrac{1}{2}; \qquad \bar{x},\ \bar{y},\ \tfrac{1}{2}; \qquad \bar{y},\ x,\ \tfrac{1}{2}; \qquad y,\ \bar{x},\ \tfrac{1}{2}$$

At the left is the Wyckoff symbol, in this case, labelled 4k. Here, the multiplicity is 4, as just four positions are generated in the unit cell for each atom placed at a 4k site. The symbol *m*.. represents the site symmetry, meaning that the atom lies on a mirror plane perpendicular to the 4-fold axis. The first dot indicates no symmetry elements running through this point along [1 0 0] and [0 1 0]: the second dot means no symmetry running through [1 1 0] and [1 $\bar{1}$ 0] (see appendix B for the table explaining the order of symbols).

Finally, at the bottom, information is given on the plane-group symmetry obtained if the space group is projected down certain directions onto a plane.

1.7.2 Non-symmorphic space groups

When one combines lattices with point-group symmetry, new types of symmetry operations are discovered. These include a translation that is less than a full lattice translation and given by the Seitz operation as

$$\{\boldsymbol{R}|\mathbf{v}\}\mathbf{r} = \boldsymbol{R}\mathbf{r} + \mathbf{v} \tag{1.28}$$

on the understanding that the infinite set of full translations will always apply in addition. Space groups that are defined in this way are known as *non-symmorphic* space groups. These contain the screw and glide operations. In total, there are 157 of these, making a total of 230 three-dimensional space-group types.

1.7.2.1 Screw operations

Screw rotations consist of a rotation plus a fractional translation along the rotation axis. The 2-fold screw operation about [0 0 1], symbol, 2_1, (figure 1.32), can be written as

$$\{2_{001}|(0, 0, ½\} \tag{1.29}$$

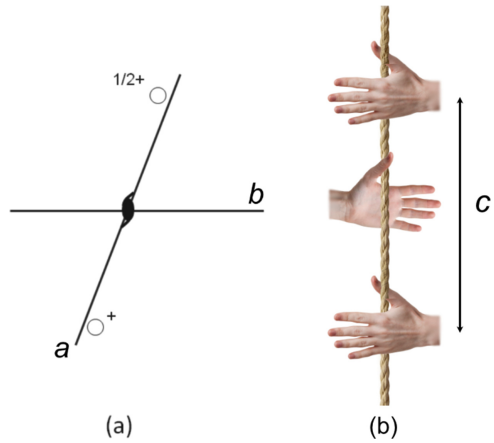

Figure 1.32. A 2_1[0 0 1] screw axis. (a) Stereographic projection. (b) An example showing hands related by a 2-fold screw axis.

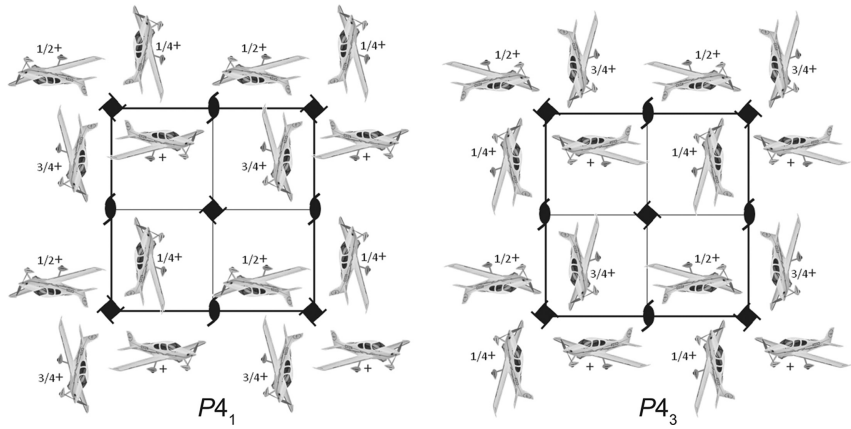

Figure 1.33. Examples of space groups $P4_1$ and $P4_3$.

Note that applying this operation twice gives

$$\{1|(0,\ 0,\ 1\} \equiv \{1|(0,\ 0,\ 0)\} \tag{1.30}$$

Because of lattice periodicity, this is equivalent to the identity operation with respect to the original unit cell.

Similarly, consider 4-fold screw axes 4_1 and 4_3 directed along [0 0 1]. Figure 1.33 shows diagrams for space groups $P4_1$ and $P4_3$. For fun, the space groups are illustrated by pictures of an aircraft undergoing barrel-rolls towards us to the left and to the right, respectively (naturally, in a real crystal, instead of an aircraft, one would have a molecule or group of atoms, but the principle is nevertheless the same). Notice that the combination of 4_1 and 4_3 axes with a primitive tetragonal lattice gives rise to 2-fold screw axes mid-way between the 4-fold screw axes. It can also be seen that 4_1 and 4_3 describe helices of opposite chirality. Thus, these two space groups are mirror images of each other, and as a result, it has been argued in the past that they should not be considered separate space groups. The International Tables nevertheless does include them separately. $P4_1$ and $P4_3$ are examples of what are termed *enantiomorphic* space-groups. There are 11 such enantiomorphic space-group types in three dimensions.

The Seitz symbols for 4_1 and 4_3 operations about the c-axis are

$$\{4_{001}|(0,0,¼)\}\text{and}\{4_{001}|(0,0,¾)\} \tag{1.31}$$

Note that there are 65 space-group types in which chiral crystal structures can form. These contain only proper rotations and/or screw rotations, and are known as *Sohncke groups* after their discoverer Leonhard Sohncke (1842–97). Note too, that there are 13 space groups, such as $P1$, $P2_1$ or $P2_12_12_1$, that do not have any special positions. These are known as *Bieberbach groups*, after Ludwig Georg Elias Moses Bieberbach (1886–1982).

1.7.2.2 Glide operations

There are several different kinds of glide operations, in which reflection is accompanied by a translation through a fraction of the unit-cell edge. As an

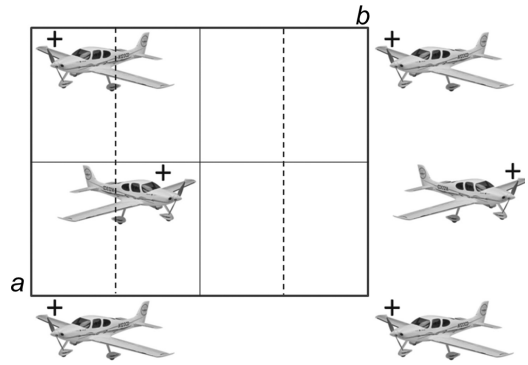

Figure 1.34. Example of an *a*-glide in space group $P1a1$ (Pa) – second setting monoclinic.

example, consider a reflection across the (0 1 0) plane plus a translation of halfway along the *a*-axis given by

$$\{m_{010}|(½,0,0)\} \tag{1.32}$$

m_{010} refers to a reflection across the plane perpendicular to the *b*-axis. This is known as an axial *a*-glide (*b* and *c*-glides involve half translations along *b* and *c*, respectively). Figure 1.34 shows space group *Pa* (or full symbol $P1a1$) using an aircraft as a general motif! Note that the two aircraft within the unit cell are mirror images of each other and are not related by rotational symmetry: look carefully at the directions of the propeller blades in each case!

There are other types of glide planes possible (diagonal, diamond and double glides). The diagonal and diamond glides again involve reflection plus translations, this time in either two or three directions (see appendix B). Thus, the Seitz symbol for a diagonal *n*-glide reflecting perpendicular to *c* with half translations along *a* and *b* is

$$\{m_{001}|(½,½,0)\} \tag{1.33}$$

For a typical diamond *d*-glide, say reflecting across *c* and quarter translations along *a* and *b*:

$$\{m_{001}|(¼,¼,0)\} \tag{1.34}$$

The *e* double glide needs special comment. This was brought into the space-group symbols relatively recently. As an example, consider the space group *Cmce*. Originally, this was called *Cmca*. However, when you look at the list of coordinate triplets, it was realized that in addition to the *a*-glide, there is also a *b*-glide present. Thus, this space group could, in principle, be called *Cmcb*. However, the *e*-glide cannot be represented by, for example, a Seitz operator, as it involves two simultaneous actions. The *e*-glide, therefore, is not a symmetry operation, but it is a symmetry element. In the list of symmetry operations in the ITA, *a* and *b* glides are seen, but not the *e*-glide.

Together with the screw axes and glide planes, it is found that there are 230 space-group types in three dimensions. For further information, I recommend consulting

Table 1.4. Space groups for some crystal structures.

Crystal	Space group	Wyckoff	Atomic coordinates
Cu	$Fm\bar{3}m$	4a	Cu: 0, 0, 0
Mo	$Im\bar{3}m$	2a	Mo: 0, 0, 0
NaCl	$Fm\bar{3}m$	4a	Na: 0, 0, 0
		4b	Cl: ½, ½, ½
CsCl	$Pm\bar{3}m$	1a	Cs: 0, 0, 0
		1b	Cl: ½, ½, ½
Diamond	$Fd\bar{3}m$	8a	C: 0, 0, 0
Zinc blende	$F\bar{4}3m$	4a	Zn: 0, 0, 0
		4c	S: ¼, ¼, ¼
Perovskite	$Pm\bar{3}m$	1b	Sr: ½, ½, ½
		1a	Ti: 0, 0, 0
		3d	O: ½, 0, 0
Wurtzite	$P6_3mc$	2b	Zn: 0, 0, 0
		2b	S: 0, 0, 0.375

the various books devoted to space groups. I have listed the crystal structures in section 1.6.3 using space-group symbols together with the atomic positions needed to generate the crystal structures (table 1.4).

1.7.3 Types

You may have noticed that the word *type* has appeared several times so far in our discussion. This word has special significance in crystal symmetry. Recall that when talking about the Bravais lattice for a particular crystal, account must be taken of both symmetry and the basis vectors making up the unit cell. For example, the copper and sodium chloride structures are face-centred cubic. They have the same lattice type (c*F*), but because their unit cells are metrically different, as well as their structures, they have different *cF*-lattices. In other words, there is an infinity of Bravais lattices but only 14 Bravais-lattice types. The same applies to space groups and space-group types. Strictly speaking, there are just 230 space-group *types* but an infinite number of space groups! For the most part, it is unnecessary to make this subtle distinction, and most crystallographers just refer to 230 space groups.

However, the concept of space-group types can be important in certain circumstances, for example, in considering group-subgroup relationships, as often occurs in solid-state phase transformations.

Definition. *A **subgroup** H consists of a subset of elements of the group G such that H also forms a group.*

As an example, consider the high-temperature phase transition from α-quartz to β-quartz, which takes place at around 574 °C. At high temperature, the structure is described by space group $P6_222$ (for right-handed quartz, $P6_422$ for left-handed

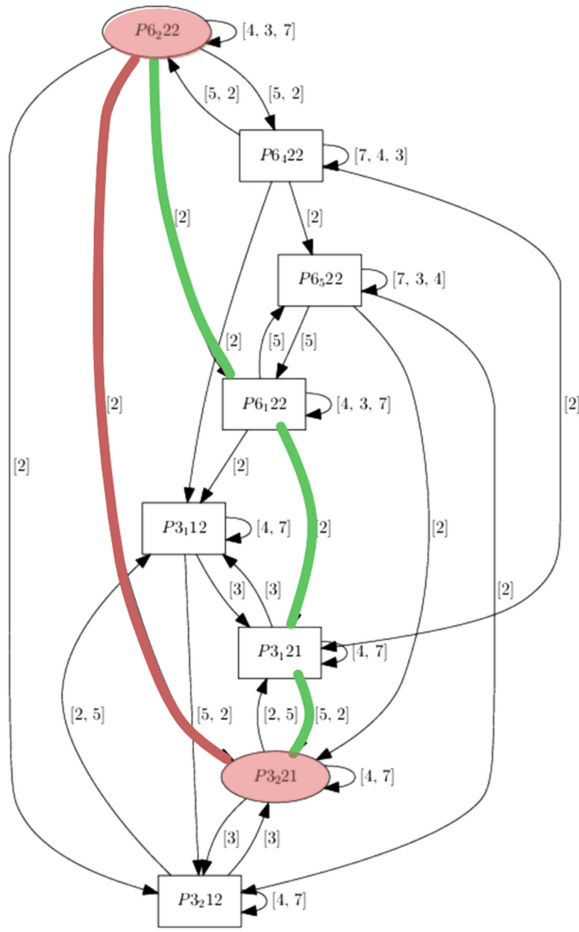

Figure 1.35. Group-subgroup graph from routine SUBGROUPGRAPH of the Bilbao Crystallographic Server [18, 19].

quartz), and on cooling, the space group changes to the subgroup $P3_221$, still right-handed ($P3_121$ for left-handed quartz). In the process, half of the symmetry operations are removed.

Figure 1.35 shows a complete group-subgroup graph from $P6_222$. You can see a direct line, coloured red, on the left between the two space groups with the figure [2] drawn beside. This is the *index* for the group-subgroup relationship, where

$$\text{index} = \frac{\text{number of elements in the group}}{\text{number of elements in the subgroup}} = \frac{12}{6} = 2 \tag{1.35}$$

This space-group change is what happens in quartz. However, there are many other routes possible between $P6_222$ and $P3_221$. For example, there is this route (in green)

$$P6_222 \xrightarrow{2c} P6_122 \longrightarrow P3_121 \xrightarrow{2c} P3_221 \tag{1.36}$$

In this case, the *c*-axis is doubled in the first change and doubled again in the last. The result is that, with this route, one might expect at low temperature a crystal structure with a unit cell four times that of quartz and with a different arrangement of atoms. Both processes involve the same space-group types but different space groups. Considerations like this can be useful in suggesting possible intermediate structures or alternative routes during, say, a phase transformation.

1.7.4 Subgroups and supergroups

The International Tables for Crystallography, Volume A1, contains a wealth of important information on subgroups and supergroups of space groups[4].

1.7.4.1 Maximal subgroups

Suppose G is a subgroup of a parent group G_0, i.e., the elements of G are all contained within G_0. G is called a *proper subgroup* if G_0 includes elements that are not in G. A subgroup H of G is called a *maximal subgroup* of G if there is no proper subgroup M of G such that H is a proper subgroup of M. In other words, G is a maximal subgroup if there is no proper subgroup of G_0, which 'lies between' G and G_0. There are two types of maximal subgroups defined in crystallographic space groups:

I translationengleiche or **t-subgroups**
II klassengleiche or **k-subgroups**

Suppose the maximal subgroup is formed from the parent group by retaining the translational elements, but the order of the point group is reduced. In that case, the subgroup is a t-subgroup or *equi-translational* subgroup. If it is formed by preserving the point group but with a loss of translations, it is a k-subgroup or *equi-class* subgroup. The k-subgroups are further subdivided:

IIa in which the conventional unit cells of G and G_0 are the same
IIb in which the conventional unit cell of G is larger than that of G_0.
IIc in which G and G_0 are isomorphic

Definition. ***Isomorphic space groups*** *have the same space-group number or are members of an enantiomorphic pair of space groups.*

Let's consider the subgroup chain (1.36). Starting with $P6_222$, space group $P6_122$ is listed as a k-maximal non-isomorphic subgroup

IIb [2] $P6_122$ ($\boldsymbol{c'} = 2\boldsymbol{c}$)

This indicates that the unit cell is doubled along *c* to achieve this change in space group, and the index for the change is 2. If we now consult space group $P6_122$, we have the following symmetry operations

[4] This information used to appear in earlier editions of the ITA, but was recently moved to a separate volume ITA1.

(1) 1	(2) $3^{+}\left(0, 0, \frac{1}{3}\right)$ 0, 0, z	(3) $3^{-}\left(0, 0, \frac{2}{3}\right)$ 0, 0, z
(4) $2\left(0, 0, \frac{1}{2}\right)$ 0, 0, z	(5) $6^{-}\left(0, 0, \frac{5}{6}\right)$ 0, 0, z	(6) $6^{+}\left(0, 0, \frac{1}{6}\right)$ 0, 0, z
(7) 2 x, x, $\frac{1}{6}$	(8) 2 x, 0, 0	(9) 2 0, y, $\frac{1}{3}$
(10) 2 x, $\overline{x}$, $\frac{5}{12}$	(11) 2 x, $2x$, $\frac{1}{4}$	(12) 2 $2x$, x, $\frac{1}{12}$

Looking through the list of maximal subgroups, we find space group $P3_121$ listed as a t-maximal non-isomorphic subgroup in this way

I[2] $P3_121$ 1:2:3:7:8:9

The six numbers refer to those symmetry operations in the parent group, $P6_122$, that are retained in the subgroup $P3_121$. Of the original 12 symmetry operations in the parent group, six have been selected to give the index as 2 for the change. Finally, when we turn to $P3_121$, we find a k-isomorphic subgroup of lowest index:

IIc[2] $P3_221$ ($\boldsymbol{c}' = 2\boldsymbol{c}$)

showing that the c-axis is doubled yet again ($P3_121$ and $P3_221$ are an enantiomorphic pair of space groups, and so are isomorphic).

1.7.4.2 Minimal non-isomorphic supergroups

Just as we could form maximal subgroups from any space group, it is possible to determine the nearest supergroups as well. If G is a group and H is a subgroup of G, then G is a supergroup of H. Moreover, if H is a maximal subgroup of G, then G is a *minimal supergroup* of H.

The minimal supergroups are also divided into two distinct types, *translationengleiche* or *t-supergroups* and *klassengleiche* or *k-supergroups*. Thus, it is possible to retrace the group-subgroup chain in reverse order: the routine CELLSUPER in the Bilbao Crystallographic server [18] is particularly suitable for this.

References

[1] Hammond C 2015 *The Basics of Crystallography and Diffraction* (Oxford: Oxford University Press)

[2] Giacovazzo C *et al* 2011 *Fundamentals of Crystallography* (Oxford: Oxford University Press)

[3] Glazer A M 2016 *Crystallography: A Very Short Introduction* (Oxford University Press)

[4] Hoffmann F 2020 *Introduction to Crystallography* (Wiesbaden: Springer International Publishing)

[5] Aroyo M I 2016 *International Tables for Crystallography* vol A (Chester: International Union of Crystallography)

[6] Kooijman H Interpretation of crystal structure determinations (http://www.cryst.chem.uu.nl/huub/notesweb.pdf)

[7] Müller U 2013 *Symmetry Relationships between Crystal Structures* (Oxford: Oxford Science Publications)
[8] Garcia-Ruiz J M 2018 2001: The crystal monolith *Substantia* **2** 19–25 (https://riviste.fupress.net/index.php/subs/article/view/57/38)
[9] Donnay J D H and LePage Y 1978 The vicissitudes of the low-quartz crystal setting or the pitfalls of enantiomorphism *Acta Crystallogr. Sect. A* **34** 584–94
[10] Glazer A M 2018 Confusion over the description of the quartz structure yet again *J. Appl. Crystallogr.* **51** 15–8
[11] Operation (Mathematics) (https://en.wikipedia.org/wiki/Operation_(mathematics))
[12] Online Dictionary of Crystallography (https://dictionary.iucr.org/Main_Page)
[13] Dove M T 2003 *Structure and Dynamics. An Atomic View of Materials* (Oxford Master Series in Condensed Matter Physics) (Oxford: Oxford University Press)
[14] Nespolo M 2019 Lattice versus structure, dimensionality versus periodicity: a crystallographic Babel? *J. Appl. Crystallogr.* **52** 451–6
[15] Nespolo M The lattice sickness pandemic, (https://www.iucr.org/news/newsletter/etc/articles?issue=142706&result_138339_result_page=7)
[16] Streitwolf H W 1967 *Group Theory in Solid State Physics* (London: Macdonald)
[17] Burns G and Glazer A M 2013 *Space Groups for Solid State Scientists* 3rd edn (Oxford: Academic)
[18] Bilbao Crystallographic Server (https://www.cryst.ehu.es/)
[19] Ivantchev S, Kroumova E, Madariaga G, Perez-Mato J M and Aroyo M I 2000 SUBGROUPGRAPH—a computer program for analysis of group-subgroup relations between space groups *J. Appl. Cryst.* **33** 1190–1

IOP Publishing

Chapter 2

The reciprocal lattice

Doc Glazer he plays with x-rays, sir
Doc Glazer, he plays with x-rays, sir
The reciprocal lattice
Who on earth knows what that is
Oh, k-space, yes, that's OK—sir!

(P A Thomas: to the tune of 'It Ain't Necessarily So' from an undergraduate party at Jesus College Oxford)

2.1 A brief history

Bravais in 1850, in addition to the normal lattice in direct space, considered another type of lattice, called the polar lattice obtained by forming points on vectors normal to the interplanar distances between lattice planes. The repeat distances between the points were proportional to the reciprocal of the interplanar distances d_{hkl} of the direct lattice according to

$$\frac{V^{2/3}}{d_{hkl}} \tag{2.1}$$

Thus, the distances in this polar lattice were expressed in Å units. Josiah Willard Gibbs (1839–1903) in the 1880s used this concept in his lectures, but with the repeat distances now in the form

$$\frac{1}{d_{hkl}} \tag{2.2}$$

and so the units of this lattice were expressed in $Å^{-1}$. However, Paul Peter Ewald (1888–1985), in or around 1913, used this definition to explain the arrangement of spots seen when a crystal diffracts x-rays. This is the form used by crystallographers to the present day in interpreting their diffraction patterns from crystals.

doi:10.1088/978-0-7503-3875-2ch2

2.2 Definition of the reciprocal lattice

In this chapter, we shall concentrate on the construction and geometry of the reciprocal lattice. To explain how to do this, let us start by defining its axes in much the same way as for direct lattices. Thus, instead of the basis vectors and angles **a**, **b**, **c**, α, β, γ defining the crystallographic unit cell of a direct lattice, we define a corresponding set denoted by **a***, **b***, **c***, α^*, β^*, γ^*. For a right-handed set, **a***, **b*** and **c*** are given by the following equations

$$\begin{aligned}\mathbf{a}^* &= 2\pi\frac{\mathbf{b}\times\mathbf{c}}{\mathbf{a}\cdot(\mathbf{b}\times\mathbf{c})} = 2\pi\frac{\mathbf{b}\times\mathbf{c}}{V}\\ \mathbf{b}^* &= 2\pi\frac{\mathbf{c}\times\mathbf{a}}{\mathbf{a}\cdot(\mathbf{b}\times\mathbf{c})} = 2\pi\frac{\mathbf{c}\times\mathbf{a}}{V}\\ \mathbf{c}^* &= 2\pi\frac{\mathbf{a}\times\mathbf{b}}{\mathbf{a}\cdot(\mathbf{b}\times\mathbf{c})} = 2\pi\frac{\mathbf{a}\times\mathbf{b}}{V}\end{aligned} \tag{2.3}$$

V is the volume of the corresponding unit cell in direct space, where

$$V = abc[(1 - \cos^2\alpha - \cos^2\beta - \cos^2\gamma) + 2(\cos\alpha\cos\beta\cos\gamma)]^{1/2} \tag{2.4}$$

It follows that the lengths of the reciprocal axes are given by

$$\begin{aligned}a^* &= 2\pi\frac{bc\sin\alpha}{V}\\ b^* &= 2\pi\frac{ca\sin\beta}{V}\\ c^* &= 2\pi\frac{ab\sin\gamma}{V}\end{aligned} \tag{2.5}$$

Taking scalar vector products

$$\begin{aligned}\mathbf{a}^*\cdot\mathbf{b}^* &= a^*b^*\cos\gamma^*\\ \mathbf{b}^*\cdot\mathbf{c}^* &= b^*c^*\cos\alpha^*\\ \mathbf{c}^*\cdot\mathbf{a}^* &= c^*a^*\cos\beta^*\end{aligned} \tag{2.6}$$

and using (2.3)

$$\begin{aligned}\mathbf{a}^*\cdot\mathbf{b}^* &= (2\pi)^2\frac{(\mathbf{b}\times\mathbf{c})\cdot(\mathbf{c}\times\mathbf{a})}{V^2}\\ \mathbf{b}^*\cdot\mathbf{c}^* &= (2\pi)^2\frac{(\mathbf{c}\times\mathbf{a})\cdot(\mathbf{a}\times\mathbf{b})}{V^2}\\ \mathbf{c}^*\cdot\mathbf{a}^* &= (2\pi)^2\frac{(\mathbf{a}\times\mathbf{b})\cdot(\mathbf{b}\times\mathbf{c})}{V^2}\end{aligned} \tag{2.7}$$

Consider, for example, the following:

$$\mathbf{b}^*\cdot\mathbf{c}^* = b^*c^*\cos\alpha^* = (2\pi)^2\frac{a^2bc\sin\beta\sin\gamma}{V^2}\cos\alpha^* \tag{2.8}$$

from (2.5) and (2.6). By applying the Binet–Cauchy vector identity

$$(\mathbf{A} \times \mathbf{B}) \cdot (\mathbf{C} \times \mathbf{D}) = (\mathbf{A} \cdot \mathbf{C})(\mathbf{B} \cdot \mathbf{D}) - (\mathbf{A} \cdot \mathbf{D})(\mathbf{B} \cdot \mathbf{C}) \tag{2.9}$$

to (2.7), we get the following

$$\begin{aligned} b^*c^* \cos\alpha^* &= (2\pi)^2 \frac{(\mathbf{c} \times \mathbf{a}) \cdot (\mathbf{a} \times \mathbf{b})}{V^2} \\ &= (2\pi)^2 \frac{(\mathbf{c} \cdot \mathbf{a})(\mathbf{a} \cdot \mathbf{b}) - (\mathbf{c} \cdot \mathbf{b})(\mathbf{a} \cdot \mathbf{a})}{V^2} \\ &= (2\pi)^2 \frac{(ca \cos\beta)(ab \cos\gamma) - (cb \cos\alpha)a^2}{V^2} \\ &= (2\pi)^2 \frac{a^2bc(\cos\beta \cos\gamma - \cos\alpha)}{V^2} \end{aligned} \tag{2.10}$$

By comparing (2.8) and (2.10), we find the formula for cos α^*. Repeating this for the other angles, we obtain the following formulae for the reciprocal angles:

$$\begin{aligned} \cos\alpha^* &= \frac{\cos\beta \cos\gamma - \cos\alpha}{\sin\beta \sin\gamma} \\ \cos\beta^* &= \frac{\cos\gamma \cos\alpha - \cos\beta}{\sin\gamma \sin\alpha} \\ \cos\gamma^* &= \frac{\cos\alpha \cos\beta - \cos\gamma}{\sin\alpha \sin\beta} \end{aligned} \tag{2.11}$$

and, of course,

$$\begin{aligned} \cos\alpha &= \frac{\cos\beta^* \cos\gamma^* - \cos\alpha^*}{\sin\beta^* \sin\gamma^*} \\ \cos\beta &= \frac{\cos\gamma^* \cos\alpha^* - \cos\beta^*}{\sin\gamma^* \sin\alpha^*} \\ \cos\gamma &= \frac{\cos\alpha^* \cos\beta^* - \cos\gamma^*}{\sin\alpha^* \sin\beta^*} \end{aligned} \tag{2.12}$$

Now, the factor 2π that appears in equation (2.3), and elsewhere, needs to be explained. This is simply a scale constant of proportionality and could be replaced by any value we choose. The factor of 2π is commonly used by condensed matter physicists [1–3], who are generally interested in the propagation of waves (electrons, phonons, etc) in crystalline solids. The modulus of the wave-vector **k** of a wave is related to the wavelength λ by:

$$k = \frac{2\pi}{\lambda} \tag{2.13}$$

On the other hand, crystallographers usually replace it with 1 for simplicity. As this book is addressed primarily to physicists who are not crystallographers, I shall continue to retain the factor of 2π throughout.

Consider now the scalar product

$$\mathbf{a} \cdot \mathbf{a}^* = 2\pi \frac{\mathbf{a} \cdot (\mathbf{b} \times \mathbf{c})}{\mathbf{a} \cdot (\mathbf{b} \times \mathbf{c})} = 2\pi \tag{2.14}$$

and also

$$\mathbf{a} \cdot \mathbf{b}^* = 2\pi \frac{\mathbf{a} \cdot (\mathbf{c} \times \mathbf{a})}{V} = 2\pi \frac{\mathbf{a} \cdot \mathbf{n} \sin \beta}{V} = 0 \tag{2.15}$$

where the vector **n** is perpendicular to the basis vectors **a** and **c**. So, one of the consequences of the definitions of the reciprocal axis vectors is that the following useful relationships between real and reciprocal axes always apply

$$\begin{aligned} &\mathbf{a} \cdot \mathbf{a}^* = \mathbf{b} \cdot \mathbf{b}^* = \mathbf{c} \cdot \mathbf{c}^* = 2\pi \\ &\mathbf{a} \cdot \mathbf{b}^* = \mathbf{a} \cdot \mathbf{c}^* = \mathbf{b} \cdot \mathbf{c}^* = \mathbf{b} \cdot \mathbf{a}^* = \mathbf{c} \cdot \mathbf{b}^* = \mathbf{c} \cdot \mathbf{a}^* = 0 \\ &\mathbf{a}^* \cdot \mathbf{a}^* = a^{*2};\ \mathbf{a}^* \cdot \mathbf{b}^* = a^* b^* \cos \gamma^*, \ldots\ldots \end{aligned} \tag{2.16}$$

Thus, we see that any direct axis, say **a**, is always perpendicular to the reciprocal **b*** and **c*** axes, with similar relationships between all the other axes.

2.3 Construction

We can now use the above definitions to construct a drawing of the reciprocal lattice starting from a direct lattice. Consider first a unit cell of a direct lattice with axes $a > b$, as shown in figure 2.1. This cell has deliberately been chosen to be oblique, with the angle between the axes denoted by γ, to illustrate a non-orthogonal case for pedagogical reasons.

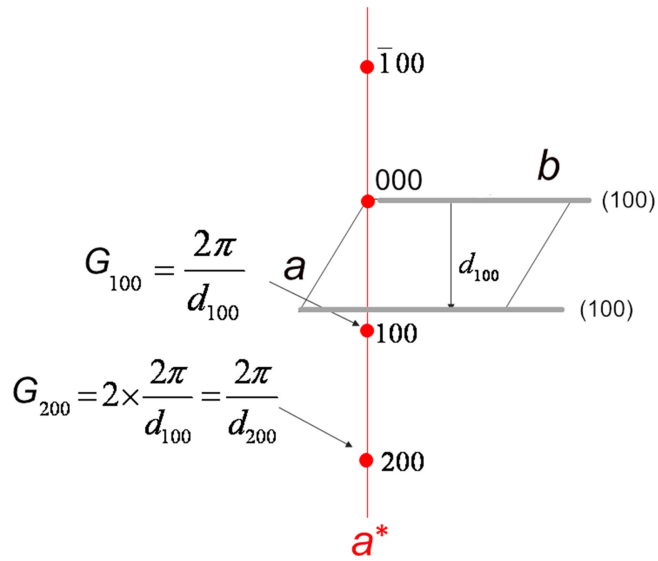

Figure 2.1. 100, 200…. reciprocal-lattice points.

Figure 2.1 shows the separation d_{100} of two of the (100) set of parallel planes marked in grey in the direct-space unit cell. Starting with a chosen origin for this unit cell, marked 000, the red line drawn perpendicular to the (100) planes is the a^*-axis. Remember from (2.16) that $\mathbf{a}^*$ is perpendicular to $\mathbf{b}$. Now mark a point, labelled 100, at a distance from the origin given by $G_{100} = 2\pi/d_{100}$. An additional point labelled 200 is added at twice this distance, thus corresponding in direct space to (200) planes, i.e., a hypothetical set of planes of half the spacing between the (100) planes. Note, therefore, that as the planes get closer together in direct space, the corresponding reciprocal-lattice points become further away from the origin. You can begin to see now why we use the term *reciprocal space*.

Proceeding in a similar way, we mark a point on the negative a^*-axis, denoted $\bar{1}00$ (note the bar placed above the 1). In figure 2.2, the same procedure has been used to mark the $\pm b^*$-axis and the set of planes (010), (020), (030), etc, plus their negative values. It can be seen that the respective points 010, 020, 030, etc, are closer together than the 100, 200 set since the corresponding real planes are farther apart.

Now choose another set of planes. Figure 2.3 shows the construction for the (110) set of planes: these planes are even closer together, and so the corresponding points 110, 220, etc, are still farther from the origin. Figure 2.4 repeats this for the (120) set of planes.

If we continue in this way for all the ($hk0$) planes, figure 2.5 is obtained, whence it can be seen that a complete two-dimensional array of points has been generated. This is a section of the *reciprocal lattice*.

Figure 2.6 shows that we can now define in two dimensions a *reciprocal unit cell* by the axes a^*, b^* and interaxial angle γ^*. It can therefore be seen from this that each reciprocal-lattice point or node corresponds to a set of parallel planes. This procedure can be carried out for all possible planes to create a three-dimensional network of points denoted by the indices hkl (figure 2.7).

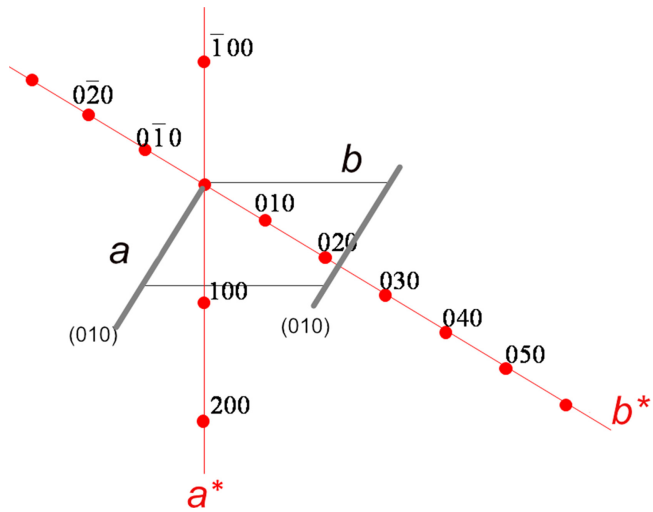

Figure 2.2. 010, 020.... reciprocal-lattice points.

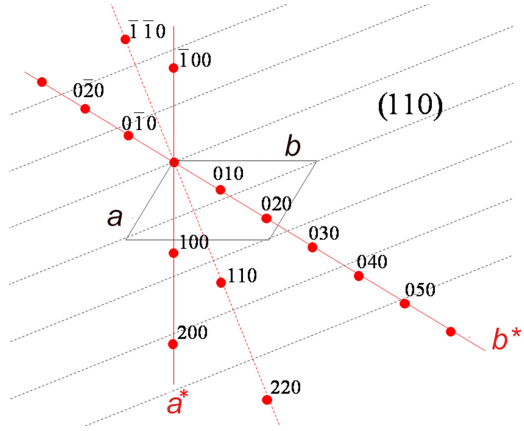

Figure 2.3. 110, 220…. reciprocal-lattice points. (110) planes marked by dashed lines.

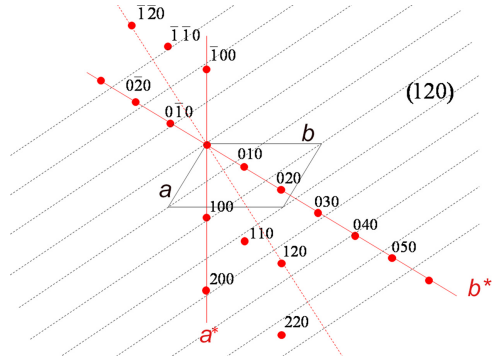

Figure 2.4. 120, 240…. reciprocal-lattice points. (120) planes marked by dashed lines.

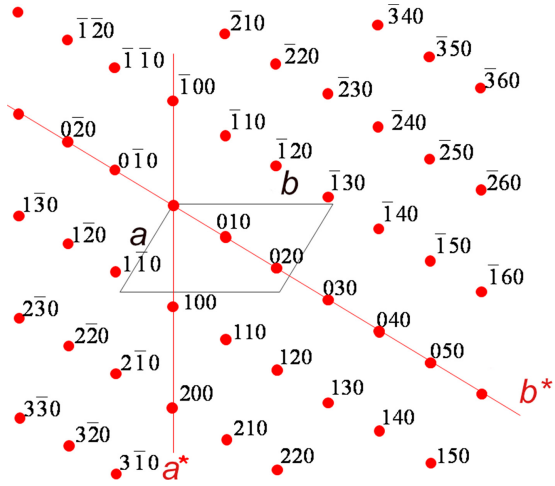

Figure 2.5. A reciprocal-lattice plane.

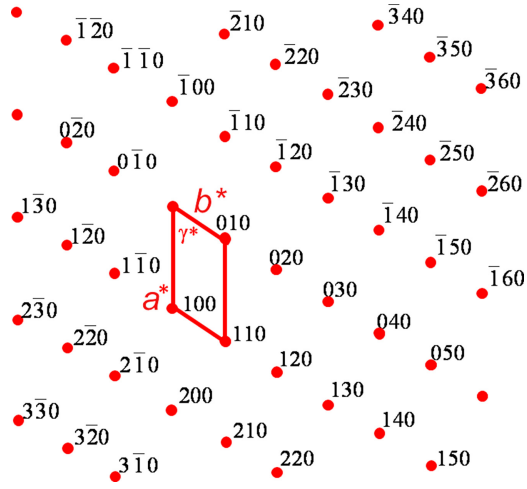

Figure 2.6. Reciprocal unit-cell axes and angle.

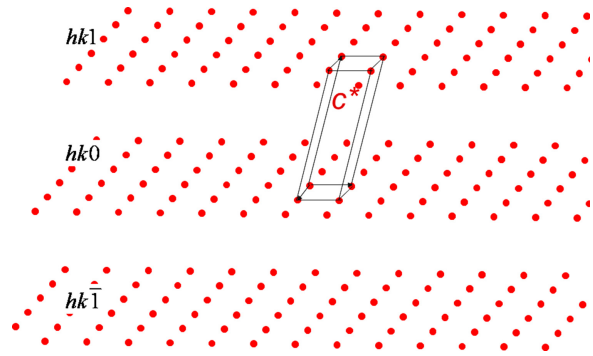

Figure 2.7. Reciprocal lattice in three dimensions: note that one way to visualize this is as a set of parallel layers of reciprocal-lattice points.

Definition ***Reciprocal-lattice vector*** $\boldsymbol{G}_{hkl}$: *The vector* $\boldsymbol{G}_{hkl} = h\boldsymbol{a}^* + k\boldsymbol{b}^* + l\boldsymbol{c}^*$ *from the origin 000 of the reciprocal lattice to a particular reciprocal-lattice point hkl.* $\boldsymbol{G}_{hkl}$ *is perpendicular to the plane (hkl). The modulus* $|\boldsymbol{G}_{hkl}| = 2\pi/d_{hkl}$.

Notation *It is conventional to denote the indices of reciprocal-lattice points by the indices hkl of the relevant planes. Note that no parentheses or brackets are used in specifying reciprocal-lattice points.*

Therefore, the reciprocal lattice can be thought of as a three-dimensional lattice of *hkl* points (or nodes) lying on layers, e.g., $hk0$, $hk1$, $hk2$, $hk\bar{1}$, $hk\bar{2}$, ……. From the construction, we see that for each direct-lattice array, there corresponds a reciprocal-lattice array whose dimensions are reciprocally related.

2.4 Geometrical calculations

Our definitions of the reciprocal axes in terms of vectors in equation (2.3) allow us to calculate many useful quantities without the need to perform some sort of elaborate geometrical construction.

2.4.1 Metric tensors

It is convenient to express the direct and reciprocal axes in a matrix form known as the **metric tensor**. In direct space, the metric tensor is given by

$$M = \begin{bmatrix} \mathbf{a}\cdot\mathbf{a} & \mathbf{a}\cdot\mathbf{b} & \mathbf{a}\cdot\mathbf{c} \\ \mathbf{b}\cdot\mathbf{a} & \mathbf{b}\cdot\mathbf{b} & \mathbf{b}\cdot\mathbf{c} \\ \mathbf{c}\cdot\mathbf{a} & \mathbf{c}\cdot\mathbf{b} & \mathbf{c}\cdot\mathbf{c} \end{bmatrix} = \begin{bmatrix} a^2 & ab\cos\gamma & ac\cos\beta \\ ba\cos\gamma & b^2 & bc\cos\alpha \\ ca\cos\beta & cb\cos\alpha & c^2 \end{bmatrix} \tag{2.17}$$

and in reciprocal space, correspondingly

$$M^* = \begin{bmatrix} \mathbf{a}^*\cdot\mathbf{a}^* & \mathbf{a}^*\cdot\mathbf{b}^* & \mathbf{a}^*\cdot\mathbf{c}^* \\ \mathbf{b}^*\cdot\mathbf{a}^* & \mathbf{b}^*\cdot\mathbf{b}^* & \mathbf{b}^*\cdot\mathbf{c}^* \\ \mathbf{c}^*\cdot\mathbf{a}^* & \mathbf{c}^*\cdot\mathbf{b}^* & \mathbf{c}^*\cdot\mathbf{c}^* \end{bmatrix} = \begin{bmatrix} a^{*2} & a^*b^*\cos\gamma^* & a^*c^*\cos\beta^* \\ b^*a^*\cos\gamma^* & b^{*2} & b^*c^*\cos\alpha^* \\ c^*a^*\cos\beta^* & c^*b^*\cos\alpha^* & c^{*2} \end{bmatrix} \tag{2.18}$$

The determinant of M gives the volume V of the unit cell in direct space:

$$V^2 = a^2b^2c^2(1 + 2\cos\alpha\cos\beta\cos\gamma - \cos^2\alpha - \cos^2\beta - \cos^2\gamma) \tag{2.19}$$

2.4.2 Interplanar distances

Suppose we want to work out the interplanar distance d_{hkl} for (hkl) planes. To do this, we simply need to find the modulus of the corresponding reciprocal-lattice vector. This can be obtained by taking the scalar product of the vector with itself, thus:

$$|\mathbf{G}_{hkl}|^2 = \left(\frac{2\pi}{d_{hkl}}\right)^2 = (h\mathbf{a}^* + k\mathbf{b}^* + l\mathbf{c}^*)\cdot(h\mathbf{a}^* + k\mathbf{b}^* + l\mathbf{c}^*) \tag{2.20}$$

or in metric tensor form

$$\begin{bmatrix} h & k & l \end{bmatrix} \begin{bmatrix} a^{*2} & a^*b^*\cos\gamma^* & a^*c^*\cos\beta^* \\ b^*a^*\cos\gamma^* & b^{*2} & b^*c^*\cos\alpha^* \\ c^*a^*\cos\beta^* & c^*b^*\cos\alpha^* & c^{*2} \end{bmatrix} \begin{bmatrix} h \\ k \\ l \end{bmatrix} \tag{2.21}$$

For the most general case of a triclinic crystal, this evaluates as

$$h^2a^{*2} + k^2b^{*2} + l^2c^{*2} + 2klb^*c^*\cos\alpha^* + 2lhc^*a^*\cos\beta^* + 2hka^*b^*\cos\gamma^* \tag{2.22}$$

a rather fearsome result needing calculation of the reciprocal axis values, it must be admitted! However, tedious though it is, it is eminently suitable for calculation by a

computer program. For crystal systems with orthogonal axes, the formulae become much more manageable. Thus, for the orthorhombic system, we have

$$a^* = \frac{2\pi}{a} \quad b^* = \frac{2\pi}{b} \quad c^* = \frac{2\pi}{c} \tag{2.23}$$

and then

$$\frac{1}{d_{hkl}^2} = \frac{h^2}{a^2} + \frac{k^2}{b^2} + \frac{l^2}{c^2} \tag{2.24}$$

For the tetragonal system

$$\frac{1}{d_{hkl}^2} = \frac{h^2 + k^2}{a^2} + \frac{l^2}{c^2} \tag{2.25}$$

while for the cubic system

$$\frac{1}{d_{hkl}^2} = \frac{h^2 + k^2 + l^2}{a^2} = \frac{N^2}{a^2} \tag{2.26}$$

where N is an integer.

As an aside, there is an interesting mathematical aspect of the cubic formula (2.26) in connection with number theory. The sum $h^2 + k^2 + l^2$ cannot equal integers like 7 and 15 (and this accounts for why in a powder x-ray diffraction pattern from a cubic material, there are missing lines corresponding to these numbers). In other words, there are specific positive integers that cannot be formed from a sum of three squared integers. How, then, can one work out which are the other missing positive integers? The formula for determining this was found by Carl Friedrich Gauss (1777–1855) and Adrien-Marie Legendre (1752–1833), who showed that the sum could not be achieved when

$$N = 4^m(8n + 7) \tag{2.27}$$

where m and n are positive integers. The following table 2.1 can then be constructed for the missing N integers:

Table 2.1. Forbidden sums.

m	n	N
0	0	7
0	1	15
0	2	23
1	0	28
0	3	31
0	4	39
0	5	47
0	6	55
1	1	60
0	7	63

2.4.3 Example calculations

2.4.3.1 Magnitude of direct-lattice vector

Consider a monoclinic crystal with $a = 0.6$ nm, $b = 0.7$ nm, $c = 0.8$ nm and $\beta = 110°$. Find the magnitude of the length denoted by the direction $[31\bar{2}]$. The metric tensor in direct space, in this case, can be written:

$$M = \begin{bmatrix} 0.36 & 0 & -0.164 \\ 0 & 0.49 & 0 \\ -0.164 & 0 & 0.64 \end{bmatrix} \text{nm}^2 \tag{2.28}$$

and so we get

$$\left([3,\ 1,\ \bar{2}] \begin{bmatrix} 0.36 & 0 & -0.164 \\ 0 & 0.49 & 0 \\ -0.164 & 0 & 0.64 \end{bmatrix} \begin{bmatrix} 3 \\ 1 \\ \bar{2} \end{bmatrix} \right)^{1/2} = 2.874 \text{ nm} \tag{2.29}$$

Alternatively, $[31\bar{2}]$ is equivalent to the vector $3\mathbf{a} + \mathbf{b} - 2\mathbf{c}$. The modulus of this vector is given by the square root of the scalar product of the vector with itself:

$$(3a + b - 2c) \cdot (3a + b - 2c) = 9a^2 + b^2 + 4c^2 - 12ac \cos\beta \tag{2.30}$$

which gives the same result.

2.4.3.2 Magnitude of reciprocal-lattice vector

This time we need the metric tensor M^* for reciprocal space. For the example above, the following values can be calculated:

$$\begin{aligned} a^* &= 2\pi \frac{1}{a \sin \beta} = 11.14 \text{ nm}^{-1} \\ b^* &= 2\pi \frac{1}{b} = 8.98 \text{ nm}^{-1} \\ c^* &= 2\pi \frac{1}{c \sin \beta} = 8.36 \text{ nm}^{-1} \\ \beta^* &= 180 - \beta = 70° \end{aligned} \tag{2.31}$$

Then

$$\left((2\pi)^2 [3,\ 1,\ \bar{2}] \begin{bmatrix} 3.14 & 0 & 0.80 \\ 0 & 2.04 & 0 \\ 0.80 & 0 & 1.77 \end{bmatrix} \begin{bmatrix} 3 \\ 1 \\ \bar{2} \end{bmatrix} \right)^{1/2} = 33.1 \text{ nm}^{-1} \tag{2.32}$$

Again, this is equivalent to calculating the modulus of the reciprocal-lattice vector using the scalar product:

$$(3a^* + b^* - 2c^*) \cdot (3a^* + b^* - 2c^*) = (2\pi)^2\left(\frac{9}{(a\sin\beta)^2} + \frac{1}{b^2} + \frac{4}{(c\sin\beta)^2} + \frac{12\cos\beta}{ac\sin^2\beta}\right) \tag{2.33}$$

2.4.3.3 Angle between reciprocal-lattice vector and direction in direct space
Again, this is a simple matter using scalar vector products; only here, the conditions in equation (2.16) make life easier still. Let's consider the above example and calculate the angle between the direction $[31\bar{2}]$ and the normal to the $(31\bar{2})$ plane (the reciprocal-lattice vector).

$$\begin{aligned}&(3a + b - 2c) \cdot (3a^* + b^* - 2c^*) = \\ &(9a^2 + b^2 + 4c^2 - 12ac\cos\beta)^{1/2}\,(9a^{*2} + b^{*2} + 4c^{*2} - 12a^*c^*\cos\beta^*)^{1/2}\cos\varphi\end{aligned} \tag{2.34}$$

The left-hand side evaluates to

$$(2\pi)^2(9 + 1 + 4) = (2\pi)^2 2.874 \times 33.1 \times \cos\varphi \tag{2.35}$$

from equation (2.16). Note that $(2\pi)^2$ cancels out on both sides. The result is $\varphi = 22.4°$.

References

[1] Kittel C 2005 *Introduction to Solid State Physics* 8th edn (New York: Wiley)
[2] Ashcroft N W and Mermin N D 1976 *Solid State Physics* (Philadelphia, PA: Saunders)
[3] Simon S H 2013 *The Oxford Solid State Basics* (Oxford: Oxford University Press)

IOP Publishing

Chapter 3

Diffraction

The electron is not as simple as it looks.

(William Lawrence Bragg)

3.1 Introduction

So far, we have learned how to construct a reciprocal lattice, and we have discovered that it enables us to make some complicated geometrical questions easier to attack. However, you will not be surprised to learn that the reciprocal-lattice concept has much more to offer. We shall now see how we can use it to understand a very practical subject, namely what happens when x-rays, neutrons, or electrons are diffracted by a crystalline material. Note that one way to define diffraction is the spreading of waves, i.e., no change in the average propagation direction, while scattering is the deflection of waves with a change of propagation direction. However, the terms 'diffraction' and 'scattering' are often used interchangeably, and hence, a clear distinction between the two is difficult to find.

In 1912, Walter Friedrich (1883–1968), Paul Knipping (1883–1935) and Max Theodor Felix Laue (1979–60) discovered that x-rays could be diffracted by crystals (figure 3.1). This showed, for the first time, that crystal structures consisted of periodic arrays of atoms and molecules with spacings comparable with the wavelength of the x-rays. This also demonstrated that x-rays could be treated as wave-like in nature (two birds with one stone!). For this discovery, Laue (by this time having been ennobled as von Laue) received the 1914 Nobel Prize in Physics.

3.2 Laue equations

To explain the observed x-ray photographs, Laue considered x-rays striking a row of atoms (or better, scatterers) spaced a distance a apart and being scattered in a different direction.

doi:10.1088/978-0-7503-3875-2ch3

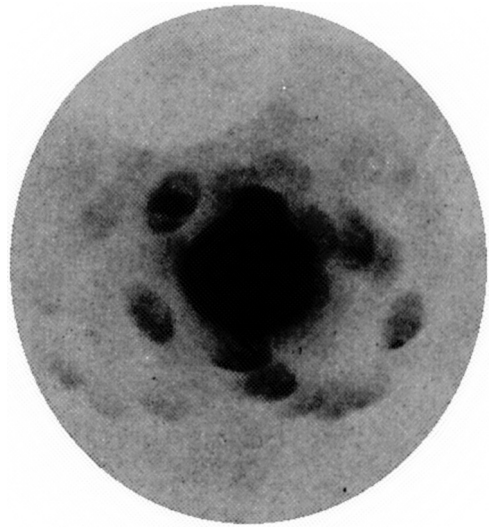

Figure 3.1. Friedrich and Knipping's first successful photograph showing that x-rays can be diffracted by a crystal of copper sulphate pentahydrate. Reproduced by permission of the International Union of Crystallography.

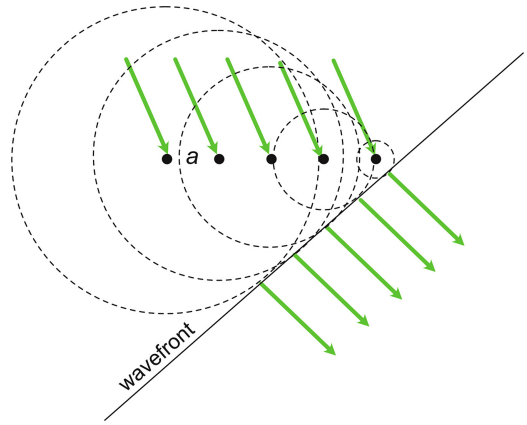

Figure 3.2. Formation of a wavefront with scattered radiation.

In figure 3.2 a beam of x-rays strikes a row of regularly spaced atoms a distance a apart at an angle to the row. Each atom acts as a centre of radiating spherical shells, creating a travelling wavefront for the diffracted beam. Figure 3.3 shows this again with the incident wave-vector $\mathbf{k}_0$ for the incident beams and $\mathbf{k}$ for the scattered beams. If we assume that the scattering is elastic, i.e., both sets of beams have the same energy, then $|\mathbf{k}_0| = |\mathbf{k}| = 2\pi/\lambda$. The path difference between any two sets of beams between neighbouring atoms distance a apart, is given by CD–AB, which, for constructive interference, must equal any integer value, h say, of the wavelength. Therefore,

$$a(\cos\alpha_1 - \cos\alpha_0) = h\lambda \tag{3.1}$$

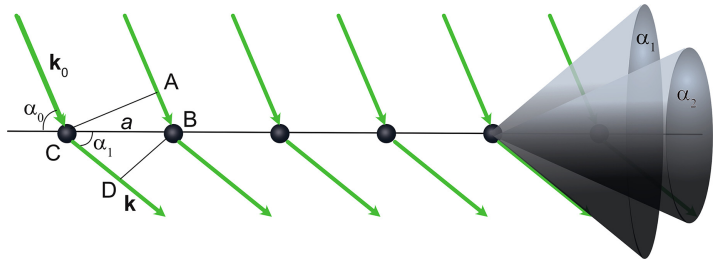

Figure 3.3. Derivation of the Laue equations and Laue cones.

Multiplying both sides by $2\pi/\lambda$ and writing in terms of vectors, we get

$$\mathbf{a} \cdot (\mathbf{k} - \mathbf{k}_0) = 2\pi h \tag{3.2}$$

In figure 3.3, the scattered beams lie in the plane of the paper. But all scattered beams with the same path difference occur at the same angle to the row of atoms, and so they all lie on cones, the *Laue cones*, centred on the atom row with half-angles α_1, α_2, α_3, … corresponding to $h = 1, 2, \ldots$.

This argument can be extended to three dimensions, where the condition is that all the atoms should scatter in phase in some direction. The three-dimensional array of atoms is described by rows of scatterers separated by vectors **a**, **b** and **c**. The result is that we can write the following set of equations

$$\begin{aligned} \mathbf{a} \cdot (\mathbf{k} - \mathbf{k}_0) &= 2\pi h \\ \mathbf{b} \cdot (\mathbf{k} - \mathbf{k}_0) &= 2\pi k \\ \mathbf{c} \cdot (\mathbf{k} - \mathbf{k}_0) &= 2\pi l \end{aligned} \tag{3.3}$$

which are known as the *Laue Equations*. All three equations must be simultaneously satisfied for constructive interference. For each row of scatterers there is a set of Laue cones coaxial with each row. Thus, in three dimensions there are intersections between three sets of cones coaxial with the three rows to form spots observed on a detector.

3.3 Bragg's Law

We now turn to one of the most famous equations in Physics: Bragg's Law. William Lawrence Bragg (1880–1971) derived the law in 1912, at the young age of 22. He found a simple way to work out the angle of diffraction from any set of crystal planes. Now, Bragg's brilliant idea was to treat the diffraction process as being similar to the reflection of x-rays from crystal planes, as if the planes acted like mirrors. This, of course, is not strictly true, as diffraction and reflection are different processes. Still, nonetheless, it does lead to a useful formula that, at least, produces the correct *positions* of the spots seen in crystal diffraction patterns. We shall see how this formula appears naturally from the concept of the reciprocal lattice (figure 3.4).

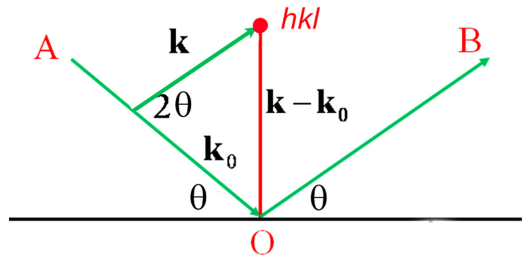

Figure 3.4. Derivation of Bragg's Law.

Notation. *Because Bragg treated diffraction in terms of reflection, it is internationally accepted that the diffraction spots arising from scattering by crystal planes are called* ***reflections*** *or sometimes* ***Bragg peaks***.

Let a beam AO of radiation strike a crystal plane at an angle θ. This angle is conventionally known as the Bragg angle. The beam is then considered to be 'reflected' through an equivalent angle along OB, just like light reflected by a mirror.

We now draw a perpendicular to the planes, and mark the corresponding reciprocal-lattice point *hkl* at a distance $2\pi/d_{hkl}$ (recall our construction of the reciprocal lattice by drawing perpendiculars to planes). Now draw a line marked $\mathbf{k}$ parallel to the reflected beam OB to meet this reciprocal-lattice point, and then we see that this makes an angle 2θ to the incident beam AO. The result is a vector triangle with incident wave-vector $\mathbf{k}_0$ and outgoing wave-vector $\mathbf{k}$. The reciprocal-lattice vector $\mathbf{G}_{hkl}$ (magnitude equals $2\pi/d_{hkl}$) is then given by

$$\mathbf{k} - \mathbf{k}_0 = \mathbf{G}_{hkl} \tag{3.4}$$

Definition. *The vector* $\mathbf{k} - \mathbf{k}_0$ *is called the* ***scattering vector***.

Therefore,

$$(\mathbf{k} - \mathbf{k}_0) \cdot (\mathbf{k} - \mathbf{k}_0) = \mathbf{G}_{hkl} \cdot \mathbf{G}_{hkl} \tag{3.5}$$

and this leads to

$$k^2 + k_0^2 - 2kk_0 \cos 2\theta = \frac{4\pi^2}{d_{hkl}^2} \tag{3.6}$$

But for elastic scattering, the wavelength λ is unchanged, and so the moduli of the wave-vectors are given by

$$k = k_0 = \frac{2\pi}{\lambda} \tag{3.7}$$

Substituting into (3.6) then gives us the well-known Bragg equation

$$\lambda = 2d \sin\theta \tag{3.8}$$

Those of you who have seen the Bragg equation before will probably have seen it in the following form

$$n\lambda = 2d \sin\theta \tag{3.9}$$

where n is a positive integer and represents the *order* of diffraction. Now, it is my experience that removing the factor n as in equation (3.8) seems to confuse students when they meet it for the first time, and so it is worth explaining the reasoning behind this.

As you will undoubtedly know, when light is diffracted from, say, a grating, one obtains a central maximum of intensity with periodic sidebands. It is then convenient to give each intensity peak a serial number denoting the order of diffraction. Suppose we consider x-rays being diffracted from, say, the (130) set of parallel planes. One way of thinking about this is to say that we obtain a set of diffracted beams at increasing angles corresponding to the increasing values of n. But another way (figure 3.5) is to forget about the order n and instead think about reflection (diffraction) from planes (130), (260), (390)…. In other words, we consider hypothetical planes halfway, third-way, etc, with respect to (130) corresponding to spacings d_{130}, d_{260}, d_{390}….

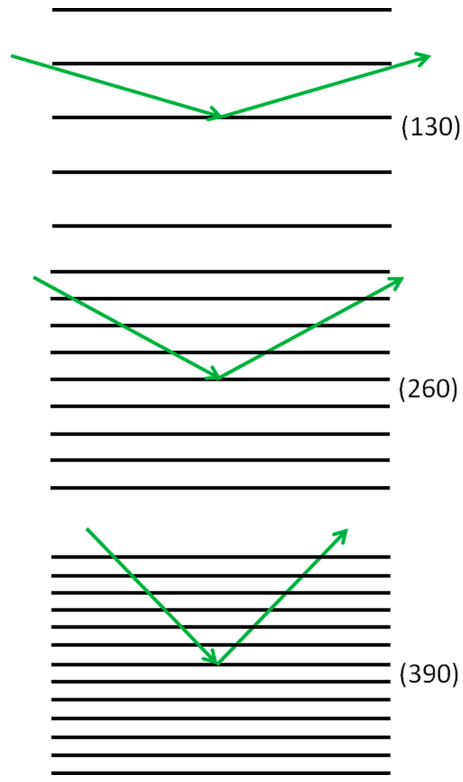

Figure 3.5. Orders of diffraction from the (130) planes.

Why should we prefer this to the more usual use of talking about an order as in optical diffraction? The point is that a crystal is a three-dimensional object described by a three-dimensional lattice. Therefore, if we think of sets of different planes such as (100), (010), (130), and so on, we could write the following:

	Orders				
(100)	1	2	3	4	5
(010)	1	2	3	4	5
(130)	1	2	3	4	5

in which case, we would have to talk about first, second, third etc, orders for (100) planes and a different set of first, second, third etc, orders for (010) and still different again for (130).

This is a messy way of labelling the reflections. Instead, if we invent hypothetical planes with corresponding interplanar spacings, we can then label the reflections like this

1 0 0	2 0 0	3 0 0	4 0 0	5 0 0
0 1 0	0 2 0	0 3 0	0 4 0	0 5 0
1 3 0	2 6 0	3 9 0	4 12 0	5 15 0

and these simply correspond to the labels for the reciprocal-lattice points we constructed in the previous chapter! (Remember that we do not use parentheses when labelling the reciprocal-lattice points.) You can now appreciate that the construction of the reciprocal lattice tells us something about the diffraction pattern obtained from a single crystal.

Definition. *The equation $\lambda = 2d \sin\theta$ is known as* ***Bragg's Law***.

Note. *The angle through which the incident beam is diffracted is equal to 2θ, i.e., twice the Bragg angle.*

Returning for the moment to the Laue equations, suppose we take the scalar product of the unit-cell vector $\mathbf{a}$ and the reciprocal-lattice vector $\mathbf{G}_{hkl}$, thus

$$\mathbf{a} \cdot \mathbf{G}_{hkl} = \mathbf{a} \cdot (h\mathbf{a}^* + k\mathbf{b}^* + l\mathbf{c}^*) = 2\pi h \tag{3.10}$$

Comparing this with the Laue equation (3.2) and equation (3.4), we note that $\mathbf{k} - \mathbf{k}_0$ is equal to the reciprocal-lattice vector $\mathbf{G}_{hkl}$. Thus, the Laue equation is consistent with the Bragg idea of treating the crystal diffraction as if it were reflection from planes, and so

$$(\mathbf{k} - \mathbf{k}_0) = \Delta\mathbf{k} = \mathbf{G}_{hkl} \tag{3.11}$$

This is known as the *Laue condition*. Essentially, this corresponds to a statement about conservation of momentum and is a consequence of the general statement that the crystal momentum is only conserved up to a reciprocal-lattice vector, while the elastic condition is the conservation of energy carried by the incident radiation.

3.4 The Ewald sphere

In 1912, when Paul Ewald introduced the reciprocal lattice, he showed how this could be used to visualize the formation of a diffraction pattern from a crystal. We have already seen this in the way Bragg's Law was derived by making use of wave-vectors. This can be developed still further by the use of a marvelous construction due to Ewald. Take a look at the following diagram (figure 3.6).

First of all, consider a beam of radiation AX reflected (diffracted) along the direction OY by a set of parallel planes O in a crystal. Now, construct a sphere of whose radius is inversely related to the wavelength of the x-rays, such that it is centred at C with O on the circumference. This is the so-called *Ewald sphere* or *sphere of reflection*. Perpendicular to the set of planes, mark in a line, which, by definition, is in the direction of the reciprocal-lattice vector $\mathbf{G}_{hkl}$ for the planes. Then draw in a line from C parallel to the outgoing ray OY. This makes an angle of 2θ to the incident beam and meets the circumference of the sphere at the same point as the reciprocal-lattice vector. Suppose now that this intersection point happens to coincide with the *hkl* reciprocal-lattice point for the planes. Draw in the line from A to the reciprocal-lattice point, and the result is a right-angled triangle. Hence, we get

$$\sin\theta = \frac{G_{hkl}}{4\pi/\lambda} = \frac{\lambda}{2d_{hkl}} \tag{3.12}$$

which is our old friend, Bragg's Law! So what does this mean exactly?

Well, what it says is that, if a reciprocal-lattice point happens to lie on the surface of the Ewald sphere, Bragg's Law is obeyed, and there will be a diffracted beam from the crystal at an angle 2θ in the direction parallel to the line from C to the reciprocal-lattice point. Conversely, if the reciprocal-lattice point does not lie on the sphere, then the corresponding set of planes will not be in the correct orientation for diffraction to occur.

3.5 Lost in reciprocal space?

The Ewald sphere construction gives us a very convenient means to enable us to find our way around reciprocal space and determine what we see in a diffraction pattern.

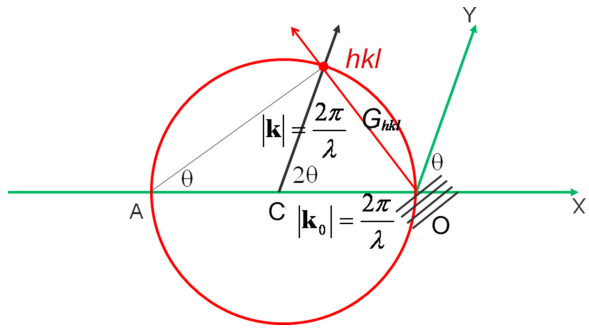

Figure 3.6. The Ewald sphere construction.

I used this myself many years ago, for instance, when I wanted to determine the presence of an extremely weak reflection. To achieve this, it was necessary to oscillate the crystal through just 1° for about one week. This was a tall order, but we managed it by carefully drawing on paper a reciprocal lattice to scale and using the Ewald sphere construction to determine where to set the crystal (this was before modern automatic diffractometers made all this trivial!).

3.5.1 Stationary crystal

Let us see how we can use the Ewald construction to understand the diffraction pattern obtained from a crystal. Suppose that the incident radiation is monochromatic and allow it to fall on a stationary crystal (figure 3.7). In this diagram, the $hk0$ section of a reciprocal lattice is shown with an x-ray (or neutron or electron) beam coming from the left (coloured green, of course!). The c-axis of the direct lattice is perpendicular to the a^*b^* plane.

It can be seen that, in this section, only reciprocal-lattice points $0\bar{3}0$ and $2\bar{3}0$ lie on the surface of the Ewald sphere (I have coloured them green to emphasize this). This results in two beams diffracted through the angles $2\theta_{0\bar{3}0}$ to the left of the incident beam and $2\theta_{2\bar{3}0}$ to the right. So, if we use a detector (film or counter) to collect reflections within this reciprocal-lattice plane, we would observe only these two reflections as spots or peaks in intensity: none of the other possible reflections would be observable in this reciprocal-lattice layer.

In figure 3.8, we see what happens in three dimensions. The drawing shows reciprocal-lattice layers perpendicular to the c-axis. We can determine the indices of the layers in the following way. Recall that the c-axis direction is, in fact, equivalent to [0 0 1], and so consider the scalar product

$$\mathbf{c} \cdot (h\mathbf{a}^* + k\mathbf{b}^* + l\mathbf{c}^*) = 0 \tag{3.13}$$

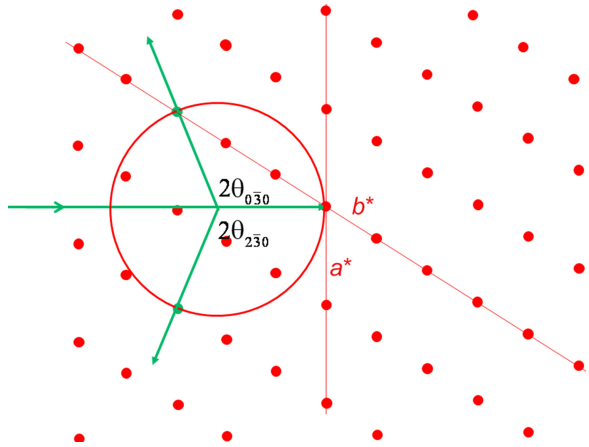

Figure 3.7. $hk0$ section of reciprocal lattice and Ewald sphere for a stationary crystal.

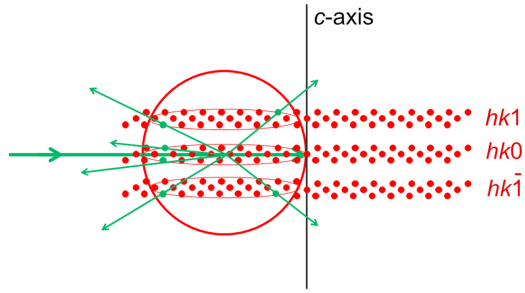

Figure 3.8. Ewald sphere for a stationary crystal.

for layers perpendicular to [0 0 1]. This gives the result

$$2\pi l = 0 \tag{3.14}$$

showing that the $hk0$ layer of nodes is perpendicular to the c-axis. The layers parallel to $hk0$ have the indices $hk0$, $hk1$, $hk\bar{1}$, $hk2$, $hk\bar{2}$, $hk3$, $hk\bar{3}$, …….

It can be seen that the layers cut through the Ewald sphere, but still only very few reciprocal-lattice points lie on the surface of the sphere. This shows that with a stationary crystal like this and a monochromatic source of incident radiation, in general, very few reflections would be expected to be observed, especially for a crystal with a small unit cell, and correspondingly a large reciprocal cell.

This points to a lesson about the original experiment carried out in 1912 by Friedrich and Knipping. They used a stationary crystal and yet observed a sufficient deflection of the x-ray beam to realize that they had found evidence of diffraction. They soon obtained beautiful photographs from ZnS, with many spots (reflections) arranged in patterns showing the underlying symmetry. The problem that they then faced was: how to interpret what they had seen? The first crystal that they used for their experiment was $CuSO_4.5H_2O$ because Laue mistakenly thought that any diffraction would be the result of scattering by a single wavelength due to secondary x-rays emanating from the copper atoms. Had this been the case, our analysis shows that they probably would not have obtained the first diffraction pattern, and they would have returned home disappointed[1]. So luck was with Friedrich and Knipping on the occasion of their seminal experiment and handed Laue his Nobel Prize. This illustrates how significant scientific advances so often occur by pure chance.

Both father and son, William Henry Bragg (1862–1942) and William Lawrence Bragg, soon set about trying to understand the ‘curious’ photographs obtained by Laue (figure 3.9); having realized that, if they assumed that the x-rays were polychromatic, they could use this knowledge to work out the first atomic structures of crystals such as NaCl. W L Bragg’s model of alternating Na and Cl atoms

[1] Laue tried, but failed, to interpret the observed photographs fully, still persisting in the belief that only one or possibly five wavelengths were involved, but it was W L Bragg who showed that the diffraction patterns could be explained if the incident radiation consisted of a continuum of wavelengths. Surprisingly, Laue should have realized his mistake, since Friedrich and Knipping obtained a good diffraction pattern from a crystal of diamond, where secondary x-rays would not be expected to play a role.

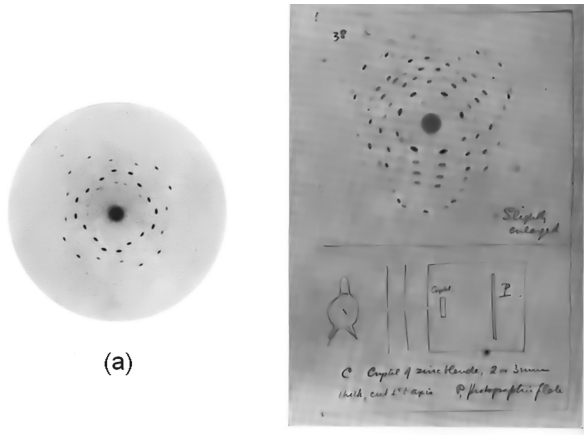

Figure 3.9. (a) One of Friedrich and Knipping's original x-ray photographs of ZnS. (b) Facsimile of W H Bragg's sketch of Laue's 'curious' x-ray effect (1912).

stretching out in all directions was not without controversy, however: see the famous letter to Nature in 1927 from Henry Edward Armstrong (1848–1937), reproduced below. Many chemists thought that NaCl should consist of molecules and for a long time resented the fact that mere physicists were telling them that they were wrong! Never mind—both father and son Bragg shared the 1915 Nobel Prize for their discovery, and the structure of NaCl has stood the test of time!

Poor Common Salt.

'Some books are lies frae end to end' says Burns. Scientific (save the mark) speculation would seem to be on the way to this state!….Professor W L Bragg asserts that 'In Sodium Chloride there appear to be no molecules represented by NaCl. The equality in number of sodium and chlorine atoms is arrived at by a chess-board pattern of these atoms; it is a result of geometry and not of a pairing of the atoms'.

This statement is more than 'repugnant to common sense'. It is absurd to the n…th degree. not chemical cricket. Chemistry is neither chess nor geometry, whatever x-ray physics might be. Such unjustified aspersion of the molecular character of our most necessary condiment must not be allowed any longer to pass unchallenged. It were time that chemists took charge of chemistry once more and protected neophytes against the worship of false gods; at least taught them to ask for something more than chess-board evidence.

(Professor H E Armstrong, Letter to Nature 1927)

3.5.2 Oscillating and rotating crystal

We have seen that with a stationary crystal and a monochromatic beam, the chances of observing diffraction are relatively minimal, at least for crystals with

small unit cells. To capture some more diffraction maxima, we need to move the crystal, and correspondingly the reciprocal lattice, in some way.

Referring to figure 3.10, imagine now that we oscillate the crystal through an angle about the axis perpendicular to the reciprocal-lattice layer shown. This can be easily seen if, instead, we keep the reciprocal lattice fixed and make the incident beam oscillate between the positions A and B, thus causing the Ewald sphere to oscillate too. It can now be seen that the shaded areas ('lunes') include several reciprocal-lattice points (green), and this means that during the oscillation, the corresponding reflections will occur on a suitably placed detector. It should be evident that, in general, in an oscillation experiment, different reflections appear on either side of the x-ray beam so that the observed pattern will generally be asymmetric unless one happens to oscillate either side of a prominent symmetry-axis direction.

If one has a crystal with a huge unit cell, such as is typically found in protein crystals, even a small oscillation range will give rise to many observed reflections (figure 3.11). In this example, the density of reflections is such that you can see the them lying on circles, corresponding to circular cuts through the Ewald sphere. Therefore, one way of thinking about this is to realize that the diffraction pattern is effectively an imprint of the reciprocal lattice, distorted by the geometry of the experimental arrangement. The varying intensities of the spots arise from the different atomic arrangements on the planes giving rise to the reflections. It is this that eventually enables crystallographers to solve the crystal structure.

It can also be seen from figure 3.10 that if we rotate the crystal (or beam) through a complete 360°, all reciprocal-lattice points within a large circle (marked in blue) will at some time pass through the circumference of the Ewald sphere and thus create a reflection on the detector. In three dimensions, this limiting circle is a sphere.

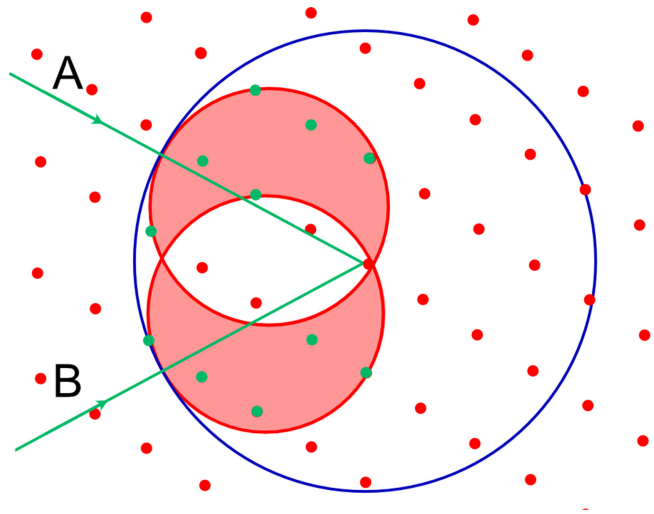

Figure 3.10. Effect of oscillating a crystal through an angle about an axis perpendicular to the page.

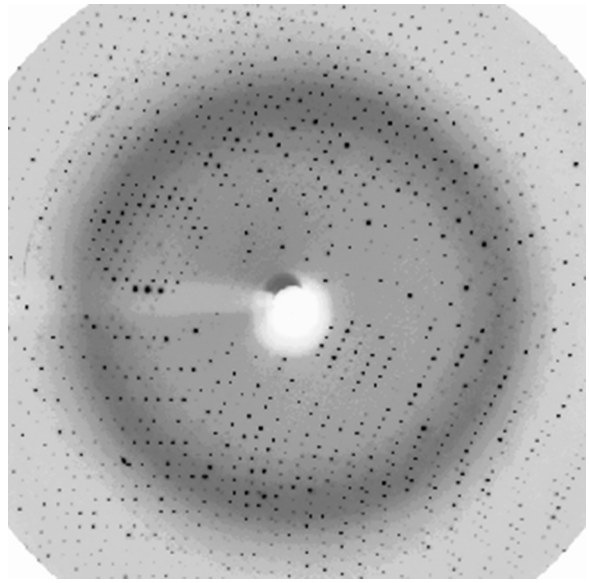

Figure 3.11. X-ray pattern, obtained using a synchrotron source, of a protein crystal oscillating over a very small angle (Reproduced by permission of the International Union of Crystallography).

Definition. *The **limiting sphere** is one that contains all the possible reciprocal-lattice points for a particular wavelength, where*

$$d_{hkl} \geqslant \frac{\lambda}{2} \tag{3.15}$$

Note that in a rotation experiment like this, the same reflections are captured on each side of the incident beam, and so the observed diffraction pattern will appear to be symmetric about the axis of rotation. One of the disadvantages of the oscillation/rotation method is that the diffraction spots will often overlap, making it difficult to measure each independent reflection. Before the modern era of computerized diffractometers, when I started crystallographic research, diffraction patterns were recorded on photographic film. To remove the overlap problem, moving film methods were used to spread the reflections out. The two most common were the so-called precession and Weissenberg techniques. These days, hardly anyone uses photographic film to record diffraction patterns. Instead, sophisticated, computer-controlled diffractometers are available that can collect complete datasets in a fraction of the time and with more precision. The average user can operate these machines with relatively little knowledge of reciprocal space. It no longer needs the operator to orient the crystal: instead, random sections of reciprocal space are recorded, and the computer is able to sort out the orientation, unit cell, space group, etc.

3.5.3 Polycrystalline powder

Suppose that, instead of using a single crystal, radiation is diffracted by a polycrystalline or powdered specimen. Now, this is simply a collection of small

crystallites, randomly oriented in the ideal case. In reciprocal space, this can be thought of by imagining spinning the reciprocal lattice about its origin.

Figure 3.12 demonstrates that by rotating about the reciprocal-lattice origin, the reflections trace out a series of concentric spheres. Figure 3.13 shows the intersection of two of these *hkl* shells around the reciprocal-lattice origin at O with the Ewald sphere centred at C. Scattered beams from C through the intersection form cones each with an internal angle $4\theta_{hkl}$, which then project rings onto a flat detector plate. For an infinite number of random crystallites, the rings will be smooth and continuous.

Clearly, if the powder does not consist of randomly oriented crystallites, the intensity around these rings will be uneven. This type of effect is known as *preferred orientation*. If the powder only consists of a tiny number of crystallites, then the rings will appear to be spotty. Thus, when carrying out a powder diffraction measurement,

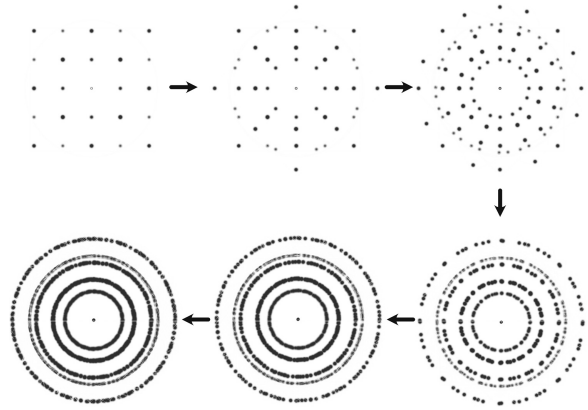

Figure 3.12. Effect of spinning the reciprocal lattice about its origin (shown in two dimensions here: in three dimensions, the spots would trace out concentric spherical shells). Here the incident beam is assumed to be perpendicular to the page.

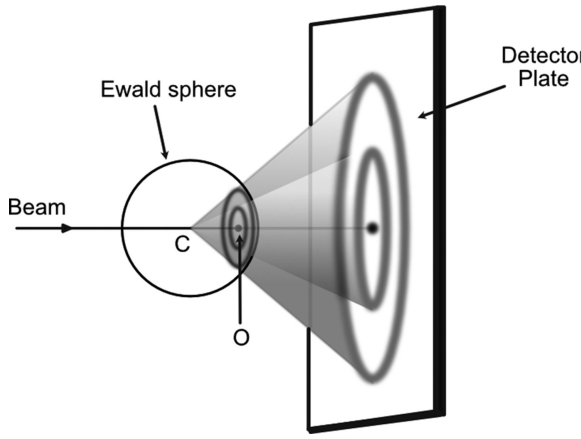

Figure 3.13. Intersection of two concentric spherical shells with the Ewald sphere forming cones of scattered beams to create powder rings projected onto a flat plate. O is the reciprocal-lattice origin.

it is usual to grind the solid up into fine particles of about 1–10 μm size. These days, rather than using photographic film (figure 3.14) to observe the powder rings, an automatic diffractometer (figure 3.15) is generally used in which a counter is scanned from low to high 2θ within a single plane. This then cuts through the diffracted rings to produce a one-dimensional pattern of intensities. A typical example of a powder pattern collected on a modern powder diffractometer is shown in figure 3.16.

3.5.4 Laue diffraction

If we go back to the original experiment of Friedrich and Knipping, we can now understand why they were able to obtain their first x-ray diffraction photographs

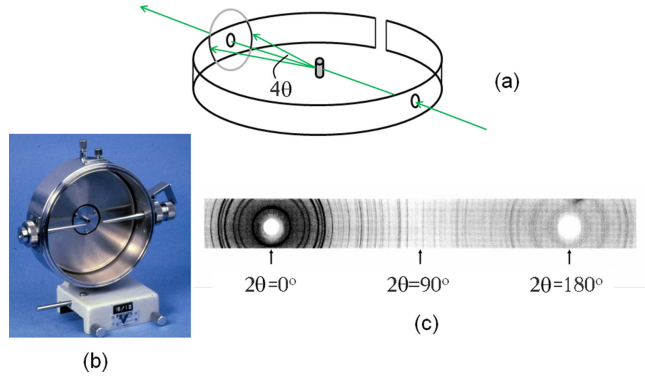

Figure 3.14. The Straumanis method of powder diffraction. (a) Schematic diagram. X-ray film is placed around the inside of a cylindrical camera. In this method, two holes are punched in the film for the incoming and outgoing incident beams. (b) Commercial powder camera. (c) Film exposed to x-rays. The two holes are centred at $2\theta = 0°$ and 180°. By measuring rings either side of the holes, it is possible to determine the exact positions of $2\theta = 0°$ and 180° and then use this to correct for errors in the film radius caused by shrinkage during the photographic development process.

Figure 3.15. Example of an x-ray powder diffractometer manufactured by Bruker AXS. Reproduced with permission of Bruker.

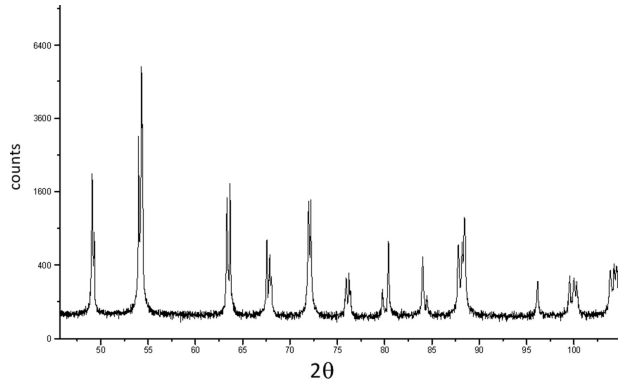

Figure 3.16. Part of an x-ray powder pattern of lead zirconate–titanate (collected with a Panalytical diffractometer and X'Celerator detector).

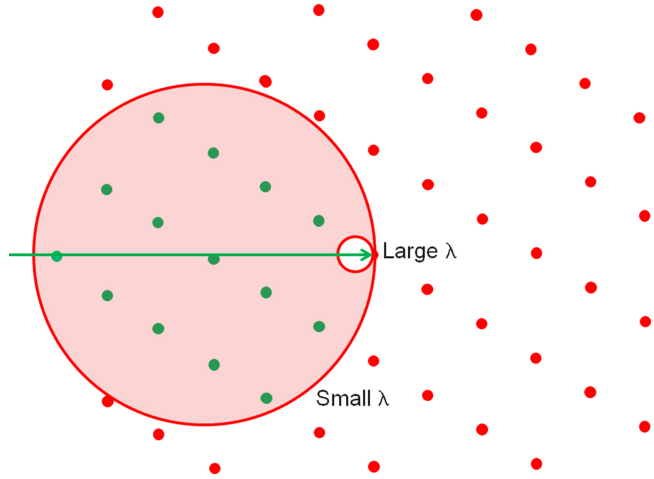

Figure 3.17. The Ewald sphere and Laue diffraction. All nodes within the pink area will give rise to reflections in principle.

using a stationary crystal. In figure 3.17, we assume that the incident radiation is polychromatic with wavelengths ranging from small to large, thus effectively creating a continuum of Ewald spheres with radii from large to small. Within this range, reciprocal-lattice points will cut through the surfaces of the Ewald spheres to give rise to diffraction spots. The result obtained on a photographic film is many diffraction spots, each spot arising from a particular wavelength.

Figure 3.18 shows simulated Laue photographs for a cubic crystal of $SrTiO_3$ in transmission and back-reflection geometry. Note how the 4-fold symmetry of the crystal is also found in the diffraction pattern. Photographs of this sort have traditionally been used for orienting crystals and establishing crystal quality, either

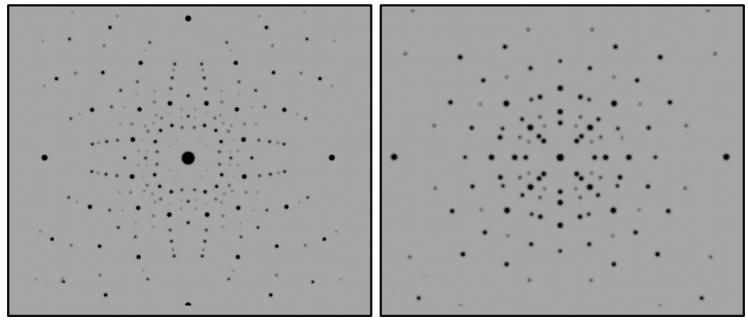

Figure 3.18. Laue photographs of $SrTiO_3$, beam along [001], flat-plate geometry. Left: transmission. Right: back-reflection. Simulated with the program SingleCrystal (CrystalMaker Software Ltd).

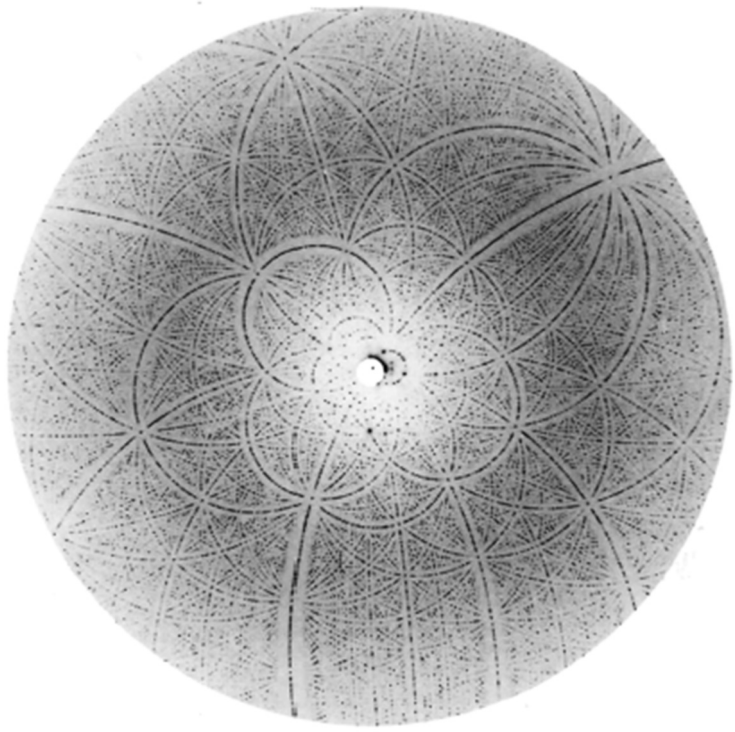

Figure 3.19. Example of a Laue photograph taken using a synchrotron for a crystal of the protein Rubisco. Reproduced from [1] by permission of the International Union of Crystallography.

in transmission or in back-reflection geometry. The back-reflection geometry is especially suited for orienting large crystals[2].

Laue photography is particularly suited to x-ray synchrotron radiation (figure 3.19), since the source of radiation is entirely polychromatic and intense. This means that

[2] I recall that my PhD supervisor, Kathleen Lonsdale (1903–1971), always insisted on seeing the Laue photographs before all else, and I was in trouble if I did not have them to hand!

diffraction information can be collected in microseconds from minute crystals. This has even been used to solve crystal structures, since so many reflections are collected at once. A useful review is given by Ren *et al* [2].

3.5.5 Energy-dispersive diffraction

One of the ways in which polychromatic sources have been used to obtain diffraction information is by collecting the diffracted intensity with a solid-state detector capable of carrying out an energy analysis of the diffracted x-rays. An example of this is in the use of synchrotron radiation (figure 3.20) on a powder sample with the detector set at a fixed 2θ angle. The detector is connected to a multi-channel analyzer, which displays the powder pattern as the number of counts against energy E in keV. Peaks then appear at different values of energy to produce a so-called energy-dispersive powder pattern. Thus, one effectively turns Bragg's Law back to front.

$$E = \frac{hc}{\lambda} = \frac{hc}{2\sin\theta} \cdot \frac{1}{d_{hkl}} \propto \frac{1}{d_{hkl}} \tag{3.16}$$

where h is Planck's constant and c is the speed of light. The real advantage of this technique is that the sample and detector are stationary, making it easier to access a sample housed in some environmental cell in which there is only a limited view. This has proved particularly useful in the study of high-pressure phases of materials, where the powder sample is placed in a fluid inside a metal gasket between two opposing diamond crystals that exert high pressure. However, the main problem with using a solid-state detector in this way is that the energy resolution is generally poor, and so it cannot compete with standard monochromatic angle-scanning methods.

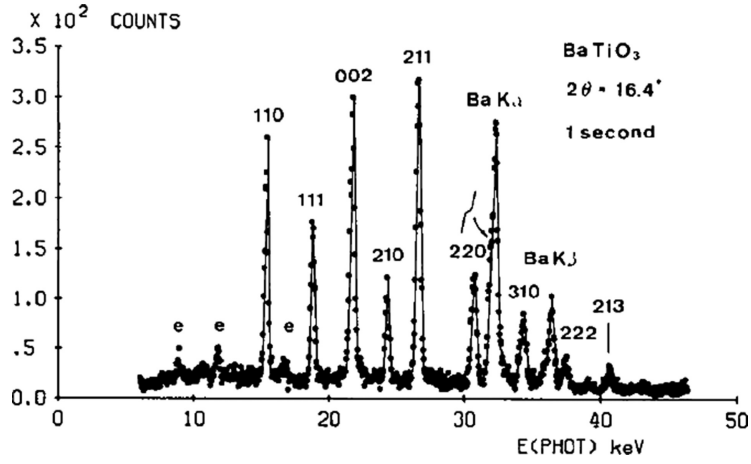

Figure 3.20. Diffraction spectrum of $BaTiO_3$ (3.7 GeV, 14 mA, $2\theta = 16.4°$) from a synchrotron source [3]. The letters e denote escape peaks. Note inclusion of the Ba $K\alpha_1$ fluorescence line. Reproduced from [3] by permission of the International Union of Crystallography.

There is another way to carry out energy-dispersive diffraction by scanning through different wavelengths with a crystal monochromator and a conventional detector at a fixed angle (figure 3.21). In this case, the almost perfectly parallel white beam of a synchrotron is used together with a silicon crystal monochromator cut to form two parallel leaves. Rotation of this channel-cut crystal changes the wavelength of the x-rays passed and, at the same time, keeps the outgoing monochromatic beam parallel to the incident beam, with only a slight change in height. This, in principle, provides a resolution in peak positions of about one part in 10^4 given by the scanning monochromator rather than by the detector.

As with x-rays, in neutron diffraction, there are two ways in which data can be collected. First of all, in the standard angle-dispersive method, neutrons, obtained typically from a nuclear reactor, are diffracted by a monochromator crystal to produce a single wavelength and then shone onto the sample. A detector is then scanned through 2θ. The second way is, again, an energy-dispersive method. A pulsed 'white' neutron source is used from a neutron spallation source: here, a polychromatic neutron beam is incident on a sample, and a bank of detectors is used to determine the time-of-flight of the scattered neutrons at various fixed angles. The momentum of a neutron with velocity v_N is given by

$$p = m_N v_N = m_N\left(\frac{l}{t}\right) = \frac{h}{\lambda} \tag{3.17}$$

where l is the distance traversed by the scattered neutron and t its time-of-flight. Then

$$d_{hkl} = \frac{\lambda}{2\sin\theta} = \frac{h}{2p\sin\theta} = \frac{ht}{2m_N l\sin\theta} \propto t \tag{3.18}$$

Thus, a detector set at a fixed angle, measuring the number of neutrons arriving for different times t, produces a diffraction pattern in which d_{hkl} is proportional to time-of-flight. Figure 3.22 shows a typical powder pattern collected in this way. Compare this pattern with that in figure 3.16, which shows the same reflections (but plotted from left to right). One of the advantages of this type of data collection is that it can rapidly access extremely high hkl values with very high resolution.

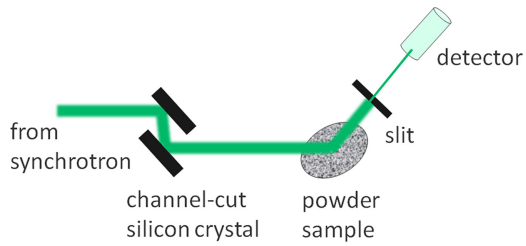

Figure 3.21. High-resolution energy-dispersive diffraction with synchrotron radiation and a channel-cut silicon crystal [4].

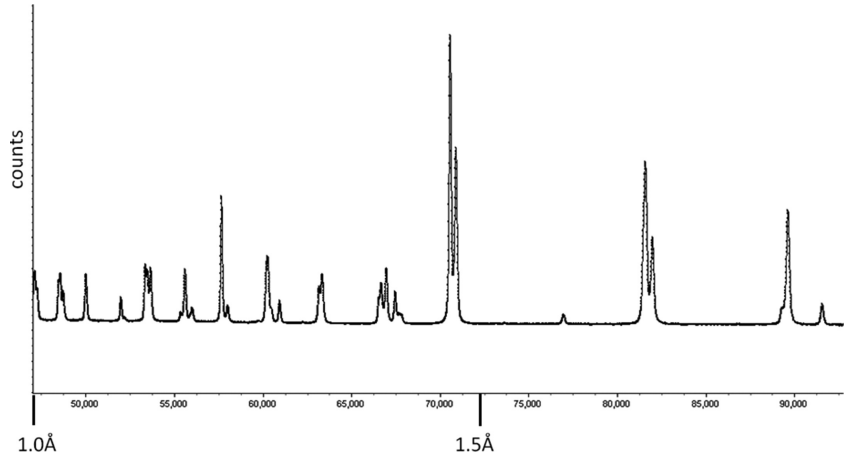

Figure 3.22. Part of a time-of-flight powder pattern of lead zirconate–titanate collected at the ISIS spallation source at the Rutherford-Appleton Laboratory (horizontal axis marked in channel numbers).

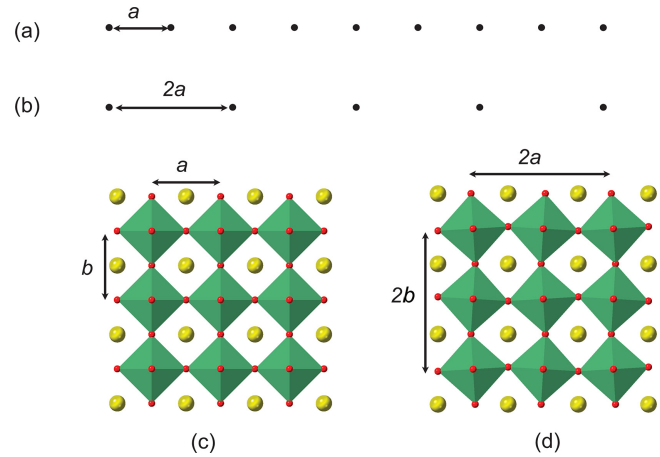

Figure 3.23. Super and sublattices and structures.

3.5.6 Confusion over sub and super?

One of the areas in which confusion occurs in the literature is in the use of terms such as superlattice, sublattice, superstructure, etc. It is worth, at this juncture, looking at where the confusion arises. Let us start with a one-dimensional lattice in direct space with a spacing given by a (figure 3.23(a)). This has the symmetry of the translation group in which the lattice points are given by symmetry operations $\mathbf{t}_i = n_i\mathbf{a}$. Suppose now we remove every other lattice point to get figure 3.23(b), where the lattice spacing becomes doubled to $2a$, and then $\mathbf{t}_i = 2n_i\mathbf{a}$. By removing alternate lattice points, half of the translational symmetry operations in the translation group have been left, so that the new translation group shown in (b) is a subgroup of index 2 of

the translation group in (a). Therefore the lattice (b) is a *sublattice* of (a); and (a) is a *superlattice* of (b). However, note that the unit cell has changed from a to $2a$, so this is a *supercell* of the original cell. We immediately see a possible source of confusion in that the prefixes *sub* and *super* are used differently for the lattice and the unit cell.

A sketch of the crystal structure of the cubic phase of the perovskite $NaNbO_3$ is shown in figure 3.23(c). Note that the oxygens form octahedra that are corner-linked in all directions. At high temperature, $NaNbO_3$ undergoes a phase transition in which the octahedra tilt slightly while still being connected by their corners (figure 3.23(d)). The effect of this tilting is to double the lattice parameters a and b while keeping c unchanged. The result is a tetragonal structure. Because of the loss of symmetry operations, the lattice for the tilted structure (d) is a sublattice of the lattice of the cubic phase (c). However, simultaneously, a supercell is created with dimensions $2a$, $2b$, c, with $a = b$, and so we would describe the crystal structure (d) as a superstructure.

To add to the confusion, consider what happens in reciprocal space. Figure 3.24 shows calculated powder diffraction plots for $NaNbO_3$ in the cubic and tetragonal phases. Notice the weak extra reflections that appear in the lower diagram. These arise purely from how the oxygen octahedra tilt, causing a doubling of the unit-cell axes. So their intensities can provide measurements of the magnitudes of the tilting. What should we call these extra peaks? In the literature, you can find many variants such as superlattice, sublattice, or superstructure peaks. In terms of the reciprocal lattice, the addition of extra peaks means that the reciprocal-lattice translation group has gained symmetry elements, and so we might call them superlattice peaks.

But on the other hand, if we refer to the lattice in direct space, where the unit cell has been increased, they could be called sublattice peaks! So, it all depends on which space, direct or reciprocal, one refers to in naming the extra diffraction peaks. I suggest, as a way out of this confusion, which, unfortunately, litters the scientific

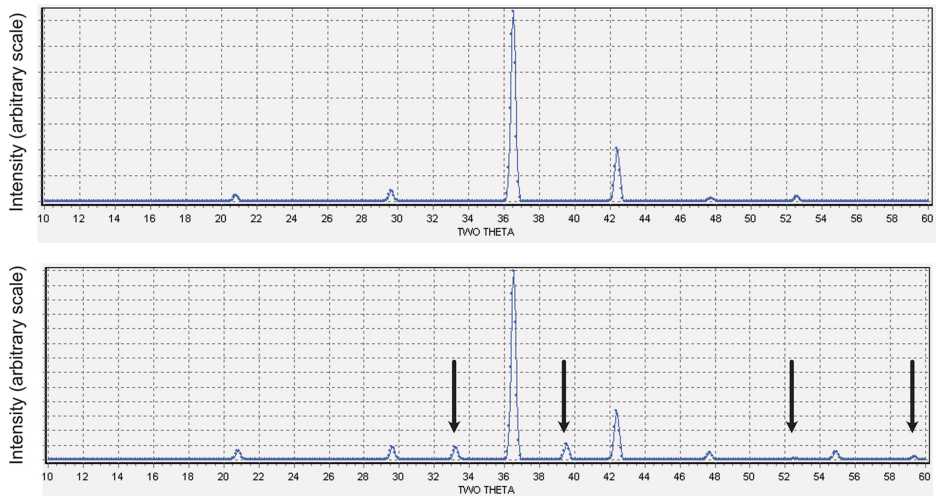

Figure 3.24. Neutron powder diffraction plots for $NaNbO_3$. Top: cubic phase, bottom: tetragonal phase.

literature, that it makes better sense to refer to the crystal structure rather than to the lattice. In this case, the extra diffraction peaks would be called superstructure peaks, as they arise from a superstructure.

3.6 Imaging

I dress for the image. Not for myself, not for the public, not for fashion, not for men.

(Marlene Dietrich)

Figure 3.25 shows a ray diagram for a converging, thin, aberration-free optical lens, and figure 3.26 shows the corresponding wave fronts focused on the back-focal plane. Parallel light incident from an object with transmission function $f(x,y)$ is imaged by the lens having focal length f. Note that all the scattered beams from the object end up at equivalent points (indicated by drawing the rays in colour in figure 3.25) on the image plane to create an inverted image, magnified by a factor R_2/R_1.

Note that all the light from everywhere in the object plane and scattered through an angle θ is brought to focus at a single point on the *back-focal plane*. The amplitude of the plane wave in the direction (θ_x,θ_y) is proportional to the Fourier transform $F(u, v)$ (appendix E) and for small angles is focused at the point $(\theta_x f, \theta_y f) = (\lambda fu, \lambda fv)$.

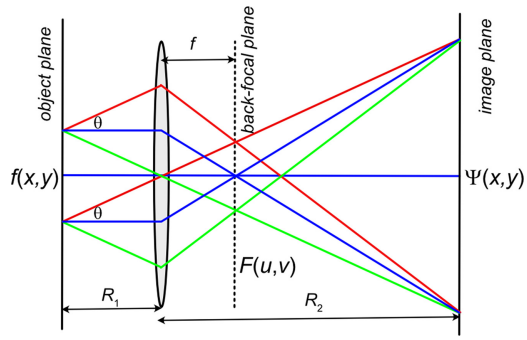

Figure 3.25. Ray diagram for a thin converging lens.

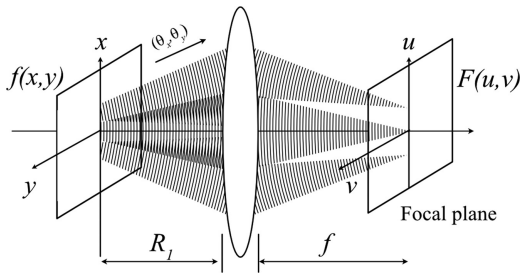

Figure 3.26. Focusing of plane wave fronts by a lens onto the back-focal plane.

In other words, every point in the focal plane receives information from all points in the object plane. This is equivalent to interference at a point at infinity. When considering diffraction from the object, the back-focal plane is also the diffraction plane. The ability to look at back-focal and image planes has been used by Harburn, Taylor and Welberry [5] in constructing their Atlas of Optical Transforms.

While lenses are available for optical wavelengths, this is not the case for x-ray or neutron beams. The exception is in electron microscopy, where magnetic lenses are available. For instance, these are exploited in the transmission electron microscope (TEM), where electromagnetic converging lenses can have their focal lengths altered by adjusting the lens currents to focus on a diffraction pattern or on an image. In figure 3.27(a), an intermediate image is formed at relatively low magnification. The intermediate lens produces a second intermediate image, which is then magnified and sent to a viewing screen by the projector lens. The final magnification is obtained by altering the focal lengths of the intermediate and projector lenses. The image can be focused on the screen by varying the focal length of the objective lens. Figure 3.27(b) shows the arrangement to send the diffracted image to the viewing screen. If the incident electron beam is parallel, then the diffracted beams are focused on the back-focal plane. From the colours of the rays drawn in the diagram, you can see that at *every* point in the back-focal plane, information is received from the *whole* of the specimen at the same time, just as with the optical lens. The diffraction pattern is seen on the viewing screen by adjusting the focal length of the intermediate lens.

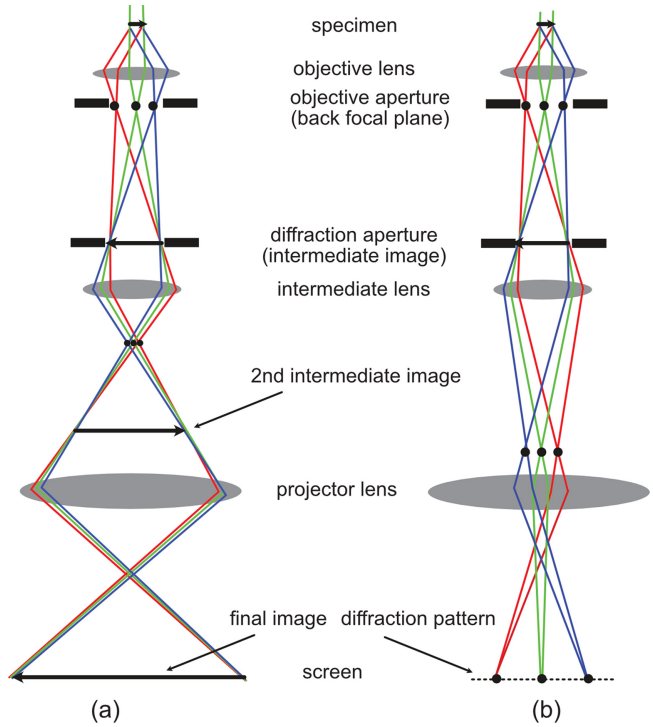

Figure 3.27. Ray diagrams for the transmission electron microscope: (a) imaging, (b) diffraction.

Note that a single diffracted beam can be selected for imaging by a suitably placed aperture in the objective lens back-focal plane to form a complete image of the specimen as a whole. Using the direct, undiffracted beam alone, a so-called bright-field image of the specimen is obtained, whereas any selected diffracted beam gives a so-called dark-field image (bright-field and dark-field images show opposite intensity contrast). However, imaging of the atoms in a crystal structure requires very high resolution and magnification, which is achieved by using many reflections at the same time. Over the years, significant advances have been made in lens design and in detectors that now enable this to be done quite routinely.

In figure 3.25, we saw how a lens forms an image by gathering the light scattered from an object and creates an amplitude distribution given by $F(u,v)$ on the back-focal plane, where u and v are coordinates in the plane. As the distances are large, $F(u, v)$ is a Fraunhofer diffraction pattern on the back-focal plane, described by the Fourier transform of the diffracting object. The radiation from the back-focal plane then forms an interference pattern on the image plane, effectively at infinity. The image thus formed is the Fourier transform of the information from the back-focal plane.

In general, when, say, x-rays are incident on a crystal, waves are diffracted (figure 3.28) at angles given by Bragg's Law, with scattered waves having different amplitudes $|F(hkl)|$ and relative phases $\phi(hkl)$ to form a pattern of diffracted intensities at the nodes of the reciprocal lattice. However, unlike in the electron microscope or normal optics, no lens is readily available to send the diffraction pattern onto a focal plane. Instead, the detector of the scattered radiation is only capable of recording diffracted intensity distributions. The intensity at the reciprocal-lattice node hkl is given by:

$$I(hkl) \propto F(hkl)F^*(hkl) = |F(hkl)|^2 \tag{3.19}$$

In crystal-structure determination, one attempts to reconstruct the scattering object (the atoms in the crystal) from the observed diffraction pattern: to do this, the amplitude and phase for each hkl reflection are required. As can be seen from equation (3.19), the phase information is lost. This difficulty in determining the appropriate phases is known as the *phase problem* to crystallographers and constitutes the main difficulty in determining crystal structures. We shall see later some of the inventive ways in which this has been overcome.

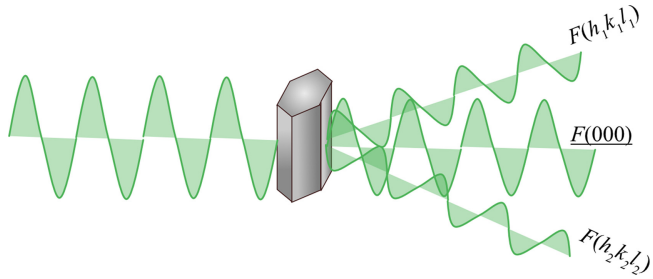

Figure 3.28. Amplitudes and phases of diffracted waves.

3.6.1 Fourier transformation

The calculation of diffraction patterns relies on Fourier transformation, for which a brief introduction is given in appendix E. In three-dimensional space, such as for a crystal, consider a small volume element dV at a position $\mathbf{r}$. The density of particles in this volume element is $\rho(\mathbf{r})$. For example, in x-ray scattering, this will be the electron density in a crystal. The scattering from the volume element is given by a complex amplitude:

$$F(\mathbf{Q}) = \int_{-\infty}^{\infty} \rho(\mathbf{r}) e^{i\mathbf{Q}\cdot\mathbf{r}} d^3\mathbf{r} \tag{3.20}$$

Also,

$$|\mathbf{Q}| = |\mathbf{k} - \mathbf{k}_0| = \frac{4\pi \sin\theta}{\lambda} \tag{3.21}$$

which is a vector in what we may call 'Fourier transform space', i.e., yet another name for reciprocal space. The integral in equation (3.20) is over all direct space (in crystallography, this refers to the crystal structure, theoretically in an ideal, infinite crystal). Note that $F(\mathbf{Q})$ is a complex number, even though the direct-space quantity $\rho(\mathbf{r})$ is real and positive. Therefore, we can write it as

$$F(\mathbf{Q}) = |F(\mathbf{Q})| e^{i\phi} \tag{3.22}$$

where ϕ is its phase. Also, one can recover the function $\rho(\mathbf{r})$ via the inverse Fourier transform given by

$$\rho(\mathbf{r}) = \frac{1}{(2\pi)^3} \int_{-\infty}^{\infty} F(\mathbf{Q}) e^{-i\mathbf{Q}\cdot\mathbf{r}} d^3\mathbf{Q} \tag{3.23}$$

Notice the change in sign in the exponential term.

3.6.1.1 Two simple 'guidelines'

I find it useful when teaching students about diffraction to visualize Fourier transformation using two simple guidelines:

1. Fundamental symmetry is preserved.
2. Large distances become small and small distances large.

Although this is a gross simplification (see appendix E for details), nonetheless, by remembering this, we can check that a calculated Fourier transformation makes sense. Let us look at a couple of examples to see how this works.

In figure 3.29, a one-dimensional vertical lattice L_1 is shown, and on the right its computed Fourier transform. First of all, note that the lattice has translational symmetry along the vertical axis, and so this symmetry will be preserved in the Fourier transform (guideline 1). However, the spacing of the lattice points will become inverted (guideline 2). Furthermore, the dimension of the one-dimensional lattice in the horizontal plane is infinitesimally small in theory, and so in Fourier space (guideline 2), it will be extended to infinity horizontally. The result is a series of infinite horizontal planes separated by translational symmetry given by $a^* = 2\pi/a$.

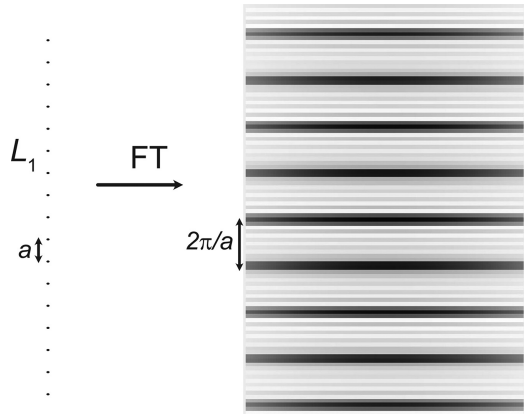

Figure 3.29. Fourier transformation of a one-dimensional lattice to give infinite repeating planes (viewed edge-on) perpendicular to a.

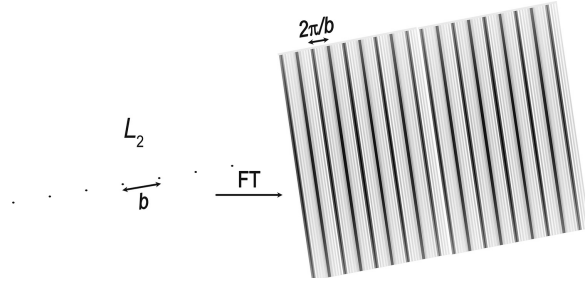

Figure 3.30. Fourier transformation of a one-dimensional lattice to give infinite repeating planes (viewed edge-on) perpendicular to b.

The fine lines between the maxima are the submaxima due to the finite height of the lattice L_1 used in this simulation. Figure 3.30 shows the Fourier transform of the lattice L_2 having spacing b.

Now consider a two-dimensional lattice (figure 3.31). This can be built from a convolution of two one-dimensional lattices L_1 and L_2. The Fourier transform, therefore, according to the convolution theorem (appendix E), will be given by the product of the Fourier transforms $\tilde{L}_1 \times \tilde{L}_2$. This means that in Fourier space, there will be one set of parallel planes perpendicular to L_1 and another set perpendicular to L_2 whose spacings are given by $2\pi/a$ and $2\pi/b$, i.e., proportional to the reciprocal of the spacings of the direct-lattice points. Note that a^* is perpendicular to b, and b^* is perpendicular to a. Because of the multiplication of the two Fourier transforms, everything will cancel except where the planes cross to give infinite rods perpendicular to the a^*b^* plane. In figure 3.32, these are denoted by the dark black crossing points: for a two-dimensional lattice, these infinite rods point out of the plane of the paper, but as one adds a third dimension, they become shorter.

It should be evident that if we introduce a third one-dimensional lattice L_3, the Fourier transform will then be $\tilde{L}_1 \times \tilde{L}_2 \times \tilde{L}_3$. The three sets of infinite planes

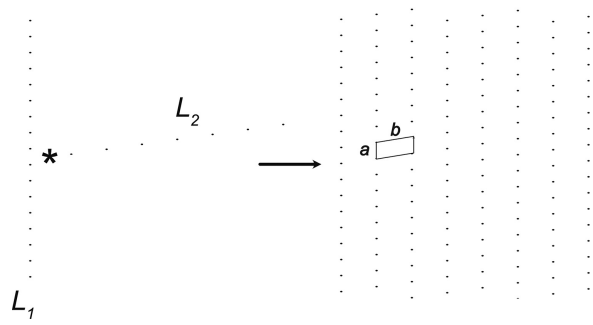

Figure 3.31. Convolution of two one-dimensional lattices to form a two-dimensional lattice.

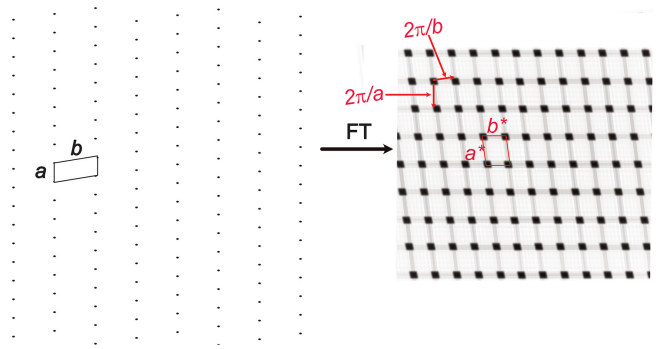

Figure 3.32. Fourier transform of a two-dimensional lattice.

produced from the Fourier transforms of the lattice functions will cross, giving zero everywhere, except where they intersect, thus creating a three-dimensional lattice of points—the reciprocal lattice again!

3.6.2 A simple view of crystal diffraction

To gain some insight into diffraction calculations for a particular crystal structure, it is instructive to go back to the way we earlier defined the crystal structure $C(\mathbf{r})$ in terms of a convolution of a lattice function $L(\mathbf{r})$

$$L(\mathbf{r}) = \sum_{uvw} \delta(\mathbf{r} - \mathbf{r}_{uvw}) \tag{3.24}$$

and a basis $B(\mathbf{r})$:

$$C(\mathbf{r}) = L(\mathbf{r}) * B(\mathbf{r}) \tag{3.25}$$

Applying this to a crystal structure, the convolution theorem gives

$$\tilde{C}(\mathbf{r}) = \tilde{L}(\mathbf{r}) \times \tilde{B}(\mathbf{r}) \tag{3.26}$$

where the Fourier transforms are again denoted by the 'squiggles'.

We can go even further with this idea. Suppose that the crystal is finite in size. We then define a shape function $S(\mathbf{r})$ that can be stated as follows

$$\begin{aligned} S(\mathbf{r}) &= 1 \text{ for } r \leqslant r_0 \\ &= 0 \text{ for } r > r_0 \end{aligned} \tag{3.27}$$

r_0 represents the boundary distance of the crystal. So, a finite crystal can be defined by

$$C(\mathbf{r}) = [S(\mathbf{r}) \times L(\mathbf{r})] \times B(\mathbf{r}) \tag{3.28}$$

Note that the shape function multiplies the lattice function $L(\mathbf{r})$, thus ensuring that there are no lattice points outside the region defined by the shape function.

Figure 3.33 illustrates how a finite crystal is built up from these three elements. According to the convolution theorem, the Fourier transform is given by (figure 3.34).

$$\tilde{C}(\mathbf{Q}) = [\tilde{S}(\mathbf{Q}) * \tilde{L}(\mathbf{Q})] \times \tilde{B}(\mathbf{Q}) \tag{3.29}$$

Note that the size of the shape function becomes inverted in reciprocal space. In the example here, $\tilde{S}(\mathbf{Q})$ is the Fourier transform of a sphere with a central maximum surrounded by rings of subsidiary maxima.

Finally, in figure 3.35, the diffraction pattern is shown. Notice that all the reciprocal-lattice points are no longer described by delta functions but are extended because of the convolution of the shape function with the reciprocal lattice. Furthermore, multiplication by the basis transform results in different intensities at the reciprocal-lattice nodes: the underlying basis transform $\tilde{B}(\mathbf{Q})$ is sampled at the reciprocal-lattice points to give the pattern of intensities. Clearly, for a large crystal, the Fourier transform of the shape function will become much smaller, and so the reflections will become much narrower in extent.

We see that, for tiny crystals, the Fourier transform of the shape function will have a central maximum surrounded by weaker subsidiary maxima. Intersection with the Ewald sphere (figure 3.36) leads to more complex intensity distributions

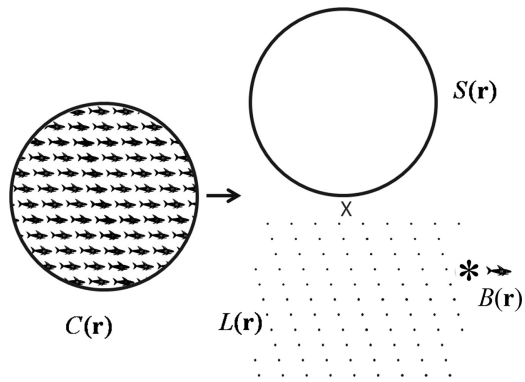

Figure 3.33. A finite crystal in terms of a shape function, a molecule (in the shape of a fish here!), and a lattice.

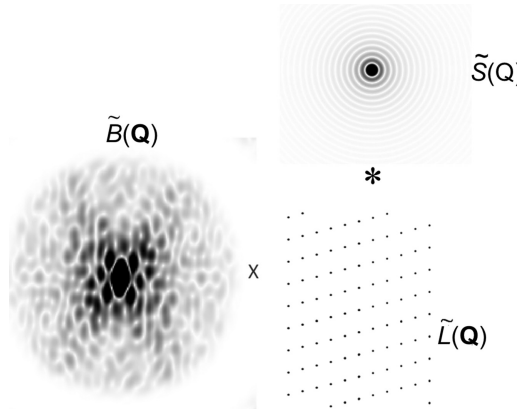

Figure 3.34. Fourier transformation of a finite crystal.

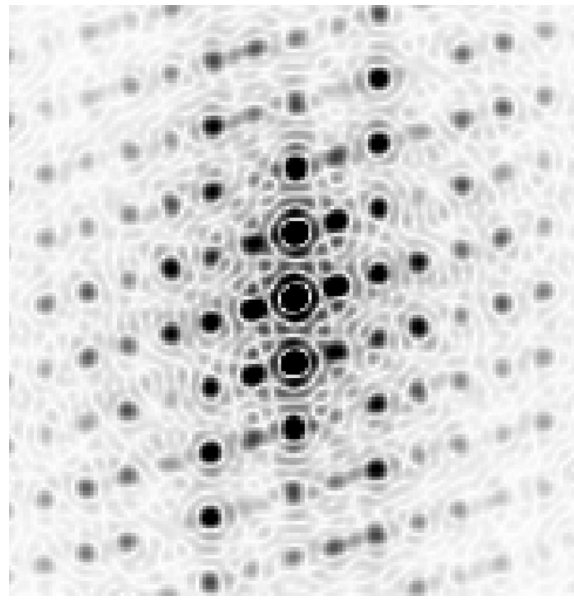

Figure 3.35. Intensity transform of a finite crystal.

around the reciprocal-lattice nodes. As the crystal is made larger, these subsidiary maxima will move into the central maximum, which will shrink in width.

Other examples of Fourier transforms are shown in figure 3.37. On the top are shown three masks in which holes have been made to represent atoms. Below are the diffraction patterns produced by the diffraction of light through the masks. It can be seen in (a) that the structure consists of hexagonal molecules stacked together in a repeating pattern based on a direct-space orthogonal lattice. The diffraction pattern below shows sharp spots of varying intensities, just as one would expect from the diffraction of x-rays by a real crystal. In (b), the intermolecular distances have been

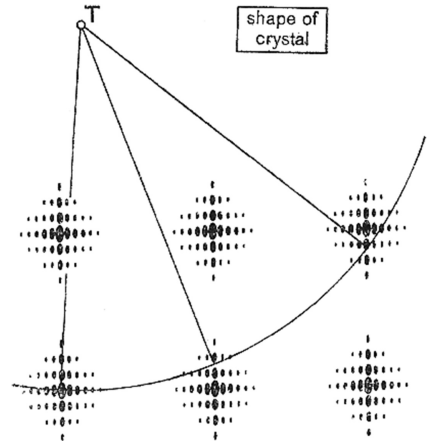

Figure 3.36. Intensity distribution surrounding reciprocal-lattice points for a finite rectangular crystal (taken from Ewald [6] with permission of Springer).

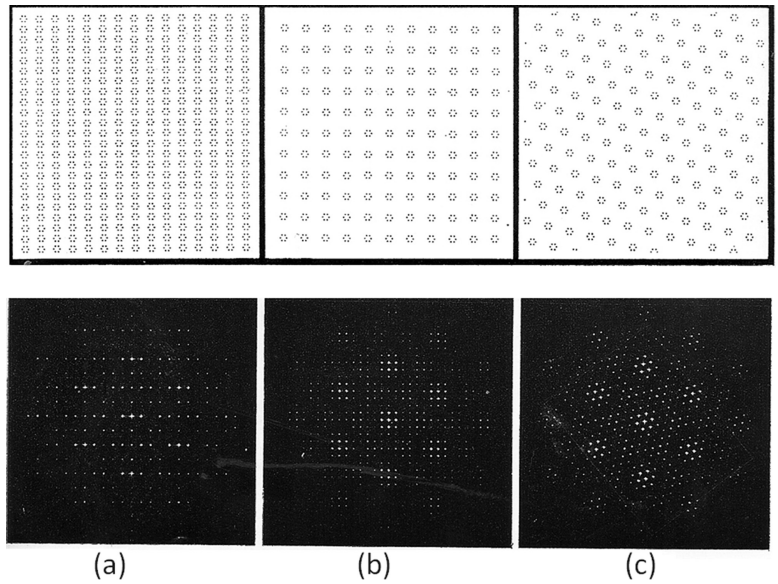

Figure 3.37. Optical transforms of a crystal structure with a molecule consisting of a hexagonal ring of atoms. Reproduced from [5].

increased. The effect of this is to create a reciprocal lattice with points closer together. It can now be seen in the diffraction pattern below how the reciprocal lattice samples the underlying transform of the molecule itself (notice the 6-fold symmetry). In (c), the molecules have been repeated on a hexagonal net, and its diffraction pattern again shows the underlying molecular transform, but the pattern of reciprocal-lattice points now has hexagonal symmetry.

In figure 3.38, the effect of crystal shape is again demonstrated. The diffraction pattern from a simple regular array of atoms is shown in (a). Note that the

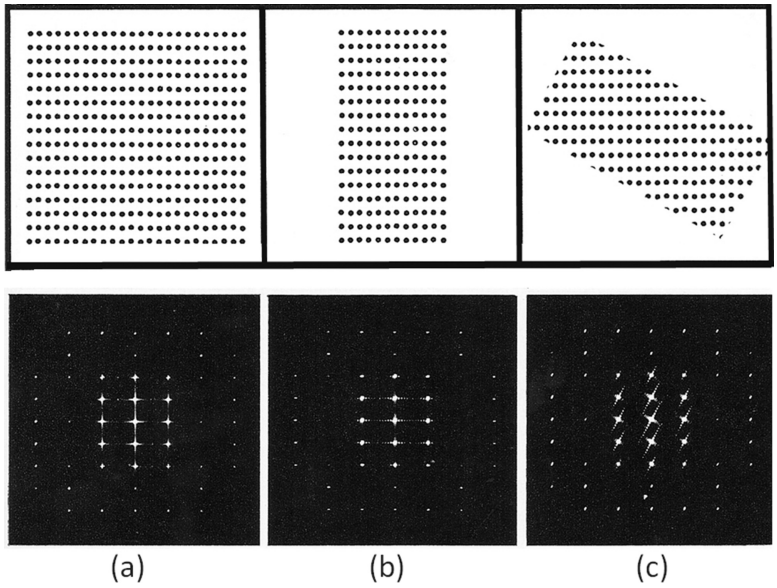

Figure 3.38. Optical transforms of an array of atoms. Reproduced from [5].

reciprocal-lattice points below have become spread vertically and horizontally: this is because the structure shown above is not infinite in extent but is bounded by the square outline of the figure. The Fourier transform of a square will be elongated in directions perpendicular to the edges of the square and contracted in the directions along the diagonals (guideline 2). In (b), the horizontal dimension of the 'crystal' has been reduced, and the transform shows the corresponding horizontal spreading of the intensity at each reciprocal-lattice node. In (c), the crystal is rotated through an angle, and we see that the spread around each node has also rotated.

3.6.3 Lattice diffraction

Let us return to the phase difference produced when waves are scattered by two different points a distance r apart. We shall assume that the so-called first Born approximation applies, namely that only a small fraction of the incident radiation is scattered. This is also known as the kinematic theory. We assume that the scattering is elastic, i.e., there is no difference in energy between the incident and diffracted waves. To understand the intensity observed in a typical diffraction pattern, we also need to realize that the observed diffraction pattern can be considered to be effectively at a very long distance from the scattering object, and so we can treat this as a case of Fraunhofer, rather than of Fresnel, diffraction.

We start by imagining that the lattice alone is involved in the diffraction process. Note that, though the lattice is actually a fictional quantity and therefore has no real existence, we can nonetheless, from a mathematical point of view, imagine that it

consists of an infinite regular array of point scatterers. From equation (3.2), the phase will then be given by

$$\phi = (\mathbf{k} - \mathbf{k}_0) \cdot \mathbf{r} = \mathbf{Q} \cdot \mathbf{r} \tag{3.30}$$

In general, the vector $\mathbf{Q}$ is the scattering vector measured from a chosen origin of reciprocal space to anywhere else in reciprocal space, i.e., it is not necessarily confined to ending at reciprocal-lattice points but can terminate between reciprocal-lattice points to sample any background scattering between the nodes. Recall from equation (3.24) that the lattice function is given by

$$L(\mathbf{r}) = \sum_{uvw} \delta(\mathbf{r} - \mathbf{r}_{uvw}) \tag{3.31}$$

with

$$\mathbf{r}_{uvw} = u\mathbf{a} + v\mathbf{b} + w\mathbf{c} \tag{3.32}$$

The scattering by the array of points will then be given by an integral over the values of $\mathbf{r}$ spanned by the lattice:

$$F(\mathbf{Q}) = \int_{-\infty}^{\infty} L(\mathbf{r}) e^{i\mathbf{Q}\cdot\mathbf{r}} d^3\mathbf{r} \tag{3.33}$$

and then

$$\begin{aligned} F(\mathbf{Q}) &= \int_{-\infty}^{\infty} \sum_{uvw} \delta(\mathbf{r} - \mathbf{r}_{uvw}) e^{i\mathbf{Q}\cdot\mathbf{r}} d^3\mathbf{r} \\ &= \sum_{uvw} \int_{-\infty}^{+\infty} \delta(\mathbf{r} - \mathbf{r}_{uvw}) e^{i\mathbf{Q}\cdot\mathbf{r}} d^3\mathbf{r} \end{aligned} \tag{3.34}$$

Now,

$$\int_{-\infty}^{\infty} \delta(\mathbf{r} - \mathbf{r}_{uvw}) d^3\mathbf{r} = 1 \tag{3.35}$$

Therefore, we can write

$$F(\mathbf{Q}) = \sum_{uvw} e^{i\mathbf{Q}.\mathbf{r}_{uvw}} \tag{3.36}$$

for all values of u, v and w. For any general $\mathbf{Q}$, the real and imaginary parts of $e^{i\mathbf{Q}.\mathbf{r}_{uvw}}$ will oscillate from positive to negative over the lattice, in which case $F(\mathbf{Q}) \simeq 0$. However, for any $\mathbf{Q}$ that satisfies

$$e^{i\mathbf{Q}.\mathbf{r}_{uvw}} = 1 \tag{3.37}$$

for all $\mathbf{r}_{uvw}$, we get that $F(\mathbf{Q})$ equals the total number of lattice points. For $\mathbf{Q}$ to satisfy this equation

$$\mathbf{Q} = \mathbf{G}_{hkl} = h\mathbf{a}^* + k\mathbf{b}^* + l\mathbf{c}^* \tag{3.38}$$

and then

$$\mathbf{Q} \cdot \mathbf{r}_{uvw} = 2\pi(hu + kv + lw) = 2\pi \times \text{integer} \tag{3.39}$$

The function $F(\mathbf{Q})$ is a three-dimensional set of δ-functions located at $\mathbf{Q}$ for which $\mathbf{Q} \cdot \mathbf{r}_{uvw}$ is an integral multiple of 2π. Note that any integral combination, $\mathbf{Q} = \mathbf{G}_{hkl}$, will also satisfy the reciprocal-lattice requirements to give in the limit u, v and w tending to infinity

$$F(\mathbf{Q}) = F(hkl) = \sum_{hkl} \delta(\mathbf{Q} - \mathbf{G}_{hkl}) \tag{3.40}$$

The implication of this is that the Fourier transform of the lattice is sharply peaked at the reciprocal-lattice nodes. In other words, we have shown that the Fourier transform of the direct lattice is the reciprocal lattice (and, of course, vice versa).

3.7 Form factors

Now I know what the atom looks like.

(Ernest Rutherford)

3.7.1 X-rays

In equation (3.20), the amplitude of scattering depended on a density function $\rho(\mathbf{r})$. In dealing with lattice diffraction, we effectively replaced this by the density of point scatterers. We now consider the scattering due to the electrons in an atom.

Let the vector $\mathbf{r}$, measured from the nucleus, make an angle θ with the scattering vector $\mathbf{Q}$. Then

$$\mathbf{r} \cdot \mathbf{Q} = rQ \cos\theta \tag{3.41}$$

In x-ray scattering, the quantity $\rho(r)$ is the electron density at any distance r from the atomic nucleus and is assumed to be spherically distributed about the atomic nucleus. This is generally a reasonable assumption for most purposes but does not take into account the much weaker effect of the electron clouds being distorted through bonding to neighbouring atoms. In this approximation, we therefore do not need to treat the distance r as a vector quantity.

From figure 3.39, the volume of an element at a distance r from the nucleus of an atom is $r^2 \sin\theta dr d\theta d\varphi$. The scattering factor f is then given by

$$\begin{aligned} f &= \int_{r=0}^{\infty}\int_{\varphi=0}^{2\pi}\int_{\theta=0}^{\pi} \rho(r) r^2 \sin\theta e^{iQr\cos\theta} dr d\theta d\varphi \\ &= \int_{r=0}^{\infty} \rho(r) r^2 dr \int_{\varphi=0}^{2\pi} d\varphi \int_{\theta=0}^{\pi} e^{iQr\cos\theta} \sin\theta d\theta \\ &= 2\pi \int_{r=0}^{\infty} \rho(r) r^2 dr \int_{\theta=0}^{\pi} e^{iQr\cos\theta} \sin\theta d\theta \end{aligned} \tag{3.42}$$

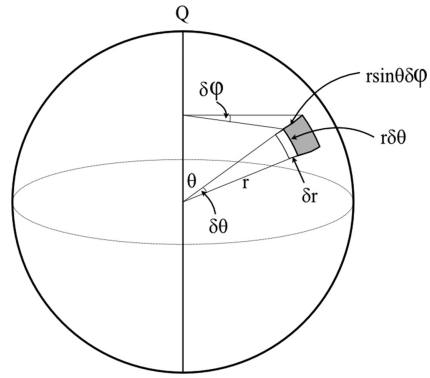

Figure 3.39. Polar coordinate system.

$\rho(r)$ is independent of the angles θ and φ, and we can write $x = \cos\theta$ and $dx = -\sin\theta d\theta$. Then

$$\int_0^{\pi} e^{iQr\cos\theta}\sin\theta d\theta = -\int_1^{-1} e^{iQrx}dx = -\left[\frac{e^{iQrx}}{iQr}\right]_1^{-1} = -\frac{1}{iQr}[e^{-iQr} - e^{iQr}] = \frac{2\sin Qr}{Qr} \tag{3.43}$$

Therefore,

$$f = 4\pi\int_0^{\infty}\rho(r)r^2\frac{\sin Qr}{Qr}dr \tag{3.44}$$

This is known as a *form factor* in general, but in x-ray crystallography, it is usually referred to as the *atomic scattering factor*. For free atoms, the electronic wave functions ψ can be calculated to good accuracy, and therefore the electron densities $|\psi\psi^*|$ can also be evaluated and the atomic scattering factors computed and tabulated. Thus, for x-rays scattered in the forward direction, $Q = 0$, all the electrons will scatter in phase, and then by l'Hôpital's rule

$$f = 4\pi\int_0^{\infty}\rho(r)r^2dr = Z_e \tag{3.45}$$

with Z_e the number of electrons in the atom[3]. As the angle of scattering 2θ increases, the diffracted waves from the electrons will destructively interfere, thus reducing the scattering factor. The atomic scattering factors can be found in standard tables, where they are usually given as a function of $\sin\theta/\lambda$.

[3] Often this is written as the atomic number, but this is only true for neutral atoms.

Note that this discussion treats the atoms as spherical and independent of one another in the unit cell. While this is adequate for most purposes, the fact is that the electron density is really extended throughout space, which is of especial importance in molecular crystals. One way to deal with this is by using multipole techniques (see the excellent review by Macchi [7]). Recently [8], an interesting new treatment that does not make the assumption of spherical atoms has been published, which should provide more precise structural information. This uses a model that takes interatomic interactions into account, and the atomic electron densities, translated to the unit-cell origin, are no longer spherical functions but are dependent on the geometry of a whole molecule. The result is that the corresponding atomic form factors are no longer real, but complex-valued functions of the reciprocal-lattice indices. Clearly, this is an area that is still growing.

In figure 3.40, the spherical scattering factors are shown plotted against sin θ/λ for different atomic and ionic species. In the left-hand diagram, you can see how the scattering factors fall off with angle, tending to level off as the angle increases. Note that hydrogen is a relatively weak scatterer, whereas the scattering power increases as the number of electrons increases.

Using the two Fourier transform guidelines, we can understand why the atomic scattering factor looks like this as a function of sin θ/λ. The electron density is taken to be spherically distributed, and so guideline 1 means that f will have isotropic symmetry in space. Guideline 2 means that for isoelectronic atoms, f will decrease with angle faster for larger *isoelectronic* atoms (more diffuse electron clouds) than for smaller isoelectronic atoms (see the right-hand diagram). For example, the Na^+ ion contains 11 protons that exert attractive forces on the 10 electrons in the ion, thus tending to pull in the electron cloud. On the other hand, Ne has 10 protons, and so the attractive effect is smaller, thus making the size of Ne greater than for Na^+. The result is that the scattering curve for Ne falls off more rapidly with angle. Similarly, F^-, which still has 11 electrons, has 9 protons making the ionic size larger, with a correspondingly faster decrease of scattering with angle.

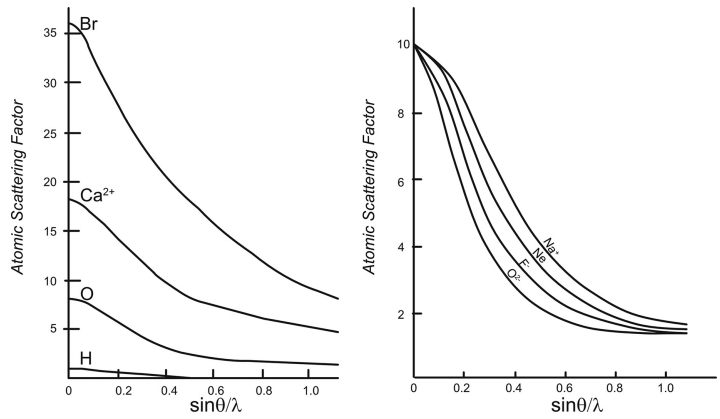

Figure 3.40. Examples of x-ray atomic scattering factors plotted as a function of sinθ/λ.

The atomic scattering factor can, in principle, be used to calculate the intensity of diffraction of x-rays by a gas of atoms. For example, Compton [9] separated the intensity into two parts, namely I_1, coherent scattering, and I_2, incoherent scattering. In this case, the intensity is given by

$$\begin{aligned} I_1 &\propto Z_e^2 f^2 \\ I_2 &\propto Z_e[1 - f^2] \end{aligned} \tag{3.46}$$

In addition to the scattering from individual atoms, there is a small extra intensity term that contains information about atom–atom distances.

3.7.2 Neutrons

The first evidence for the diffraction of neutrons was discovered in 1936 by D P Mitchell and P N Powers [10] and by Hans Heinrich von Halban (1908–64) and Peter Preiswerk (1907–72) [11]. But it was Bertram Brockhouse (1918–2003) and Clifford Shull (1915–2001) who developed neutron spectroscopy and diffraction in the 1940s and shared the Nobel Prize for this work as late as 1994. For a thorough treatment of neutron scattering, I recommend the book by Boothroyd [12].

In neutron diffraction, the scattering objects are the atomic nuclei. The neutron of mass m_N travels with a velocity v_N, and then according to the de Broglie relationship, has a wavelength given by

$$\lambda = \frac{h}{m_N v_N} \tag{3.47}$$

which for thermal neutrons is of the same order as the x-ray wavelengths used in diffraction, although their energies are very different. For example, a wavelength of approximately 0.1 nm corresponds to a neutron energy of 0.1 eV, to be compared with x-rays with energy 12.5 keV. The neutron form factor is conventionally given by b, the *scattering length*, or σ, the *scattering cross-section*. The scattering length is measured in femtometres (1×10^{-15} m) and the cross-section in barns (1×10^{-24} cm^2).

Now, if we follow the Fourier transform guidelines, the scattering will again be isotropic, as we can assume that the scattering object, the nucleus, is spherically symmetric. The nucleus is tiny compared with the electron cloud around the nucleus so that in Fourier space, the observed nuclear scattering length will persist to very high angles. So much so that it can be taken to be independent of angle. Table 3.1 gives a few example values.

In this table, coherent and incoherent scattering components are listed: the coherent terms give rise to sharp Bragg reflections. In contrast, the incoherent terms contribute to background scattering. Because the mass of a ^{1}H nucleus is almost the same as that of a neutron, it can be displaced by collision with the incoming neutron. This results in a large incoherent cross-section. Therefore, neutron diffraction from a crystal containing substantial amounts of hydrogen can be compromised by creating too much background scattering. For this reason, neutron diffraction studies of hydrogen-containing crystals are often done with the hydrogen nuclei substituted by

Table 3.1. Neutron scattering lengths and cross-sections.

Isotope	$b_{coh}(fm)$	$b_{inc}(fm)$	$\sigma_{coh}(barns)$	$\sigma_{Inc}(barns)$
^{1}H	−3.74	25.27	1.76	80.27
^{2}H	6.67	4.04	5.59	2.05
$^{16}0$	5.80	0	4.23	0
^{39}K	3.74	1.4	1.76	0.25
^{35}Cl	11.65	6.1	17.06	4.7

deuterium ^{2}H, for which the incoherent scattering length is much smaller. Note also that the nuclear scattering length can be negative, unlike x-ray form factors, signifying that the outgoing wave has the sign of its phase reversed compared with the equivalent x-ray wave. ^{39}K and ^{35}Cl nuclei have quite different scattering lengths so that, with neutron diffraction, it is easy to distinguish between the effects of these nuclei. Contrast this with the case of x-ray scattering, where the atomic scattering factors of K^+ and Cl^- ions are almost identical. For instance, an x-ray powder pattern of KCl will look like it is primitive cubic rather than face-centred cubic since the K^+ and Cl^- ions will be almost indistinguishable from one another.

There is also another type of neutron scattering that needs to be considered. The neutron possesses spin, which means it can also interact with magnetic moments, such as those due to unpaired electrons in an atom. This gives rise to an additional diffraction pattern superimposed upon the nuclear diffraction pattern. Note that in magnetic scattering, the scattering is due to the electrons around a nucleus, and so, as in x-ray diffraction, its form factor falls off rapidly with angle. The effect of magnetic neutron scattering can be particularly easily seen for antiferromagnetic crystals, where the magnetic moment may alternate in direction, thus cancelling out the net magnetization. In such cases, the magnetic moments repeat at a multiple, say double, of the repeat distance of the nuclei, thus doubling the nuclear unit cell. This leads to magnetic superstructure reflections appearing halfway between those due to the nuclear scattering.

3.7.3 Electrons

The diffraction of electrons by atoms in crystals was discovered by Clinton Davisson (1881–1958) and by George Paget Thomson[4] (1892–1975), who shared the Nobel Prize in 1937. Good introductory books on electron diffraction are by Zou, Hovmöller and Oleynikov [13], and by Grundy and Jones [14].

In electron diffraction, the scattering is via the electrons in the solid with the atoms subject to a periodic potential energy $V(\mathbf{r})$. Assuming spherically symmetric

[4] Son of Joseph John Thomson, the discoverer of the electron. It is interesting to note that while his father proposed the electron to be a particle, his son showed it was a wave! Similarly, some years earlier, W H Bragg believed that x-rays consisted of neutral particles, but his son, W L Bragg, showed that they were waves, in agreement with Laue. We now understand that quantum mechanics permits electrons and x-rays to be treated both as particles and waves.

atoms, elastic scattering, and the first Born approximation with incident electron energy $E \gg V(\mathbf{r})$

$$\begin{aligned} f^{el} &= \frac{me}{2\pi\hbar^2}\int_{-\infty}^{\infty} V(\mathbf{r})e^{i\mathbf{Q}\cdot\mathbf{r}}d^3\mathbf{r} \\ &= -\frac{me}{2\pi\hbar^2 Q^2}\int_{-\infty}^{\infty} V(\mathbf{r})\nabla^2(e^{i\mathbf{Q}\cdot\mathbf{r}})d^3\mathbf{r} \end{aligned} \tag{3.48}$$

Integrating by parts and using $V(\infty) = V(-\infty) = 0$

$$f^{el} = -\frac{me}{2\pi\hbar^2 Q^2}\int_{-\infty}^{\infty} e^{i\mathbf{Q}\cdot\mathbf{r}}\nabla^2 V(\mathbf{r})d^3\mathbf{r} \tag{3.49}$$

Using Poisson's equation relating the potential and charge distributions

$$\nabla^2 V(\mathbf{r}) = -\frac{e[Z\delta(\mathbf{r}) - \rho(\mathbf{r})]}{\varepsilon_0} \tag{3.50}$$

where $Z\delta(\mathbf{r})$ is the nuclear point charge and ε_0 is the permittivity of free space. Therefore,

$$f^{el} = \frac{me^2}{2\pi\hbar^2\varepsilon_0 Q^2}\int_{-\infty}^{\infty}[Z\delta(\mathbf{r}) - \rho(\mathbf{r})]e^{i\mathbf{Q}\cdot\mathbf{r}}d^3\mathbf{r} \tag{3.51}$$

We then obtain the Mott–Bethe formula:

$$f^{el} = \frac{me^2}{2\pi\hbar^2\varepsilon_0 Q^2}[Z - f^X] \tag{3.52}$$

where f^X is the x-ray form factor. Typically, f^{el} is in the range 1–10 Å, whereas $r^e f^X$ (r^e is the classical electron radius) is of the order of 10^{-4} Å, and so electrons are scattered more strongly than x-rays (or neutrons). Therefore, the angular range for electron scattering is very small, and hence the scattering is strongly peaked in the forward direction. For 100 keV electrons

$$\lambda = \frac{h}{\sqrt{2m_e \mathrm{V}}} = \frac{12.6}{\sqrt{\mathrm{V}}} \simeq 0.04\text{Å} \tag{3.53}$$

Therefore, assuming the atomic radius is about 1 Å,

$$\begin{aligned} \Delta\left(\frac{\sin\theta}{\lambda}\right) &= \frac{1}{2\Delta d} \\ \Delta(\sin\theta) \simeq \Delta\theta &= \frac{\lambda}{2\Delta d} = 0.02 \text{ radians} \end{aligned} \tag{3.54}$$

and

$$\Delta\theta \simeq 2 \times 10^{-2} \text{ rad} \simeq 1^\circ \tag{3.55}$$

We can also see this in terms of Fourier transforms. The periodic potential extends over an extended range. According to the guidelines, the scattered electrons

Table 3.2. Typical voltages used in electron diffraction.

V (volts)	λ(Å)	v/c	Name
10	3.9	0.006	LEED
10^2	1.2	0.02	LEED
10^3	0.39	0.06	MEED
10^4	0.12	0.19	MEED
10^5	0.037[a]	0.54	HEED
10^6	0.009[a]	0.94	HEED

[a] relativistic correction of ~5% at 10^5 volts.

will be confined to a very narrow angular range about the incident electron beam. The typical voltages (wavelengths) used in electron diffraction are shown in table 3.2 where LEED means low-energy electron diffraction, MEED medium-energy electron diffraction, and HEED high-energy electron diffraction. v/c is the fraction of the electron velocity compared with the velocity of light. For excitation voltages less than about 100 V the electrons are very strongly absorbed, and so they only penetrate a few atomic layers of a crystal. Thus, LEED tends to be used for surface studies, whereas standard transmission electron diffraction and microscopy use voltages above 10^5 V. In transmission electron diffraction, because of the high absorption, very thin crystals are customarily used.

It is instructive to consider the reciprocal lattice and the Ewald sphere construction in this case (figure 3.41). A thin sample is placed at the sample-stage position with a perpendicular incident beam of electrons in the electron microscope. Now, because the electron beam's wavelength is much smaller than that generally used with x-rays, the radius of the corresponding Ewald sphere is relatively very large, making its surface flatter. Because the crystal is thin, then according to the Fourier transform guidelines, the reciprocal-lattice points will be extended to form truncated rods in a direction perpendicular to the crystal plane. The surface of the Ewald sphere then cuts through many reciprocal-lattice rods. The result is that even though the crystal is stationary, the diffraction image shows many reflections simultaneously. In figure 3.42, the spots observed near the centre are those for which the Ewald sphere intersects the rods in the $hk0$ layer while the outer ring of spots comes from the $hk1$ layer. These circular areas of diffraction are commonly known by electron diffractionists as *Laue zones*.

3.8 Structure factors

We now turn to the calculation of diffracted intensities from the crystal structure. As usual, $F(\mathbf{Q})$ anywhere in reciprocal space is given by equation (3.20), where $\rho(\mathbf{r})$ is the volume density of the scattering material, which in x-ray diffraction is the electron density for each atom. As unit cells are repeated according to the lattice, we can write the volume density for the crystal as

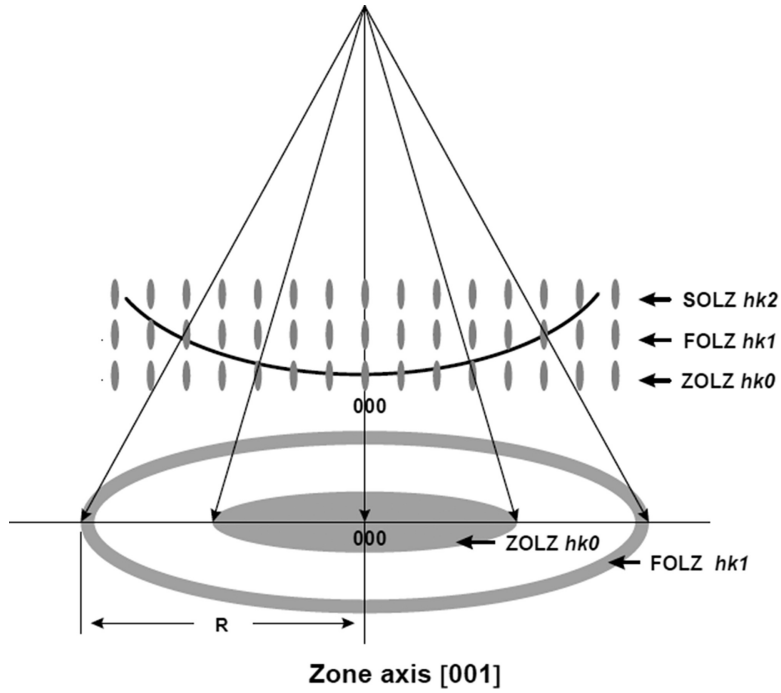

Figure 3.41. Ewald sphere construction in transmission electron microscopy (TEM). Here the *c*-axis of the crystal is perpendicular to the crystal plate. ZOLZ = zero-order Laue zone; FOLZ = first-order Laue zone; SOLZ = second-order Laue zone (from [13]).

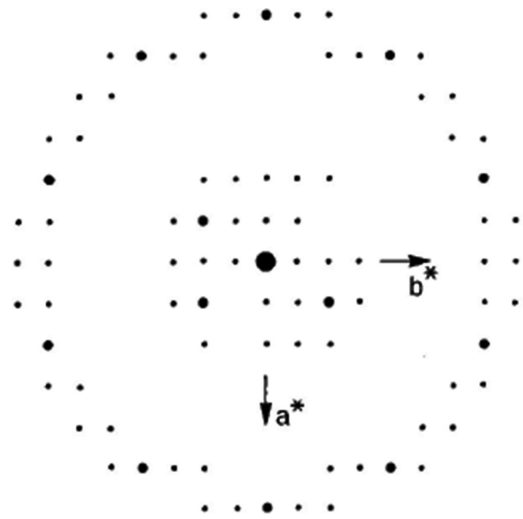

Figure 3.42. Electron diffraction image from a thin crystal.

$$\rho_{\text{crystal}}(\mathbf{r}) = \sum_{uvw} \rho_{\substack{\text{unit}\\\text{cell}}}(\mathbf{r}) \;*\; \delta(\mathbf{r} - \mathbf{r}_{uvw}) \tag{3.56}$$

Now, the Fourier transform of $\delta(\mathbf{r} - \mathbf{r}_{\text{uvw}})$ is given by $\delta(\mathbf{Q} - \mathbf{G})$. According to the convolution theorem, therefore,

$$F_{\text{crystal}}(\mathbf{Q}) = \sum_{uvw} \tilde{\rho}_{\substack{\text{unit}\\\text{cell}}}(\mathbf{r}) \times \delta(\mathbf{Q} - \mathbf{G}) \tag{3.57}$$

This is valid for a crystal with a very large number of unit cells in which particle size broadening is negligible. At the reciprocal-lattice nodes, $\mathbf{Q} = \mathbf{k}—\mathbf{k}_0 = \mathbf{G} = h\mathbf{a}^* + k\mathbf{b} + l\mathbf{c}^*$ (Laue condition). To a good approximation, we can assume that the unit-cell density can be considered a superposition of isolated, spherical atoms j located at $\mathbf{r}_j$ with respect to the unit-cell origin. Therefore,

$$\rho_{\substack{\text{unit}\\\text{cell}}}(\mathbf{r}) = \sum_j \rho_j(\mathbf{r}) * \delta(\mathbf{r} - \mathbf{r}_j) \tag{3.58}$$

and so for a unit cell

$$F(\mathbf{Q}) = \tilde{\rho}_{\substack{\text{unit}\\\text{cell}}}(\mathbf{r}) = \sum_j \tilde{\rho}_j(\mathbf{r}) \times \delta(\mathbf{Q} - \mathbf{G}) = \sum_j f_j e^{\mathbf{Q}\cdot\mathbf{r}_j} \tag{3.59}$$

where

$$\begin{aligned} \mathbf{Q} \cdot \mathbf{r}_j = \mathbf{G} \cdot \mathbf{r}_j &= (h\mathbf{a}^* + k\mathbf{b}^* + l\mathbf{c}^*) \cdot (x_j\mathbf{a} + y_j\mathbf{b} + z_j\mathbf{c}) \\ &= 2\pi(hx_j + ky_j + lz_j) \end{aligned} \tag{3.60}$$

from which we get

$$F(hkl) = \sum_j f_j e^{2\pi i(hx_j + ky_j + lz_j)} \tag{3.61}$$

Definition. *F(h k l) is known as the* ***structure factor****, and its modulus |F(h k l)| is known as the* ***structure amplitude****.*

The structure factor can also be written as

$$\begin{aligned} F(hkl) &= \sum_j f_j \;\cos 2\pi(hx_j + ky_j + lz_j) \\ &\quad + i\sum_j f_j \;\sin 2\pi(hx_j + ky_j + lz_j) \\ &= A(hkl) + iB(hkl) \end{aligned} \tag{3.62}$$

and then the phase angle is given by

$$\tan \phi(hkl) = \frac{B(hkl)}{A(hkl)} \tag{3.63}$$

This gives

$$F(hkl) = |F(hkl)|e^{i\phi} \tag{3.64}$$

For a centrosymmetric crystal, in which the unit-cell origin is chosen to lie on a centre of inversion, for every x, y, z, there is an equivalent atom at $-x$, $-y$, $-z$. Therefore, the sine terms vanish, and one can write the structure factor as

$$F(hkl) = 2\sum_j f_j \cos 2\pi(hx_j + ky_j + lz_j) \tag{3.65}$$

where the summation is over one half of the centrosymmetrically-related atoms and $\phi = 0$ or 180°. The structure factor is then

$$F(hkl) = \pm|F(hkl)| \tag{3.66}$$

For non-centrosymmetric crystals, the phase angle can have any value.

We saw in figure 3.25 that the diffraction image is found on the back-focal plane of a lens and that every point was receiving information from the whole of the scattering object. This is true even for a lens-less system, such with x-ray and neutron diffraction, since the diffraction pattern is determined by the Fourier transform of the scattering object. You may be wondering whether this means that scattering by *all* the atoms in the crystal contributes to the intensity seen at any single reciprocal node. The answer to this is yes, it does! Recall that the Fourier transform function (appendix E) involves an integration over the whole of one vector space to calculate a value at a single point in the other vector space. By making use of crystal periodicity, we can calculate the amplitude via the contents of a unit cell, i.e., use the structure factor formula (3.61). To obtain the correct intensity of a single reflection, all the atomic positions and scattering factors in the unit cell are added together. Miss one atom out, and you get the wrong answer, so scattering from every atom in the unit cell (and hence the crystal) contributes to each individual reflection, even to those that calculate to have zero intensity. Therefore, in principle, any single reflection contains information derived from all the atoms in the *entire* crystal. Of course, to form a meaningful image of the crystal structure, one needs to combine data from several reflections in order to obtain a sufficient degree of structural resolution.

3.9 Thermal scattering

So far, we have considered the atoms to be fixed in space. However, we also know that the atoms must vibrate within the crystal, with amplitudes depending on the temperature.

To include the effect of temperature, consider the atoms as being slightly displaced from their time-averaged positions $\mathbf{r}_n$ by a small amount, $\mathbf{u}_n$. Assume also that the average $\langle \mathbf{u}_n \rangle = 0$. The intensity of scattering, according to equation (3.19), is then given by

$$\begin{aligned} I &\propto \left\langle \sum_m f(\mathbf{Q}) e^{i\mathbf{Q}\cdot(\mathbf{r}_m+\mathbf{u}_m)} \sum_n f(\mathbf{Q}) e^{-i\mathbf{Q}\cdot(\mathbf{r}_n+\mathbf{u}_n)} \right\rangle \\ &= \sum_m \sum_n f^2(\mathbf{Q}) e^{i\mathbf{Q}\cdot(\mathbf{r}_m-\mathbf{r}_n)} \langle e^{i\mathbf{Q}\cdot(\mathbf{u}_m-\mathbf{u}_n)} \rangle \\ &= \sum_m \sum_n f^2(\mathbf{Q}) e^{i\mathbf{Q}\cdot(\mathbf{r}_m-\mathbf{r}_n)} \langle e^{iQ(u_m-u_n)} \rangle \end{aligned} \tag{3.67}$$

The last line follows if we assume that u_m and u_n are components of the displacements parallel to the scattering vector $\mathbf{Q}$. Since the displacements are small, we can write that

$$\begin{aligned} \langle e^{iQ(u_m-u_n)} \rangle &= \langle e^{ix} \rangle = \langle 1 + ix - \tfrac{1}{2}x^2 \ldots \rangle \simeq \langle 1 - \tfrac{1}{2}x^2 \rangle \simeq e^{-\frac{1}{2}\langle x^2 \rangle} \\ &= e^{-\frac{1}{2}\langle [Q(u_m-u_n)]^2 \rangle} = e^{-\frac{1}{2}Q^2\langle u_m^2 \rangle} e^{-\frac{1}{2}Q^2\langle u_n^2 \rangle} e^{Q^2\langle u_m u_n \rangle} \end{aligned} \tag{3.68}$$

The last term can be written as

$$e^{Q^2\langle u_m u_n \rangle} = 1 + [e^{Q^2\langle u_m u_n \rangle}] - 1 \tag{3.69}$$

We then split the scattered intensity into two terms

$$\begin{aligned} I \propto & \sum_m \sum_n f^2(\mathbf{Q}) e^{i\mathbf{Q}\cdot\mathbf{r}_m} e^{-\frac{1}{2}Q^2\langle u_m^2 \rangle} e^{-i\mathbf{Q}\cdot\mathbf{r}_n} e^{-\frac{1}{2}Q^2\langle u_n^2 \rangle} \\ & + \sum_m \sum_n f^2(\mathbf{Q}) e^{i\mathbf{Q}\cdot\mathbf{r}_m} e^{-i\mathbf{Q}\cdot\mathbf{r}_n} [e^{Q^2\langle u_m u_n \rangle} - 1] \end{aligned} \tag{3.70}$$

The first term is recognizable as the elastic scattering given by the usual structure factor in which the form factor for an atom has been replaced by

$$f \to f(\mathbf{Q}) e^{-\frac{1}{2}Q^2\langle u^2 \rangle} \equiv f(\mathbf{Q}) e^{-M} \tag{3.71}$$

The exponential term is known as the *Debye–Waller* factor, where

$$M = 8\pi^2 \langle u^2 \rangle \sin^2 \theta / \lambda^2 = B_T \left(\frac{\sin \theta}{\lambda} \right)^2 \tag{3.72}$$

The structure factor then becomes

$$F(hkl) = \sum_j f_j e^{-M} e^{2\pi i(hx_j + ky_j + lz_j)} \tag{3.73}$$

As temperature rises, the Debye–Waller factor generally increases as the atomic displacements increase. Note that this multiplies the form factor in the structure factor formula and so does not change the widths of the reflections but reduces their intensities towards high angles. You can see this in figure 3.43. The consequence of this is that crystallographers often cool their crystals to be able to collect more data at a high angle and thus achieve higher resolution when solving for the crystal structure.

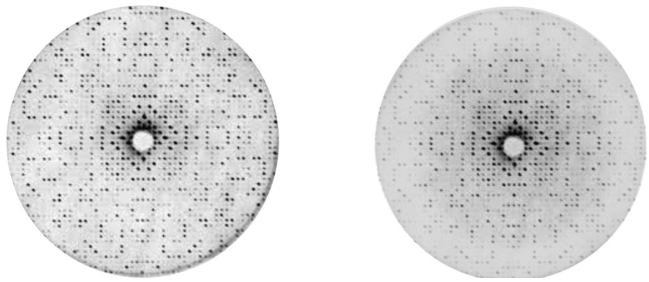

Figure 3.43. Effect on a diffraction pattern of raising the temperature. Left: room temperature, right: high temperature.

I think that it is instructive to see how this can be explained by using the convolution theorem. The position of all vibrating atoms in the basis can be thought of as being slightly smeared with respect to their average positions. This thermal motion can be simulated by introducing a 'smearing' function, $\Omega(\mathbf{r})$, which is convoluted with all the atoms in the basis, $B(\mathbf{r})$. $\Omega(\mathbf{r})$ depends on many factors. It is approximately inversely proportional to chemical bonding forces and the atomic mass, but it is proportional to temperature. The crystal is described by

$$C(\mathbf{r}) = L(\mathbf{r}) * [B(\mathbf{r}) * \Omega(\mathbf{r})] \tag{3.74}$$

and then the Fourier transform is given by

$$\tilde{C}(\mathbf{Q}) = \tilde{L}(\mathbf{Q}) \times \tilde{B}(\mathbf{Q}) \times \tilde{\Omega}(\mathbf{Q}) \tag{3.75}$$

If $\Omega(\mathbf{r})$ has spherical symmetry, its Fourier transform will be isotropic (guideline 1) and fall off with scattering angle. Because of the multiplication by $\tilde{\Omega}(\mathbf{Q})$, this means that high-angle reflections will be reduced in intensity, but the peak widths will be unaffected. The higher the temperature, the larger $\Omega(\mathbf{r})$, and, correspondingly, $\tilde{\Omega}(\mathbf{Q})$ will be smaller (guideline 2), and the fall-off steeper with angle.

The Debye–Waller factor acts as a global thermal vibration term for the crystal. However, it is possible in crystal-structure determination to refine independent isotropic temperature factors for each atom separately. Also, with a good structure determination, anisotropic temperature factors T_j can be refined for each atom. These are given by

$$T_j = \exp\begin{bmatrix} -\tfrac{1}{2}(U_{11}h^2a^{*2} + U_{22}k^2b^{*2} + U_{33}l^2c^{*2} + 2U_{23}klb^*c^* \\ + 2U_{31}lhc^*a^* + 2U_{12}hka^*b^*) \end{bmatrix} \tag{3.76}$$

The six U_{ij} terms define a tensor of rank 2 for an atom at a general position and are represented by a probability ellipsoid. For atoms at special positions, the number of independent U_{ij} terms is reduced, but for an atom at a general position, six values need to be determined (three diagonal and three off-diagonal). Figure 3.44 shows an example of thermal ellipsoids that have been refined for the crystal structure of quartz in space group $P3_221$. Note how the vibrational amplitudes of the oxygens are greater than for the heavier silicon atoms.

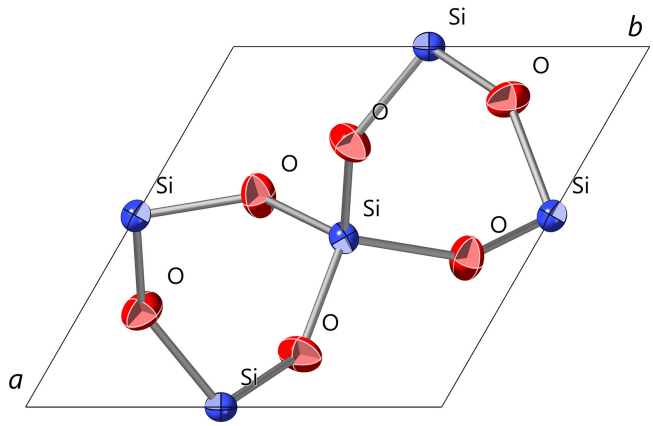

Figure 3.44. Crystal structure of quartz projected on (001) showing anisotropic thermal ellipsoids at 75% probability. Silicon on 2-fold axes (three independent terms): oxygen at general positions (six independent terms).

These days, the thermal factors are better called *displacement parameters*: *isotropic* or *anisotropic displacement parameters*. This is because, unless one is sure that they are thermal in origin, similar probability distributions are found when the atoms exhibit disorder that is not of thermal origin. For instance, if an atom occupies a slightly different position from unit cell to unit cell, solution of the crystal structure using the reflection intensities will give its average position but with a large displacement parameter. Without experiments to prove whether the disorder is thermal or static in origin, the IUCr prefers not to use the term *thermal*.

The second term in (3.70) has a different character. It gives rise to an intensity that increases as the mean-squared displacements increase and has a width determined by the correlations $\langle u_m u_n \rangle$ between the displacements of different atoms. The correlations tend to occur only over a few unit cells, and the scattering widths are greater than that of a Bragg peak. This is known as *thermal diffuse scattering*, or TDS for short. TDS is often ignored as it is much weaker than the usual Bragg scattering. Figure 3.45 shows TDS observed in an electron microscope for a crystal of strontium titanate. Again, in some cases, the observed diffuse scattering may not be due to thermal vibrations, but instead to disordering of the atoms (either displacement or substitutional disorder) with some degree of correlation between them (discussed later in section 3.15).

Finally, although the above theory of thermal scattering is found in many standard textbooks, for example, in Als-Nielsen and McMorrow [16], it has been questioned by Castellano and Main [17]. They argue that the physical model is too simple and is incompatible with the concept of probability ellipsoids. Instead, they consider the atomic oscillators to follow a Boltzmann-like distribution as a function of energy. The probability density can then be cast as a normalized Gaussian function:

$$P(u) = (2\pi\langle u^2\rangle)^{-½} e^{-u^2/2\langle u^2\rangle} \tag{3.77}$$

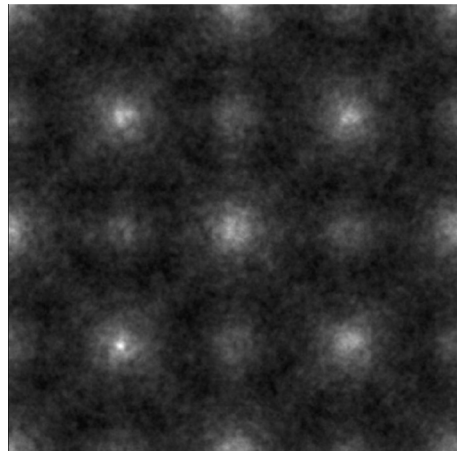

Figure 3.45. Thermal diffuse scattering in $SrTiO_3$ in electron diffraction. Reproduced from [15] with permission from Elsevier.

where $\langle u^2 \rangle$ is the average of u^2 for each atom over the whole range of energies. The application of this formula leads to the result (3.72). They conclude that it is the spatial average over a large number of oscillators with a Boltzmann distribution of energy that yields the Debye–Waller factor, and not the time-average over a single oscillator.

3.10 Intensities of reflections

The intensity of a reflection is given by equation (3.19), where the constant of proportionality is a scale factor that has to be determined usually by experiment. The full formulae, adapted from Zachariasen [18], for the integrated intensities are given in table 3.3.

If all measurements are on the same scale (after any geometric/polarisation corrections have been made), one obtains a list of *relative* intensities. Furthermore, to be correct, the measurement of the reflection intensity needs to be made by integration over the whole of a Bragg peak. Note that the height of a Bragg peak is proportional to the square of the number of atoms/molecules in the crystal. At the same time, the angle-integrated intensity is proportional to their number and inversely proportional to the size of the unit cell (see appendix E).

To calculate the relative intensity, it is necessary first to work out a value for the structure factor. Consider the diamond crystal structure (1.6.3.5), which contains eight carbon atoms in a face-centred cubic unit cell. It would be straightforward to use the structure factor formula and sum over all eight atoms. However, by making use of the convolution theorem, we can simplify the process using equation (3.26):

$$F(hkl) = \left[f_C + f_C e^{i\pi\left(\frac{h+k+l}{2}\right)} \right] [1 + e^{i\pi(h+k)} + e^{i\pi(h+l)} + e^{i\pi(k+l)}] \tag{3.78}$$

The first term is the Fourier transform of the basis alone, and this is multiplied by the second term, which is the transform of the all-face-centred lattice. This second term

Table 3.3. Integrated intensities.

Laue method	$I(hkl) = I_o v \left(\frac{e^2}{m_e c^2 V}\right)^2 p \frac{\lvert F(hkl)\rvert \lambda^4}{2 \sin^2 \theta}$
Rotating single crystal	$I(hkl) = I_o v \left(\frac{e^2}{m_e c^2 V}\right)^2 p \frac{\lvert F(hkl)\rvert \lambda^3}{\sin \psi \cos \varphi \cos \chi} \Delta\lambda$
Powder method	$I(hkl) = I_o v \left(\frac{e^2}{m_e c^2 V}\right)^2 p \frac{\lvert F(hkl)\rvert \lambda^3}{4 \sin \theta} \Delta\lambda$

I_0	Incident intensity
v	Unit-cell volume
V	Crystal volume
p	Polarization factor (= 1 for neutron diffraction, $(1 + \cos^2 2\theta)/2$ from a conventional x-ray tube)
$\Delta\lambda$	Spectral width
ψ, φ, χ	Diffractometer angles $\cos 2\theta = \cos\psi \cos\varphi \cos\chi + \sin\psi \sin\chi$

$$1 + e^{i\pi(h+k)} + e^{i\pi(h+l)} + e^{i\pi(k+l)} \neq 0 \tag{3.79}$$

provided that h, k and l are all even or all odd integers. Because the two terms are multiplied together, this condition will be valid for *any* all-face-centred crystal, irrespective of any crystal system or basis. This is a general condition that used to be known as a *systematic absence*, although today, the ITA prefers to refer to allowed *reflection conditions*. This can be used, therefore, to identify the lattice type of any crystal, just by searching for those reflections that are unobserved. Generalizing this to all lattice types, we obtain table 3.4.

In addition to lattice absences, non-symmorphic symmetry operations also can give rise to cancellations of intensity. For example, consider a screw axis along $[001] = \{2_{001}|0,0,½\}$. This affects every atom in the unit cell, and so each atom in the basis at x, y, z has an equivalent one at $\bar{x}$, $\bar{y}$, $z+½$. Therefore, we can write for each atom j in the unit cell the exponential term as

$$e^{2\pi i(hx_j+ky_j+lz_j)} + e^{2\pi i(-hx_j-ky_j+lz_j+lz_j/2)} \tag{3.80}$$

This equals zero for any reflection $00l$ with l odd. Similar conditions apply to glide operations. Table 3.5 gives examples of reflection conditions for several non-symmorphic operations. It is by searching for absent reflections in the diffraction pattern, whether due to the lattice type and/or to non-symmorphic operations, that the crystallographer finds clues to the likely space group of a crystal. This is usually the first step in determining the crystal structure.

Note that the reflection condition for any all-face-centred F lattice means that reflections such as 100, 010, 001, 111, 211, etc, will be absent in the diffraction pattern (these points in reciprocal space will be missing). Figure 3.46 shows what

Table 3.4. List of allowed lattice reflection conditions.

Lattice	Lattice points	$F(hkl)$	Reflection conditions
P	0,0,0	1	None
I	0,0,0 ½,½,½	$1 + \exp[\pi i(h + k + l)]$	$h+k+l = 2n$
F	0,0,0 ½,½,0 ½,0,½ 0,½,½	$1 + \exp[\pi i(h + k) + \pi i(k + l) + \pi i(l + h)]$	*h, k, l all even or all odd*
A	0,0,0 0,½,½	$1 + \exp[\pi i(k + l)]$	$k + l = 2n$
B	0,0,0 ½,0,½	$1 + \exp[\pi i(h + l)]$	$h + l = 2n$
C	0,0,0 ½,½,0	$1 + \exp[\pi i(h + k)]$	$h + k = 2n$
R_{obverse} (hexagonal axes)	0,0,0 ⅔,⅓,⅓ ⅓,⅔,⅔	$1 + \exp\left[1 + \pi i\left(\frac{4}{3}h + \frac{2}{3}k + \frac{2}{3}l\right) + \pi i\left(\frac{2}{3}h + \frac{4}{3}k + \frac{4}{3}l\right)\right]$	$-h + k + l = 3n$
R_{reverse} (hexagonal axes)	0,0,0 ⅓,⅔,⅓ ⅔,⅓,⅔	$1 + \exp\left[1 + \pi i\left(\frac{2}{3}h + \frac{4}{3}k + \frac{2}{3}l\right) + \pi i\left(\frac{4}{3}h + \frac{2}{3}k + \frac{4}{3}l\right)\right]$	$h - k + l = 3n$

Table 3.5. Some examples of reflection conditions for non-symmorphic operations.

Operation	Seitz operator	Reflection type	Reflection condition
a-glide	$\{m_{001}\|(½,0,0)\}$	$hk0$	$h = 2n$
b-glide	$\{m_{001}\|(0,½,0)\}$	$hk0$	$k = 2n$
n-glide	$\{m_{001}\|(½,½,0)\}$	$hk0$	$h + k = 2n$
d-glide	$\{m_{001}\|(¼,\pm¼,0)\}$	$hk0$	$h + k = 4n$ (h, $k = 2n$)
2_1 screw	$\{2_{100}\|(½,0,0)\}$	$h00$	$h = 2n$
2_1 screw	$\{2_{010}\|(0,½,0)\}$	$0k0$	$k = 2n$
2_1 screw	$\{2_{001}\|(0,0,½)\}$	$00l$	$l = 2n$
3_1 screw	$\{3_{001}\|(0,0,⅓)\}$	$00l$	$l = 3n$
4_1 screw	$\{4_{001}\|(0,0,¼)\}$	$00l$	$l = 4n$
6_1 screw	$\{6_{001}\|(0,0,⅙)\}$	$00l$	$l = 6n$
6_2 screw	$\{6_{001}\|(0,0,⅓)\}$	$00l$	$l = 3n$
6_3 screw	$\{6_{001}\|(0,0,½)\}$	$00l$	$l = 2n$

happens to the reciprocal lattice when this condition applies. The black points are the reciprocal-lattice points for which the indices are either all odd or all even, whereas the open circles represent those points that are not allowed.

It can be seen that the unit cell in reciprocal space has become body-centred. In other words, the Fourier transform of an all-face-centred lattice is a body-centred lattice and vice versa. Therefore, there are the following symmetry relationships between real and reciprocal lattices.

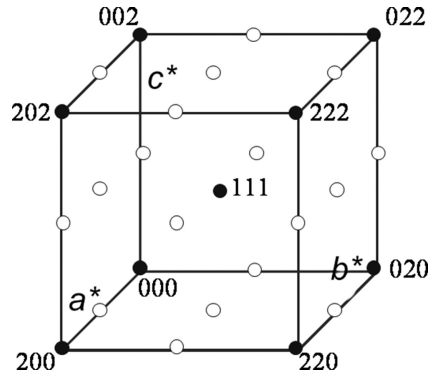

Figure 3.46. A reciprocal unit cell for an all-face-centred direct lattice. Open circles denote points that are missing in the reciprocal lattice, where *h k l* are not all even or all odd. Closed circles are for *h k l* that are all even or all odd. The result is that the reciprocal unit cell is body-centred.

$$\begin{aligned} P &\leftrightarrow P \\ A &\leftrightarrow A \\ B &\leftrightarrow B \\ C &\leftrightarrow C \\ I &\leftrightarrow F \\ F &\leftrightarrow I \end{aligned}$$

Returning now to equation (3.78), let us take a closer look at the first term, the basis transform, and ask the question whether this too can become equal to zero. In other words, we wish to determine the conditions when

$$f_C\left[1 + e^{i\pi\left(\frac{h+k+l}{2}\right)}\right] = 0 \tag{3.81}$$

Multiplying this term by its complex conjugate to calculate the intensity contribution

$$\left[1 + e^{i\pi\left(\frac{h+k+l}{2}\right)}\right]\left[1 + e^{-i\pi\left(\frac{h+k+l}{2}\right)}\right] = 2 + 2\cos\pi\left(\frac{h+k+l}{2}\right) = 0 \tag{3.82}$$

whence

$$\begin{aligned} &\cos\pi\left(\frac{h+k+l}{2}\right) = -1 \\ \therefore \quad &\frac{h+k+l}{2} = 2n+1 \\ \text{or} \quad &h+k+l = 4n+2 \end{aligned} \tag{3.83}$$

Thus, reflections like 222 will be absent in the diffraction pattern. This is not a lattice condition, but a special condition caused by accidental cancellation of terms in the basis transform, and so is specific to the diamond type of structure. If we change the

two carbon atoms in the basis so that they are different, for example, In and As, then the 222 reflection would be allowed, but the all-face-centring lattice conditions would still apply.

By the way, the fact that the 222 reflection is missing for this structure is useful in the design of crystal monochromators. For example, a Si or Ge crystal cut on the (111) plane is often used because a white beam of radiation incident on it will, in general, pass intensity corresponding to the wavelengths λ, $\lambda/2$, $\lambda/3$, etc. Because the 222 intensity is equal to zero, the harmonic intensity due to $\lambda/2$ will not be present, and the higher harmonics will be sufficiently weak so as not to contribute too much. However, the absence of the 222 intensity is not strictly true. A very weak 222 signal can be seen by x-ray diffraction. This is believed to arise from an asymmetry in the electron cloud around each carbon nucleus (the atomic scattering factor is based on the assumption that the atom is spherical). Such asymmetry arises from anharmonic vibrations and the bond charge distribution. Therefore, the weakly allowed 222 x-ray reflection in silicon can be useful for studying bond charges.

Consider, now, the difference in x-ray and neutron powder diffraction patterns for KCl, which we know to have an all-face-centred cubic lattice. This is shown in figure 3.47. Note that the neutron pattern appears to show more peaks than the x-ray pattern. Table 3.6 shows the measured 2θ values for the x-ray pattern.

To index the lines, first of all, convert the 2θ values to interplanar spacings d using Bragg's Law and then construct the set of $1/d^2$. As we know that KCl is cubic, we can then find the ratios of these values (rounded to the nearest integer), and then the indices from

$$h^2 + k^2 + l^2 = \frac{a^2}{d^2} = \text{Ratio} \tag{3.84}$$

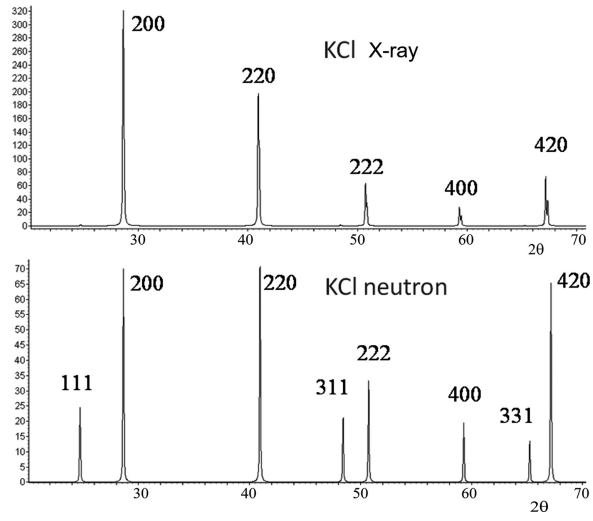

Figure 3.47. Computed powder diffraction patterns for KCl using x-rays and neutrons. λ = 1.5418 Å. The splitting seen for peaks in the x-ray pattern, especially as 2θ increases, arises from the fact that the x-ray beam is a close doublet $CuK\alpha_1$ and $CuK\alpha_2$, with λ = 1.54051 Å and 1.54403 Å, respectively.

Table 3.6. Indexing of KCl x-ray powder pattern.

$2\theta°$	d (Å)	$1/d^2$ (Å^{-2})	Integer ratio	$h\ k\ l$
28.642	3.114	0.1031	1	100
40.951	2.202	0.2062	2	110
50.74	1.798	0.3094	3	111
59.30	1.557	0.4125	4	200
67.16	1.393	0.5156	5	210

This list of indices suggests that KCl is primitive cubic with $a = 3.114$ Å. However, if we repeat the process with neutron data, the sequence of $h\ k\ l$ values is now 111, 200, 220, 311, 222, 400, 331 and 420. These indices are all even or odd, indicating that the lattice is all-face-centred and $a = 6.228$ Å. Therefore, the indices used in the x-ray pattern need to be doubled to be consistent with the neutron data. The cause of this difference is that x-rays are unable to distinguish easily between scattering by K^+ and Cl^- ions since they each contain the same numbers of electrons and hence have very similar x-ray atomic scattering factors. Had the diffraction pattern been from, say, NaCl, which is of the same structure type, this ambiguity would not occur.

3.11 Laue classes

An aspect of the symmetry of diffraction patterns is that, to a first approximation, they appear to be centrosymmetric. We can see this as follows. Consider the structure factors for reflections $h\ k\ l$ and $\bar{h}\ \bar{k}\ \bar{l}$:

$$F(hkl) = \sum_j f_j e^{2\pi i(hx_j+ky_j+lz_j)} \tag{3.85}$$

and

$$F(\bar{h}\bar{k}\bar{l}) = \sum_j f_j e^{-2\pi i(hx_j+ky_j+lz_j)} \tag{3.86}$$

But the intensity is proportional to the structure factor multiplied by its complex conjugate, whence

$$I(hkl) \propto F(hkl)F(hkl)^* = F(\bar{h}\bar{k}\bar{l})F(\bar{h}\bar{k}\bar{l})^* \tag{3.87}$$

Therefore, $I(hkl) = I(\bar{h}\bar{k}\bar{l})$, and so the diffraction pattern appears to be centrosymmetric. This is known as *Friedel's Law*.

This implies that the crystal diffraction pattern appears to be centrosymmetric, even when the crystal is non-centrosymmetric. Thus, if a series of diffraction images are taken to determine the symmetry of the crystal, it is not always easy to determine whether a crystal is centrosymmetric or not. Diffraction, therefore, has the effect of adding a centre of inversion to the point group of the crystal. This means that one can only distinguish directly between the 11 centrosymmetric groups. We may therefore

Table 3.7. The 11 Laue classes (the centrosymmetric groups are marked in bold).

Triclinic	Monoclinic	Orthorhombic	Tetragonal	Trigonal	Hexagonal	Cubic
1	2	222	4	3	6	23
	m	*mm*2	$\bar{4}$		$\bar{6}$	
$\bar{1}$	**2/*m***	***mmm***	**4/*m***	**$\bar{3}$**	**6/*m***	***m*$\bar{3}$**
			422	32	622	432
			4*mm*	3*m*	6*mm*	
			$\bar{4}$2*m*		$\bar{6}$*m*2	$\bar{4}$3*m*
			4/*mmm*	***$\bar{3}$m***	**6/*mmm***	***m*$\bar{3}$*m***

classify each of the 32 point groups as members of *Laue classes*. For instance, point groups 4 and $\bar{4}$ belong in the same Laue class denoted by 4/*m*, i.e., the diffraction pattern from a crystal having 4 or $\bar{4}$ symmetry will appear to show 4/*m* symmetry.

In table 3.7 the 11 laue classes with all the point groups associated with them are listed. Note that, in the 1965 edition of the International Tables, the term 'Laue groups' was defined as 'groups of point groups that become identical when a centre of symmetry is added to those that lack it'. However, the collections of point groups associated in each Laue class taken together do *not* strictly constitute groups in the mathematical sense. The more recent editions of the International Tables do not, however, make this mistake.

3.12 Anomalous dispersion

In discussing the atomic scattering factor for x-rays, we need to consider what happens when x-rays are strongly absorbed by the electrons in an atom. The effect is to cause the electrons to undergo inter-shell transitions at specific energies.

Consider the formula for the standard damped harmonic motion of a classical electron in an oscillating electric field $E_0e^{i\omega t}$:

$$\ddot{x} + \gamma\dot{x} + \omega_0^2 = \frac{e}{m_e}E_0e^{i\omega t} \tag{3.88}$$

γ is a damping constant, and ω_0 is the resonant frequency of the bound electron. If we take the solution to be of the form

$$x = x_0e^{i\omega t} \tag{3.89}$$

we then get

$$x = \frac{e}{m_e}\left(\frac{E_0e^{i\omega t}}{\omega_0^2 - \omega^2 + i\gamma\omega}\right) \tag{3.90}$$

x then characterises an oscillating electron dipole, which acts as a source of scattered electromagnetic radiation. Seen from a large distance, R, the wave can be thought of as spherical, and its electric vector in the plane perpendicular to the dipole is $\omega^2/c^2|\mathbf{R}|$

times the dipole moment ex at the time $t - |\mathbf{R}|/c$. Then the amplitude of the scattered wave is

$$\frac{e^2}{m_e c^2}\left(\frac{\omega^2 E_0}{\omega_0^2 - \omega^2 + i\gamma\omega}\right) \tag{3.91}$$

The atomic scattering factor f is given by the ratio of the amplitude scattered by the oscillator to that scattered by a free classical electron, where $\omega_0 = 0$ and $\gamma = 0$. The amplitude for the free electron therefore is

$$-\frac{e^2}{m_e c^2}E_0 \tag{3.92}$$

which means that the wave scattered by the free electron in the forward direction has the opposite phase to that of the incident wave. Therefore, we find that for a positive value of f

$$f = \frac{\omega^2}{\omega_0^2 - \omega^2 + i\gamma\omega} \tag{3.93}$$

We can then generalize the formula for the atomic scattering factor as

$$f = f_0 + \Delta f' + \Delta f'' \tag{3.94}$$

where f_0 is the Fourier transform of the electron distribution in the atom. $\Delta f'$ is a real quantity, while $\Delta f''$ is imaginary. This is known as *anomalous dispersion* or *resonant scattering*.

Figure 3.48 shows a plot of the real and imaginary anomalous dispersion terms as a function of wavelength for the metal platinum. Provided that one is not close to one of the dipole resonances, the second and third terms are relatively small and can be ignored. However, when working with x-rays close to the absorption edge for a particular atom, the additional terms do become important. Because of the imaginary term, $\Delta f''$, Friedel's Law no longer holds true.

Figure 3.49 shows, in an Argand diagram, the effect of having a unit cell with two atoms, one of which has $\Delta f'' = 0$ and another with $\Delta f'' > 0$. $F1(h)$ is the structure factor component from the first atom for reflection $h\ k\ l$ and $F1(-h)$ the structure factor for reflection $\bar{h}\bar{k}\bar{l}$. Adding the contribution from the second atom, to these vectors are added $F'2(h)$ and $F'2(\text{-}h)$, the real parts of the structure factors for atom 2. The red arrows are the corresponding vectors $F''2(h)$ and $F''2(-h)$ for the imaginary contributions to the structure factors of atom 2. Finally, the green arrows are the resultant vectors for the total structure factors in each case. Notice that they are different in length, thus breaking Friedel's Law.

The breaking of the centre of symmetry of the diffraction pattern can be used, for instance, to determine, in a structurally polar crystal, such as a ferroelectric, which way certain atoms are displaced in order to link this with the sign of the macroscopic polarisation. Similarly, it can be used to differentiate between two isostructural optically-active chiral materials (i.e., those that rotate the plane of polarised light either to the right or to the left). In 1951, Johannes Martin Bijvoet (1892–1980) and

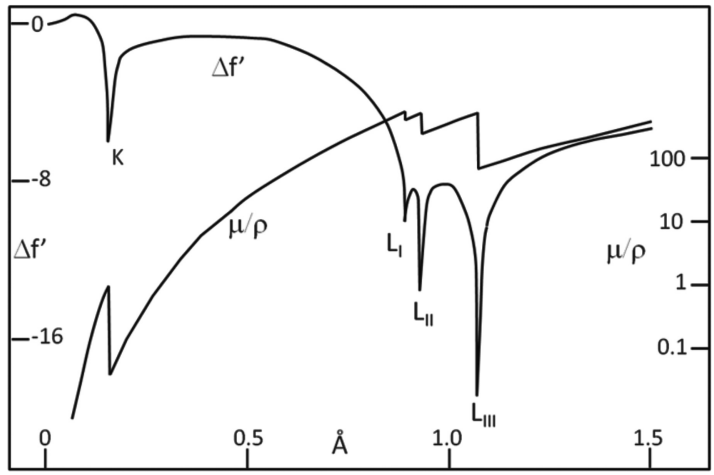

Figure 3.48. Theoretical x-ray dispersion corrections for platinum. $\Delta f'$ is effectively measured in numbers of electrons. μ/ρ is the mass absorption coefficient in cm^2/g and is proportional to $\Delta f''$. Reprinted from [19].

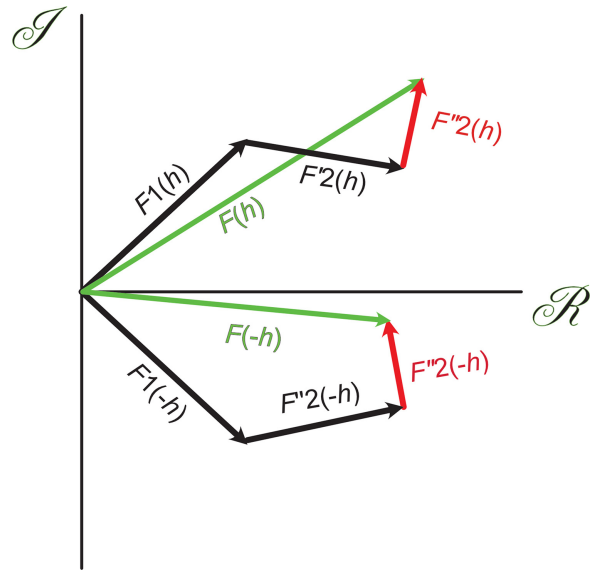

Figure 3.49. Argand diagram illustrating the effect of an anomalous dispersion contribution.

his research group used this anomalous scattering effect to determine successfully for the first time the absolute configuration of an optically-active crystal, sodium rubidium tartrate. A more recent example is that of $LiIO_3$ [20]. Anomalous dispersion with multiple wavelengths (multi-wavelength anomalous dispersion, MAD) has been used to solve the phase problem for complex protein structures with thousands of atoms in a unit cell.

3.13 Solution of crystal structures

I miss the old days when nearly every problem in x-ray crystallography was a puzzle that could be solved only by much thinking.

(Linus Pauling)

3.13.1 The phase problem

To determine crystal structures (see [21–23]), i.e., the location of all the atomic positions in a crystal, we need to calculate the density $\rho(xyz)$ at any place in the unit cell from the known structure factors using the standard Fourier transformation formula:

$$\rho(\mathbf{r}) = \frac{1}{(2\pi)^3}\int F(\mathbf{Q})e^{-i\mathbf{Q}\cdot\mathbf{r}}d^3\mathbf{Q} \tag{3.95}$$

Notice the minus sign in the exponent: this is because we are now changing from reciprocal space back to direct space. Thus, corresponding to the structure factor formula (3.85), we can write

$$\rho(xyz) = \frac{1}{V}\sum_{\bar{h}\bar{k}\bar{l}}^{hkl} F(hkl)e^{-2\pi i(hx+ky+lz)} \tag{3.96}$$

V is the volume of the unit cell. Note that the summation is over all reflections from $\bar{h}\bar{k}\bar{l}$ to hkl, i.e., over all possible reflections.

In x-ray diffraction, $\rho(xyz)$ is the electron density at the point (x,y,z) in the unit cell. In neutron diffraction, it is the nuclear density. This formula is not particularly convenient in its present form for calculating the electron density in practice and can be simplified. Consider the term in the summation in (3.96)

$$F(hkl)e^{-2\pi i(hx+ky+lz)} = e^{-2\pi i(hx+ky+lz)}\sum_j f_j e^{2\pi i(hx_j+ky_j+lz_j)} \tag{3.97}$$

which can be written as

$$\{\cos 2\pi(hx + ky + lz) - i\sin 2\pi(hx + ky + lz)\}\{A(hkl) + iB(hkl)\} \tag{3.98}$$

where

$$\begin{aligned} A(h\ k\ l) &= \sum_j f_j \cos 2\pi(hx_j + ky_j + lz_j) \\ B(h\ k\ l) &= \sum_j f_j \sin 2\pi(hx_j + ky_j + lz_j) \end{aligned} \tag{3.99}$$

Combining with the complex conjugate, we get

$$\begin{aligned}&\{A(h\ k\ l) + iB(h\ k\ l\}\{\cos 2\pi(hx + ky + lz) - i\sin 2\pi(hx + ky + lz)\}\\&+\left\{A(\bar{h}\ \bar{k}\ \bar{l}) + iB(\bar{h}\ \bar{k}\ \bar{l}\right\}\left\{\cos 2\pi(hx + ky + lz) + i\sin 2\pi(hx + ky + lz)\right\}\\&= 2A(h\ k\ l)\cos 2\pi(hx + ky + lz) + 2B(h\ k\ l)\sin 2\pi(hx + ky + lz)\end{aligned} \tag{3.100}$$

Now, $A(\bar{h}\bar{k}\bar{l}) = A(hkl)$ and $B(\bar{h}\bar{k}\bar{l}) = -B(hkl)$ in the absence of anomalous dispersion.

Then

$$\rho(x\ y\ z) = \frac{1}{V}\left[\begin{aligned}&F(000) + 2\sum_{h>0\ -k\ -l}^{h\ k\ l}[A(h\ k\ l)\cos 2\pi(hx + ky + lz)\\&+ B(h\ k\ l)\sin 2\pi(hx + ky + lz)]\end{aligned}\right] \tag{3.101}$$

The summation here is taken only for reflections with $h > 0$, i.e., over half of reciprocal space. Note that $F(000)$ is excluded from the summation as it has no separate conjugate. We can now simplify this expression still further by introducing the phase angle $\phi(hkl)$, defined by

$$\tan\phi(hkl) = \frac{B(hkl)}{A(hkl)} \tag{3.102}$$

and then

$$\rho(xyz) = \frac{1}{V}\left[F(000) + 2\sum_{h>0\ -k\ -l}^{hkl}|F(hkl)|\cos\{2\pi(hx + ky + lz) - \phi(hkl)\}\right] \tag{3.103}$$

This result shows that to compute the density $\rho(xyz)$, it is necessary to know the values of the structure amplitudes $|F(hkl)|$ and also the phases $\phi(hkl)$. The structure amplitudes come directly from the measurements of the relative intensities (3.19)

$$I(hkl) \propto |F(hkl)|^2 \tag{3.104}$$

but in general, the phases are not known. This *phase problem* has been a challenge towards automatic structure determination since the beginning of x-ray crystallography. Some of the methods developed to handle this are:

1. Trial and error—guess a model or part model, and then to reveal the remaining atoms, construct a Fourier map based on the *difference* between observed and calculated structure factors to find any remaining atoms

$$\begin{aligned}\Delta\rho(x\ y\ z) = \frac{2}{V}\sum_{h>0\ -k\ -l}^{hkl}&[|F_{\text{obs}}(hkl)| - |F_{\text{cal}}(hkl)|]\\&\times\cos\{2\pi(hx + ky + lz) - \phi(hkl)\}\end{aligned} \tag{3.105}$$

   The starting model is then normally refined using non-linear least-squares algorithms.

2. Heavy atom method—if there is a heavy atom, e.g., Hg, present in the structure, the x-ray intensities are so dominated by its contribution that one can consider the phases to be essentially due to this single atom alone. The calculated phases based on a crystal structure consisting of this atom alone can be used together with the observed structure factors to obtain an initial model.
3. Isomorphous replacement—compare diffracted intensities from two crystals in which one atom type has been replaced by another. This is particularly useful in protein structure determination. This replacement can be done by chemical means or by tuning the wavelength of incident synchrotron radiation.
4. Anomalous dispersion—makes use of the fact that the atomic scattering factor contains real and imaginary parts that are large, especially close to an x-ray atomic absorption edge.
5. Direct methods—use the statistical distribution of intensities in reciprocal space to find relationships between phases of different reflections. Thus, if one starts with a couple of trial phases, direct methods enable likely phases of other reflections to be found. This is particularly useful for small-molecule problems and is widely used as a nearly automatic method of solving crystal structures. The pioneering work on this resulted in the Nobel Prize awarded in 1986 to Jerome Karle (1918–2013) and Herman Aaron Hauptmann (1917–2011).
6. Synchrotron and x-ray free-electron laser experiments—conventional Bragg crystallography requires only that the coherence width across the beam be larger than the unit cell, not the crystal. However, with the advent of new radiation sources in recent years, the coherence width of the beam typically exceeds the dimensions of the crystals, producing interference effects between Bragg reflections. This introduces the possibility of new methods for finding the phases.

We shall see below a couple of ways in which the phase problem has been handled, but before this, let's consider how the formula (3.103) can be used to locate the atomic positions, assuming that the phases are known.

3.13.2 Fourier synthesis

To obtain a map of the density representing the contents of the unit cell in a crystal structure, it is necessary to add together all of the waves described by amplitudes $|F(hkl)|$ together with their phases $\phi(hkl)$. As a simple example, consider figure 3.50 (a)–(d), where four plane waves with phase angle $\phi = 0°$ are added together.

In (a), the plane wave is for the 100 reflection. In this case, the peaks lie on the (100) planes with the troughs halfway between. $|F(hkl)|$ is a measure of the height of this wave, represented by the amount of shading. In (b), the plane wave for the 010 reflection has been added, in (c) the wave corresponding to the 110 reflection, and finally in (d) the wave for the $\bar{1}10$ reflection. It can be seen that with these four reflections alone, it is apparent that density is being built up on the corners of the unit cell with a weaker component at the centre of the unit cell. In (e), the phases for the

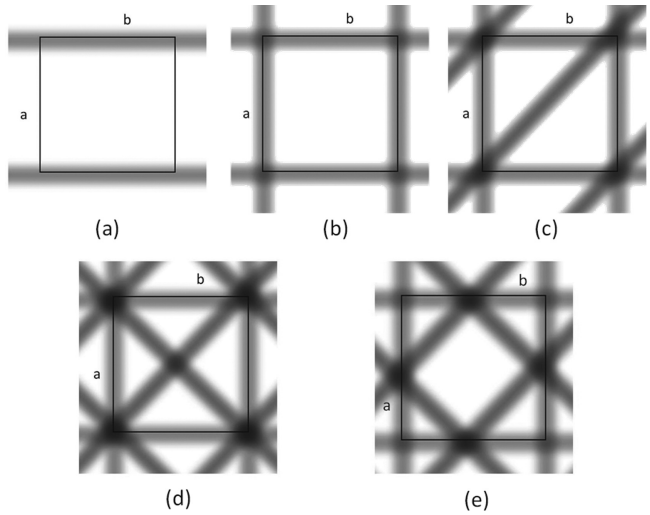

Figure 3.50. Example of the addition of planes waves in Fourier synthesis of electron density.

110 and $\bar{1}10$ reflections have been changed by $\pi/2$. By shifting the maxima of these two waves, density is now seen to form halfway along the unit-cell axes, with little density at the centre of the unit cell, a completely different structure from before.

In figure 3.51 one can see what might be the result of summing the Fourier series over a very large number of *h k l* reflections starting from figure 3.50(d) and (e). The effect is to concentrate the density into the atomic positions with little or no observable density between. We end up with something resembling a photograph of the atoms in the structure. The main difference obtained between the two structures shows that it is the phases that are crucial for correct structure determination, rather than merely the structure amplitudes.

Figure 3.52 illustrates the critical fact that it is the phases that dominate in Fourier synthesis rather than the amplitudes of the waves. At the top, we see photographs of the Nobel Prize winners, father and son, William Henry Bragg and William Lawrence Bragg on the left. On the right, the images have been reconstructed by swapping the phases but keeping the amplitudes. The result clearly shows that most of the information has been switched too.

Before the advent of computers, various creative photographic techniques were invented to perform Fourier syntheses in this way. The author is sufficiently advanced in years to have used one called the 'von Eller photosommateur' during his graduate studies (figure 3.53). I present it here for its pedagogical value. This consisted of a cylindrical light-tight can. At one end, a lamp illuminated a glass mask on which were a set of cosinusoidal fringes. The light then passed through this to a photographic plate outside the can, to which was taped a scale drawing of the reciprocal lattice. By rotating the photographic plate (and, therefore, the reciprocal lattice) and at the same time winding a cursor up and down, it was possible to position the cursor directly onto a reciprocal-lattice point. This had the effect of orienting the relevant reciprocal-lattice vector perpendicular to the image of the

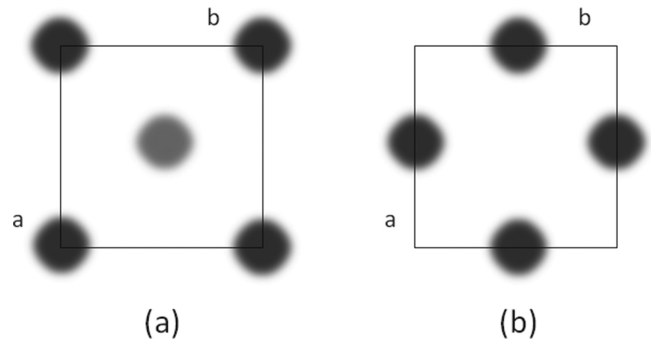

Figure 3.51. Fourier synthesis using a large number of reflections.

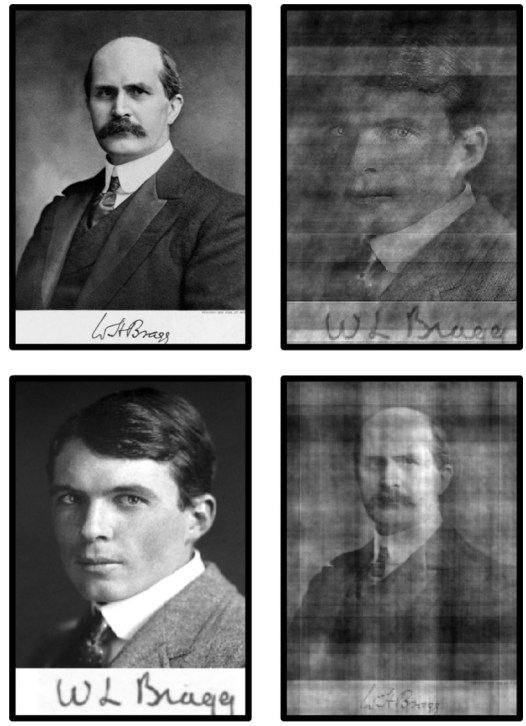

Figure 3.52. The relative importance of phases over amplitudes.

cosine mask. Simultaneously, the mask automatically moved forward or backward, thus changing the apparent fringe spacing projected onto the photographic plate.

Furthermore, left and right movements of the mask enabled the correct phase to be set up. The light was then exposed for several seconds in proportion to the structure amplitude for the relevant reflection, and the whole process repeated for the next reciprocal-lattice point. The result was something that looked like a photograph of the atoms in the crystal structure. Figure 3.54 shows the result of using this technique to plot a projection on (010) of the crystal structure of urea together, for comparison,

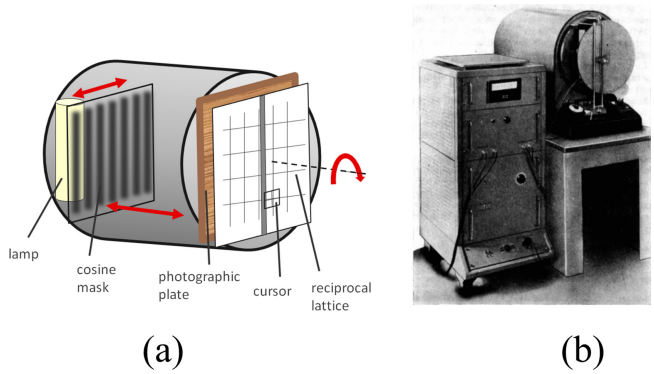

Figure 3.53. (a) Schematic diagram of von Eller photosommateur. (b) Photograph of the original photosommateur. Reproduced by permission of the International Union of Crystallography.

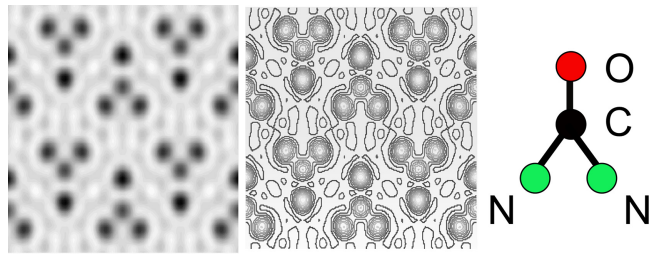

Figure 3.54. Fourier maps of the crystal structure of urea on (010): left, performed with the von Eller photosommateur, middle computer-generated [24]; right, the urea molecule (hydrogens omitted).

with a modern computer-generated contour map. Although one would not dream of using such a method today, it was a fun way to learn about Fourier syntheses [24].

Before the general use of computers became standard after the mid-1960s, many different and cunning techniques like this were devised to locate the atomic positions from the data, even though the intensities of the reflections were often simply estimated by eye on an arbitrary scale! Today, with modern computers and new data collection methods, it is commonplace to determine crystal structures routinely with literally hundreds or even thousands of atoms in the unit cell. To do this, of course, one has first to deal with the phase problem. Many techniques for doing this have been developed over the last decades. In the next sections, we shall look at just a couple of methods by which this has been done successfully.

3.13.3 The Patterson method

This method of getting at the phases was first demonstrated by Arthur Lindo Patterson (1902–66) in 1934. He introduced a new function based on the convolution of the electron density with itself:

$$P(\mathbf{u}) = \rho(\mathbf{r}) * \rho(-\mathbf{r}) = \int \rho(\mathbf{r})\rho(\mathbf{u}+\mathbf{r})d\mathbf{r} \tag{3.106}$$

After some manipulation (appendix F), the following formula is obtained

$$P(uvw) = \frac{2}{V}\sum_{h>0}\sum_{k}\sum_{l}|F(hkl)|^2 \cos 2\pi(hu + kv + lw) \tag{3.107}$$

The importance of this formula is that no phase information is involved. Because of the starting point as an autocorrelation between two electron densities at different positions, the Patterson function provides information on *vectors* between atoms, but not on individual atoms themselves. Thus, one can construct a Fourier map using this function by using the squares of structure amplitudes with all plane waves having their phases set to zero. It is evident that in such a map, all the waves will add together at the origin of the Patterson unit cell, corresponding to self-vectors (i.e., vectors of zero length corresponding to the atomic distance from each atom to itself). Peaks elsewhere in the map will correspond to vectors between different atoms. I find that a useful way to think of this is to remember the following quotation I heard while attending lectures at Birkbeck College London by the crystallographer C H (Harry) Carlisle: 'All vectors to a common origin'. He used to call this the 'peasant's definition of the Patterson function'. Let's see an example in practice to get the idea.

Figure 3.55 shows how to build up a Patterson map from a known structure. On the left-hand side is a hypothetical crystal structure consisting of three atoms, for convenience, coloured red, yellow and green, with decreasing numbers Z_1, Z_2, Z_3 of electrons. The right-hand side shows the Patterson map in the process of construction.

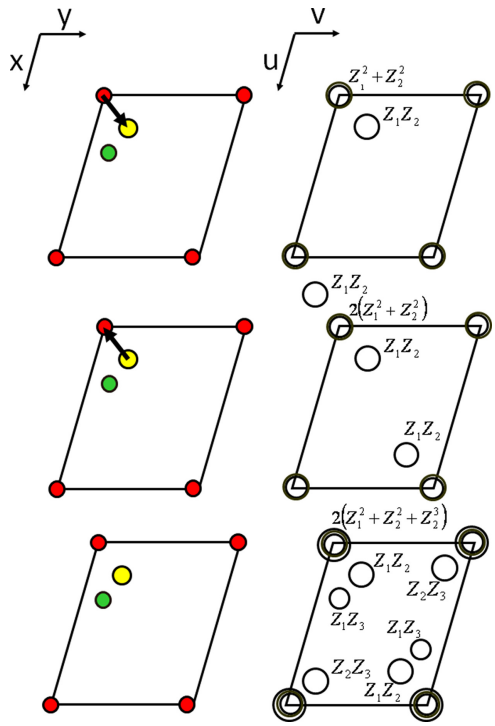

Figure 3.55. Construction of a Patterson map.

Starting with the red atoms alone, the self-vector (red atom to red atom) creates a peak at the origin of the Patterson cell approximately of height Z_1^2. Now consider the vector from a red atom at the corner of the unit cell to the nearby yellow atom (top diagram). Placing the origin of this vector at the Patterson cell origin creates a peak in the Patterson map of height proportional to Z_1Z_2 (remember 'all vectors to a common origin'). At the origin, we also add Z_2^2 for the yellow atomic self-vector. However, one has to consider the reverse vector from yellow atom to red atom, which creates another peak of height Z_1Z_2 outside the Patterson cell, which by translational symmetry gives a peak inside the lower right of the cell (middle diagram). Finally, we add the vectors green to red, red to green, green to yellow, and yellow to green to lead to the distribution of Patterson peaks shown at the bottom right of the figure. Despite not knowing the phases of the reflections, the result gives rise to a map on which the peaks are closely related to the underlying crystal structure. It is then the crystallographer's task to deconvolute this map to reveal the most likely model for the structure. This is not always unique since different models can give very similar Patterson maps, but, at least, the number of models is finite. These days, solving Patterson maps can be done automatically by computer programs. Note that the Patterson map is always centrosymmetric, because, for each vector in one direction, there will always be another in the opposite direction.

Figure 3.56 shows a simulated Fourier density map for a hypothetical crystal structure (a), and in (b) the same map with interatomic vectors drawn in. The Patterson map is shown in (c), where all interatomic vectors have been moved to the origin of the Patterson map (in each corner of the diagram).

The Patterson map always has a large peak of approximate height $\sum Z_e^2$ at the unit-cell origin due to the summation of self-vectors for all the atoms. This can be eliminated by subtracting the self-vector terms, thus

$$|F'(hkl)|^2 = |F(hkl)|^2 - \sum_j f_j^2 \tag{3.108}$$

3.13.4 Charge flipping

Charge flipping is one of the most recent and possibly most exciting developments in phase determination, demonstrated by two Hungarian optical physicists, Gabor

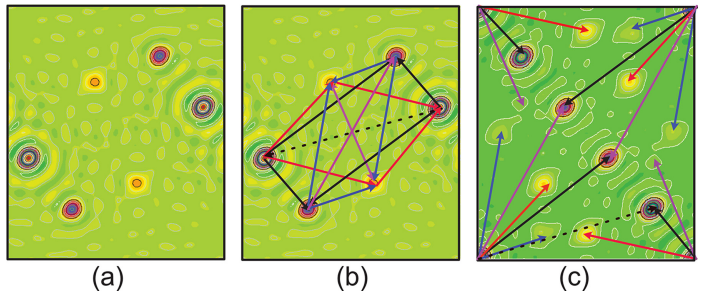

Figure 3.56. Simulation of the Patterson projection from a crystal structure. (a) Fourier map of the hypothetical structure. (b) Interatomic vectors. (c) Patterson map with interatomic vectors added. The extra ripples are caused by series termination as a result of using a finite number of reflections.

Oszlányi and András Sütő, in 2004 [25]. The basic idea behind this owes much to algorithms developed years earlier for optical image processing. The procedure is amazingly simple to follow in principle and to code into software. The charge-flipping algorithm is an iterative process starting with a complete set of diffraction intensities in order to achieve atomic resolution. The algorithm does not require any *a priori* information about the symmetry of the structure or its chemical composition. These properties can be included in the model later after the application of charge flipping and can be, even to a large extent, derived directly from the result of charge flipping. The iterative process is illustrated in figure 3.57.

First of all, start with a set of observed structure amplitudes $|F(hkl)|$ and assign random phases to each. Fourier transformation is then used to create an electron density map $\rho(xyz)$, which will initially appear unrecognizable. A cut-off density δ is assigned, and all densities below this value have their signs reversed to produce a new map $\rho'(xyz)$. Fourier transformation of this gives a new set of structure factors $F'(hkl)$ with new phases. We now take the new phases and apply them to the original set of observed structure amplitudes. The cycle is then repeated continuously until density maps showing the crystal structure are obtained. The whole process seems to work like magic and is very entertaining to watch. Figure 3.58 shows a few slides taken from a Java applet available at [26]. The reader is strongly encouraged to try this out.

3.13.5 Rietveld refinement

In 1969, Hugo Rietveld (1932–2016) published a landmark paper in the field of powder diffraction analysis [27]. Up to this time, powder diffraction had principally been used to identify materials and obtain lattice-parameter information and generally held little interest beyond this. However, Rietveld showed that if one had a reasonable model of the crystal structure of a material, it was possible to refine, by least-squares, the positions of the atoms by fitting a calculated powder pattern to the total observed data without the need to separate out the individual structure factors making up the peak intensities. This launched an enormous renewed interest in powder diffraction so that these days there are whole conferences devoted to this subject. Rietveld refinement is now an entirely accepted and standard

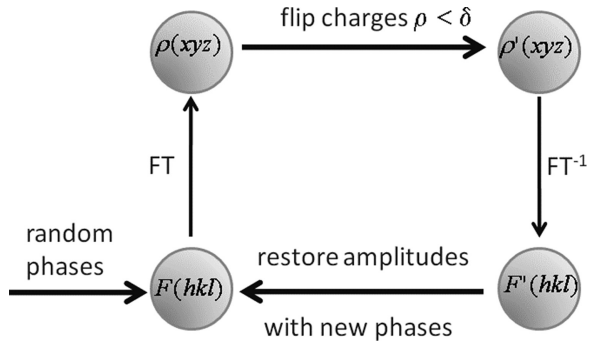

Figure 3.57. Charge-flipping flow diagram.

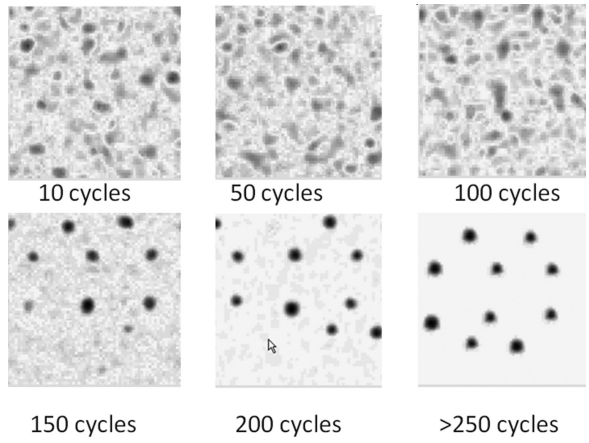

Figure 3.58. Sequence of electron density calculations as a function of the number of cycles. In the last picture, the origin has been shifted for convenience to show the whole molecule.

method to refine crystal structure information. It is particularly useful for situations where single crystals are not readily available (by far the majority of cases). The basic idea is to consider the contributions to the intensity y_i of the measured peak profile at positions $2\theta_i$. Assuming a Gaussian shape to the profiles

$$y_i = tF^2(hkl)m_jL_j\frac{2\sqrt{\ln 2}}{H_j\sqrt{\pi}}e^{-4\ln 2\{(2\theta_i-2\theta_j)/H_j\}^2} \tag{3.109}$$

where

t = step width of the counter
m_j = multiplicity of jth reflection
L_j = Lorentz factor (for x-rays, one needs to include also a polarisation factor)
$2\theta_j$ = calculated positions of the jth Bragg peak
H_j = full width of a peak at half-height.

This Rietveld equation has since been modified for different peak shape functions, and other parameters have been added, but the basic idea remains true. The parameter H_j is often given by the relationship

$$H_j^2 = U\tan^2\theta_j + V\tan\theta_j + W \tag{3.110}$$

where U, V and W are parameters that can be refined during the process. We see from this that the parameters to be refined can be considered in two parts:

1. $F(hkl)$ contains all the structural parameters of interest (coordinates, displacement parameters, occupation factors, etc). Also, $2\theta_j$ is determined by refining the unit-cell parameters.
2. Geometrical factors are used to fit the profile pattern, including any zero error, H_j (with parameters U, V and W), absorption correction parameters, preferred orientation, peak asymmetry, etc.

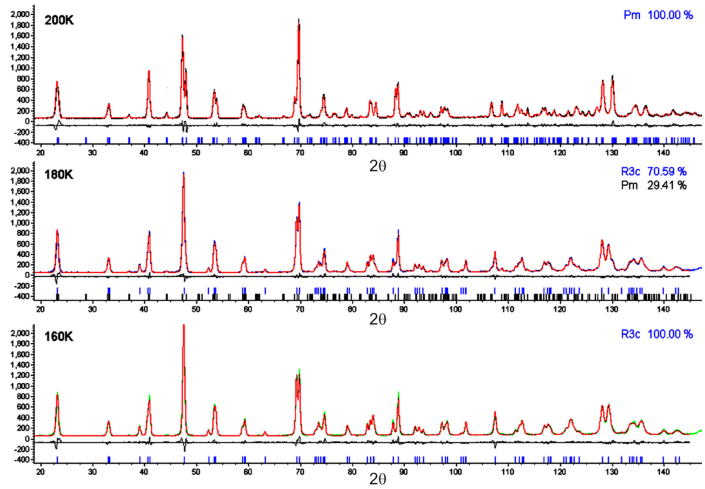

Figure 3.59. Rietveld refinements using TOPAS [28] for neutron powder patterns of $Na_{0.7}K_{0.3}NbO_3$ ($\lambda = 0.16$ nm) at 160 K, 180 K and 200 K, collected on the D2B diffractometer (Institut Laue-Langevin). The red line marks the fitted data. A plot, in black, of the difference between the observed and calculated patterns, is shown immediately below, and below this, ticks indicating the positions of the expected reflections.

For most users of the method, only the parameters in (1) are of any real interest, while the geometrical factors (2) are often ignored. They are parameters that are needed mainly to help with the fitting of the profiles.

Figure 3.59 shows Rietveld fits using neutron diffraction for the compound $Na_{0.7}K_{0.3}NbO_3$ at three different temperatures. At 200 K, the space group fits best in space group *Pm*, while at 160 K, it is *R*3*c*. In the intermediate temperature 180 K, a two-phase mixture was refined. The Rietveld analysis not only gave an excellent fit to the data but was able also to estimate the percentage of each phase. In addition to using the Rietveld process on angle-dispersive data such as this, it has also been applied to neutron time-of-flight data (figure 3.60). With good data such as this, it can be seen that Rietveld refinement is capable of detecting subtle differences in the refined structure.

3.13.6 Total scattering analysis

A more recent development in the extraction of crystal structure information from powder diffraction is the so-called total scattering or PDF (pair distribution function) analysis. Essentially, this is to consider the whole diffraction pattern, peaks plus background, and treat it as if one were dealing with diffraction somewhat like that from a liquid or amorphous material. The method has usually been applied with neutron scattering, although x-rays are also being used more recently. For this method to work, the data must extend to very high Q values. While this can be achieved easily with time-of-flight neutron sources, it is more difficult with conventional x-ray sources: synchrotron sources, however, do achieve high Q data.

Suppose there are n different atomic species in a material. Let c_j be the concentration of atomic species j and b_j the effective, coherent bound neutron

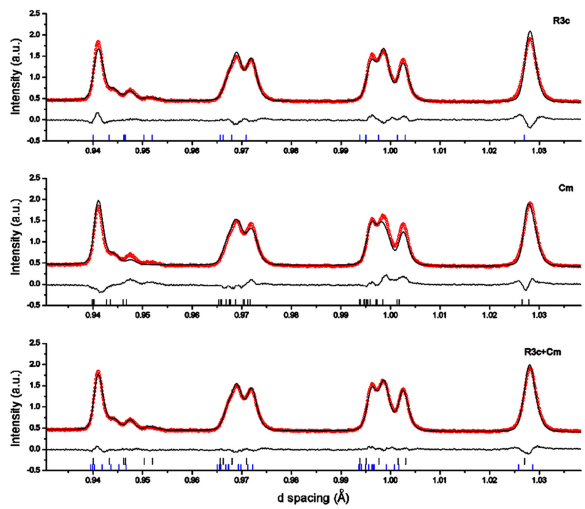

Figure 3.60. Neutron time-of-flight Rietveld fit for $PbZr_{0.7}Ti_{0.3}O_3$ ceramic, data collected on HRPD (ISIS, UK), showing best fit to a mixture of phases with space groups *R*3*c* and *Cm* [29].

scattering length. The total scattering factor $F(\mathbf{Q})$ is related to the total radial distribution $G(r)$ by

$$F(\mathbf{Q}) = \langle \rho \rangle \int_0^\infty 4\pi r^2 G(r) \frac{\sin Qr}{Qr} dr \tag{3.111}$$

where (ρ) is the average number density (in atoms $Å^{-3}$).

Definition *The **radial distribution function**, G(r), or **pair correlation function**, is a measure of the correlation between atoms within a system. It is a measure of the average probability of finding an atom at a distance r away from a given reference atom. It determines how many other atoms are within distances of r and r + dr away from any particular atom.*

$G(r)$ can be defined in terms of partial radial distribution functions $G_{ij}(r)$:

$$G(r) = \sum_{i,j=1}^{n} c_i c_j \langle b_i \rangle \langle b_j \rangle [G_{ij}(r) - 1] \tag{3.112}$$

where

$$G_{ij}(r) = \frac{n_{ij}(r)}{4\pi r^2 \rho_j dr} \tag{3.113}$$

$n_{ij}(r)$ is the number of atoms of type j within distances of r and $r + dr$ from an atom of type i, and $\rho_j = c_j\langle \rho \rangle$. For a fully-ordered crystal, $G(r)$ gives rise to a series of sharp peaks with relatively low background. However, as disorder is introduced into the structure, the peaks become broader. Nonetheless, their positions as a function of distance r provide useful information about atomic separations.

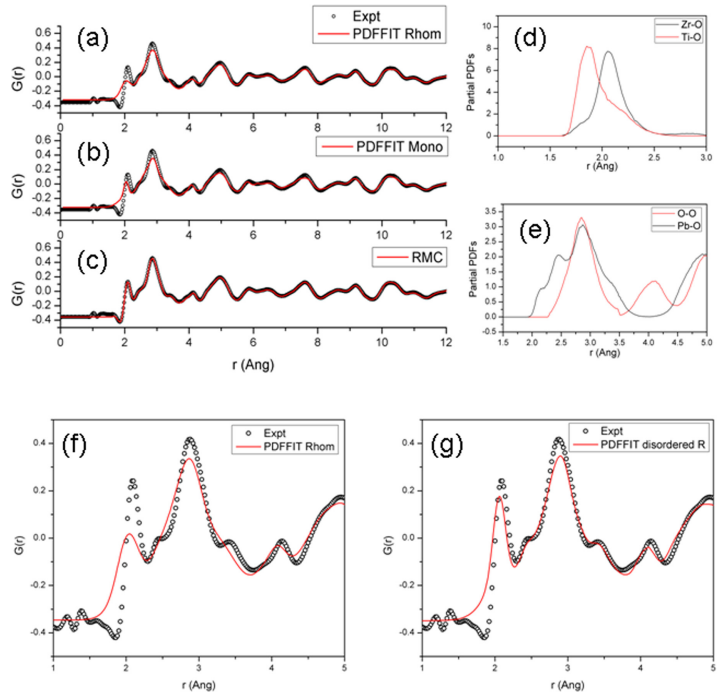

Figure 3.61. (a) PDFFIT for $PbZr_{1-x}Ti_xO_3$ with $x = 0.3$ at room temperature using a rhombohedral model structure, (b) using a monoclinic structure. (c) Fitting by the reverse Monte Carlo (RMC) method. (d) Partial PDF peaks for Zr–O and Ti–O. (e) Partial PDF peaks for Pb–O and O–O from the RMC modelling. (f) Enlargement of (a) showing the disagreement between the observed and fitted results. (g) The addition of disordered Pb displacements around the [111] direction in the structure now gives rise to the shoulders on the main Pb–O peak (from [31]).

Figure 3.61 shows some total scattering results for the important piezoelectric ceramic $PbZr_{1-x}Ti_xO_3$ (PZT). In (a), the experimental $G(r)$ is shown as a function of distance r. The red curve is a fit to the observed data with a computer program called PDFFIT. This used the known average crystal structure, assumed to be rhombohedral, as derived from Rietveld refinement. However, the structure of PZT has always been controversial, with some evidence that it is, in fact, monoclinic at the local scale, but effectively rhombohedral on average at the large scale. Figure 3.61(b) shows the fit for the monoclinic structure, and (c) shows the result of what is known as reverse Monte Carlo (RMC) modelling. Here, a computer simulation is set up in which there is a large array of unit cells containing the atoms in their average positions. The atoms are then allowed to move within certain limits while monitoring a fit to the total scattering and the peaks seen in the Rietveld analysis. It can be seen that the fit is very close. In (d), two peaks in $G(r)$ have been identified as corresponding to the Zr–O and Ti–O distances, and in (e), the O–O and Pb–O distances are observed. The PDFFIT to the first few peaks is shown in (f), where there is considerable disagreement with the experimental plot. However, once one allows for the Pb positions to have a degree of disorder in the structure, an excellent fit is obtained. The results of this analysis have played an important role in

understanding the property of enhanced piezoelectricity in ceramic PZT. Total scattering analysis plus RMC modelling is an example where both direct and reciprocal space refinements are made simultaneously.

It can be seen that total scattering provides a large amount of useful information about crystal structures, especially on the local scale, which, when taken together with the long-range average structure, can be of great use in understanding the role of atomic positions and displacements in the physical properties of materials. Note that the technique does not require knowledge of the phases of reflections.

3.13.7 What's new?

Despite the field of crystallography having a long and distinguished history, significant developments have continued to be made right up to the present time. Probably the biggest advances have been in the fields of computing, and apparatus for data collection. Up to the 1960s, measurement of x-ray single-crystal data could take several days or even weeks, mainly using photographic film. Analysis of the data and subsequent structure determination could take months, such that the determination of a couple of crystal structures could be sufficient to earn a PhD. Faster computing and development of precise diffractometers has now reduced the time for a typical structure determination in a standard laboratory down to around one or two hours.

For many years, x-ray diffraction was carried out using sealed x-ray tubes, based on the original designs made at the beginning of the 20th century. However, in the early 1970s, synchrotron x-radiation became available, where electrons circulating in an evacuated ring are accelerated and steered by magnets to speeds approaching the speed of light. The acceleration of the electrons produces Larmor radiation, which spans the whole range of wavelengths from x-rays up to infra-red. Since then, many new techniques have been developed using synchrotron radiation's special properties (e.g., high flux, high collimation, plane polarisation, high coherence).

In a further advance, the free-electron laser (figure 3.62) has become available in the last few years. This produces femtosecond pulses of high-intensity and coherent x-rays. This is done by accelerating electrons to near relativistic speeds to create a

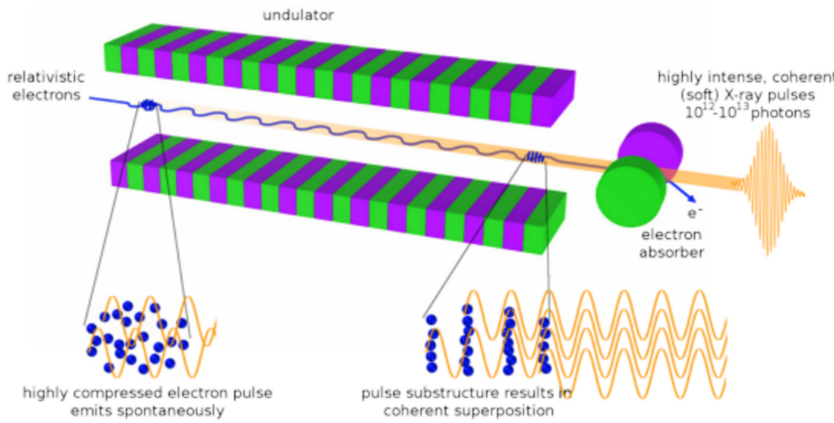

Figure 3.62. Schematic diagram of the free-electron laser (by permission of Daniela Rupp, ETH Zürich) [32].

highly compressed electron pulse. The pulses of electrons are made to accelerate along a linear path where magnets shape the pulses to make them extremely short. These pulses then pass through a magnetic undulator. As the electrons wiggle back and forth, they create radiation, which in turn interacts with the electrons to form a high-intensity coherent, and tuneable x-ray beam.

Also, new neutron sources have been set up, the so-called spallation sources, in which protons are accelerated to high velocities and then beamed onto a target metal, such as tungsten, to produce a high-intensity, white and pulsed beam of neutrons. In addition, recent developments in electron diffraction have been made possible through the development of new lenses and detectors.

Let us look at just a couple of the new techniques, which are particularly exciting. A fascinating use of the x-ray free-electron laser is where extremely rapid diffraction data collections can be made with tiny crystals of proteins (figure 3.63). Henry Chapman, Janos Hajdu and John Spence developed the technique in which a fine powder of small protein crystallites is injected through the beam. The energy of the x-rays is such as to destroy each tiny crystal, but not before a diffraction pattern is recorded on an imaging detector. Each flash image can be recorded within approximately 25 femtoseconds, and many hundreds and thousands of diffraction images are collected. As the crystallites pass through the beam, the diffraction patterns are recorded from all their random orientations. Post-processing by computer has enabled these to be sorted out, and the data used to solve the protein crystal structures. As this technique works with such tiny samples, it is unnecessary to have to grow single crystals on the scale used in synchrotron crystallography. For more details, see the article by Spence [33].

Another recent and significant development in structure solution is the MicroED method in electron diffraction. For a long time, measurement of diffracted intensities in electron diffraction was limited owing to multiple scattering effects and problems with detectors. However, in the last few years, it has become possible to measure structure factors using the TEM. The MicroED technique was developed

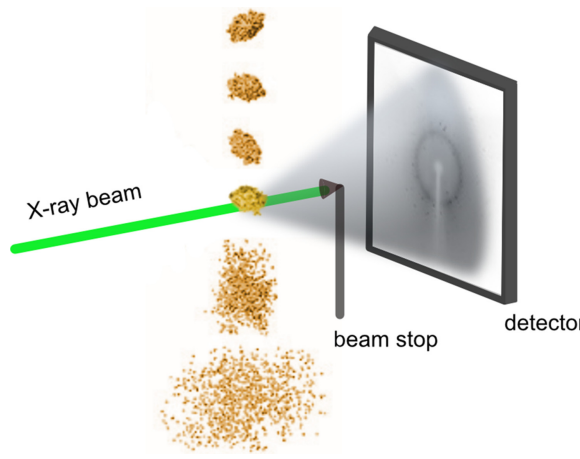

Figure 3.63. Use of free-electron laser radiation in protein crystallography. Reproduced from [33] by permission of the International Union of Crystallography.

in 2013 by Tamir Gonen and his group at the Howard Hughes Medical Institute in Virginia, USA. This uses very tiny crystals, approximately one-billionth the size needed for conventional x-ray diffraction. The samples are first frozen, and the TEM is used in diffraction mode with an extremely low electron exposure. Each nanocrystal is exposed to the diffracting beam and continuously rotated while diffraction patterns are collected on a fast camera to make a movie (see the video at https://www.youtube.com/watch?v=RxOp9NP3uho). The measured data are then processed using traditional x-ray crystallographic methods using the standard software for structure analysis and refinement. This is in effect a modern version of the traditional crystal rotation method of data collecting (see section 3.5.2). The first demonstration of this method's viability was made with the enzyme lysozyme, but since then it has been used for many organic crystal-structure determinations. MicroED is a development of an earlier precession method in a TEM, where the electron beam is rotated rather than the crystal. This has been successfully used in determining structures of inorganic crystals. In both methods, errors in intensity measurement due to multiple scattering have been shown to be very low. For a good review, see [34].

The pace of development in crystallographic techniques has been astonishing in recent times. One thing is for sure: these are leading to exciting new fields of study, and we can expect tremendous advances in crystallographic research in the future.

3.14 Aperiodic crystals

> *I told everyone who was ready to listen that I had material with pentagonal symmetry. People just laughed at me.*
>
> (Dan Shechtman)

Just when you think that everything about crystal symmetry must be known, nature retaliates by throwing a curveball. We have already seen that the basic idea of periodicity defines a crystal, but the scientific world was unprepared for a significant discovery that subsequently altered our perception of what is meant by a crystal.

In 1984, a rapidly-cooled metallic Al_4Mn alloy was observed by the Israeli-born materials scientist Daniel Shechtman (1941–) to exhibit 10-fold symmetry in its electron diffraction pattern. This seemed to show that these materials, in some way, violated the rule that crystal lattices could not show 5 or 10-fold symmetry (figure 3.64(a)). Such materials were termed quasiperiodic crystals or quasicrystals, and they clearly could not be explained by conventional crystal-symmetry arguments. Initially, this discovery was met with disbelief, and Shechtman's original paper was rejected for publication. Even the Nobel Laureate, Linus Pauling (1901–94), claimed that the effect could be explained as a form of multiple twinning, a mixture of different crystal orientations. However, Shechtman's work was extremely precise and methodical, and to his credit, he pursued this discovery against all the opposition. He was subsequently proved correct and was eventually awarded the 2011 Nobel Prize in Chemistry for this discovery. Other examples appeared after this initial discovery, including naturally formed icosahedrite, a mineral with the composition $Al_{63}Cu_{24}Fe_{13}$. This was found in the Koryak Mountains in Russia, apparently coming from a meteorite. We now know

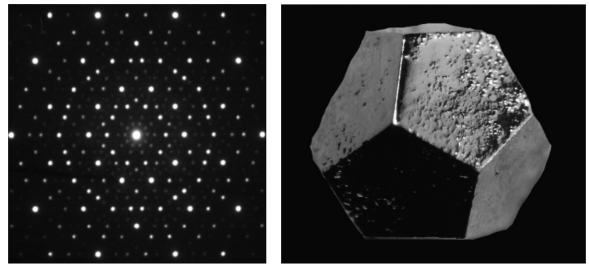

Figure 3.64. (a) Electron diffraction showing 10-fold symmetry from an icosahedral quasicrystal of Ho–Mg–Zn (Materialscientist (CCBY SA 3.0); (b) Ho–Mg–Zn quasicrystal, laboratory-grown [35].

that such quasicrystals are not exceptionally rare, especially in metal alloys, and one can even grow crystals with observable faces exhibiting 5-fold symmetries (figure 3.64).

Two types of quasicrystals are known. The first type, polygonal (dihedral) quasicrystals, have an axis of 8, 10, or 12-fold local symmetry (octagonal, decagonal, or dodecagonal quasicrystals, respectively). They are periodic along this axis and quasiperiodic in planes perpendicular to it. The second type, icosahedral quasicrystals, is aperiodic in all directions.

How, then, can we explain this apparent violation of fundamental lattice symmetry? A convenient way to do this is to think of different ways to tile a floor without leaving gaps. In the conventional approach, if we use a set of identical regular tiles, one ends up with periodicity and the restriction that 5 and 7-fold symmetries are not allowed. However, if one is prepared to use differently-shaped tiles, one can obtain many arrangements with local 5 or 7-fold symmetries. Such structures are not periodic in the traditional sense but are ordered since they occur according to specific rules.

Interestingly, this subject has an old history. As far back as 1619, Johannes Kepler showed how to fill a two-dimensional space with *different* 5 and 10-fold symmetric tiles (figure 3.65(a)), realizing that it was not possible with just one type of tile. Figure 3.65(b) shows an example of tiling in two dimensions, where two different shapes are used, from an idea proposed by Roger Penrose (1931–) in Oxford, UK. We see that with appropriate rules for stacking, fat and thin rhomb shapes can be placed together to fill two-dimensional space. Such an arrangement never repeats, although it does show local orientational symmetry of a 5-fold kind. Interestingly, if one superimposes a series of lines, due to Robert Ammann (1946–94), as shown, the sets of lines together show evidence of 5-fold symmetries! Furthermore, the lines are spaced by long (L) and short (S) distances in the sequence L S L L S L S L… This sequence has an interesting property. If you replace every L by L S and every S by L, you find the series L S L L S L S L L S L L S…. This is simply a copy of the original sequence. This type of sequence is found in many places in nature and was discovered by the Italian mathematician Leonardo Pisano Bigollo (1170–1250), also called Leonardo of Pisa, or simply Fibonacci. It is interesting to note that the ratio L/S is the 'golden mean' $\tau = (1+\sqrt{5})/2 = 1.61803\ldots$, well known to artists who use this ratio to design a pleasing

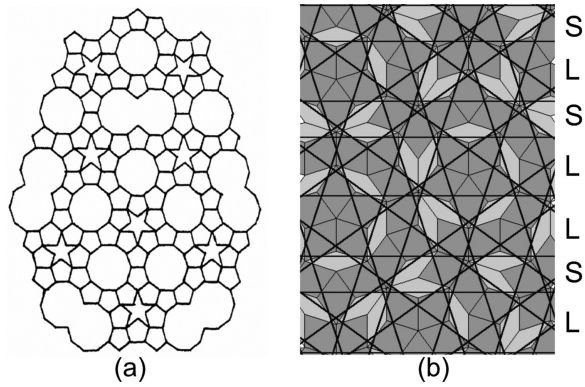

Figure 3.65. (a) Kepler's tiling. (b) Penrose tiling of two types of rhomb-shaped cell.

layout for a painting. Thus, we see that this arrangement is not random, nor is it periodic. Instead, the term *quasiperiodic* is used to describe it. It is not obvious what the overall symmetry is of an aperiodic arrangement in direct space, such as in the Penrose tiling example, where the 5-fold symmetries are local. However, in reciprocal space, as seen through diffraction, the symmetry is revealed.

Notation. *The term **aperiodic** applies to those cases where long-range periodicity is not a feature of the solid, such as in amorphous (non-crystalline) materials like glass. The term **aperiodic crystal** is used to describe crystals where translational periodicity does not apply. Nonetheless, the atoms or molecules are arranged in some sort of order governed by different rules from the usual periodic rules.*

As a consequence of Shechtman's discovery, in 1992, the International Union of Crystallography [36] revised the definition of a crystal in terms of reciprocal space.

Definition. *A material is a crystal if it has **essentially** a sharp diffraction pattern. The word **essentially** means that most of the intensity of the diffraction is concentrated in relatively sharp Bragg peaks, besides the always present diffuse scattering. In all cases, the positions of the diffraction peaks can be expressed by*

$$\mathbf{H} = \sum_{i=1}^{n} h_i \mathbf{a}_i^* \; (n \geqslant 3) \tag{3.114}$$

Here $\mathbf{a}_i^*$ and h_i are the basis vectors of the reciprocal lattice and integer coefficients, respectively. The number n is the minimum for which the positions of the peaks can be described with integer coefficient h_i. The conventional crystals are a special class, though very large, for which $n = 3$.

Notice that instead of defining a crystal as a physical object in direct space, as we did in chapter 1, this new definition relies on the observation of sharp diffraction peaks in reciprocal space. Both definitions are not perfect, since they rely on a certain amount of fuzziness. The direct-space definition relies on *average* periodic order:

average because in real crystals there is never perfect periodicity, owing to thermal vibrations and defects. At what point does breakdown in periodic order mean that something is not to be considered a crystal? Similarly, the reciprocal-space definition depends on the meaning of *essentially sharp*. When do peaks become sufficiently broad not to be considered sharp enough to define a crystal? (*NB. At the time of writing, the Nomenclature Commission of the IUCr has just revised the definition of a crystal to include the direct-space definition*, see [36].)

Conventional crystals, then, are a particular class where $n = 3$, whereas aperiodic crystals are described as periodic in a higher-dimensional space, $n > 3$, with symmetries described by appropriate superspace groups. Quasiperiodicity can be shown to arise by considering a regular periodic reciprocal lattice of points in this higher-dimensional space. If a cut is then made through such a lattice and projected onto two- or three-dimensional space, the projection will obviously still consist of points. If the cut and projection are made in the right way, it turns out that an array of points can be obtained with, say, local 5-fold symmetries, and with perfect 5-fold symmetry of their two-point correlations, resulting in perfect symmetry of their diffraction patterns. The positional ordering of the points along particular directions is again found to obey a rule such as the Fibonacci sequence. So that the quasicrystal itself be aperiodic, this slice must avoid any lattice plane of the higher-dimensional lattice.

Figure 3.66 gives an example of using the strip/projection method from a two-dimensional square lattice onto a one-dimensional lattice. A strip of width $a(\cos\alpha + \sin\alpha)$ is made and drawn with an irrational slope given by $\tan\alpha = \tau$. Then points within the strip are projected onto the line OR to form a series of points (marked by red stars in the figure) with a series of long and short spacings.

Nicolaas De Bruijn (1918–2012) [37] showed that Penrose tilings could be viewed as two-dimensional slices of five-dimensional hypercubic structures. Equivalently, the Fourier transform of such a quasicrystal is nonzero only at a dense set of points spanned by integer multiples of a finite set of basis vectors (the projections of the

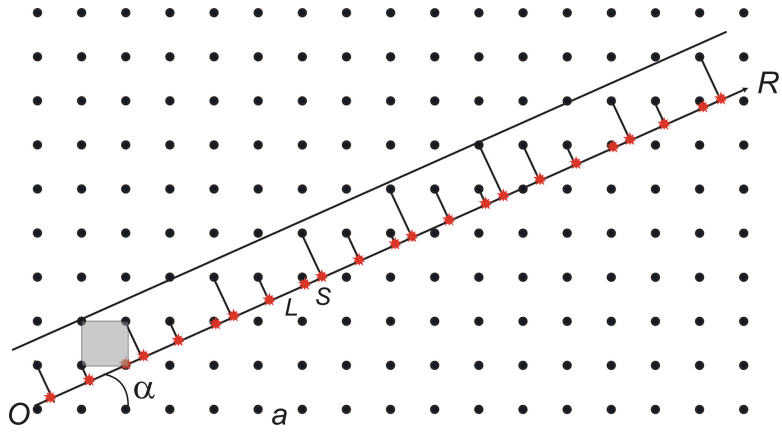

Figure 3.66. Illustration of the strip/projection method from two dimensions to one dimension.

primitive reciprocal-lattice vectors of the higher-dimensional lattice). In polygonal quasicrystals the projection is from a dimension of 4, whereas for icosahedral quasicrystals, it is 6. For further reading about quasicrystals, I recommend Janot [38].

Aperiodic crystals also include the so-called incommensurate or modulated crystals, where superimposed on a fundamentally periodic arrangement, there are long-range periodic wave-like disturbances to the atomic positions so that the structure never actually repeats. This is illustrated in figure 3.67, where (a) shows a normal commensurate structure, using the Statue of Liberty as a 'basis'. In (b), another commensurate structure is shown, but with twice the repeat determined by a wave-like modulation. In (c), the modulating wave is not commensurate with the fundamental repeat of the Statue of Liberty, thus creating a one-dimensional incommensurate structure. In diffraction space, a three-dimensional incommensurate crystal structure results in extra reflections that do not lie on the nodes of the usual reciprocal lattice. We can describe the crystal in the following way

$$C(\mathbf{r}) = (B(\mathbf{r}) * L_1) \times L_2 \tag{3.115}$$

L_2 is the long-period modulation wave, with periodicity greater than L_1. Using the convolution theorem,

$$\tilde{C}(\mathbf{r}) = (\tilde{B}(\mathbf{r}) \times \tilde{L}_1) * \tilde{L}_2 \tag{3.116}$$

The periodicity of $\tilde{L}_2$ is less than that of $\tilde{L}_1$ and so the convolution of the two results in reciprocal space in main peaks with associated satellites.

However, going to a higher dimension, the spots will lie on regular reciprocal-lattice nodes. For instance, consider the case of a three-dimensional reciprocal lattice with an additional one-dimensional modulation. From (3.114)

$$\mathbf{a}_4^* = \mathbf{q} = q_1\mathbf{a}_1^* + q_2\mathbf{a}_2^* + q_3\mathbf{a}_3^* \tag{3.117}$$

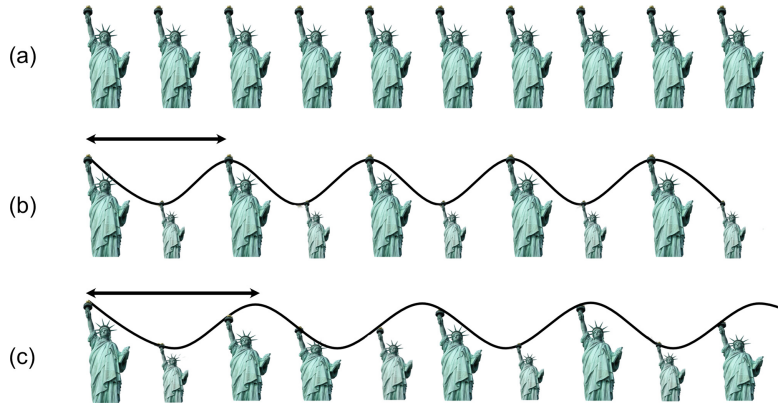

Figure 3.67. Commensurate and incommensurate modulations: (a) regular periodicity, (b) commensurate modulation, (c) incommensurate modulation.

where at least one of the q_i is irrational to give extra reflections in the diffraction pattern. We see from this that such a reciprocal lattice with its additional satellite points can be treated as a true periodic lattice within a four-dimensional space. The space symmetry of such a crystal structure would then be described by a four-dimensional superspace group. This idea was first reported for the crystal structure of Na_2CO_3 during the IUCr Congress in Kyoto (1972) by Pim de Wolff (1919–98) [39]. I was present when he presented his paper, and I recall that it was received with considerable hostility and argument. But since then, this has become widely accepted. Interestingly, as mentioned in section 1.2, the faces of crystals of the mineral calaverite, $AuTe_2$, disobeyed the Law of Rational Indices, and subsequently, it was determined that calaverite was, in fact, an example of an incommensurate material, where the modulation arises from Te valence fluctuations [40].

Finally, I should make a comment about the concept of *order*. Humans have a natural tendency to recognise patterns, and so we might conclude that we know order when we see it. However, order turns out to be very difficult to define, at least mathematically. The observation of peaks in a diffraction pattern is one way to think of order. However, another might be in real space connected with rules in positioning the atoms. Both ways of thinking about order, it seems to me, are not perfect. If we think in terms of Fourier transforms, the intensity at any point in reciprocal space arises from two-point correlations for diffraction from conventional crystals. This type of correlation corresponds to calculating an autocorrelation function (such as the Patterson function). One problem, here, is that starting from the Fourier transform of the autocorrelation function, and working back to direct space, does not necessarily provide a unique solution for the crystal structure, and so does not give a complete characterisation of structures that show pure point diffraction. Such different structures are called *homometric*. As explained by Uwe Grimm, in a highly recommended and profound paper [41], if we think of order as being equivalent to having a deterministic rule, it is possible, at least mathematically, to construct toy models in which the scatterers are arranged according to rules, but at the same time display a continuous diffraction pattern, rather than Bragg peaks.

Grimm also points out that we do not know of any materials that have aperiodically-ordered structures beyond incommensurate and quasicrystals, but this does not rule out the possibility that materials with other symmetries might be discovered in the future. Therefore, the definitions of a crystal (real or reciprocal) should be seen as working definitions that may need to be revised in future.

3.15 Disordered and partially-ordered crystals

So far, we have considered crystals in terms of the average positions of atoms in the solid. However, in reality, the atoms are in a state of thermal agitation, and so the information contained within the Bragg intensities is essentially a time-average of the crystal structure. Furthermore, there is spatial disorder in many crystals, for example, where certain atoms are replaced by different atoms or molecules are oriented differently from the average. This disorder may not be completely random, but there may be some partial or short-range order, where statistically ordered

arrangements exist in the crystal. The disordered part of the structure gives rise to extra, so-called diffuse, scattering superimposed on the Bragg intensity pattern so that we can write the diffraction intensity as the sum of two terms (see section 3.9):

$$I = I_{\text{Bragg}} + I_{\text{diffuse}} \tag{3.118}$$

By conservation of energy, the more disorder that is present, the lower I_{Bragg} and the higher I_{diffuse}. So, measurements of the Bragg intensities alone give information about the *average* crystal structure, whereas the diffuse intensity tells us about the *departures* from the average structure.

There are two ways to compute the diffracted intensity.

1. $\rho(\mathbf{r}) \xrightarrow{FT} F(\mathbf{Q}) \Rightarrow I(\mathbf{Q}) = F(\mathbf{Q})F(\mathbf{Q})^*$
2. $\rho(\mathbf{r}) \overset{\text{autocorrelation}}{\rightarrow} A(\mathbf{r}) = \int \rho(\mathbf{r}')\rho(\mathbf{r}+\mathbf{r}')d^3\mathbf{r} \Rightarrow I(\mathbf{Q}) = \int A(\mathbf{r})e^{i\mathbf{Q}\cdot\mathbf{r}}d^3\mathbf{r}$

The second method, using an autocorrelation function approach, is generally preferred in considering diffraction from disordered structures, where the arrangements of atomic or molecular species are governed by probability functions.

To understand this further, consider figure 3.68, where black and white horses represent two sorts of molecule or atom. In (a), you will note that there are domains containing just white horses and domains containing only black horses. So, the long-range order has been broken, and the effect of this in diffraction space is to increase I_{diffuse} with respect to I_{Bragg}. This results in broad diffuse peaks sitting beneath the Bragg reflections. In (b), the correlated regions tend to have alternating black and white horses, so that there is a tendency to double the unit-cell repeat distances. This gives rise to a broad diffuse peak halfway between the reciprocal-lattice nodes,

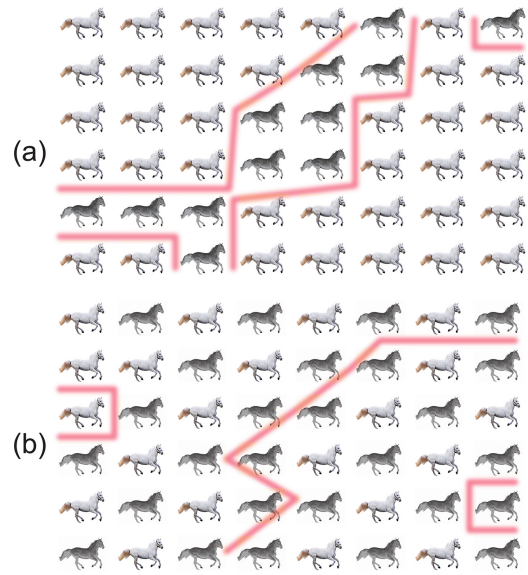

Figure 3.68. Short-range domains.

i.e., between the Bragg peaks. In both cases, the widths of the diffuse peaks are inversely proportional to the average sizes of the correlated domains. When the horses are randomly distributed with respect to the lattice sites, diffuse intensity will add to the overall background in the diffraction pattern.

Suppose the white and black horses, or two atom types, are labelled A and B with scattering factors f_A and f_B. Let $P_{AB(r)}$ be the probability of finding A given B at a distance r, and $P_{AA(r)}$ be the probability of finding A given A at a distance r. Then

$$H = P_{AA(r)}f_A^2 + P_{BB(r)}f_B^2 + (P_{AB(r)} + P_{BA(r)})f_Af_B \tag{3.119}$$

H is the height of the autocorrelation function (as in the Patterson function, see equation (3.106)). Now let $P_{AA(r)} = P_{BB(r)}$ and $P_{AB(r)} = P_{BA(r)}$. Then

$$P_{AB(r)} = ½ - P_{BB(r)} = ½ - P_{AA(r)} \tag{3.120}$$

and

$$H = P_{AA(r)}f_A^2 + P_{AA(r)}f_B^2 + (1 - 2P_{AA(r)})f_Af_B \tag{3.121}$$

This can be divided into two terms, thus

$$H = ¼(f_A + f_B)^2 + (P_{AA(r)} - ¼)(f_A - f_B)^2 \tag{3.122}$$

This shows that the autocorrelation function has two terms. The first one is simply the average of the two scattering factors, corresponding to the information obtained from Bragg scattering. The second term is a probability function multiplied by the difference in scattering factors, and it is this term that gives rise to the diffuse scattering.

There are many ways to calculate short-range order diffuse scattering. For example, let's look at stacking disorder, where layers h are partially ordered one-dimensionally in a particular direction. This was initially treated by A J C (Arthur James Cochran) Wilson (1914–95) [42]. Consider N layers of atoms of type A and B, and let α be the probability of a 'mistake' in the stacking of the layers. Then

α close to 0 implies $AAAAAAAA|BBBBBBBB|AAA|BBBBB|\ldots\ldots$
α close to 1 implies $ABABAB|BABABABA|ABAB|BABABA|\ldots\ldots$

Let

$$\delta = \alpha - ½ \tag{3.123}$$

Wilson was then able to obtain the following expression:

$$\begin{aligned} I(h) = {} & ¼(f_A + f_B)^2\left[N + 2\sum_{n=1}^{N}(N-n)\cos 2\pi h\right] \\ & + ¼(f_A - f_B)^2\left[N + 2\sum_{n=1}^{N}(N-n)(-2\delta)^n \cos 2\pi h\right] \end{aligned} \tag{3.124}$$

and then

$$I(h) = ¼(f_A + f_B)^2 \frac{\sin^2 \pi Nh}{\sin^2 \pi h} + ¼(f_A - f_B)^2 N \frac{1 - (-2\delta)^2}{1 + (-2\delta)^2 - 2(-2\delta)\cos \pi h)} \tag{3.125}$$

This can be written as

$$I(h) = (\langle f \rangle)^2 \frac{\sin^2 \pi Nh}{\sin^2 \pi h} + ¼(\Delta f)^2 N \frac{1 - (-2\delta)^2}{1 + (-2\delta)^2 - 2(-2\delta)\cos \pi h)} \tag{3.126}$$

The first term is I_{Bragg} and gives sharp diffraction peaks corresponding to the average scattering factors from A's and B's. The second term is I_{diffuse}, and this depends on the difference in scattering between species A and B, so this formula would also apply to a one-dimensional atomic or molecular substitutional disorder. Figure 3.69 illustrates, schematically, the formation of this type of diffuse scattering for different values of δ. For $\delta = 0$, there is a random distribution of A's and B's, thus creating a low and constant background between the reciprocal-lattice nodes, ignoring any instrumental correction factors. In practice, the scattering is likely to be weak and difficult to observe. When δ is negative, the scattering gathers under the Bragg peaks at the reciprocal-lattice nodes, and when it is positive, the extra scattering forms halfway between the Bragg peaks.

Two consequences of the theory are that for diffuse scattering passing through Bragg peaks, according to equation (3.126):

1. if the disorder involves substitution of atomic species it also passes through the origin of reciprocal space;
2. if the disorder is related to atomic or molecular displacement/orientation it disappears close to the origin of reciprocal space.

Considerable progress has been made in recent years in the study of complex diffuse scattering, not only with x-rays but also with neutron and electron diffraction. An excellent example is given in figure 3.70, where neutron scattering has revealed a wealth of diffuse scattering detail. Analysis of the diffuse scattering from the organic

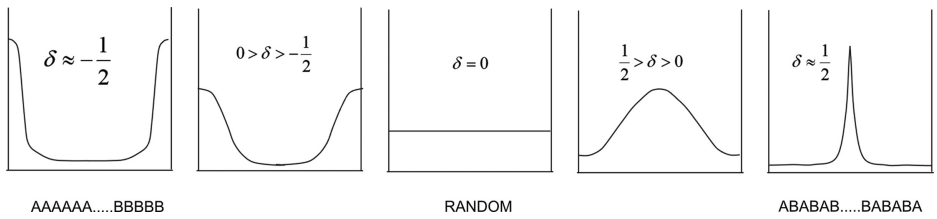

Figure 3.69. Diffuse scattering for different probabilities of 'mistakes'.

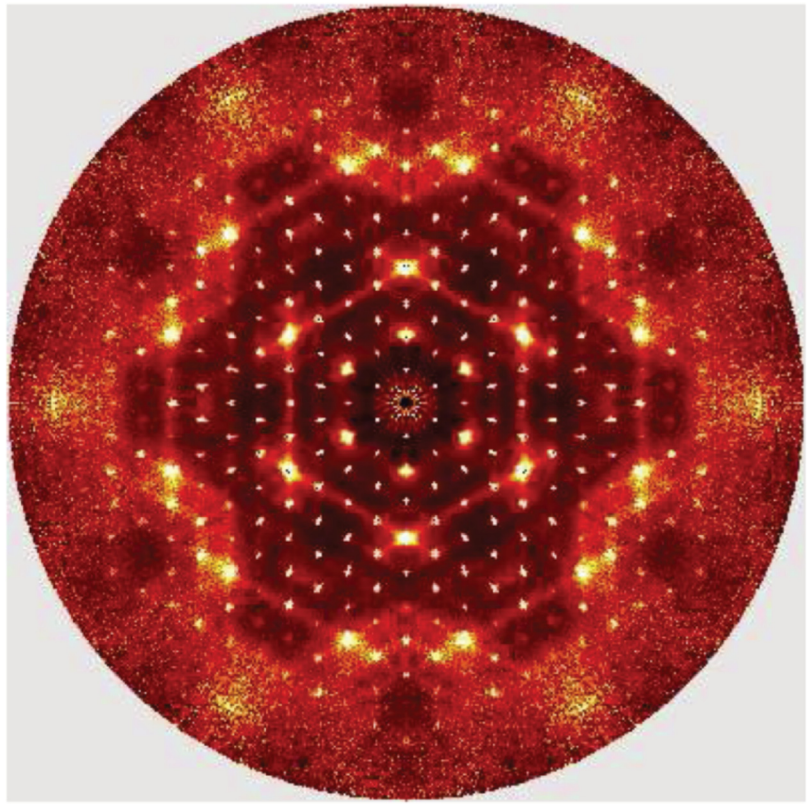

Figure 3.70. Diffuse scattering from a crystal of benzil, using neutron scattering by Welberry and Whitfield. Reprinted from [43] with permission from MDPI.

molecular crystal, benzil ($C_{14}H_{10}O_2$), by Welberry *et al* [44] has shown that the scattering is thermal in origin, and quite clearly that the diffuse lines, that feature so prominently in the observed diffraction patterns, are due to strong longitudinal displacement correlations (note that the diffuse lines do not pass through the origin). These are transmitted from molecule to molecule via a network of intermolecular contacts. Longitudinal correlation means that the direction of displacement and the direction of correlation are the same. For more details about diffuse scattering, see the review by Welberry [45], where many more examples are given.

References

[1] Clifton I J, Elder M and Hajdu J 1991 Experimental strategies in Laue crystallography *J. Appl. Crystallogr.* **24** 267–77

[2] Ren Z, Bourgeois D, Helliwell J R, Moffat K, Šrajer V and Stoddard B L 1999 Laue crystallography: coming of age *J. Synchrotron Radiat.* **6** 891–917

[3] Buras B, Gerward L, Glazer A M, Hidaka M and Olsen J S 1979 Quantitative structural studies by means of the energy-dispersive method with x-rays from a storage ring *J. Appl. Crystallogr.* **12** 531–6

[4] Bourdillon A J, Glazer A M, Hidaka M and Bordas J 1978 High-resolution energy-dispersive diffraction using synchrotron radiation *J. Appl. Cryst.* **11** 684–7
[5] Harburn G, Taylor C and Welberry T R 1975 *Atlas of Optical Transforms* (Ithaca, NY: Cornell University Press)
[6] Ewald P P (ed) 1962 *Fifty Years of X-Ray Diffraction* (Boston, MA: Springer US)
[7] Macchi P 2020 The connubium between crystallography and quantum mechanics *Crystallogr. Rev.* **26** 209–68
[8] Kleemiss F *et al* 2021 Accurate crystal structures and chemical properties from NoSpherA2 *Chem. Sci.*
[9] Compton A H 1930 The determination of electron distributions from measurements of scattered x-rays *Phys. Rev.* **35** 925–38
[10] Mitchell D P and Powers P N 1936 Bragg reflection of slow neutrons *Phys. Rev.* **50** 486–7
[11] von Halban H and Preiswerk P 1936 Experimental evidence of neutron diffraction *C.R. Hebd. Séances Acad* **203** 73
[12] Boothroyd A T 2020 *Principles of Neutron Scattering from Condensed Matter* (Oxford: Oxford University Press)
[13] Zou X, Hovmöller S and Oleynikov P 2011 *Electron Crystallography: Electron Microscopy and Electron Diffraction* (Oxford: Oxford University Press)
[14] Grundy P J and Jones G A 1976 *Electron Microscopy in the Study of Materials* (London: Edward Arnold)
[15] Forbes B D *et al* 2011 Thermal diffuse scattering in transmission electron microscopy *Ultramicroscopy* **111** 1670–80
[16] Als-Nielsen J and McMorrow D 2011 *Elements of Modern X-ray Physics* (New York: Wiley)
[17] Castellano E E and Main P 1985 On the classical interpretation of thermal probability ellipsoids and the Debye–Waller factor *Acta Crystallogr. Sect.* A **41** 156–7
[18] Zachariasen W H 1945 *Theory of X-ray Diffraction in Crystals* (Toronto: General Publishing Co. Ltd)
[19] Glazer A M and Hart M 1980 A new era in crystallography *Phys. Bull.* **31** 278–80
[20] Stadnicka K, Glazer A M and Moxon J R L 1985 The structural chirality and optical activity of α-$LiIO_3$ *J. Appl. Cryst.* **18** 237–40
[21] Giacovazzo C *et al* 2011 *Fundamentals of Crystallography* (Oxford: Oxford University Press)
[22] Ladd M and Palmer R 2003 *Structure Determination by X-ray Crystallography* (New York: Springer US)
[23] Clegg W 2015 *X-ray Crystallography* (Oxford Chemistry Primers) (Oxford: Oxford University Press)
[24] Glazer A M 2016 FOURIER2D and FOURIER3D: programs to demonstrate Fourier synthesis in crystallography *J. Appl. Crystallogr.* **49** 2276–8
[25] Oszlányi G and Sütő A 2004 *Ab initio* structure solution by charge flipping *Acta Crystallogr. Sect. A: Found. Crystallogr.* **60** 134–41
[26] Chapuis G e-Crystallography (https://www.epfl.ch/schools/sb/research/iphys/teaching/crystallography/)
[27] Rietveld H M and IUCr 1969 A profile refinement method for nuclear and magnetic structures *J. Appl. Crystallogr.* **2** 65–71
[28] Coehlo A Topas Academic (http://www.topas-academic.net/)
[29] Yokota H, Zhang N, Taylor A E, Thomas P A and Glazer A M 2009 Crystal structure of the rhombohedral phase of $PbZr_{1-x}Ti_xO_3$ ceramics at room temperature *Phys. Rev. B—Condens. Matter Mater. Phys.* **80** 104109

[30] Peel M D, Thompson S P, Daoud-Aladine A, Ashbrook S E and Lightfoot P 2012 New twists on the perovskite theme: crystal structures of the elusive phases R and S of $NaNbO_3$ *Inorg. Chem.* **51** 6876–89
[31] Zhang N *et al* 2014 The missing boundary in the phase diagram of $PbZr_{1-x}Ti_xO_3$ *Nat. Commun.* **5** 5231
[32] Kerenyi N X-ray free-electron laser science (https://nux.ethz.ch/research/x-ray-free-electron-laser-science.html)
[33] Spence J C H Serial crystallography at XFELS and synchrotrons (https://www.iucr.org/news/newsletter/etc/articles?issue=150473&result_138339_result_page=5)
[34] Nannenga B L and Gonen T 2019 The cryo-EM method microcrystal electron diffraction (MicroED) *Nat. Methods* **16** 369–79
[35] Quasicrystal (https://en.wikipedia.org/wiki/Quasicrystal)
[36] Online Dictionary of Crystallography (https://dictionary.iucr.org/Main_Page)
[37] de Bruijn N G 1981 Algebraic theory of Penrose's non-periodic tilings of the plane. I *Indigationes Math.* **84** 39–52
[38] Janot C 1994 *Quasicrystals. A Primer* (Oxford: Oxford University Press)
[39] de Wolff P M 1974 The pseudo-symmetry of modulated crystal structures *Acta Cryst.* **A30** 777–85
[40] Schutte W J and de Boer J L 1988 Valence fluctuations in the incommensurately modulated structure of calaverite *Acta Crystallogr. Sect. B Struct. Crystallogr. Cryst. Chem.* **B44** 486–94
[41] Grimm U 2015 Aperiodic crystals and beyond *Acta Cryst.* **B71** 258–74
[42] Wilson A J C 1949 *X-Ray Optics. The Diffraction of X-Rays by Finite and Imperfect Crystals* (London: Methuen)
[43] Welberry T R and Whitfield R 2018 Single crystal neutron diffuse scattering *Quantum Beam Sci.* **2** 2–11
[44] Welberry T R, Goossens D J, Edwards A J and David W I F 2001 Diffuse x-ray scattering from benzil: analysis via automatic refinement of a Monte Carlo model *Acta Crystallogr. Sect.* A **A57** 101–9
[45] Welberry T R 2004 *Diffuse X-ray Scattering and Models of Disorder* (Oxford: Oxford University Press)

IOP Publishing

A Journey into Reciprocal Space (Second Edition)
A crystallographer's perspective
Anthony Michael Glazer

Chapter 4

Dynamical diffraction

X-rays… I am afraid of them. I stopped experimenting with them two years ago, when I came near to losing my eyesight, and Dally, my assistant, practically lost the use of both of his arms.

(Thomas Edison)

4.1 Multiple scattering

So far, we have confined ourselves to cases where the kinematic approximation applies: that is, the interaction between the beam and the crystal is 'weak'. In other words, only a small fraction of the incident radiation is diffracted. In terms of quantum mechanics, this is also a result of the so-called first Born approximation. However, consider what can happen (figure 4.1) if the beam is scattered by planes in a perfect crystal, i.e., one without any defects or dislocations [1, 2]. As usual, some of the incident beam can be thought of as being 'reflected' by the first plane it meets, following Bragg's Law, while the remainder continues to the next plane. This plane, too, reflects the beam in the same way, but notice how this time it is also reflected back by the first plane. This continues with the next plane and so on, to give a series of multiple scatterings.

The upshot of this is that our assumption that most of the incident radiation passes through the crystal and is not diffracted is not correct when the crystal is perfect! This surprising result means that to use diffraction intensities to solve the crystal structure, crystallographers working on structure determination do not want perfect crystals, contrary to what you might expect.

Instead, the requirement is for so-called 'ideally imperfect' crystals: that is just enough imperfections to hinder the multiple scattering but not so much as to destroy the crystal's integrity. Sometimes, crystallographers will deliberately drop a crystal into liquid nitrogen to introduce some mosaicity by thermally shocking it for this

doi:10.1088/978-0-7503-3875-2ch4

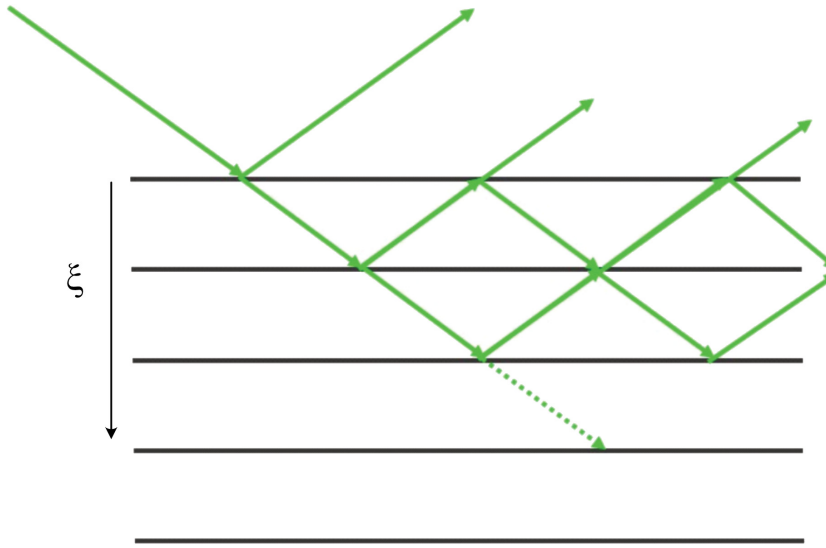

Figure 4.1. The effect of diffraction (reflection) by successive planes in a perfect crystal. ξ is known as the extinction distance.

purpose. Even so, it is often found that the intensities of some reflections are less than those calculated theoretically from the crystal structure. Crystallographers know this as *extinction*, and it is often corrected for in crystallographic computer programs, usually by empirical correction factors. There are two types of extinction recognized by crystallographers.

1. *Primary extinction*—loss of intensity due to multiple scattering inside every block of a mosaic crystal. A mosaic crystal is described as a conglomerate of minute crystalline blocks, tilted with respect to each other by fractions of a minute of arc. Each block is separated from the surrounding blocks by faults and cracks. At the Bragg angle, each incident wave can undergo multiple reflections from different atomic planes; each scattering event causes a phase difference of $\lambda/4 = \pi/2$ so that along each direction, waves differing by an even number of scatterings, i.e., by $n\pi$ in phase, interfere, and the intensity decreases rapidly with the number of scatterings. This causes a significant difference in intensity and an overall reduction of the intensity as given by the kinematic theory.
2. *Secondary extinction*—the loss of intensity when the incident beam passes through mosaic blocks in a crystal that are closely aligned. If two successive blocks are aligned, some of the incident intensity is reflected away by the first block before it reaches the second. Secondary extinction is equivalent to an increase of the linear absorption coefficient, but it is negligible for sufficiently small crystals.

Definition *The quantity ξ is known as the* ***extinction distance*** *and can be thought of as a mean free path for the transmitted wave.*

In transmission electron diffraction, multiple scattering is a more severe problem because of the strong Coulombic interaction of electrons with those in the crystal. The result is that the central beam intensity can appear weaker than some of the diffracted beams. On average, dynamical scattering increases the intensity of weaker reflections, whereas strong reflections become less intense. This can make all the diffraction spots have nearly the same intensity. Crystal size is an important factor affecting dynamical scattering, as the probability of multiple scattering events increases with sample thickness.

4.2 Renninger effect

Multiple scattering can be a severe problem in determining crystal structures by x-ray, neutron, or electron diffraction. A particular case can arise when the diffracted beam is so intense that it effectively acts as a second incident beam in the crystal. Consider a beam along CO with wave-vector $\mathbf{k}_0$ and a strongly diffracted beam CA with wave-vector $\mathbf{k}_1$ to the reciprocal-lattice node at $h_1k_1l_1$ in figure 4.2. We can then draw a new Ewald sphere (dashed curve) centred at C′ with an incident beam along C′O. C′O is parallel to CA and has the same length.

Now suppose for the dashed circle, we draw the line C′B′ corresponding to wave-vector $\mathbf{k}_2$ ending on a reciprocal-lattice node $h_2k_2l_2$ at B′. Simple geometry shows

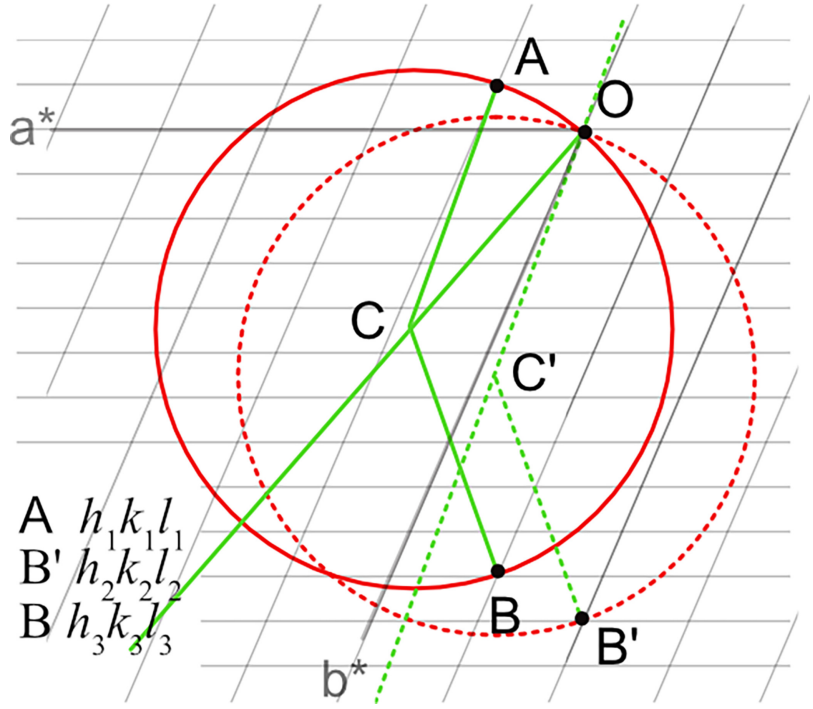

Figure 4.2. Renninger effect produced when two reciprocal-lattice points lie simultaneously on the Ewald sphere.

that a line CB drawn parallel to C′B′ must end on a reciprocal-lattice node, $h_3k_3l_3$ at B. We can then write

$$\begin{aligned} \mathbf{k}_1 - \mathbf{k}_0 &= h_1\mathbf{a}^* + k_1\mathbf{b}^* + l_1\mathbf{c}^* \quad \text{triangle CAO} \\ \mathbf{k}_2 - \mathbf{k}_1 &= h_2\mathbf{a}^* + k_2\mathbf{b}^* + l_2\mathbf{c}^* \quad \text{triangle C}'\text{B}'\text{O} \end{aligned} \tag{4.1}$$

Adding the two equations

$$\mathbf{k}_2 - \mathbf{k}_0 = (h_1 + h_2)\mathbf{a}^* + (k_1 + k_2)\mathbf{b}^* + (l_1 + l_2)\mathbf{c}^* \tag{4.2}$$

Then for triangle CBO the node at B is given by

$$h_3 = h_1 + h_2 \quad k_3 = k_1 + k_2 \quad l_3 = l_1 + l_2 \tag{4.3}$$

The effect, therefore, is to add intensity to the node $h_3k_3l_3$. In the figure, the indices are

A	$1\ \bar{1}\ 0$
B′	$\bar{2}\ 1\ 1\ 0$
B	$\bar{1}\ 1\ 0\ 0$

Generally, such extra so-called Renninger reflections tend to be weak but may appear in places where the space-group symmetry dictates that there should be an absence of intensity. Therefore, it is important in using diffraction data to recognize the existence of these extra reflections when present, and remove them from the list of usable reflections (they can sometimes be identified by being sharper than the normal Bragg reflections). In some cases, interference from Renninger effects can be a serious matter: for instance, in the structure determination of the material $LiNbO_3$, a total of 42 Renninger reflections was observed!

4.3 Darwin's dynamical theory

There are several different theories to explain dynamical diffraction. In this section, I shall briefly outline one of the early ideas due to Charles Galton Darwin (1887–1962) [3]. This was extended shortly after by Ewald, who introduced the idea of wave-fields, and then again by von Laue. For thorough treatments of dynamical scattering, I recommend the books by Warren [4] and Authier [2]. Darwin's basic idea was to calculate the scattering amplitude due to an entire plane of atoms. In the kinematic theory of scattering, it is assumed that the far-field approximation applies, namely that the source to crystal distance is much larger than the distance between the crystal and a detector. However, for an ideal, perfect crystal, this condition needs to be relaxed with a geometry such as that represented in figure 4.3. S is the source of a beam at a distance R, and D is a detector for reflection, and D′ is for transmission, both at a distance r. No far-field approximation is made.

In the theory, the diffracted wave is calculated as a superposition of plane waves reflected from and transmitted through individual atomic planes, and multiple

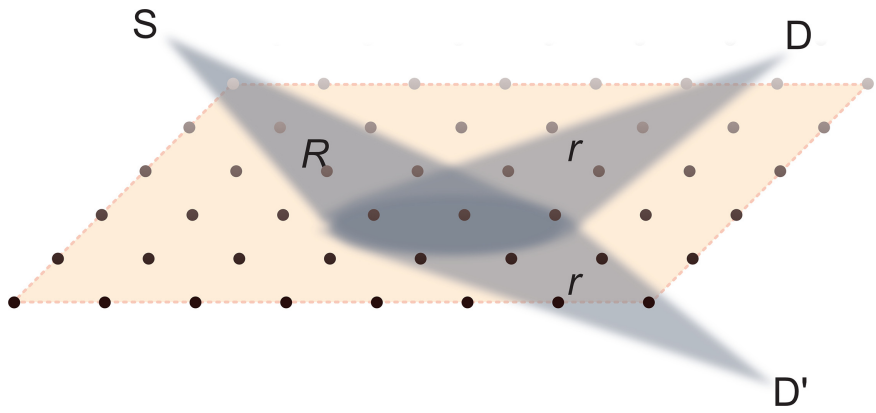

Figure 4.3. Scattering from a perfect, extended plane of atoms.

reflection is included. To do this, Darwin summed up all the contributions from transmission and reflection for all the planes, where

$$\begin{aligned} t_0 &= 1 - iq_0 \\ r_h &= -iq_h \end{aligned} \tag{4.4}$$

q_0 and q_h are the transmission and reflection coefficients, respectively, and t_0 and r_h are the transmissivity and reflectivity.

Darwin was able to show that the real scattered amplitude is proportional to the *density* of scatterers, rather than the total number of atoms, a departure from the kinematic approximation. In transmission, Darwin's theory gives the refractive index for x-rays as:

$$n = 1 - r_e \frac{N\lambda^2 Z_e}{2\pi} < 1 \tag{4.5}$$

Here, N is the number of atoms per unit volume, and Z_e is the number of electrons per atom. r_e is the classical electron radius ($2.817\,9403 \times 10^{-15}$ m). This result shows that the refractive index is less than 1, thus predicting that x-rays undergo total external reflection from the surfaces of materials. A typical refractive index for x-rays is around 10^{-5} to 10^{-6} less than 1, and the critical angle for total external reflection is around 10^{-3} degrees. This fact is often used in the construction of x-ray mirrors and focusing devices for experiments using synchrotron radiation.

Another finding from Darwin's theory is that the angular region, where the x-ray beam shows total reflection, is given by

$$|\theta - \theta_{\text{Bragg}}| < r_e \frac{F(hkl)\lambda^2}{\pi V \sin(2\theta)} = s \tag{4.6}$$

The angular difference s is known as the *Darwin width*. Figure 4.4 shows the shape of the reflection profile for x-rays, in the absence of any absorption, according to Darwin's theory. In this case, for a perfect, infinite crystal, the Bragg peak width is

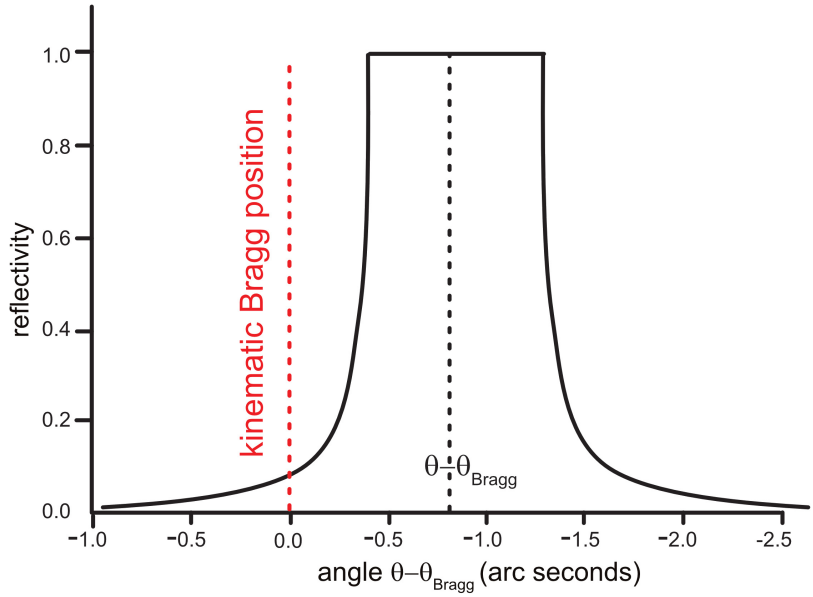

Figure 4.4. Reflectivity profile according to Darwin's theory. Calculated for silicon (111) slice, 10 mm thick, 60 keV (adapted from [5]).

not given by a delta function but is finite. Outside this total reflection region, where $|\theta - \theta_{\mathrm{Bragg}}|/s > 1.0$, the scattered intensity decays polynomially. Note that the angular position of the kinematic Bragg reflection is displaced from the centre position of the Darwin curve. This arises from the fact that the x-ray wavelength and phase velocity inside the crystal are slightly greater than in free space.

In considering the diffraction geometry, there are two basic arrangements: Laue and Bragg. Figure 4.5 shows the reflectivity profile for a silicon crystal in the Bragg geometry, where the incident beam is reflected from horizontal planes. The example shown includes absorption of the x-ray beam, which smooths out the flat region of the Darwin profile in figure 4.4. As the crystal is thick, very little, if any, of the incident intensity passes through the crystal.

The Laue case is shown in figure 4.6. Here we see that the incident beam emerges from the opposite face of the crystal, split into two components. The profiles for reflectivity and transmissivity, in this case, show a central maximum (or minimum) together with subsidiary maxima and minima. If the absorption is high, one might expect that the emerging beams should be very weak. However, it has been found that at any arbitrary angle, the intensities of the two beams are zero, as expected. But at the Bragg angle, both the reflected and transmitted beam have, roughly, equally strong intensity. This surprising observation was first discovered by Gerhard Borrmann (1908–2006) in 1941 [6] and later interpreted by von Laue [7]. This is an example of the so-called *Borrmann effect*, sometimes known as the *anomalous transmission effect* [8]. The Borrmann effect is one of the most remarkable manifestations of the dynamical diffraction of x-rays. The beam, which enters the

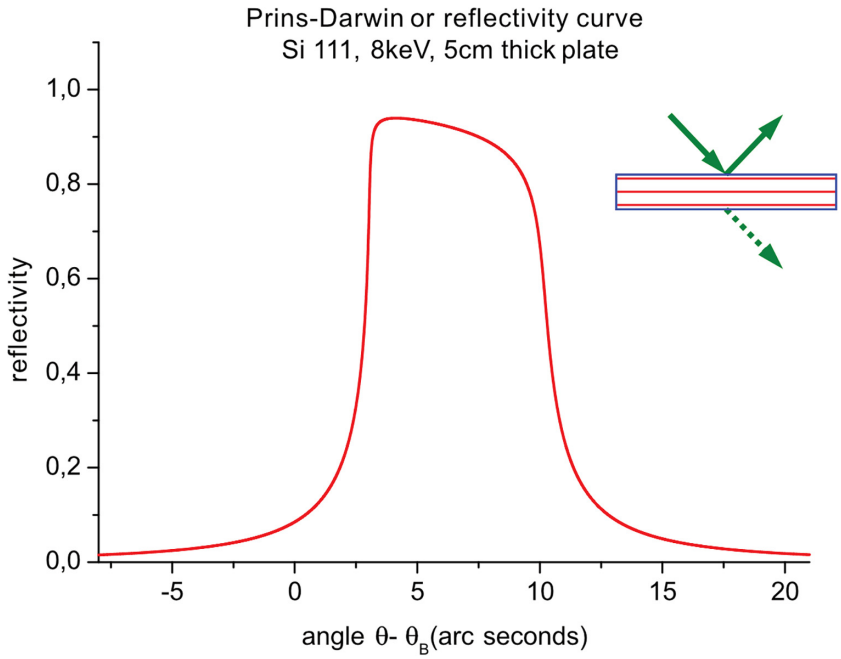

Figure 4.5. Effect of absorption and crystal thickness on reflectivity in a Bragg case (adapted from [5]).

sample face on the top, is a single plane wave. Initially, the x-ray beam undergoes normal absorption. However, as it penetrates further into the crystal, an increasing fraction of its energy is transferred to the diffracted beam. Note that the two beams emerge directly from the opposite point to the incident beam, suggesting that the combination of the two beams has travelled through the crystal parallel to the diffracting planes.

It is also instructive to see how the reflectivity depends on crystal thickness for different situations. In figure 4.7, the reflectivity is plotted in terms of the crystal thickness for three cases in the absence of absorption. In the kinematic approximation, this is a straight line, while in the Bragg dynamical diffraction geometry, once the thickness exceeds the extinction distance, the reflectivity remains constant. In the Laue geometry, we see a succession of oscillations starting roughly just above the extinction distance.

Finally, in the absence of any absorption, the area under the reflectivity curve is proportional to $V|F(hkl)|^2$ in the kinematic limit, where V is the illuminated volume of the crystal. In dynamical theory, on the other hand, it is found that

$$\begin{aligned} R_{ref} &\sim |F(hkl)| \text{ for the Laue case} \\ R_{ref} &\sim 2|F(hkl)| \text{ for the Bragg case} \end{aligned} \tag{4.7}$$

4.4 Bloch's theorem

In condensed matter physics, Bloch's theorem states that solutions to the Schrödinger equation in a periodic potential $V(\mathbf{r})$ take the form of a plane wave

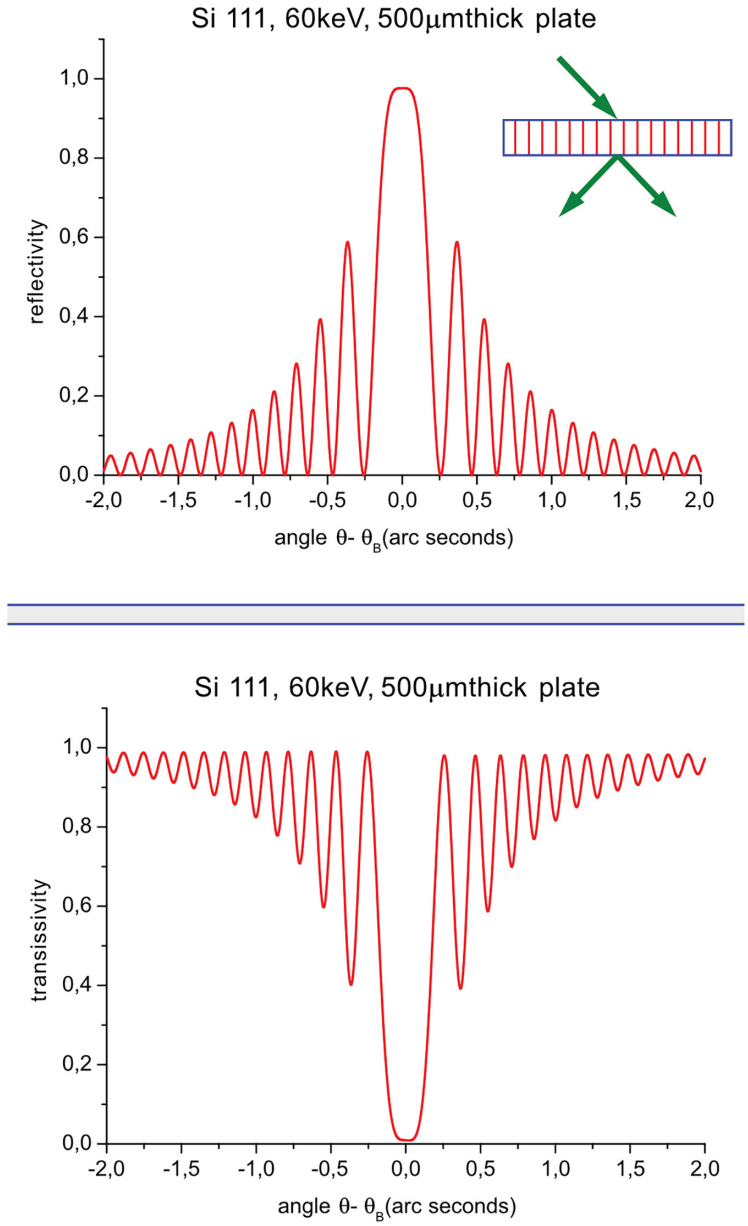

Figure 4.6. Effect of absorption and crystal thickness on reflectivity and transmissivity in a Laue case (adapted from [5]).

modulated by a periodic function. These solutions, sometimes known as Bloch states, are eigenstates in energy and serve as a suitable basis for the wave functions of electrons in crystalline solids.

Consider the effect of the lattice translation Seitz operator $\{1|\mathbf{t}_n\}$ acting as a *function space operator* on the basis function $e^{i\mathbf{k}\cdot\mathbf{r}}$. Then

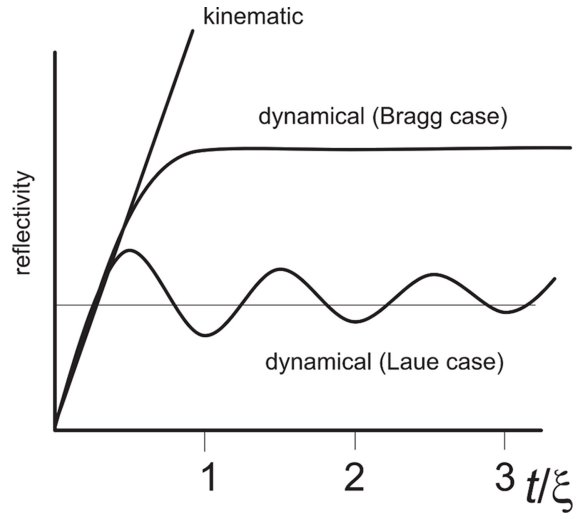

Figure 4.7. Integrated intensity for kinematic and dynamical scattering.

$$\{1|\mathbf{t}_n\}e^{i\mathbf{k}\cdot\mathbf{r}} = e^{i\mathbf{k}\cdot\{1|\mathbf{t}_n\}^{-1}\mathbf{r}} = e^{i\mathbf{k}\cdot(\mathbf{r}-\mathbf{t}_n)} \tag{4.8}$$

This can be rewritten

$$\{1|\mathbf{t}_n\}e^{i\mathbf{k}\cdot\mathbf{r}} = e^{i\mathbf{k}\cdot\mathbf{r}}e^{-i\mathbf{k}\cdot\mathbf{t}_n} \tag{4.9}$$

Now, instead of $e^{i\mathbf{k}\cdot\mathbf{r}}$ we can use any function of the form

$$\psi_{\mathbf{k}}(\mathbf{r}) = u_{\mathbf{k}}(\mathbf{r})e^{i\mathbf{k}\cdot\mathbf{r}} \tag{4.10}$$

where

$$u_{\mathbf{k}}(\mathbf{r}) = u_{\mathbf{k}}(\mathbf{r} + \mathbf{t}_n) \tag{4.11}$$

for all values of $\mathbf{t}_n$. The basis functions of the translation group $\mathbf{T}$ are of the form defined by equations (4.10) and (4.11), where $\mathbf{T}$ is given by the set $\{1|n_1\mathbf{t}_1 + n_2\mathbf{t}_2 + n_3\mathbf{t}_3\}$, and n_1, n_2 and n_3 are integers.

Definition. ***Bloch's theorem*** *states that the wave function for a particle moving in a periodic potential* $V(\mathbf{r})$ *with periodicity defined by* $\mathbf{T}$ *is given by* $\psi_{\mathbf{k}}(\mathbf{r}) = u_{\mathbf{k}}(\mathbf{r})e^{i\mathbf{k}\cdot\mathbf{r}}$.

The periodic function $u_{\mathbf{k}}$ is usually known as a *Bloch function*, which represents the atoms in a unit cell. It can be written as a sum over reciprocal-lattice vectors

$$u_{\mathbf{k}}(\mathbf{r}) = \sum_{\mathbf{G}} C_{\mathbf{G}}e^{i\mathbf{G}\cdot\mathbf{r}} \tag{4.12}$$

This form guarantees that $u_{\mathbf{k}}(\mathbf{r}) = u_{\mathbf{k}}(\mathbf{r} + \mathbf{T})$ for any $\mathbf{T}$. Therefore, the full wave function is expressed as

$$\psi_{\mathbf{k}}(\mathbf{r}) = \sum_{\mathbf{G}} C_{\mathbf{G}}e^{i(\mathbf{G}+\mathbf{k})\cdot\mathbf{r}} \tag{4.13}$$

This means that each eigenstate is made up of a sum of plane-wave states **k** that differ by reciprocal-lattice vectors **G**. Thus, the quantum-mechanical matrix elements for scattering $<\mathbf{k}|V(\mathbf{r})|\mathbf{k}_0>$ are zero unless **k** and $\mathbf{k}_0$ differ by a reciprocal-lattice vector, a statement corresponding to the Laue condition.

Although the Bloch function is an eigenfunction of the Hamiltonian $\hat{\mathcal{H}}$, let us see if it is an eigenfunction of the momentum operator $\hat{p}$. Consider, for example, a Bloch function in one dimension along x:

$$\begin{aligned}\hat{p}_x|\psi(x)> &= -i\hbar\frac{d}{dx}[u_k(x)e^{ikx}] \\ &= -i\hbar\left[ike^{ikx}u_k(x) + e^{ikx}\frac{d}{dx}u_k(x)\right] \\ &= \hbar k\psi(x) - i\hbar e^{ikx}\frac{d}{dx}u_k(x)\end{aligned} \tag{4.14}$$

from which we see that it is not an eigenfunction of the momentum operator. Therefore, $\hbar k$ is not strictly a momentum for a Bloch function, in which case, it is referred to as the *crystal momentum*. It only is a true momentum if the derivative of $u_{\mathbf{k}}$ is equal to zero, which, of course, it cannot be in a crystal.

4.5 Two-beam approximation in electron diffraction

Problems with multiple scattering are of particular relevance to transmission electron diffraction and the analysis of the diffraction conditions. The theory of contrast in electron microscope images is complicated (see [9, 10]), and for a useful review, see Humphreys [11]. Unfortunately, as he points out, the notation tends to vary considerably, depending on the author. For instance, while condensed matter physicists think of a wave-vector as $k = 2\pi/\lambda$ and $G = 2\pi/d$, most papers by electron diffractionists tend to use $k = 1/\lambda$ and $G = 1/d$, or even sometimes a hybrid system, with $k = 2\pi/\lambda$ and $G = 1/d$. This can be quite confusing when reading the literature. Here, I shall continue to use the notation used in condensed matter physics. Note that the results of the dynamical theory for electrons are similar to those for x-ray scattering by perfect crystals.

One can learn how to approach the subject by considering the two-beam approximation to the dynamical theory. While this is not entirely general, it still fits most situations quite well. Consider two electron beams interacting, i.e., two reciprocal-lattice points lie on the Ewald sphere simultaneously for a perfect crystal. We start by writing the electron plane-wave function as

$$\psi(\mathbf{r}) = u_k e^{i\mathbf{k}\cdot\mathbf{r}} \tag{4.15}$$

According to Bloch's theorem, we can write

$$\psi(\mathbf{r}) = e^{i\mathbf{k}\cdot\mathbf{r}}\sum_{\mathbf{G}} C_{\mathbf{G}}e^{i\mathbf{G}\cdot\mathbf{r}} \tag{4.16}$$

For the two-beam case, we take just two terms

$$\psi(\mathbf{r}) = C_0 e^{i\mathbf{k}\cdot\mathbf{r}} + C_\mathbf{G} e^{i(\mathbf{k}+\mathbf{G})\cdot\mathbf{r}} \tag{4.17}$$

Now the electron wave interacts with a periodic potential $V(\mathbf{r})$ in the crystal due to the presence of the atomic nuclei, and this can be written as a Fourier series:

$$V(\mathbf{r}) = \sum_\mathbf{G} V_\mathbf{G} e^{i\mathbf{G}\cdot\mathbf{r}} \tag{4.18}$$

We now define

$$U_\mathbf{G} = \frac{2m_e}{\hbar^2} V_\mathbf{G} \tag{4.19}$$

and

$$K^2 = \frac{2m_e}{\hbar^2}(E - V_0) \tag{4.20}$$

E is the energy of the incident electrons, and K is the modulus of the electron wave-vector, taking into account the refractive index of the crystal. This is related to the wave-vector K_{vac} *in vacuo* by

$$K^2 + \frac{2m_e}{\hbar^2} V_0 = \frac{2m_e}{\hbar^2} E = K_{vac}^2 \tag{4.21}$$

Then, applying the time-independent Schrödinger equation to (4.17)

$$-\frac{\hbar^2}{2m_e}\nabla^2\psi(\mathbf{r}) + V(\mathbf{r})\psi = E\psi(\mathbf{r}) \tag{4.22}$$

we get

$$\begin{aligned} &-\frac{\hbar^2}{2m_e}[-\mathbf{k}^2 C_0 e^{i\mathbf{k}\cdot\mathbf{r}} - (\mathbf{k}+\mathbf{G})^2 C_G e^{i(\mathbf{k}+\mathbf{G})\cdot\mathbf{r}}] \\ &\quad + \sum_\mathbf{G} V_\mathbf{G} e^{i\mathbf{G}\cdot\mathbf{r}}[C_0 e^{i\mathbf{k}\cdot\mathbf{r}} + C_\mathbf{G} e^{i(\mathbf{k}+\mathbf{G})\cdot\mathbf{r}}] \\ &= E[C_0 e^{i\mathbf{k}\cdot\mathbf{r}} + C_\mathbf{G} e^{i(\mathbf{k}+\mathbf{G})\cdot\mathbf{r}}] \end{aligned} \tag{4.23}$$

Comparing coefficients of $e^{i\mathbf{k}\cdot\mathbf{r}}$ and $e^{i(\mathbf{k}+\mathbf{G})\cdot\mathbf{r}}$ on both sides of this equation, we then obtain two simultaneous equations:

$$\begin{aligned} \frac{\hbar^2}{2m_e}\mathbf{k}^2 C_0 + V_0 C_0 + V_{-\mathbf{G}} C_\mathbf{G} &= E C_0 \\ \frac{\hbar^2}{2m_e}(\mathbf{k}+\mathbf{G})^2 C_\mathbf{G} + V_0 C_\mathbf{G} + V_\mathbf{G} C_0 &= E C_\mathbf{G} \end{aligned} \tag{4.24}$$

Rearranging and using (4.19) and (4.20)

$$\begin{aligned}(K^2 - |\mathbf{k}|^2)C_0 + U_{-\mathbf{G}}C_{\mathbf{G}} &= 0\\ U_{\mathbf{G}}C_0 + (K^2 - |\mathbf{k} + \mathbf{G}|^2)C_{\mathbf{G}} &= 0\end{aligned} \tag{4.25}$$

For a non-trivial solution

$$\begin{vmatrix} K^2 - |\mathbf{k}|^2 & U_{-\mathbf{G}} \\ U_{\mathbf{G}} & K^2 - |\mathbf{k} + \mathbf{G}|^2 \end{vmatrix} = 0 \tag{4.26}$$

and so

$$(K^2 - |\mathbf{k}|^2)(K^2 - |\mathbf{k} + \mathbf{G}|^2) = -U_{\mathbf{G}}U_{-\mathbf{G}} \tag{4.27}$$

As K, $|\mathbf{k}|$ and $|\mathbf{k} + \mathbf{G}|$ are very large compared with the differences between them (because the periodic potential is much smaller than that of the electron beam), this equation becomes

$$(|\mathbf{k}| - K)(|\mathbf{k} + \mathbf{G}| - K) = \frac{U_{\mathbf{G}}U_{-\mathbf{G}}}{4K^2} = \frac{|U_{\mathbf{G}}|^2}{4K^2} \tag{4.28}$$

It can be seen that the result is a quadratic equation in K, showing that there are two solutions. Consider the special case $\mathbf{k} = \mathbf{k} + \mathbf{G}$ where a standing solution occurs. Then equation (4.27) becomes

$$(|\mathbf{k}|^2 - K^2) = \pm|U_{\mathbf{G}}| \tag{4.29}$$

Solving for the roots $\mathbf{k}_1$ and $\mathbf{k}_2$

$$(k_1 + k_2)(k_1 - k_2) = 2U_G \tag{4.30}$$

and then

$$\Delta k = (k_1 - k_2) \simeq \frac{2U_{\mathbf{G}}}{2K} = \frac{2m_e V_{\mathbf{G}}}{\hbar^2 K} = \frac{2\pi}{\xi} \tag{4.31}$$

The extinction distance allows one to define what is meant by thin and thick crystals, thus

$$\frac{\pi t}{\xi} \ll 1 \text{ “thin”crystal, kinematic and dynamical theory valid}$$

$$\frac{\pi t}{\xi} \gg 1 \text{ “thick”crystal, only dynamical theory valid}$$

The crystal splits the incident beam into two Bloch waves, each with different wave-vectors. This means that there will be phase differences between the two waves, and hence they can interfere with each other to produce interference fringes. The crystal, therefore, acts as its own interferometer.

To understand this better, consider figure 4.8, which shows the situation for the kinematic case. The full circle is the usual Ewald sphere, for which the wave-vector

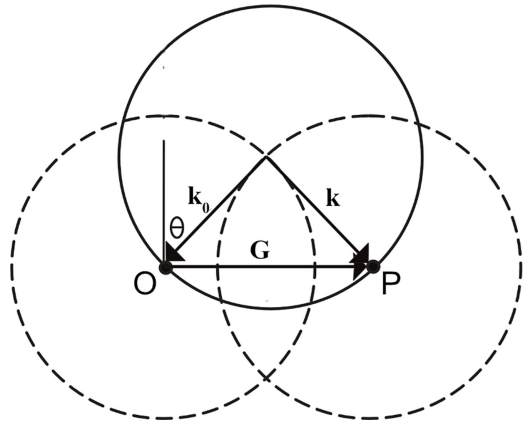

Figure 4.8. Ewald sphere in the kinematic approximation.

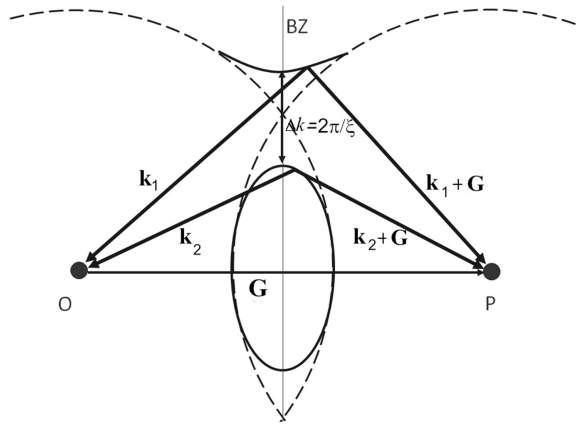

Figure 4.9. Dispersion surface for two-beam dynamical diffraction.

$\mathbf{k}_0$ represents the incident wave and $\mathbf{k}$ the diffracted wave. Now in the dynamical theory, the two beams share energy rather like in a balanced pendulum, since in a perfect crystal, both may be intense waves within the crystal. If we construct the loci of the centres of the Ewald sphere around the two reciprocal-lattice nodes O and P, the dashed spheres are obtained. Now, in the two-beam dynamical case, for high electron energies, equation (4.28) defines a *dispersion surface* that has two branches asymptotic to the spherical surfaces (figure 4.9) separated at the centre by $\Delta k = 2\pi\xi^{-1}$.

This means that instead of a single wave-vector to the point O, as in the kinematic approximation, there are two wave-vectors $\mathbf{k}_1$ and $\mathbf{k}_2$, one from each branch, and similarly $\mathbf{k}_1 + \mathbf{G}$ and $\mathbf{k}_2 + \mathbf{G}$ to the point P. The central line BZ denotes the so-called Brillouin zone boundary corresponding to the Bragg reflection condition. Wave-vectors coming from the two points on the upper and lower branches on BZ signify standing-wave solutions. Note that as the extinction distance increases, the two

branches become close together until they finally touch and the kinematic situation is recovered (in this case, the electron can be represented by a single plane wave of wave-vector **k** or **k** + **G**). The extinction distance is therefore integrally linked to the breakdown of the first Born approximation.

Figure 4.10 shows the energy surfaces around the reciprocal-lattice points in a repeated zone scheme. The total wave functions for the two solutions are given by

$$\begin{aligned}\psi_1 &= C_0(1)e^{i\mathbf{k}_1\cdot\mathbf{r}} + C_g(1)e^{i(\mathbf{k}_1+\mathbf{G})\cdot\mathbf{r}}\\ \psi_2 &= C_0(2)e^{i\mathbf{k}_2\cdot\mathbf{r}} + C_g(2)e^{i(\mathbf{k}_2+\mathbf{G})\cdot\mathbf{r}}\end{aligned} \tag{4.32}$$

In the Bragg reflection position, we can express the normalised wave functions as

$$\begin{aligned}\psi_1 &= \frac{1}{\sqrt{2}}C\{e^{i\mathbf{k}_1\cdot\mathbf{r}} - e^{i(\mathbf{k}_1+\mathbf{G})\cdot\mathbf{r}}\}\\ \psi_2 &= \frac{1}{\sqrt{2}}C\{e^{i\mathbf{k}_2\cdot\mathbf{r}} + e^{i(\mathbf{k}_2+\mathbf{G})\cdot\mathbf{r}}\}\end{aligned} \tag{4.33}$$

If we take $\mathbf{k}_1 = \mathbf{k}_2 = -\mathbf{G}/2$

$$\begin{aligned}\psi_1 &= -\sqrt{2}\,iC\,\sin \tfrac{1}{2}\mathbf{G}\cdot\mathbf{r}\\ \psi_2 &= \sqrt{2}\,C\,\cos \tfrac{1}{2}\mathbf{G}\cdot\mathbf{r}\end{aligned} \tag{4.34}$$

and then

$$\begin{aligned}\psi_1\psi_1^* &= |\psi_1|^2 = 2C^2\sin^2(\tfrac{1}{2}\mathbf{G}\cdot\mathbf{r})\\ \psi_2\psi_2^* &= |\psi_2|^2 = 2C^2\cos^2(\tfrac{1}{2}\mathbf{G}\cdot\mathbf{r})\end{aligned} \tag{4.35}$$

We can get an idea of what this means by considering each of the waves with respect to the arrangement of atoms (figure 4.11). For wave (1), the maxima lie

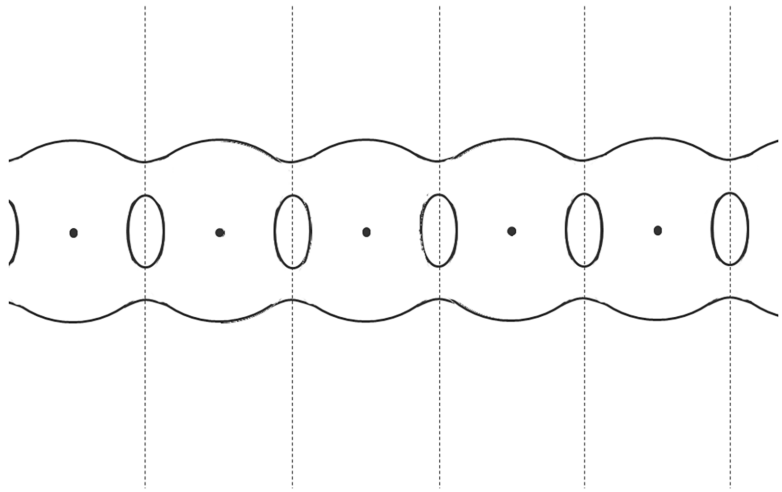

Figure 4.10. Energy dispersion surface in a repeated zone scheme.

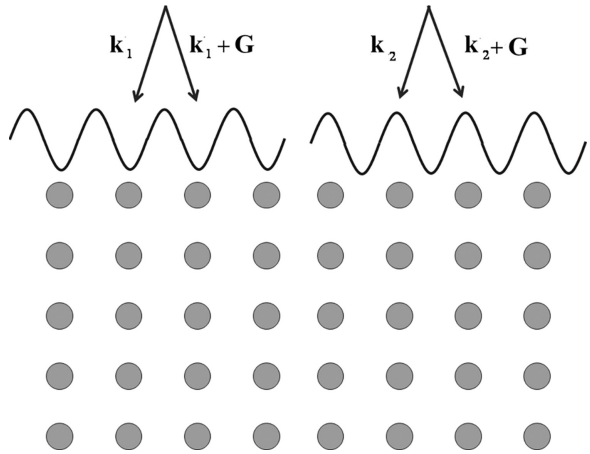

Figure 4.11. Schematic diagram of the two types of wave field at the Bragg reflecting position. The current flow vector is parallel to the reflecting planes.

between the atomic planes, whereas for wave (2), they lie *on* the atomic planes. Both Bloch waves have the same total energy, but since electrons in wave (2) are concentrated in a region of low potential energy, they must, on average, have higher kinetic energy than electrons in wave (1). It is this difference that is the reason for the separation of the dispersion branches by Δk. It also follows that wave (2) is scattered more than wave (1) because it is concentrated close to the atoms where there is a greater likelihood of interaction with the atoms, thus causing a strong absorption. On the other hand, wave (1) is concentrated between the atoms, leading to an anomalously high transmission (the Borrmann effect).

It is interesting to see what happens inside a perfect crystal at the maximum of the Bragg position. Figure 4.12 shows the pattern of standing waves inside a perfect crystal, where the Bragg condition is fulfilled at the maximum of the reflectivity curve. The wavelength of the standing-wave pattern is equal to the spacing of the reflecting planes. Figure 4.13 shows the stationary wave pattern inside the crystal for the Laue case.

We note in passing that this treatment is closely similar to that used in electronic band theory. The main difference is that here the energy is fixed and one solves for the wave-vectors, whereas there, it is the other way round, with the wave-vectors fixed and the Schrödinger equation solved for energy solutions. Furthermore, although this theory has been applied here to electron diffraction, the same type of dispersion is obtained for x-ray and neutron diffraction from perfect crystals.

4.6 Pendellösung or thickness fringes

An example of how the two-beam theory can be used is in finding the effect of the thickness of a crystal on the contrast in an image. For a thickness t, the amplitude of the directly transmitted beam at the bottom of the crystal is given by

$$\psi_0(t) = C_0(1)e^{ik_1 t} + C_0(2)e^{ik_2 t} \tag{4.36}$$

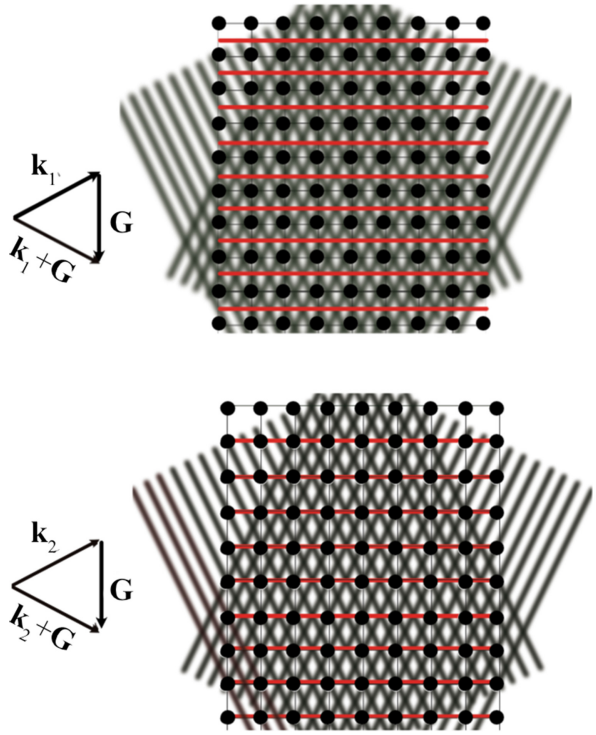

Figure 4.12. Standing waves inside a perfect crystal under Bragg diffraction due to the two beams. The red lines parallel to the reflecting planes mark the lines of nodes and antinodes.

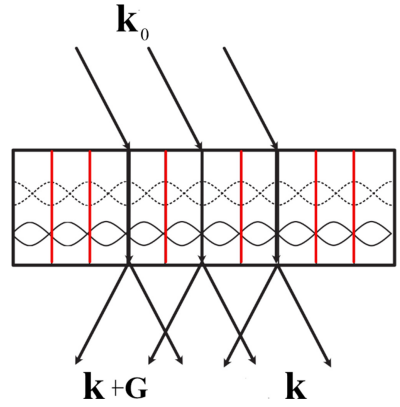

Figure 4.13. Standing waves inside a perfect crystal for Laue diffraction. The vertical red lines indicate the scattering planes. The wave field splits up at the lower exit surface.

where k_1 and k_2 are components perpendicular to the crystal surface. At the Bragg reflecting position

$$C_0(1) = C_0(2) \tag{4.37}$$

The intensity for the transmitted beam is then given by

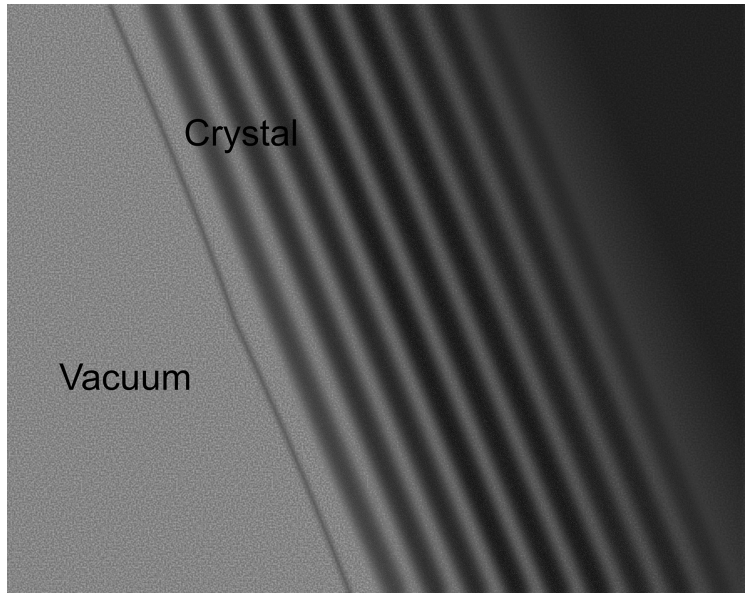

Figure 4.14. Simulated thickness fringes shown by a wedge-shaped crystal of AlCu alloy in an electron microscope image.

$$I_0 = \psi_0(t)\psi_0^*(t) \propto 1 + 1 + 2\cos(k_1 - k_2)t \tag{4.38}$$

Therefore,

$$I_0 \propto \cos^2[(k_1 - k_2)t/2] = \cos^2[\pi t/\xi] \tag{4.39}$$

Similarly, for the diffracted beam

$$I_G \propto \sin^2[(k_1 - k_2)t/2] = \sin^2[\pi t/\xi] \tag{4.40}$$

and then

$$I_0 + I_G = \text{constant} \tag{4.41}$$

When t is varied, there is an interchange of intensity between the two beams, rather like the sharing of energy between coupled pendulums, thus the name Pendellösung. For $t = n\xi$, the intensity is zero (hence the term extinction distance).

Therefore, the effect of this is to create within an image of a wedge-shaped crystal a set of contrast fringes. The periodicity of the fringes can then, in principle, be used to estimate the angle of the wedge-shaped crystal. Note that inelastic scattering processes cause absorption in practice so that the intensity tends to decay with increasing thickness. An example of thickness fringes is shown in figure 4.14.

References

[1] Als-Nielsen J and McMorrow D 2011 *Elements of Modern X-ray Physics* (New York: Wiley)
[2] Authier A 2003 *Dynamical Theory of X-Ray Diffraction* (Oxford: Oxford University Press)

[3] Darwin C G 1914 The theory of X-ray reflexion *Phil. Mag.* **27** 315–33
[4] Warren B E 1969 *X-ray Diffraction* (New York: Dover)
[5] Härtwig J Introduction into the dynamical theory of X-ray diffraction for perfect crystals (https://www.researchgate.net/publication/303400758_Introduction_dynamical_theory_at_IFPAN_in_Warsaw2016)
[6] Borrmann G 1941 Uber Extinktionsdiagramme von Quarz *Zeits. für Phys.* **9/10** 157–62
[7] von Laue M 1949 Die Absorption der Röntgenstrahlen in Kristallen im Interferenzfall *Acta Cryst.* **2** 106–13
[8] Collins S P, Tolkiehn M, Laurus T and Dimitrienko V E 2012 Anisotropy in Borrmann spectroscopy *Eur. Phys. J. Spec. Top.* **208** 75–87
[9] Grundy P J and Jones G A 1976 *Electron Microscopy in the Study of Materials* (London: Edward Arnold)
[10] Hirsch P, Howie A, Nicholson R, Pashley D W and Whelan M J 1977 *Electron Microscopy of Thin Crystals* (Malabar, FL: R.E. Krieger Pub. Co)
[11] Humphreys C J 1979 The scattering of fast electrons by crystals *Reports Prog. Phys.* **42** 1825–87

IOP Publishing

A Journey into Reciprocal Space (Second Edition)
A crystallographer's perspective
Anthony Michael Glazer

Chapter 5

Waves in a periodic medium

Physicists use the wave theory on Mondays, Wednesdays, and Fridays, and the particle theory on Tuesdays, Thursdays, and Saturdays.

(William Henry Bragg)

5.1 Waves in space

We shall now look at how reciprocal space can be used to describe the quantum states for various waves travelling in a periodic medium, i.e., in a crystal. These waves arise through elementary excitations, such as for electrons or phonons. We have already seen how the incidence of x-ray, neutron and electron beams leads to diffraction by the crystal and how that can be described through the Ewald construction applied to the reciprocal lattice. In much the same way, waves corresponding to elementary excitations can be considered to be scattered or diffracted by the underlying crystal potential. For this reason, in the case of elastic scattering, where there is no difference in energy between the incident and diffracted waves, the corresponding wave-vectors are related by:

$$k_0 = k \tag{5.1}$$

Also, the Ewald construction has shown that

$$\mathbf{k} - \mathbf{k}_0 = \mathbf{G} \tag{5.2}$$

is the condition for a wave to be diffracted, or turning this around, the scattered wave-vector $\mathbf{k}$ is

$$\mathbf{k} = \mathbf{k}_0 + \mathbf{G} \tag{5.3}$$

doi:10.1088/978-0-7503-3875-2ch5

In terms of conservation of crystal momentum, the scattered crystal momentum is

$$\hbar\mathbf{k} = \hbar\mathbf{k}_0 + \hbar\mathbf{G} \tag{5.4}$$

Notation. *Reciprocal space is sometimes called* ***k-space*** *or* ***momentum space***.

Correspondingly, for elastic scattering, the energy between the incident and scattered waves is also conserved:

$$\hbar\omega_0 = \hbar\omega \tag{5.5}$$

5.2 Periodic boundary conditions

We now consider how to specify the quantum states for waves travelling in a crystal, bearing in mind that waves or elementary excitations corresponding to electrons and phonons have many wavelengths with scales varying from the crystal dimensions down to atomic distances. The problem that needs to be addressed is: how can one fit all these waves within the crystal's confines? Now one way to do this is to recognize that, for most purposes, the surfaces of the crystal are so far away with respect to the unit-cell dimensions that we can treat the crystal as if it were infinite in extent. Given this, we can then, without loss of generality, treat the problem mathematically as if one end of the crystal, at ∞ is connected to the other at $-\infty$. This tying together of opposite ends is known as a *Periodic Boundary Condition*. The simplest way to see this is to take a one-dimensional example.

Figure 5.1 illustrates this with a simple example of 12 points spaced a apart and arranged on a circle of circumference L (to describe a real crystal of normal size, more like 10^{25} points would be needed). The idea now is to consider possible wave motions that will displace these points from their ideal positions (a mechanical analogue would have a circular string of atoms set into vibrational motion). Furthermore, any

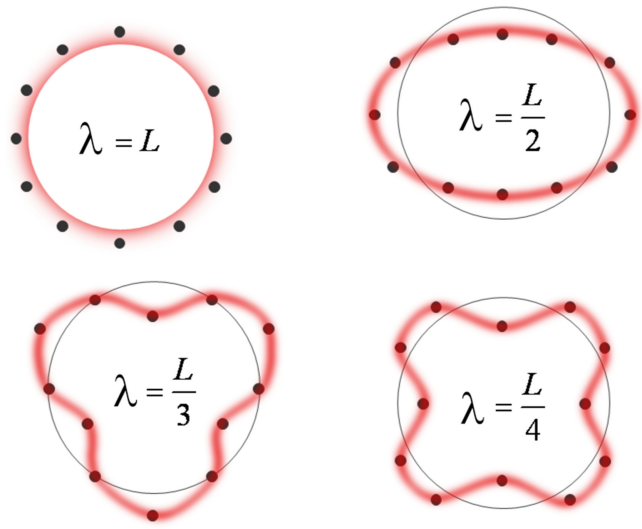

Figure 5.1. Examples of different waves for a circular array of repeating points.

wave around this circular string must be continuous and not have any discontinuities. The fundamental wave will then have a wavelength equal to the circle's circumference, and the first harmonic will have a wavelength equal to half the circumference, and so on. The wavelengths therefore are

$$L \; \frac{L}{2} \; \frac{L}{3} \; \frac{L}{4} \; \frac{L}{5} \; \frac{L}{6} \ldots \tag{5.6}$$

Now, if instead, we write this sequence in terms of wave-vectors, we get the following nice series:

$$\pm\frac{2\pi}{L} \; \pm\frac{4\pi}{L} \; \pm\frac{6\pi}{L} \; \pm\frac{8\pi}{L} \; \pm\frac{10\pi}{L} \; \pm\frac{12\pi}{L} \ldots \tag{5.7}$$

The ± signs have been included to allow for the wave-vectors to point in positive and negative directions. The advantage of specifying the waves by wave-vectors rather than wavelengths should be apparent: we end up with a series of points in k-space, each equally separated by a fixed reciprocal distance of $2\pi/L$. Furthermore, because L is so much bigger than the unit-cell distance, we can see that, on the reciprocal-lattice scale, these points are extremely close together compared with the separation of the reciprocal-lattice points and, for most purposes, can be considered to form a quasi-continuum.

Figure 5.2 illustrates this schematically, where

$$\frac{2\pi}{L} \ll \frac{2\pi}{a} \tag{5.8}$$

This can be repeated in three dimensions for a crystal of dimensions $L \times L \times L$. The result is that the reciprocal space is filled with a fine mesh of points representing all the quantum states for elementary excitations in the crystal. Figure 5.3 shows what this looks like in two dimensions; an orthogonal reciprocal lattice has been drawn for simplicity.

You will notice that the wave states have been marked in all over reciprocal space. This is because the solutions to the wave equation are periodic in the reciprocal lattice. In other words, the wave solutions are invariant under addition or subtraction of integer multiples of the reciprocal vector **G**. We see that subtracting the vector $\mathbf{G}_{100}$ from the wave-vector **k** with respect to the origin at (0, 0) leads to the vector $\mathbf{k}–\mathbf{G}_{100}$ with a component pointing to the left. But it is also equivalent to the wave-vector **k′** pointing to the right with respect to an origin chosen at $(-2\pi/a, 0)$. This illustrates an important idea. It shows that, because the reciprocal lattice is translationally invariant, all wave solutions, as expressed by Bloch waves, also will be translationally invariant. This is equivalent to saying that in direct space, the crystal structure is translationally invariant. Therefore, it means that we can define all the wave states within a unit cell in

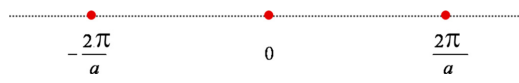

Figure 5.2. One-dimensional reciprocal lattice (red points) spaced $2\pi/a$ and wave-vectors (black points) spaced $2\pi/L$ apart.

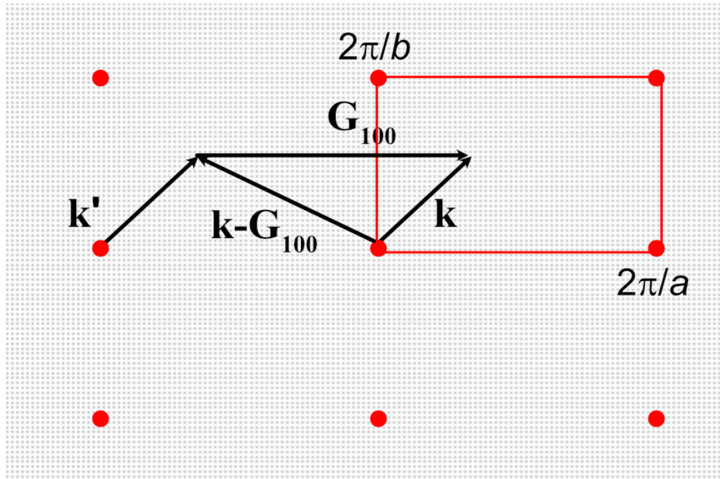

Figure 5.3. Two-dimensional reciprocal lattice (red points) spaced $2\pi/a$ by $2\pi/b$, and wave-vectors (black points) spaced $2\pi/L$ by $2\pi/L$. The red box is an example of a primitive unit cell in the reciprocal lattice.

reciprocal space, and then all other reciprocal unit cells will contain the same wave states. In this sense, the reciprocal lattice behaves just like a direct lattice, in the way it acts as a template for translational symmetry. In direct space, we have atoms inside direct unit cells, but in reciprocal space, we have wave states inside reciprocal unit cells.

5.3 Brillouin zones

As explained above, for waves propagating in a periodic medium, there are always other wave-equation solutions. Suppose we have waves described by the following wave-vector components $\mathbf{k}_1$ and $\mathbf{k}_2$ projected along the $\pm\mathbf{a}^*$ axis in figure 5.3, such that

$$\begin{aligned} \mathbf{k}_1 &= +\tfrac{1}{2}\,\mathbf{G}_{100} \\ \mathbf{k}_2 &= -\tfrac{1}{2}\,\mathbf{G}_{100} \\ \therefore k_1 = k_2 &= \frac{\pi}{a} \end{aligned} \tag{5.9}$$

Therefore,

$$\begin{aligned} k_1 = k_2 &= \frac{2\pi}{\lambda} = \frac{\pi}{a} \\ \therefore \lambda &= 2a = 2d_{100} \end{aligned} \tag{5.10}$$

which is simply Bragg's Law, where $2\theta = 180°$. This means that the wave component k_1 is back-scattered (reflected) to k_2 and vice versa. In other words, with respect to the chosen origin in reciprocal space, there are two waves of equal wave-vector magnitude travelling in opposite directions, i.e., a standing wave consisting of two opposite real components. Such a pair of waves is said to end on the so-called Brillouin zone boundary. We met this earlier when discussing the two-beam approximation in dynamical scattering.

What about waves with wave-vectors that do not end on the Brillouin zone boundary? There are still other solutions to the wave equation. Suppose one is for $\mathbf{k}$ and the other for $\mathbf{k} - \mathbf{G}_{100}$. Referring back to figure 5.3, with the origin at the centre of the diagram, the vector $\mathbf{k}$ represents a wave solution within the specified reciprocal unit cell with a *component* travelling to the right, whereas $\mathbf{k} - \mathbf{G}_{100}$ is for a wave whose wave-vector lies outside the reciprocal unit cell: this corresponds to a solution with a *component* travelling to the left. The two wave solutions in figure 5.3 differ in wave-vector by $\mathbf{G}_{100}$. Thus, in terms of wave-vector components $\mathbf{k}_1$ and $\mathbf{k}_2$ parallel to $\mathbf{G}_{100}$ we can write

$$\mathbf{k}_1 - \mathbf{G}_{100} = \mathbf{k}_2 \tag{5.11}$$

Therefore,

$$\begin{aligned} \frac{2\pi}{\lambda_1} - \frac{2\pi}{a} &= -\frac{2\pi}{\lambda_2} \\ \therefore a &= \frac{\lambda_1\lambda_2}{\lambda_2 + \lambda_1} \end{aligned} \tag{5.12}$$

where a is the unit-cell repeat distance.

Definition. *The **Brillouin zone** corresponds to a unit cell in reciprocal space.*

Now, this definition may surprise you, for it is not the way it is usually defined in most textbooks. The point about this definition is that the Brillouin zone is a region of reciprocal space that contains *all* the allowed wave states. This can be compared with how a direct unit cell contains all the atoms needed to describe the whole crystal. What is often not realized is that the Brillouin zone can be constructed in an infinite number of ways in reciprocal space, because, like all unit cells, it can be drawn in any way we want: it just has to satisfy the notion that when repeated, it fills all (reciprocal) space [1, 2].

Let's look at a particular construction (figure 5.4). The red box is a conventional reciprocal unit cell with lattice points at each corner.

Because there is only one lattice point in this cell, it is primitive. Now the blue cell is the same unit cell but with its origin displaced so that a lattice point now lies at its centre. The regions ABC and D together contain all the allowed wave states (property of a reciprocal unit cell), and their counterparts can be found in the blue cell as A′ B′ C and D′. Notice that this, too, according to our definition, is a Brillouin zone. The only difference is in the way we have defined the origin and axes. However, instead of thinking of the blue cell as a simple translation of the red cell, there is another way of obtaining it.

5.4 Wigner–Seitz cell

The Wigner–Seitz cell (sometimes referred to as a *proximity* cell, or *Dirichlet* domain or a *Voronoi* cell) is a unit cell in a lattice constructed in a particular way. It can be

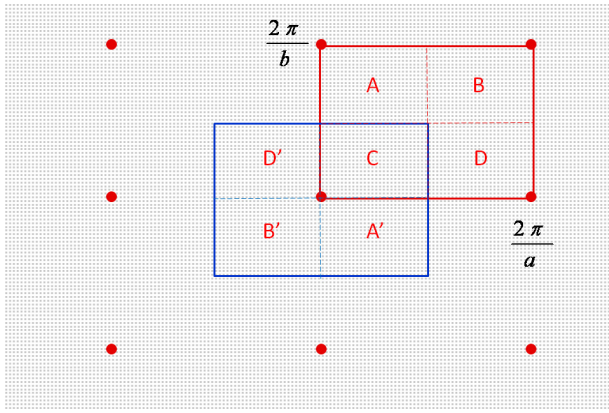

Figure 5.4. Two-dimensional reciprocal lattice with two unit cells.

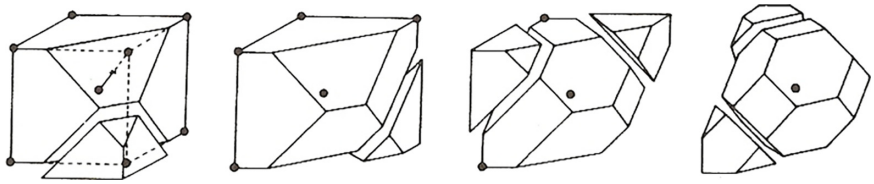

Figure 5.5. The construction of a Wigner–Seitz cell for a cubic I-lattice. The lattice points at the origin and neighbouring sites are shown.

used in direct space, although with not much practical use for our purposes here, and in reciprocal space. To carry out the construction:

1. choose a lattice point;
2. draw vectors from this lattice point to all other lattice points;
3. bisect each of these vectors by planes *perpendicular* to the vectors;
4. the Wigner–Seitz cell is the smallest enclosed volume around the initial lattice point.

It can be seen that the blue unit cell in figure 5.4 can be obtained by this procedure.

Suppose now we consider a centred lattice. For example, take a cubic body-centred lattice. Figure 5.5 shows the various stages in constructing the Wigner–Seitz cell. The result looks very different from the parallelepiped-shaped unit cells that we have used so far. Nevertheless, it is a unit cell, as when stacked together with identical copies, it fills all space without leaving gaps, the requirement for being a general unit cell. This can be seen in figure 5.6.

So, the question that has to be asked is: why use such a peculiar construction to describe wave states in reciprocal space? One answer to this is that, because it is constructed around a single lattice point, the Wigner–Seitz cell is always a primitive unit cell and, therefore, the smallest volume possible. This means that if we are counting quantum states, we need only do this once, whereas if we use a conventional centred unit cell, we would then have to count the same states several times

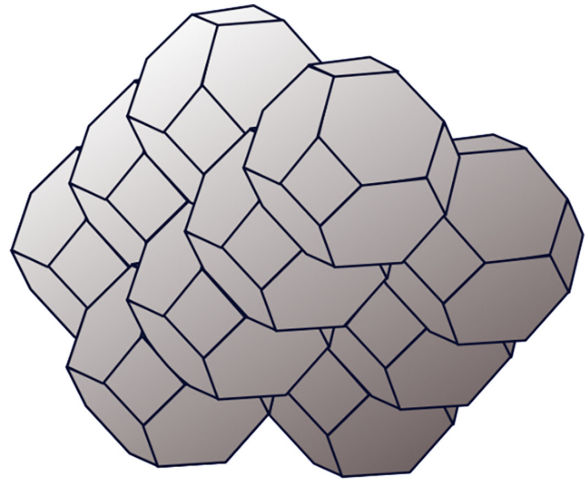

Figure 5.6. The stacking of Wigner–Seitz cells for a body-centred cubic lattice.

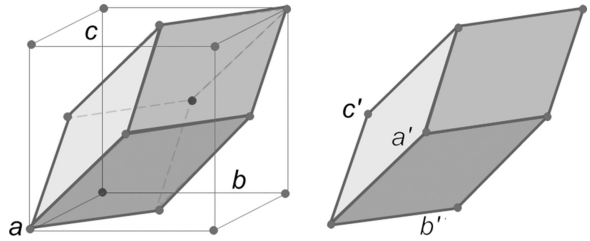

Figure 5.7. An example of the construction of a parallelepiped-shaped primitive unit cell out of an all-face-centred cubic unit cell.

over. The second advantage of this construction is that this type of unit cell, when looked at in isolation, readily shows the full point symmetry of the underlying lattice from which it has been constructed. In the example above, we can immediately see in the shape of the cell that there are four 3-fold axes of symmetry, thus showing that it has been derived within a cubic lattice. Suppose that, instead of using a Wigner–Seitz construction, we defined a primitive parallelepiped-shaped cell. For example, consider in figure 5.7, a cubic all-face-centred unit cell. The shaded cell is one of the infinite numbers of primitive unit cells that can be constructed with this lattice and, because it is primitive, it has one quarter of the *F*-cell volume.

The following equation gives the relationship between the two choices of unit cell

$$\begin{bmatrix} \mathbf{a}' \\ \mathbf{b}' \\ \mathbf{c}' \end{bmatrix} = \begin{bmatrix} \frac{1}{2} & 0 & \frac{1}{2} \\ \frac{1}{2} & \frac{1}{2} & 0 \\ 0 & \frac{1}{2} & \frac{1}{2} \end{bmatrix} \begin{bmatrix} \mathbf{a} \\ \mathbf{b} \\ \mathbf{c} \end{bmatrix} \tag{5.13}$$

In figure 5.7, the primitive cell is shown on the right-hand side in isolation. The problem is that if you now hand this unit cell to someone and ask them to which crystal system this belongs, the likely answer will be trigonal. This is because it is easy to spot a 3-fold axis of symmetry along the long diagonal, but it is not obvious how to locate the remaining three 3-fold axes needed to define a cubic crystal. The angle α between the axes can be found from (5.13) using

$$\frac{1}{2}(\mathbf{a}+\mathbf{c})\cdot\frac{1}{2}(\mathbf{a}+\mathbf{b})=\frac{1}{4}a^2=\left|\frac{1}{2}(\mathbf{a}+\mathbf{c})\right|\left|\frac{1}{2}(\mathbf{a}+\mathbf{b})\right|\cos\alpha \tag{5.14}$$

to be precisely 60°. Therefore, this rhombohedral shape is a very special one, but by merely looking at it, we cannot be sure if α is exactly 60° without very careful measurement. The Wigner–Seitz cells for centred cubic lattices are shown in figure 5.8, where the four 3-fold axes can easily be seen.

Thus, the Wigner–Seitz unit cell in reciprocal space is a convenient container for all the allowed wave states, and so is a useful way of describing a Brillouin zone. However, while this is fine for high-symmetry systems, the Wigner–Seitz construction becomes complicated for low symmetries, such as in monoclinic and triclinic lattices. As far as I know, this was first pointed out by Bradley and Cracknell [1]. The exact shapes of the Wigner–Seitz cells are not unique, as they depend on the ratios of the unit-cell axes and angles, and so it is easy to make mistakes in trying to draw

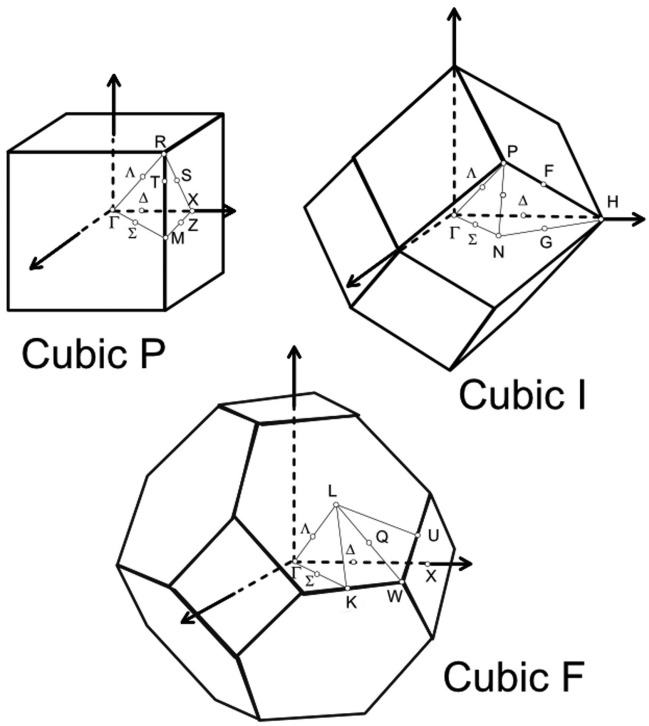

Figure 5.8. Brillouin zones using Wigner–Seitz constructions for cubic lattices.

them. These days computer programs can handle the Wigner–Seitz shapes, even for low-symmetry lattices, and so, perhaps, this concern is less serious than in earlier times. To be sure, the majority of textbooks *define* the Brillouin zone *as* the Wigner–Seitz cell. On the other hand, the Bilbao Crystallographic Server agrees with Bradley and Cracknell and draws monoclinic and triclinic Brillouin zones using a parallelepiped cell (see figure 5.9).

Note that labels have been given to various particular points in the Brillouin zones. These are known as *critical points* because they occur at particular positions of interest. Unfortunately, there is no internationally-accepted consensus on their use, although the ones shown here are the most used these days. Table 5.1 shows a list of some of the more commonly used critical points in the primitive cubic system (the symbol Γ is universally accepted to represent the centre of the Brillouin zone for all crystal systems):

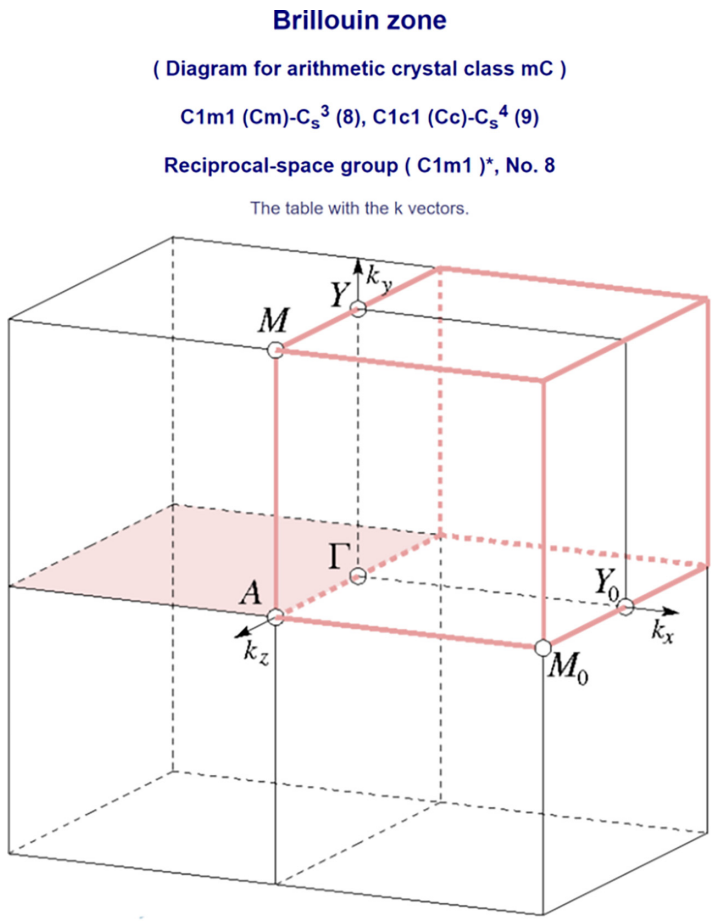

Figure 5.9. Brillouin zone for the monoclinic arithmetic class *mC* from routine KVEC of the Bilbao Crystallographic Server [3, 4].

Table 5.1. Symbols for some critical points in the primitive cubic Wigner–Seitz unit cell.

Symbol	Fraction	Coordinate
Γ	0 0 0	0 0 0
R	½ ½ ½	π/a π/a π/a
M	½ ½ 0	π/a π/a 0
X	½ 0 0	π/a 0 0

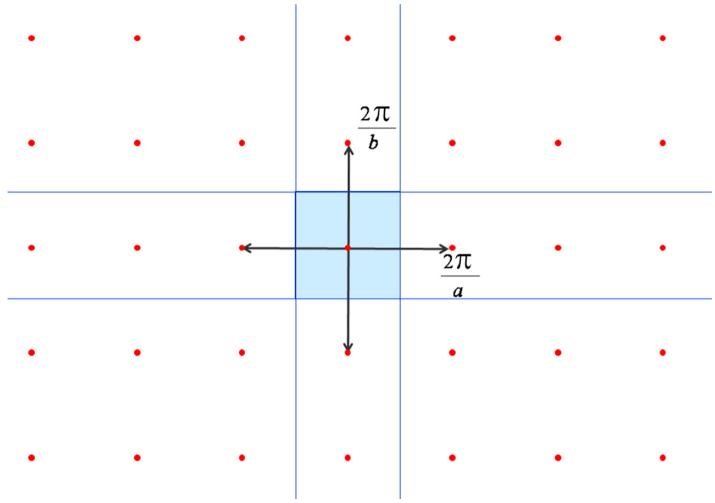

Figure 5.10. Construction of a first Brillouin zone (blue) for a square reciprocal lattice.

5.5 Higher-order Brillouin zones

Brillouin zones defined by the Wigner–Seitz construction, as described above, are often referred to as first *Brillouin zones*, for reasons that will become apparent when we later discuss how to treat elementary excitations. However, sometimes one meets the so-called second, third, and so on Brillouin zones. Their construction simply follows the same procedure as for Wigner–Seitz first Brillouin zones, except that the construction is extended further out in reciprocal space. We proceed by example to demonstrate how this is done for the simple case of a square reciprocal lattice.

Figure 5.10 shows how to construct the first Brillouin zone by drawing in vectors to the reciprocal-lattice points at $\pm 2\pi/a$ and $\pm 2\pi/b$. These lines are then bisected by perpendicular lines (planes in a three-dimensional lattice) running through $\pm\pi/a$ and $\pm\pi/b$ to contain a square region (shown in blue). As explained above, this is a primitive unit cell in reciprocal space and contains all the allowed wave-vectors for the elementary excitations.

In figure 5.11, vectors are now drawn to the reciprocal-lattice points at $(\pm 2\pi/a, \pm 2\pi/b)$. These, too, are bisected perpendicularly to enclose the first Brillouin zone and a region marked in pink. Note that the pink region has the

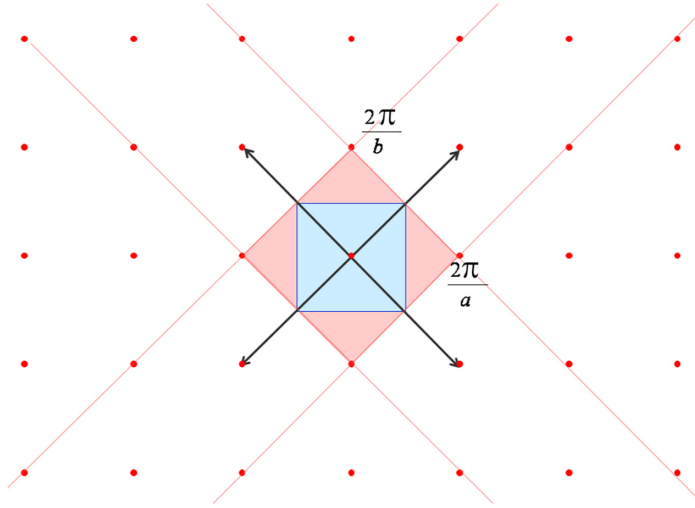

Figure 5.11. Construction of the second Brillouin zone (pink) for a square reciprocal lattice.

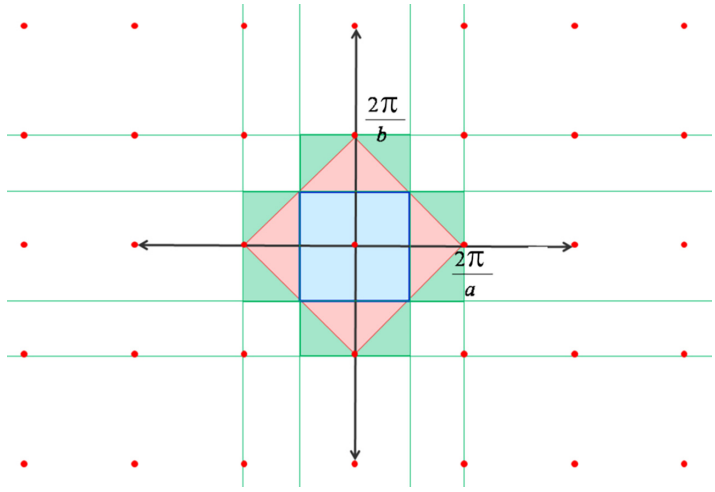

Figure 5.12. Construction of a third Brillouin zone (green) for a square reciprocal lattice.

same area (volume in three dimensions) as the first Brillouin zone, and so by translational symmetry must also contain the same wave states.

Figure 5.12 shows this process continued by drawing in the vectors to ($\pm 4\pi/a$, 0) and (0, $\pm 4\pi/b$). The lines that perpendicularly bisect these vectors are marked in green and enclose the green area. This again has the same area (or volume) as the blue and pink regions and denotes the third Brillouin zone. Figure 5.13 shows the higher-order zones for a square lattice. Obviously, in principle, one could continue with this process, but you can see that the diagrams become ever more complicated. For lower-symmetry reciprocal lattices, the complexity of doing this is hardly worth the effort. As a result, wave information is usually not presented in this form in practice, but, instead, use is made of the so-called *reduced zone scheme*.

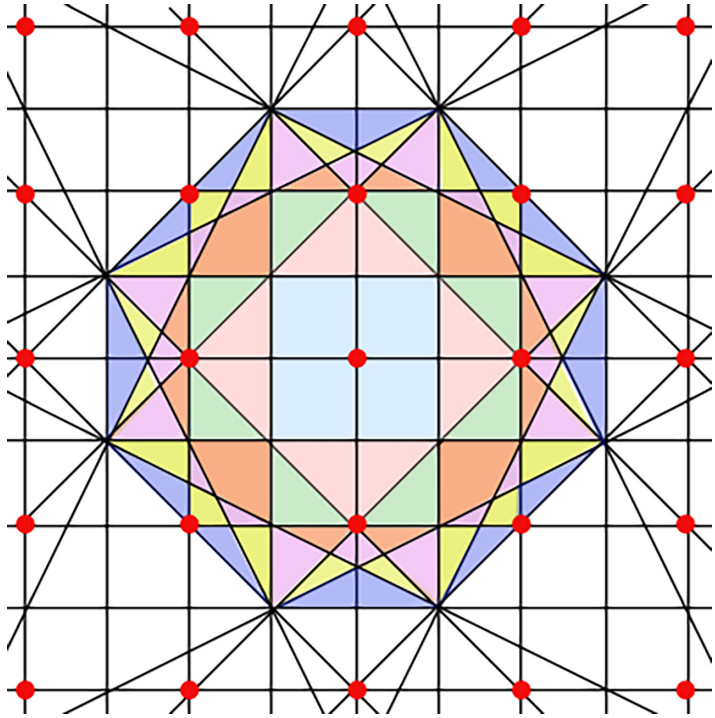

Figure 5.13. Wigner–Seitz zones for a two-dimensional square lattice (the first seven zones shown coloured). Reproduced from [5] with permission of Springer.

Definition *The pieces of each higher zone can be transferred into the first zone through moving the separate regions by subtracting appropriate reciprocal-lattice vectors, and the states of each zone form a continuous energy band over the first zone; this is called the* ***reduced zone scheme****, whereas the use of all Brillouin zones (first, second, third, etc) is known as the* ***extended zone scheme****.*

5.6 Density of states

We now turn to a most important topic in connection with describing the wave states and how they relate to energy or frequency. The concept of the *density of states* lies at the heart of much of statistical mechanics and condensed matter physics. It is important for understanding behaviour such as the thermal and electronic properties of a crystalline solid.

We start by working out the number of states within a wave-vector range. We shall do this for an isotropic system, as this is sufficient for most illustrative purposes. We start by calculating the number of wave states within a bounded region in **k**-space. In three dimensions, for a cubic lattice, this bounded region is a sphere. Figure 5.14 shows a sphere of radius k containing a number of states N_{states}.

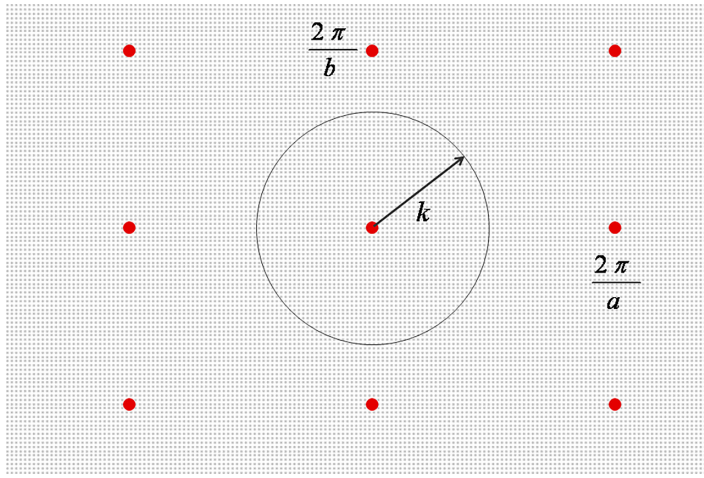

Figure 5.14. Calculation of the number of states within a sphere of radius k.

Now each state is separated from its neighbour by $2\pi/L$, and so the volume around each state is given by

$$V_{\text{state}} = \left(\frac{2\pi}{L}\right)^3 = \frac{8\pi^3}{V_{\text{crystal}}} \tag{5.15}$$

The number of states, N_{states}, is then found by dividing the volume of the sphere by V_{state}:

$$N_{\text{states}} = \frac{4}{3}\pi k^3 \div \frac{8\pi^3}{V_{\text{crystal}}} = \frac{V_{\text{crystal}} k^3}{6\pi^2} \tag{5.16}$$

Then, because, in reality, the number of states is enormous for a normal-sized crystal, we can treat N_{states} as representing a continuum, and so we can calculate the number of occupied states within a range dk by

$$\frac{dN_{\text{states}}}{dk} = \frac{V_{\text{crystal}} k^2}{2\pi^2} \tag{5.17}$$

This defines the *density of states* in k-space.

Definition. *The **density of states** in k-space is the number of states within the range k and k + dk.*

This, however, is not the usual way in which this concept is used. Instead, it is the energy (or because $E = \hbar\omega$) frequency density of states that is employed. To find this, we make use of the identity

$$D(E) = \frac{dN_{\text{states}}}{dE} = \frac{dN_{\text{states}}}{dk}\frac{dk}{dE} \tag{5.18}$$

or

$$D(\omega) = \frac{dN_{\text{states}}}{d\omega} = \frac{dN_{\text{states}}}{dk}\frac{dk}{d\omega} \tag{5.19}$$

We, therefore, modify our definition of the density of states as follows.

Definition. *The **energy (or frequency) density of states** $D(E)$ or $D(\omega)$ is the number of states within the range E and $E + dE$ (or ω and $\omega + d\omega$).*

To proceed further, we need to evaluate either dk/dE or $dk/d\omega$, and so we need a formula relating E (or ω) to k. This depends on the specific problem that needs addressing. We shall see later how this is used in understanding the thermal and electronic properties of crystalline solids.

The formulae (5.16) and (5.17) were found for a three-dimensional system. Clearly, this can be generalized for systems of any dimensions. Some examples are given in table 5.2.

Notice that the density of states is proportional to the crystal size. Therefore, for a large crystal, the number of wave states contained within the Brillouin zone is huge and closely spaced, and so can be treated to a good approximation as a continuum of states. As the crystal size diminishes, the distances between the wave-vectors increase, thus decreasing the number of wave states within the Brillouin zone, making them less like a continuum.

V_{cell} is the volume of a primitive unit cell in direct space. The number of **k**-states in the Brillouin zone is

$$\begin{aligned} N_{\text{states}} &= \frac{V_{BZ}}{V_{\text{state}}} \\ &= \frac{8\pi^3}{V_{\text{cell}}}\frac{V_{\text{crystal}}}{8\pi^3} \\ &= \frac{V_{\text{crystal}}}{V_{\text{cell}}} \\ &= N_{\text{cell}} \end{aligned} \tag{5.20}$$

Table 5.2. Numbers and density of k-states for different dimensions.

Dimension	N_{states}	dN_{states}/dk
1	$\frac{L_{\text{crystal}}k}{2\pi}$	$\frac{L_{\text{crystal}}}{2\pi}$
2	$\frac{A_{\text{crystal}}k^2}{4\pi}$	$\frac{A_{\text{crystal}}k}{2\pi}$
3	$\frac{V_{\text{crystal}}k^3}{6\pi^2}$	$\frac{V_{\text{crystal}}k^2}{2\pi^2}$

This makes an important point relating direct and reciprocal space, namely that, in general, *the number of* ***k****-states in the Brillouin zone is equal to the number of primitive cells in the crystal.*

References

[1] Bradley C J and Cracknell A P 1972 The mathematical theory of symmetry in solids: representation theory for point groups and space groups (Oxford: Oxford University Press)
[2] Burns G and Glazer A M 2013 *Space Groups for Solid State Scientists* (Oxford: Academic)
[3] Bilbao Crystallographic Server (https://www.cryst.ehu.es/)
[4] Aroyo M I, Orobengoa D, de la Flor G, Tasci E S, Perez-Mato J M and Wondratschek H 2015 Brillouin-zone database on the Bilbao Crystallographic Server *Acta Cryst.* **A70** 126–37
[5] Brillouin L 1946 *Wave Propagation in Periodic Structures* (New York: McGraw-Hill)

IOP Publishing

A Journey into Reciprocal Space (Second Edition)
A crystallographer's perspective
Anthony Michael Glazer

Chapter 6

Thermal and electronic properties

If you can't stand the heat, then get out of the kitchen!

(Harry S Truman)

6.1 Heat capacity of solids

In this chapter, we shall look at a couple of physical properties of solids that illustrate the principles described so far, starting with thermal effects. There has long been a historical interest in determining the heat capacity of solids, going back to 1819 when Pierre Louis Dulong (1785–1838) and Alexis Therese Petit (1791–1830) found, or so they thought, that all solids had the same value for the heat capacity multiplied by the atomic weights. The Law of Dulong and Petit can be related to Maxwell's equipartition theorem, whereby the internal energy is given by ½ k_BT per degree of freedom. k_B is Boltzmann's constant.

Definition. *The* ***number of degrees of freedom*** *of a system is the number of independent variables needed to describe that system. It is also equal to the number of quadratic terms in the classical expression of energy.*

The number of degrees of freedom is often considered to be the same as the number of normal modes of a system. However, this statement needs some clarification, as it depends on how you define degrees of freedom. In molecules, the number of degrees of freedom does indeed equate to the number of translational and rotational modes, but in the case of vibrational modes, there is a factor of 2 for the number of degrees of freedom. Two independent variables describe each normal vibrational mode (a vibrational coordinate and its time derivative, which enter into the potential and kinetic energies, respectively).

For example, in a diatomic molecule, there is one normal mode of oscillation (the atoms moving towards and away from each other with respect to the centre of mass)

doi:10.1088/978-0-7503-3875-2ch6

but two degrees of freedom. According to Maxwell's equipartition theorem, each degree of freedom contributes ½k_BT to the thermal energy, and so for the diatomic molecule, the energy per molecule of the normal vibrational mode is k_BT, i.e., there are 2 degrees of freedom per normal vibrational mode[1].

In a three-dimensional solid, each atom, therefore, should provide a contribution to the energy of $3 \times 2k_BT/2$ for vibration in all three dimensions, i.e., 3 degrees of freedom × 2. Therefore, for a solid, the total internal energy is given by

$$E = 3N_Ak_BT \tag{6.1}$$

where N_A is Avogadro's number: $6.022\,1415 \times 10^{23}$ mol^{-1}. Then the heat capacity at constant volume is

$$C_V = 3N_Ak_B = 3R \tag{6.2}$$

where R is the gas constant. This is equal to the Dulong and Petit value of 24.94 J K^{-1} mol^{-1}. Nice though this is, it turned out that experimentally this was only true at high temperatures, and at lower temperatures, the heat capacity was lower and temperature-dependent. This observation heralded the concept of energy levels in quantum theory. As a result, several theories were proposed to explain the observed behaviour, the two most popular due to Einstein and Debye.

6.1.1 Einstein model

Einstein's approach owed much to the work of others such as Planck and Boltzmann and is a simple modification of the Dulong and Petit model. To introduce a temperature-dependence into the theory, he considered the atomic vibrations to be quantized harmonic oscillators, all with a single frequency ω_E. This is a gross approximation, but as we shall see, it does have features that fit rather well with the observed data. For a quantized harmonic oscillator

$$E = \left(n + \frac{1}{2}\right)\hbar\omega \tag{6.3}$$

The single-particle partition function is given by

$$\begin{aligned} Z_{sp} &= \sum_n e^{-\left(n+\frac{1}{2}\right)\hbar\omega_E/k_BT} \\ &= e^{-\frac{1}{2}\hbar\omega_E/k_BT}\left(1 + e^{-\hbar\omega_E/k_BT} + e^{-2\hbar\omega_E/k_BT} + e^{-3\hbar\omega_E/k_BT} + \ldots\right) \\ &= \frac{e^{-\frac{1}{2}\hbar\omega_E/k_BT}}{1 - e^{-\hbar\omega_E/k_BT}} \end{aligned} \tag{6.4}$$

[1] But, as Tabor [14] pointed out, some authorities refer to vibration as possessing a *single* degree of freedom of energy k_BT.

The mean internal energy is then given by

$$\begin{aligned} E &= 3N_A k_B T^2 \frac{\partial \ln Z_{sp}}{\partial T} \\ &= 3N_A \hbar\omega_E \left\{ \frac{1}{2} - \frac{1}{e^{\hbar\omega_E/k_B T} - 1} \right\} \end{aligned} \tag{6.5}$$

and then the heat capacity is

$$\begin{aligned} C_V &= \frac{3N_A}{k_B T^2} \frac{(\hbar\omega_E)^2 e^{\hbar\omega_E/k_B T}}{(e^{\hbar\omega_E/k_B T} - 1)^2} \\ &= 3R \left(\frac{\Theta_E}{T} \right)^2 \frac{e^{\Theta_E/T}}{(e^{\Theta_E/T} - 1)^2} \end{aligned} \tag{6.6}$$

and the *Einstein temperature* $\Theta_E = \hbar\omega_E/k_B$. For high temperatures where $T \gg \Theta_E$, $k_B T \gg \hbar\omega_E$, this expression tends to

$$C_V \to 3R \tag{6.7}$$

the Dulong and Petit law. On the other hand, for very low temperatures

$$C_V \to 3R \left(\frac{\Theta_E}{T} \right)^2 e^{-\Theta_E/T} \tag{6.8}$$

which tends to zero as $T \to 0$.

The Einstein model agrees surprisingly well with observed heat capacity measurements for several metals. However, in reality, the heat capacities of solids do not approach zero quite as quickly as suggested by Einstein's model when $T \to 0$. In practice, it often looks more like

$$C_V \propto T^3 \tag{6.9}$$

6.1.2 Debye model

Peter Joseph William Debye (1884–1966) achieved a more complete description of the heat capacity in 1912. Einstein's model is based on oscillating atoms. Debye's treatment is at the other extreme, in which case the solid is treated somewhat like an elastic continuum, and atoms are not considered *per se*. Here, the thermal energy is involved in creating waves that distort the solid in some way. Using the language of quantum mechanics, then, such waves can also be interpreted in terms of particles called *phonons*. This name is derived from the fact that typical low-frequency waves are in many respects similar to sound waves. Symmetric wave functions describe phonons, and so, from a statistical mechanics point of view, they are bosons. As they have no physical existence outside the solid, they are, in fact, examples of what are termed *quasiparticles*.

Debye makes the following assumptions:

1. The solid can be treated as if it were an elastic continuum.
2. Phonons are created as temperature increases.

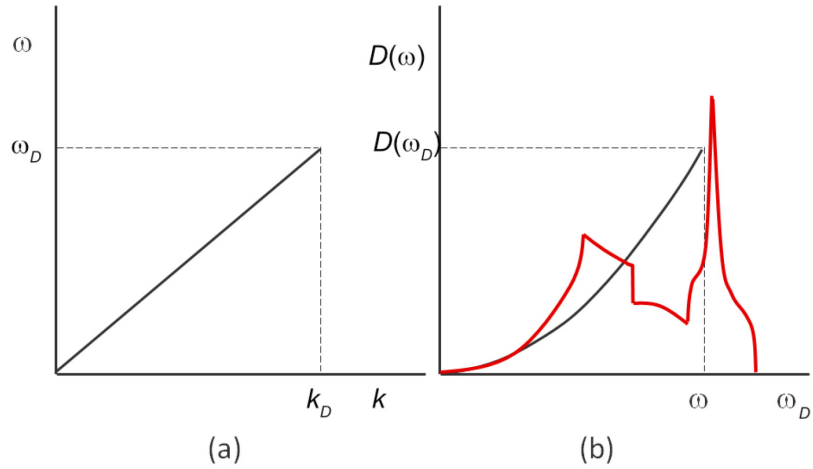

Figure 6.1. Assumptions of the Debye model of heat capacities. (a) No dispersion. (b) Parabolic density of states. The red curve is an experimental trace for aluminium.

3. There is no frequency dispersion in the solid, i.e., $\omega = vk$, where v is the wave velocity (figure 6.1(a)).
4. There is a cut-off frequency ω_D (and wave-vector k_D) above which no phonons exist in the solid (figure 6.1(a)).

For a three-dimensional solid, the density of states is

$$D(\omega) = 3 \times \frac{V_{\text{crystal}}\, k^2}{2\pi^2} \frac{dk}{d\omega} \tag{6.10}$$

An extra factor of three has been added to account that the phonons have three polarisations, two of which are transverse and one of which is longitudinal. Since there is no dispersion in this approximation

$$D(\omega) = \frac{3 V_{\text{crystal}}\, \omega^2}{2\pi^2 v^3} \tag{6.11}$$

This is shown in figure 6.1(b). The number of states is then given by

$$\begin{aligned} N_{\text{states}} &= \frac{3 V_{\text{crystal}}}{2\pi^2 v^3} \int_0^{\omega_D} \omega^2 d\omega \\ &= \frac{V_{\text{crystal}}}{2\pi^2 v^3} \left(\frac{k_B \Theta_D}{\hbar} \right)^3 \end{aligned} \tag{6.12}$$

where Θ_D is the so-called Debye temperature. The integral is used here since we assume the sample to be sufficiently large that the density of states forms a quasi-continuum. The upper limit of the integral is set at the Debye cut-off frequency.

Since we are dealing with phonons, we can now introduce the Bose–Einstein factor $f(\omega, T)$ but with the chemical potential $\mu = 0$, as the numbers of phonons are not conserved as temperature changes:

$$f(\omega, T) = \frac{1}{e^{\hbar\omega/k_B T} - 1} \tag{6.13}$$

The internal energy is then given by

$$\begin{aligned} E &= \int_0^{\omega_D} \hbar\omega D(\omega) f(\omega, T) d\omega \\ &= \frac{3V_{\text{crystal}}}{2\pi^2 v^3} \int_0^{\omega_D} \frac{\hbar\omega^3}{e^{\hbar\omega/k_B T} - 1} d\omega \\ &= 3N_{\text{states}} \left(\frac{\hbar}{k_B \Theta_D}\right)^3 \int_0^{\omega_D} \frac{\hbar\omega^3}{e^{\hbar\omega/k_B T} - 1} d\omega \end{aligned} \tag{6.14}$$

This integral is fearsome, and to simplify it, we make the substitution

$$x = \frac{\hbar\omega}{k_B T} \tag{6.15}$$

and then

$$E = 3N_{\text{states}} k_B T \left(\frac{T}{\Theta_D}\right)^3 \int_0^{x_D} \frac{x^3}{e^x - 1} dx \tag{6.16}$$

Now, for high temperatures, $k_B T \gg \hbar\omega$, the integral is close to zero. We can then make the following approximation

$$\frac{x^3}{e^x - 1} \simeq \frac{x^3}{1 + x - 1} = x^2 \tag{6.17}$$

and then

$$\begin{aligned} E &= 3N_{\text{states}} k_B T \left(\frac{T}{\Theta_D}\right)^3 \int_0^{x_D} x^2 dx \\ &= N_{\text{states}} k_B T \left(\frac{T}{\Theta_D}\right)^3 \left[x^3\right]_0^{x_D} \end{aligned} \tag{6.18}$$

But

$$x_D = \frac{\Theta_D}{T} \tag{6.19}$$

and so

$$\begin{aligned} E &= N_{\text{states}} k_B T \\ \therefore C_V &= N_{\text{states}} k_B \end{aligned} \tag{6.20}$$

Note that N_{states} appears in this result rather than N_A, Avogadro's number. It is a common mistake to confuse the numbers of states with numbers of atoms. In this case, if we can assume that the number of states equals three times the number of atoms (each atom has three vibrational degrees of freedom) in the crystal, then we get the Dulong and Petit Law

$$C_V = 3N_A k_B \tag{6.21}$$

However, one has to be careful here because you cannot generally assume that the number of states is equal to three times the number of atoms. The number of states has nothing to do with the number of atoms, as it is equal to three times the number of primitive unit cells in the crystal (note that the derivation of the density of states does not involve atoms at all!). If we write $N_{\text{states}} = 3N_A$ we are, in fact, assuming that there is one atom per primitive unit cell. This problem was discussed several years ago by Ziman [1]. So why do we get away with this formulation? The reason is subtle and is due to the type of vibration mode that is primarily responsible for heat capacity. As we shall see later, every atom can oscillate in three orthogonal directions, so that if in any primitive unit cell there are N atoms, there will be $3N$ modes of vibration. The three lowest-energy modes (the so-called acoustic modes) are the main contributors to the Debye heat capacity, especially at low temperatures. As every crystal has at least one atom in the primitive unit cell, the heat capacity is dominated by the three acoustic modes. This is why we can treat the number of states in the Debye approximation as equivalent to having one atom in the primitive unit cell in practice.

Now, consider what happens at low temperatures where $k_B T \ll \hbar\omega$. The heat capacity is then given by (appendix H)

$$C_V = \frac{12\pi^4}{15} N_{\text{states}} k_B \left(\frac{T}{\Theta_D}\right)^3 \tag{6.22}$$

correctly showing that $C_V \propto T^3$ in line with experiment.

The Debye model can be improved in various ways. For instance, instead of assuming that all three acoustic waves have the same velocity, one can use

$$\frac{1}{v^3} = \frac{1}{v_{\text{trans}}^3} + \frac{1}{v_{\text{trans}}^3} + \frac{1}{v_{\text{long}}^3} \tag{6.23}$$

for the two transverse polarisations and one longitudinal polarisation. Note, too, that the result depends on the system's dimensionality since the density of states depends on the dimensionality m of the system. Therefore, at low temperature

$$C_V \propto T^m \tag{6.24}$$

For instance, graphite crystals have layers of carbon atoms strongly bound together in planes with weak van der Waals interactions between the layers. Measurements of the heat capacity find $C_V \propto T^{2.4}$ at very low temperatures.

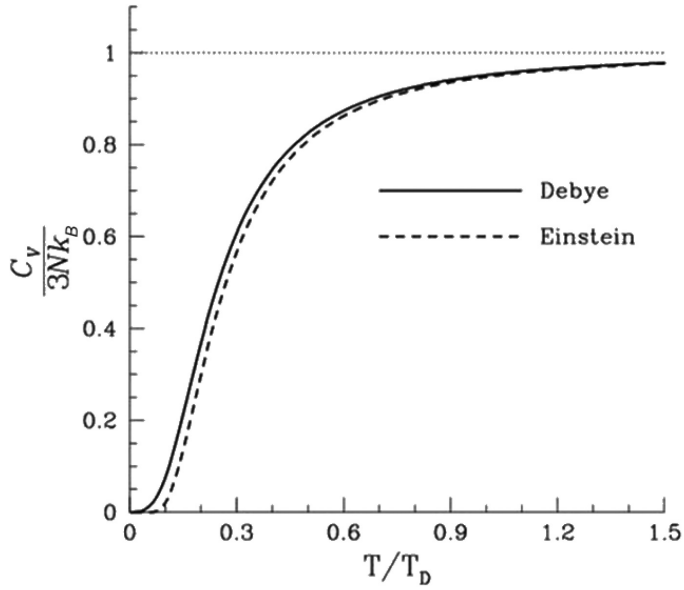

Figure 6.2. Comparison between Debye and Einstein models. From [11].

The significance of the Debye temperature is that this is the temperature where the maximum number of phonons are created by thermal energy, above which the classical Dulong and Petit behaviour is expected. This is a function of the strength of the bonding between the atoms in the crystal, with strong bonds meaning stiff force constants between the atoms leading to higher-frequency phonons; hence higher Debye temperatures. Thus, for example, crystals of diamond, one of the hardest materials known, and in which carbon atoms are strongly covalently bonded, have a Debye temperature of 2250 K. On the other hand, a softer material such as aluminium has a Debye temperature of 428 K.

Figure 6.2 shows a comparison between the Einstein and Debye models, where it is seen that, while both saturate at high temperatures to the same value, the Einstein model underestimates the heat capacity as the temperature decreases.

6.2 Vibrations of atoms

When a crystal is heated, the main result is an increase in the atoms' vibrational amplitudes and frequencies. Because the atoms interact with each other through the periodic potential, the motion of one atom affects the surrounding atoms, the result being that wave-like vibrational modes are set up. There are several ways this can be described, and we shall see that the concept of reciprocal space plays an integral part in this. We shall begin here with a very simple way of viewing vibrational behaviour in direct space from an atomistic point of view using purely classical physics (although we should bear in mind that, in reality, the solutions that we obtain are quantum states: we get away with the classical approach because the density of states in a typical solid is very large and the quantum states constitute a quasi-continuum).

6.2.1 One-dimensional monatomic chain

A standard problem, discussed in most solid-state texts, is that of a one-dimensional linear chain of atoms separated by a distance a along which waves can propagate. In this case, the distance a is also the primitive unit-cell repeat length (i.e., a one-dimensional unit cell containing 1 atom). Although the atoms repeat in one dimension, we can consider the motion of the atoms to be in three dimensions. These waves can be transverse (in which case there are two such transverse, degenerate components) or longitudinal (figure 6.3).

To determine this simple system's characteristics, we need to define the classical equation of motion for the atoms. In its simplest form, we can use the harmonic approximation. This is done using Hooke's Law and thinking of the bonds between the atoms as if they were springs with force constant C. As one atom moves, it influences its neighbours, next-neighbours, and so on, causing them to move in sympathy. It is this that creates the wave. Here, for illustrative purposes, we shall take the trivial approach of just having nearest-neighbour force constants, but it is relatively easy to incorporate higher-order forces if required.

Figure 6.4(a) shows a row of lattice points of spacing a and (b) a set of identical atoms of mass M joined by springs. Consider the displacement of the atom s denoted by u_s.

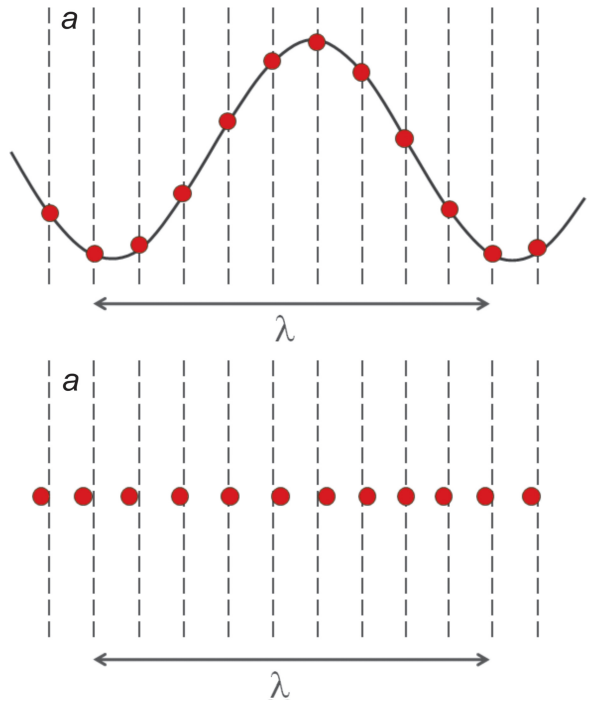

Figure 6.3. Examples of waves propagating on a one-dimensional linear chain of atoms spacing a. The upper wave is transverse, and the lower wave is longitudinal.

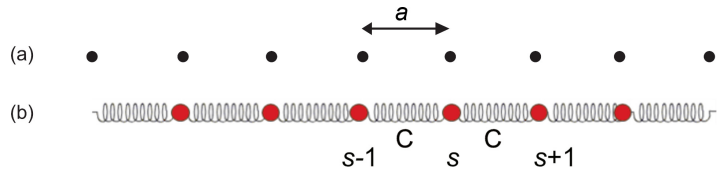

Figure 6.4. A linear chain of atoms of mass M with repeat distance a.

According to Hooke's Law, the equation of motion is then given by

$$M\ddot{u}_s = C(u_{s+1} - u_s) + C(u_{s-1} - u_s) \tag{6.25}$$

If we now assume a nearest-neighbour wave-like solution of the form

$$u_s = Ue^{i(ksa-\omega t)} \tag{6.26}$$

we then get

$$\begin{aligned} -M\omega^2 &= C(e^{ika} + e^{-ika} - 2) \\ &= 2C(\cos ka - 1) \end{aligned} \tag{6.27}$$

Therefore, we find that the frequency is

$$\omega = \sqrt{\frac{4C}{M}} \left|\sin\frac{ka}{2}\right| = \omega_{\max} \left|\sin\frac{ka}{2}\right| \tag{6.28}$$

The group velocity of this wave is given by

$$v_g = \frac{d\omega}{dk} = \sqrt{\frac{Ca^2}{M}} \cos\frac{ka}{2} = \frac{a\omega_{\max}}{2} \cos\frac{ka}{2} \tag{6.29}$$

The frequency is plotted as a function of the wave-vector in figure 6.5, and the group velocity in figure 6.6.

Definition. *The plot of frequency against the wave-vector for a vibrating system is known as a* ***dispersion curve***.

The first thing to notice is that the curve is periodic in k-space with a periodicity of $2\pi/a$. Also shown in both figures are the first, second and third Brillouin zones (coloured blue, pink and green, respectively), where it can be seen that the same solutions appear in each. Therefore, it is evident that all the information needed to construct these curves is contained in one half of the first Brillouin zone within the range 0 to π/a. In other words, it is not necessary to consider higher-order Brillouin zones in practice (figure 6.6).

Note that the group velocity is highest at $k = 0$ but drops to zero at the values $\pm(2n+1)\pi/a$, or for the first Brillouin zone at $\pm\pi/a$. These points differ by a reciprocal-lattice vector distance 2π/a. So the solution at π/a is for a travelling wave to the right while $-\pi/a$ is for an equal amplitude wave travelling to the left. In other words, on the Brillouin zone boundary, the solution is that of a standing wave,

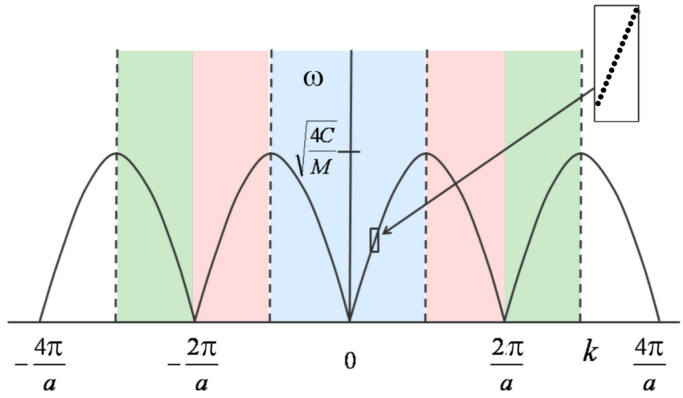

Figure 6.5. Frequency of vibration for a monatomic chain plotted as a function of wave-vector. First Brillouin zone = blue; second Brillouin zone = pink; third Brillouin zone = green. The inset diagram is a magnified view of the curve, showing that it consists of several wave states close together to form a quasi-continuum. The smaller the chain's length, the fewer such wave states will exist within the Brillouin zone, and the smaller the density of states.

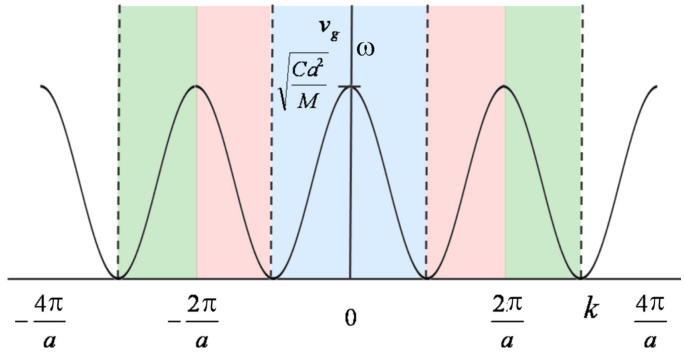

Figure 6.6. Group velocity for the monatomic chain as a function of wave-vector. First Brillouin zone = blue; second Brillouin zone = pink; third Brillouin zone = green.

i.e., two equivalent waves travelling in opposite directions. One can think of this as a wave travelling to the right being reflected (Bragg-scattered) to the left, provided that its wavelength corresponds to a wave-vector ending on the Brillouin zone boundary (see section 5.3).

Therefore, it can be seen that there are, in principle, for any wave, an infinite number of solutions consistent with the periodicity of the reciprocal and direct lattices. In general, the wave-vector solutions are given by $\pm k \pm \frac{2n\pi}{a}$ where n is an integer. Figure 6.7 shows three such wave-vector solutions corresponding to $k = \frac{\pi}{2a}$, $\frac{3\pi}{2a}$ and $\frac{7\pi}{2a}$, the second and third solutions corresponding to waves travelling in the opposite direction to the first. All these solutions are equivalent, but it can also be seen that only the wave with $k = \frac{\pi}{2a}$ needs to be considered, as all other solutions carry no further information. The wave with $k = \frac{\pi}{2a}$ is the only one that lies *within* the first Brillouin zone.

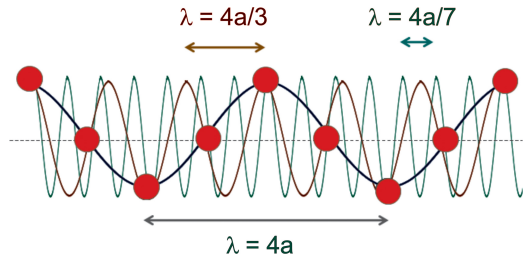

Figure 6.7. Example of three transverse waves for the monatomic chain. Although the wavelengths are different, they are all possible solutions.

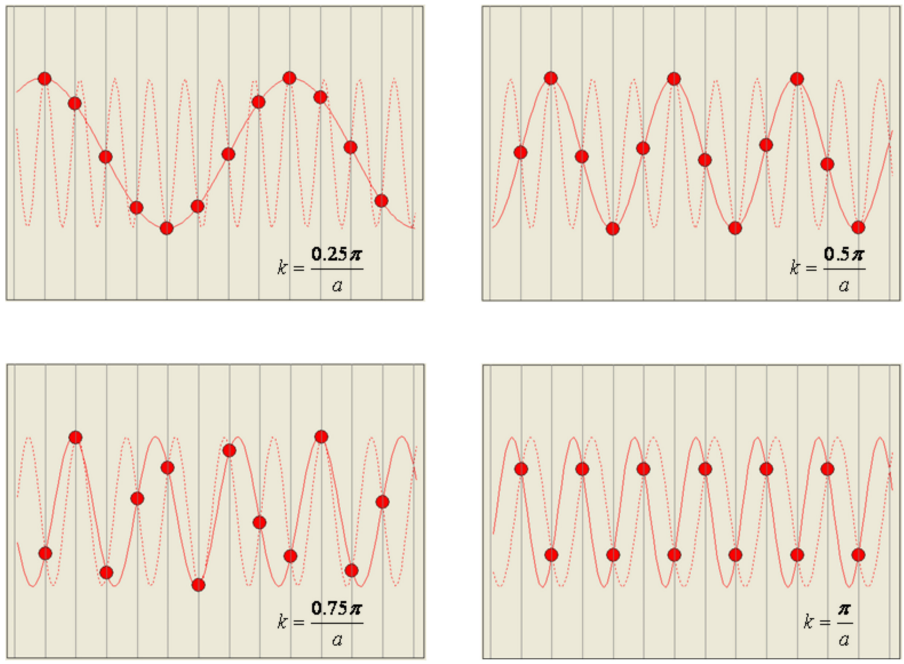

Figure 6.8. Examples of transverse oscillations in a monatomic chain for different values of the wave-vector. Simulations by the program CHAINPLOT are obtainable from [2].

Therefore, in general, starting from the centre of the first Brillouin zone, where $k = 0$ and $\lambda = \infty$, as k increases, the wavelength decreases until the point where k reaches the Brillouin zone boundary. Here, $k = \pm\pi/a$, and the wavelength is equal to $2a$. All wave-vectors outside the Brillouin zone boundary then have shorter wavelengths. But then these waves rise and fall between the atomic sites, unlike the ones with wave-vectors inside the Brillouin zone. It is, therefore, somewhat meaningless to ask if such waves describe the same vibrational wave used in equation (6.26). I understand that radio engineers call the phenomenon, where two or more waves with different wavelengths look the same if they are sampled only at the lattice positions, *aliasing* of waves.

Figure 6.8 shows some examples of transverse waves computed by the program CHAINPLOT [2]. The dashed curves show the solutions where a reciprocal-lattice

vector has been subtracted, corresponding to a wave travelling to the left. Only for $k = \pi/a$ (diagram at bottom right) do we obtain two equal solutions travelling in opposite directions to form a standing wave.

Finally, consider the density of states for this system. For a one-dimensional system, this is given by

$$D(\omega) = \frac{3L}{\pi}\frac{dk}{d\omega} \tag{6.30}$$

The factor of three arises here because there are three possible modes, two transverse and one longitudinal.

Therefore,

$$\begin{aligned}\frac{d\omega}{dk} &= \frac{a\omega_{\max}}{2}\cos\frac{ka}{2} \\ &= \frac{a\omega_{\max}}{2}\left(1 - \sin^2\frac{ka}{2}\right)^{\frac{1}{2}} \\ &= \frac{a\omega_{\max}}{2}\left(1 - \left[\frac{\omega}{\omega_{\max}}\right]^2\right)^{\frac{1}{2}} \\ &= \frac{a}{2}(\omega_{\max}^2 - \omega^2)^{\frac{1}{2}}\end{aligned} \tag{6.31}$$

and this results in

$$D(\omega) = \frac{6L}{\pi a}\frac{1}{(\omega_{\max}^2 - \omega^2)^{\frac{1}{2}}} \tag{6.32}$$

The density of states, therefore, shows a singularity when $\omega = \omega_{\max}$ (corresponding to $k = \pm \pi/a$, the zone boundary value).

6.2.2 One-dimensional diatomic chain

We now consider what happens if, within the repeat distance a there are two atoms of differing mass M_1 and M_2. Figure 6.9 shows such an alternating array. It is most important to emphasize that the distance a, as indicated in the lattice in figure 6.9(a), is not the distance between atoms, but it is the *repeat* distance. In other words, it is a

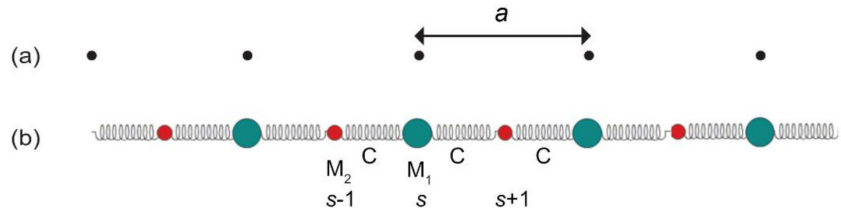

Figure 6.9. The diatomic chain with alternating atoms of different mass $M_1 > M_2$ but with equal force constants C between them.

unit-cell length for a one-dimensional primitive unit cell containing two different atoms. Be aware that some treatments in the literature write a for the distance between the atoms.

Once again, using Hooke's Law, we now have two equations of motion:

$$\begin{aligned} M_1\ddot{u}_s &= C[u_{s+1} - u_s] + C[u_{s-1} - u_s] \\ M_2\ddot{u}_{s+1} &= C[u_{s+2} - u_{s+1}] + C[u_s - u_{s+1}] \end{aligned} \tag{6.33}$$

Then, assuming two wave-like solutions

$$\begin{aligned} u_s &= Ue^{i(ksa/2-\omega t)} \\ u_{s+1} &= Ve^{i(k(s+1)a/2-\omega t)} \end{aligned} \tag{6.34}$$

This gives rise to the following two equations

$$\begin{aligned} -M_1\omega^2 U &= 2CV\cos k\frac{a}{2} - 2CU \\ -M_2\omega^2 V &= 2CU\cos k\frac{a}{2} - 2CV \end{aligned} \tag{6.35}$$

For a non-trivial solution

$$\begin{vmatrix} 2C - M_1\omega^2 & 2C\cos k\dfrac{a}{2} \\ 2C\cos k\dfrac{a}{2} & 2C - M_2\omega^2 \end{vmatrix} = 0 \tag{6.36}$$

Hence,

$$(2C - M_1\omega^2)(2C - M_2\omega^2) - 4C^2\cos^2\frac{ka}{2} = 0 \tag{6.37}$$

Finally, this gives the result

$$\omega^2 = \frac{C(M_1 + M_2)}{M_1M_2} \pm C\left[\left(\frac{M_1 + M_2}{M_1M_2}\right)^2 - \frac{4}{M_1M_2}\sin^2 ka/2\right]^{\frac{1}{2}} \tag{6.38}$$

This is plotted in figure 6.10. As with the monatomic chain, we see that the dispersion is periodic in the reciprocal lattice with Brillouin zone boundaries at $\pm(2n+1)\pi/a$. However, this time for any value of wave-vector $\mathbf{k}$, there are two solutions, one at low frequency and one at high frequency. The lower-frequency curve is known as the *acoustic branch*, and the higher-frequency curve is called the *optic branch*. The acoustic branch is so-called because, at small values of k, the frequency is approximately linearly related to the wave-vector, i.e., it is almost dispersionless, and in real solids corresponds to a velocity similar to that for sound waves. The optic branch, on the other hand, corresponds to frequencies typically seen in the optical region. The amplitudes are given by

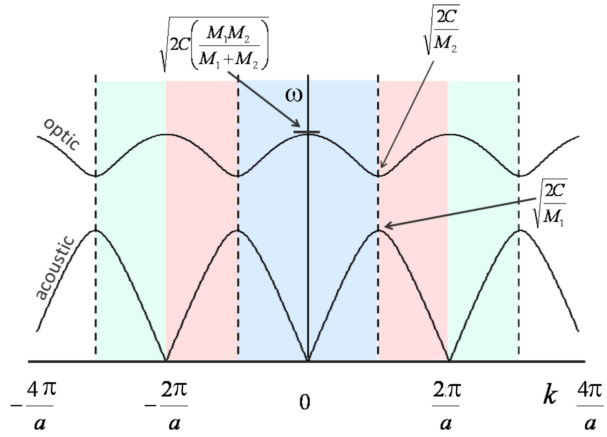

Figure 6.10. Dispersion curves for a diatomic chain in which $M_1 > M_2$. First Brillouin zone = blue; second Brillouin zone = pink; third Brillouin zone = green.

$$\begin{aligned}\frac{U}{V} &= \frac{2C\cos ½ka}{2C - M_1\omega^2} \text{ acoustic branch}\\ \frac{V}{U} &= \frac{2C\cos ½ka}{2C - M_2\omega^2} \text{ optic branch}\end{aligned} \tag{6.39}$$

Notice how on the Brillouin zone boundaries, where $k = \pm\pi/a$, the two solutions are

$$\begin{aligned}\omega_{\text{acoustic}} &= \sqrt{\frac{2C}{M_1}} \text{ and } U = 0\\ \omega_{\text{optic}} &= \sqrt{\frac{2C}{M_2}} \text{ and } V = 0\end{aligned} \tag{6.40}$$

This tells us that, for this wave-vector value, the acoustic mode only involves the motion of the heavy atoms, and the light ones are not oscillating at all. On the optic branch at this wave-vector, the lighter atoms are vibrating, while the heavier ones remain stationary. If we make the two masses closer in magnitude, the gap between the optic and acoustic modes will become narrower. Therefore, it is instructive to consider what happens to the dispersion curve as the two atoms become increasingly alike (figure 6.11).

This diagram plots the first and second Brillouin zones with the heavy line marking the diatomic dispersion curves. If we now imagine that we somehow magically managed to change the masses until $M_1 = M_2$, the gap at the zone boundary closes up, and the dispersion curve follows along the dashed trace. But, of course, when this happens, we are simply back to the monatomic case. This means that the Brillouin zone boundary is moved from π/a to $2\pi/a$. In this case, the repeat distance now becomes equivalent to the interatomic spacing $a_0 = a/2$, so that the Brillouin zone boundary is now at π/a_0. In this situation, the optic branches no longer exist, and only the acoustic branch is left (figure 6.12).

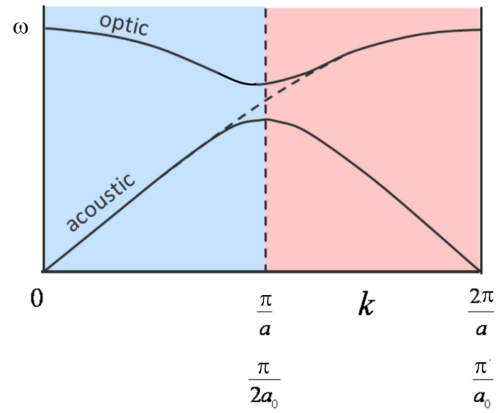

Figure 6.11. Diatomic chain related to the monatomic chain.

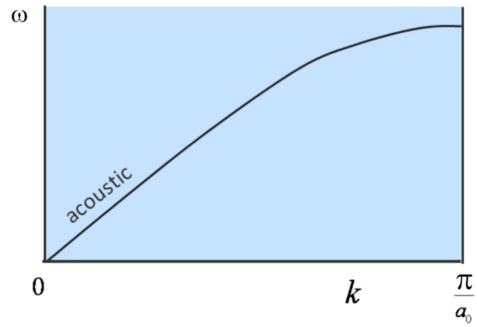

Figure 6.12. Result of making the two atoms in a diatomic chain equivalent in mass. First Brillouin zone = blue.

This tells us a couple of important things. First of all, there will always be acoustic branches for vibrations in a solid: in general, there will be three such branches, two transverse and one longitudinal, although they may turn out for symmetry reasons to be frequency-degenerate. Secondly, this also shows that, when there is more than one atom in the primitive unit cell, say n, at any value of k, we have $3n$-3 optic modes plus three acoustic modes.

So now, we can begin to understand a bit more about the significance of the extended Brillouin zones. Imagine doing the reverse of the procedure above by starting from the monatomic chain and then causing every second atom to have a higher mass, thus changing the system back to a diatomic chain. Figure 6.13 shows what would happen just as the two types of atom are differentiated. Halfway between the zone centre and the zone boundary for the monatomic case, splitting of the curve occurs, and this then becomes the new Brillouin zone boundary. This alternative view has the optic branch in the second Brillouin zone and the acoustic branch in the first Brillouin zone. By appealing to the periodicity of the reciprocal lattice, we can fold back all the solutions across the Brillouin zone boundaries to

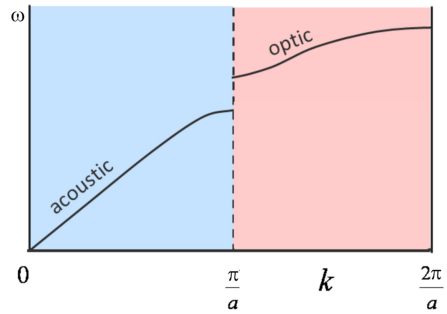

Figure 6.13. Alternative view of the dispersion curves for a diatomic chain.

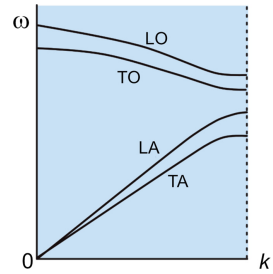

Figure 6.14. Reduced zone scheme for a diatomic chain showing longitudinal acoustic (LA), longitudinal optic (LO), transverse acoustic (TA) and transverse optic (TO) branches.

obtain figure 6.10, and then instead of using an extended zone scheme, use a reduced zone scheme instead (figure 6.14).

In this diagram, the longitudinal and transverse acoustic and optic branches are plotted. Bonds are compressed and stretched in longitudinal motion, whereas in transverse motion, it is the bond angles that change. The former involves higher force constants, and so we expect to find that the longitudinal modes are of higher frequency than the transverse modes. Furthermore, in this example, there are two degenerate transverse oscillations with the atomic motions perpendicular to each other, and so we only see single TA and TO curves plotted.

Note. *For any crystal, the number of normal mode branches at any value of k will be equal to* $3N$ *where* N *is the number of atoms in the* ***primitive*** *unit cell.*

Figures 6.15 and 6.16 illustrate some simulations of the transverse motion of the atoms in a diatomic chain. The dashed curves represent solutions for each atom type, where a reciprocal-lattice vector has been subtracted, and correspond to waves travelling in the opposite direction to those described by the full curves.

In the acoustic case for $k < \pi/a$, the tendency is for all atoms to move in the same direction, particularly obvious for low values of k. For $k < \pi/a$, the solutions correspond to running waves and the heavy and light atoms execute motion described by two waves, according to equations (6.39) and (6.34) (red and green sinusoidal traces). The dashed traces are for corresponding waves where a reciprocal-lattice vector has been

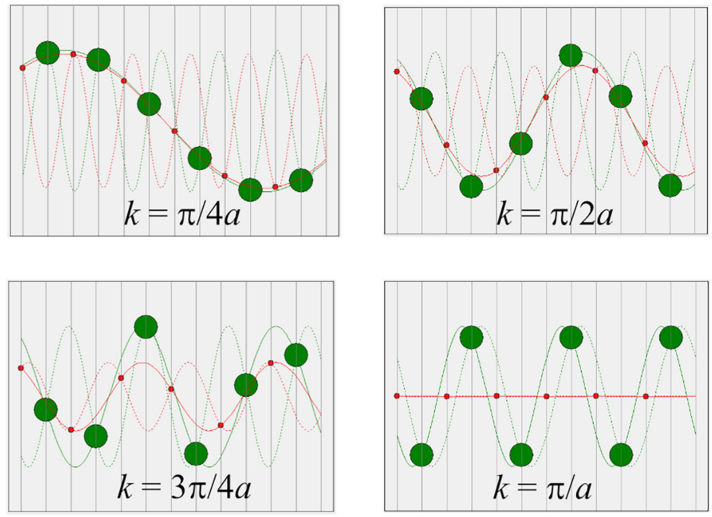

Figure 6.15. Examples of transverse oscillations in a diatomic chain ($M_1/M_2 = 4$) for different values of wave-vector (acoustic branch). Simulations by the program CHAINPLOT are obtainable from [2].

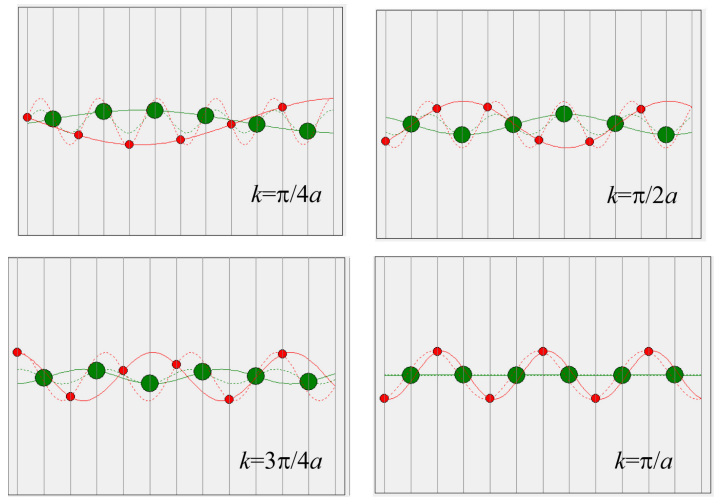

Figure 6.16. Examples of transverse oscillation in a diatomic chain ($M_1/M_2 = 2$) for different values of wave-vector (0ptic branch). Simulations by the program CHAINPLOT are obtainable from [2].

subtracted from k and thus correspond to running waves travelling in the opposite direction. As k approaches zero, all the atoms move in the same direction but with very low frequency. Generalizing to a real solid, such low-frequency acoustic modes, therefore, lead to bulk distortions of the solid. So their study is important for the understanding of its elastic properties. When $k = \pi/a$, the Brillouin zone boundary, the light atoms remain stationary, and the heavy atoms oscillate about their mean positions in accordance with the solutions (6.40). The dashed and full curves, in this case, constitute a standing wave solution. The effect is to double the unit-cell repeat from a to

$2a$. If we were to freeze the motion in this configuration, such as might occur at a phase transition, the result would be that we would have to use a new reciprocal lattice with new lattice points halfway between the former points.

In the optic case (figure 6.16), the tendency is for the two types of atom to move in opposing directions. The frequencies here are high, typically similar to optical frequencies. At very low k, the chain of heavy atoms will move in one direction while the light ones will move in the opposite directions. If the two types of atoms happen to be ions, this will result in charge separation, i.e., oscillating dipoles (for example, in NaCl). The existence of oscillating dipoles will mean that a solid with this type of motion would absorb electromagnetic radiation, typically in the infra-red region. Again, when $k = \pi/a$, the motion effectively doubles the unit-cell repeat length, as in the acoustic case, but this time it is only the light atoms that oscillate. We can also see that a study of low-k optic modes gives information about relative atomic motions within a unit cell.

These simulation diagrams also illustrate something that seems to be ignored in almost all books published since the 1960s. Notice in figure 6.17 how the light and heavy atoms seem to sit on a single sinusoidal wave. What has been forgotten here is that, except for $k = \pi/a$, the wave solutions are running waves, not stationary! You might think that because we have used periodic boundary conditions, the waves must all be stationary, but remember that dispersion curves, such as those shown in figure 6.14, are usually plotted as travelling waves in half the Brillouin zone, with the other unplotted half corresponding to equivalent waves travelling in the opposite direction. It is when taken together that one has stationary waves. Therefore, if the acoustic case looked like that shown in figure 6.17, then as the crest of the wave moves from left to right, both heavy and light atoms would have to execute the same amplitude. But this cannot be so, as equations (6.34) imply. In reality, there are two sinusoidal waves with the same frequency and phase but with different amplitudes, one for the heavy atoms and one for the light atoms, as seen in the simulations earlier. In general, we can say that each atom must lie on its own travelling sinusoidal wave, as can be seen in figures 6.15 and 6.16. Figure 6.17 is, therefore, misleading by giving the wrong impression. The diagrams in the books by Brillouin [3] and by Wannier [4] are among the few that make this clear.

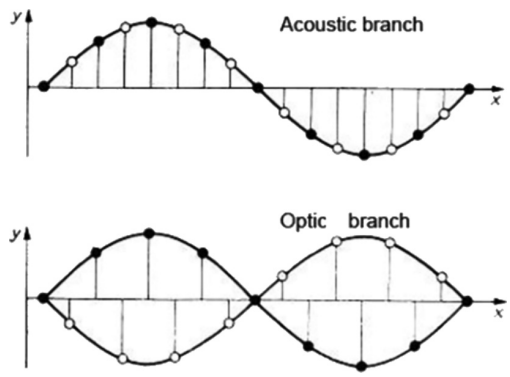

Figure 6.17. Typical diagrams of atomic displacements for the diatomic chains, as seen in many textbooks.

6.2.3 Lattice dynamics

Real solids are generally not one-dimensional, and so we need a way to handle the more complicated case of a three-dimensional crystal. The term lattice dynamics describes this subject, although this title demonstrates the usual confusion between atoms and lattice points. It is not the lattice that vibrates but the atoms! Perhaps it would be better if we called this atom dynamics, but I guess it is too late for that. I shall only give a brief introduction to the subject here, but for more details, I recommend the books by Dove [5, 6].

Once again, we shall adopt a semi-classical approach. Let us start by defining the kinetic energy of the atoms

$$T = \frac{1}{2}\sum_{ls\alpha} M_s \dot{u}_\alpha^2\begin{pmatrix} l \\ s \end{pmatrix} \tag{6.41}$$

Here, l is the unit-cell index, s the atom index within a unit cell, and α the Cartesian component of direction. The potential energy can be expressed as a power series via a Taylor expansion in the atomic displacements:

$$V = V_0 + \sum_{ls}\sum_{\alpha}\phi_\alpha\begin{pmatrix} l \\ s \end{pmatrix}u_\alpha\begin{pmatrix} l \\ s \end{pmatrix} + \frac{1}{2}\sum_{\substack{ls \\ l's'}}\sum_{\alpha\beta}\phi_{\alpha\beta}\begin{pmatrix} ll' \\ ss' \end{pmatrix}u_\alpha\begin{pmatrix} l \\ s \end{pmatrix}u_\beta\begin{pmatrix} l' \\ s' \end{pmatrix} + \cdots \tag{6.42}$$

$\phi_{\alpha\beta}\begin{pmatrix} ll' \\ ss' \end{pmatrix}$ represents the force in the α direction on atom ls when the atom $l's'$ is displaced along β. In general, we can write

$$V = V_0 + V_1 + V_2 + \cdots \tag{6.43}$$

and then

$$\phi_\alpha\begin{pmatrix} l \\ s \end{pmatrix} = \left[\frac{\partial V_1}{\partial u_\alpha\begin{pmatrix} l \\ s \end{pmatrix}}\right]_0 \tag{6.44}$$

at equilibrium. Also at equilibrium

$$\phi_{\alpha\beta}\begin{pmatrix} ll' \\ ss' \end{pmatrix} = \left[\frac{\partial^2 V_2}{\partial u_\alpha\begin{pmatrix} l \\ s \end{pmatrix}\partial u_\beta\begin{pmatrix} l' \\ s' \end{pmatrix}}\right]_0 \tag{6.45}$$

In the harmonic approximation, we neglect all higher-order terms. V_0 is a static term and can be ignored. Also, $V_1 = 0$ because $\phi_\alpha\begin{pmatrix} l \\ s \end{pmatrix}$ is the negative of the force acting on the atom ls, and this is zero at equilibrium. Therefore, for harmonic motion, the Hamiltonian is given by

$$\mathcal{H} = V_0 + \frac{1}{2}\sum_{ls\alpha} M_s \dot{u}_\alpha^2\begin{pmatrix} l \\ s \end{pmatrix} + \frac{1}{2}\sum_{\substack{ls \\ l's'}}\sum_{\alpha\beta}\phi_{\alpha\beta}\begin{pmatrix} ll' \\ ss' \end{pmatrix} u_\alpha\begin{pmatrix} l \\ s \end{pmatrix} u_\beta\begin{pmatrix} l' \\ s' \end{pmatrix} \tag{6.46}$$

The equation of motion for atom ls is (omitting α and β for simplicity)

$$M_s \ddot{u}\begin{pmatrix} l \\ s \end{pmatrix} = -\frac{\partial V}{\partial u\begin{pmatrix} l \\ s \end{pmatrix}} = -\sum_{l's'}\phi\begin{pmatrix} ll' \\ ss' \end{pmatrix} u\begin{pmatrix} l' \\ s' \end{pmatrix} \tag{6.47}$$

This gives an infinite number of coupled differential equations to solve, and this can be simplified by making use of lattice periodicity. From the Bloch theorem $u(l, s) = e^{i\mathbf{k}\cdot\mathbf{r}}u(0, s)$, for corresponding atoms s, in different unit cells, e.g. (l, s) and (l', s), the motions differ only in phase, and therefore only on the relative positions of the cells. So

$$u\begin{pmatrix} l \\ s \end{pmatrix} = M_s^{-\frac{1}{2}} U_s e^{-i\omega t} e^{i\mathbf{k}\cdot\mathbf{r}(l)} \tag{6.48}$$

Therefore,

$$\begin{aligned} M_s \ddot{u}\begin{pmatrix} l \\ s \end{pmatrix} &= -\omega^2 M_s^{\frac{1}{2}} U_s e^{-i\omega t} e^{i\mathbf{k}\cdot\mathbf{r}(l)} \\ &= -\sum_{l's'}\phi\begin{pmatrix} 0l' \\ ss' \end{pmatrix} M_{s'}^{-\frac{1}{2}} U_{s'} e^{-i\omega t} e^{i\mathbf{k}\cdot\mathbf{r}(l')} \end{aligned} \tag{6.49}$$

Rearranging and reintroducing directions α and β

$$\begin{aligned} \omega^2 U_{\alpha s} &= \sum_{\beta l s'}\phi\begin{pmatrix} 0l' \\ ss' \end{pmatrix} \frac{1}{\sqrt{M_s M_{s'}}} U_{\beta s'} e^{-i\omega t} e^{i\mathbf{k}\cdot[\mathbf{r}(l') - \mathbf{r}(l)]} \\ &= \sum_{\beta s'} D_{\alpha\beta}(ss', \mathbf{k}) U_{\beta s'} \end{aligned} \tag{6.50}$$

$D(ss', \mathbf{k})$ is known as the *dynamical matrix*. In this way, the problem is reduced to the solution of $3n$ equations, where n is the number of atoms in a *primitive* unit cell. A non-trivial solution is found when

$$|D_{\alpha\beta}(ss', \mathbf{k}) - \omega^2\delta_{\alpha\beta}\delta_{ss'}| = 0 \tag{6.51}$$

The dynamical matrix is Hermitian, and so the eigenvalues are real. Therefore, we obtain $3n$ solutions for ω^2 at any value of $\mathbf{k}$. By diagonalizing the dynamical matrix, the problem is then re-specified by new coordinates, the so-called *normal coordinates*. The resulting solutions then correspond to $3n$ independent *normal modes*.

In principle, solving the full lattice dynamics problem in this way should be straightforward for any crystal structure, and indeed computer programs are now available that attempt to do just that. However, the task is complicated because the force constants are of variable origin and are often unknown. For example, just

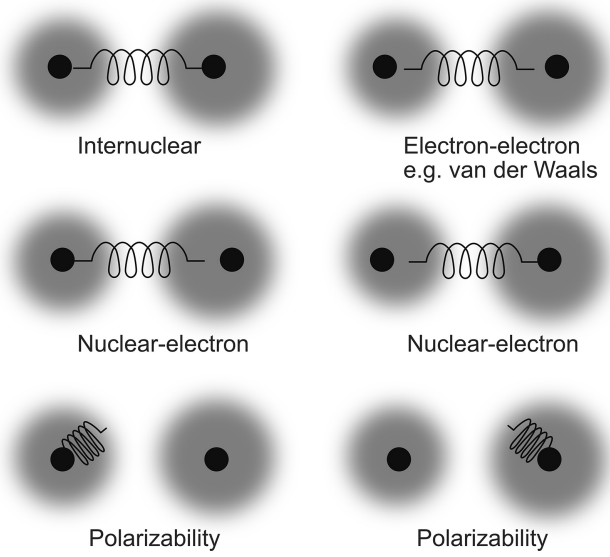

Figure 6.18. The force constant information needed to describe a diatomic molecule in full.

consider the trivial case of a diatomic molecule consisting of two different atoms (figure 6.18). It can be seen that, even in this simple molecule, we require a great deal of information to fully determine the eigenvalue frequencies of vibration for the individual atoms. However, by group-theoretical arguments, we can easily use symmetry to determine the directions of movement (the eigenvectors). In this example, we know that the mode of vibration is simply described by the two atoms moving towards and away from each other. Determination of the frequency requires knowledge of at least the most important force constants, so it is not trivial after all!

A simple approach that works quite well for ionic crystals is through the shell model, in which only two types of interaction are assumed. One is the core interaction of each atom representing the nucleus and inner electrons (polarisability term), and the other is the shell representing the outer electrons (electron–electron term). Good models can be made for these two interactions. Although other interactions are ignored, it turns out that these are sufficiently strong to enable a reasonable computation to be made. The core and shell are charged, and typically interact via a simple harmonic potential.The shell is treated as having no mass. So the dynamical equations are written in such a way that the positions of the shells are assumed to relax instantaneously when the positions of interacting neighbouring atoms change (the *adiabatic approximation*). Because the shells represent the outer electrons, it is often assumed that the interatomic interactions are represented by interactions between neighbouring shells.

Figure 6.19 shows a couple of examples of dispersion curves that have been calculated using an *ab initio* force constant model and compared with measurements for two relatively straightforward cases, diamond (all-face-centred cubic) and graphite (hexagonal). The curves are shown for different paths in the Brillouin zones, and the letters indicate the critical points. The agreement between measured

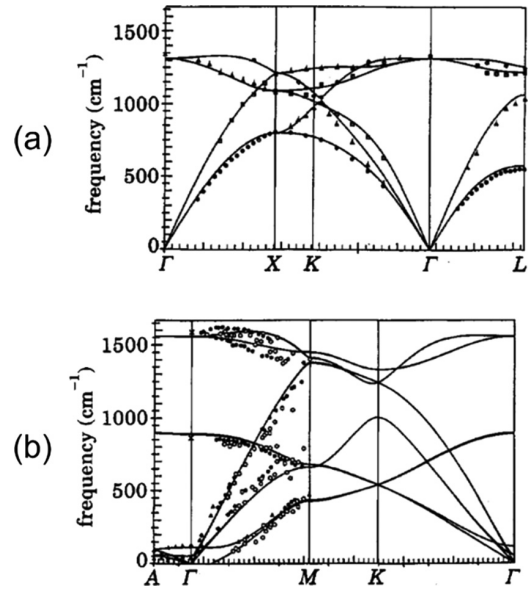

Figure 6.19. Observed and calculated phonon dispersion curves for (a) diamond and (b) graphite [12], copyright IOP Publishing. Reproduced with permission. All rights reserved.

and calculated curves is excellent in these cases, but with crystal structures of lower symmetry, it may be more challenging to obtain such good agreement.

6.3 Heat conduction

Another thermal process in which reciprocal space plays a significant role is thermal conduction. Obviously, phonons carry thermal energy across the solid, but what is it that results in some materials conducting heat less efficiently than others? Why are some materials, like diamond, good thermal conductors, while others are good thermal insulators? To explain this, we need to understand that thermal energy is conducted through the material by two types of quantum quasiparticle, phonons and electrons. If we restrict ourselves to electrically insulating materials, then it is principally phonons that are responsible for the heat conduction. To limit phonon heat conduction, in other words, create thermal resistivity, we need a mechanism whereby the flow of phonons is in some way impeded. One possibility is that impurities and imperfections within the crystal structure will tend to impede phonon propagation. But the other important mechanism, which occurs even in the purest of crystalline materials, is through phonon–phonon collisions. Phonon collisions are examples of anharmonic interactions that we have so far ignored. There are two collision-dominated regimes that need to be considered.

6.3.1 Normal processes

Consider two phonons with wave-vectors $\mathbf{k}_1$ and $\mathbf{k}_2$ travelling with components from left to right with respect to our choice of axes.

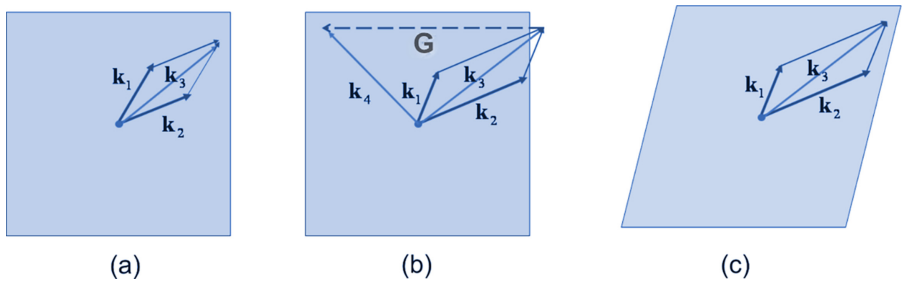

Figure 6.20. (a) Normal process, (b) Umklapp, (c) Umklapp or not? A different choice of Brillouin zone.

Figure 6.20(a) shows what happens when the two phonons interact to create a third phonon:

$$\mathbf{k}_1 + \mathbf{k}_2 = \mathbf{k}_3 \tag{6.52}$$

or in terms of crystal momentum conservation

$$\hbar\mathbf{k}_1 + \hbar\mathbf{k}_2 = \hbar\mathbf{k}_3 \tag{6.53}$$

such that wave-vector $\mathbf{k}_3$ still lies within the first Brillouin zone. In other words, a collision between two waves with horizontal components travelling from left to right creates another wave, also with a horizontal component travelling from left to right. The effect of the collision is to create some resistance to the flow of thermal energy. This type of collision is called a *normal process*.

6.3.2 Umklapp processes

There is a more important, although less well understood, type of phonon collision that needs to be considered as a mechanism limiting heat propagation. Once again (figure 6.20(b)), consider two phonons with wave-vectors $\mathbf{k}_1$ and $\mathbf{k}_2$ having horizontal components travelling from left to right. As before, they interact to produce a third phonon with wave-vector given by

$$\mathbf{k}_3 = \mathbf{k}_1 + \mathbf{k}_2 \tag{6.54}$$

However, this time the initial wave-vectors are sufficiently large that the new phonon wave-vector lies outside the first Brillouin zone. We can now appeal to the reciprocal lattice's translational periodicity, and via the Bloch Theorem subtract a reciprocal-lattice vector $\mathbf{G}$ from $\mathbf{k}_3$. The result is now a wave-vector $\mathbf{k}_4$ that lies within the first Brillouin zone but has its horizontal component now pointing from right to left:

$$\mathbf{k}_4 = \mathbf{k}_1 + \mathbf{k}_2 - \mathbf{G} \tag{6.55}$$

So, two waves travelling from left to right collide and produce a new wave effectively reflected. Such a collision therefore has the effect of reversing the horizontal flow of thermal energy, and so a large thermal resistivity is obtained. This is known as an *Umklapp process*.

We need, however, to inject a word of caution here. Recall that a Brillouin zone is simply a unit cell in reciprocal space [7] and so it can be defined in an infinite number of ways. The first Brillouin zone in figure 6.20 has been drawn using the Wigner–Seitz construction, perfectly acceptable given the high symmetry of the reciprocal lattice in our example. But suppose we choose a different shape for the unit cell (figure 6.20(c)). This time the wave-vector $\mathbf{k}_3$ lies within this definition of the Brillouin zone (see Cracknell [8]). So what has happened to Umklapp? As Cracknell explained, in the past, those writers, who are careful about this matter, have appreciated that a change in the choice of the description of the Brillouin zone will alter the division into normal and Umklapp processes.

Let us look at a particular case. The mineral diamond is unusual in that, unlike a metal, it is an excellent electrical insulator, but it is a superb thermal conductor. It is such a good thermal conductor that it is sometimes used as a heat sink for electronic components. By the way, one way to distinguish between a genuine and a fake diamond is to place it on the tongue. A real diamond should feel cold like a metal. The question we need to address here is: why is diamond such a good thermal conductor but at the same time a good electrical insulator? The following statements answer this:

- Diamond has covalent bonding between carbon atoms.
- This makes diamond very hard, as covalent bonds are very stiff.
- Therefore, diamond has a high Debye temperature of 2250 K.
- At room temperature, diamond is far below the Debye temperature.
- This means that most phonons at room temperature are of low frequency, hence long wavelength.
- So, most of the phonons in diamond at room temperature have short wave-vectors.
- Therefore, there are few opportunities for Umklapp to occur.
- The covalent bonding means that the electrons are tightly bound so that diamond is a good electrical insulator.

Metals are good electrical and good thermal conductors, because then heat is transported by both electrons and phonons (and the Debye temperature is relatively low).

6.4 Measurement of phonon dispersion

We discuss here three principal methods that can provide phonon dispersion information: optical (infra-red) absorption, Raman scattering and inelastic neutron scattering. Typical optical wavelengths are in the region of 3000–8000 μm. The wave-vectors are between about 1.2×10^{-4} and 3×10^{-4} Å^{-1}, to be compared with a typical reciprocal-lattice distance of about 1 Å^{-1}. Therefore, optical wavelengths can be used to probe phonons with $k \approx 0$ (figure 6.21), where the phonon wavelengths are very large. This can be done by optical absorption spectroscopy or by inelastic light scattering. In the latter case, there are two regimes to consider: Raman scattering will enable the optic modes close to $k = 0$ to be studied, while Brillouin scattering

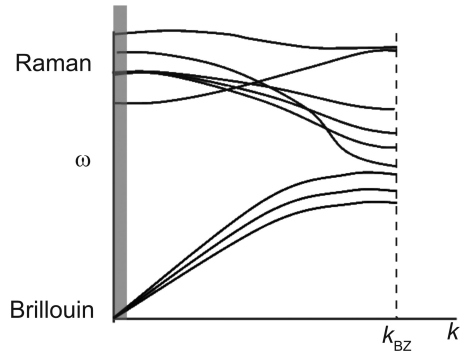

Figure 6.21. Regions of the phonon dispersion curves accessible to different radiations (reduced zone scheme).

will cover the acoustic modes. The primary way of studying phonons at higher wavevectors is by inelastic neutron scattering. This works because thermal neutrons have energies in the meV range, and this is comparable with typical phonon energies. Also, typical thermal neutron wavelengths are in the Ångström range, and so most of the Brillouin zone can be accessed.

6.4.1 Absorption spectroscopy

Typically, infra-red radiation is used, since optic phonon frequencies tend to lie in this region of the electromagnetic spectrum. A transition between an initial state $|\phi_i\rangle$ and a final state $\langle\phi_f|$ is only possible when the matrix element

$$\langle\phi_f|\hat{\mathcal{H}}|\phi_i\rangle \neq 0 \tag{6.56}$$

The resulting function must have even symmetry for this element to be non-zero. In optical absorption spectroscopy, the electric field $\mathbf{E}(t)$ of the light couples with an oscillating dipole $\mathbf{p}(t)$, described by a time-dependent Hamiltonian. Therefore, the transition occurs for

$$\langle\phi_f|\hat{\mathcal{H}}'|\phi_i\rangle \neq 0 \tag{6.57}$$

where $\hat{H}'$ represents the additional energy acquired when the light is absorbed. Therefore,

$$\begin{aligned}\langle\phi_f|\hat{\mathcal{H}}'|\phi_i\rangle &= \langle\phi_f|\mathbf{p}(t)\cdot\mathbf{E}(t)|\phi_i\rangle \\ &= e\langle\phi_f|\mathbf{r}(t)\cdot\mathbf{E}(t)|\phi_i\rangle \\ &\neq 0\end{aligned} \tag{6.58}$$

The vector $\mathbf{r}(t)$ is the time-dependent position vector for an atom. Provided that the atom is charged, i.e., an ion, an oscillating dipole exists, and absorption can occur. From a symmetry point of view, the initial ground state is a symmetric, therefore even, function. Therefore, $\langle\phi_f|\hat{\mathcal{H}}'$ must also be even symmetric for the matrix

element to be non-zero. Since the dipole term has odd symmetry like a coordinate axis, e.g., x, y or z, the symmetry of $\langle \phi_f |$ must also be odd.

Alkali halides are ionic crystals, and in the optic modes, the positive cations move towards and away from the negative anions, thus creating oscillating dipoles. The consequence is that there is a large absorption of light at a frequency matching the relevant optic mode frequency. However, note that diamond is not ionic, yet a certain amount of weak absorption is seen in the infra-red. This has been much discussed in the literature, with the suggestion that it arises either from impurities or defects or from two-photon absorption. The latter manifests itself as a secondary effect caused by the deformation of the charge distribution during vibration leading to a second-order dipole moment.

6.4.2 Inelastic scattering of light

The two optical inelastic scattering techniques to be discussed are Raman and Brillouin scattering [9]. In both cases, a monochromatic optical beam, typically from a laser, is incident on the sample, and the frequency spectrum is analyzed at some angle from the incident-beam direction. To understand the process involved, first, consider a light wave with an oscillating electric field **E** given by

$$\mathbf{E} = \mathbf{E}_0 e^{i(\mathbf{k}_0 \cdot \mathbf{r} - \omega t)} \tag{6.59}$$

On encountering an atom in the crystal, this electric field polarises the electron cloud, thus *inducing* a dipole moment (Figure 6.22), which fluctuates with time with the incident electric field.

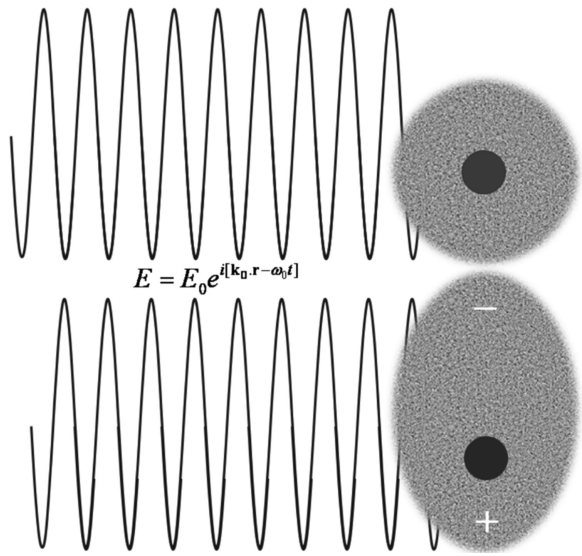

Figure 6.22. The effect of an incident light wave on an atom is to momentarily displace the electron cloud around the nucleus, thus inducing an electric dipole.

The polarisation at any point in time then will be given by

$$\mathbf{P} = \alpha \mathbf{E} \tag{6.60}$$

where α is the electronic polarisability. This is actually given by a 2nd-rank tensor:

$$\mathbf{P}_l = \alpha_{lm} \mathbf{E}_m \tag{6.61}$$

so that α_{lm} creates a polarisation in direction l when the optical field is polarised along direction m. The atom in the crystal is not static but oscillates with a normal coordinate given by

$$U_j(t) = U_j^0 e^{i(k_j \cdot r - \omega_j t)} \tag{6.62}$$

for the jth phonon. This makes the polarisability itself dependent on this normal coordinate:

$$\alpha(t) = \alpha(\mathbf{U}_j, t) \tag{6.63}$$

Expanding in a Taylor series about the static polarisability α(0)

$$\alpha(t) = \alpha(0) + \sum_j \left(\frac{\partial \alpha(t)}{\partial \mathbf{U}_j(t)} \right)_0 \mathbf{U}_j(t) + \frac{1}{2} \sum_j \sum_{j'} \left(\frac{\partial^2 \alpha(t)}{\partial \mathbf{U}_j(t) \partial \mathbf{U}_{j'}(t)} \right)_0 \mathbf{U}_j(t) \mathbf{U}_{j'}(t) + \ldots \tag{6.64}$$

Multiplying by the electric field and substituting by (6.62) we get

$$\begin{aligned} P(t) = {} & \alpha(0) E_0 e^{i(k_0 \cdot r - \omega_0 t)} \\ & + \sum_j \left(\frac{\partial \alpha(t)}{\partial U_j(t)} \right)_0 E_0 U_j^0 e^{i[(k_0 \pm k_j) \cdot r - (\omega_0 \pm \omega_j) t)]} \\ & + \frac{1}{2} \sum_j \sum_{j'} \left(\frac{\partial^2 \alpha(t)}{\partial U_j(t) \partial U_{j'}(t)} \right)_0 E_0 U_j^0 U_{j'}^0 e^{i[(k_0 \pm k_j \pm k_{j'}) \cdot r - (\omega_0 \pm \omega_j \pm \omega_{j'}) t)]} + \ldots \end{aligned} \tag{6.65}$$

The scattered intensity is then given by

$$I(t) \propto \mathbf{P}(t) \mathbf{P}(t)^* \tag{6.66}$$

Let us look at each of the terms in equation (6.65) in turn. The first term represents the light scattered with the same frequency as the incident light frequency and therefore corresponds to straightforward elastic scattering. In the second term, the incident light momentum has been changed according to

$$\hbar \mathbf{k}_s = \hbar \mathbf{k}_0 \pm \hbar \mathbf{k}_j \tag{6.67}$$

and the light energy according to

$$\hbar \omega_s = \hbar \omega_0 \pm \hbar \omega_j \tag{6.68}$$

The incident light frequency has increased by destroying a phonon j or decreased by creating a phonon j (the two regimes are known as the anti-Stokes and Stokes

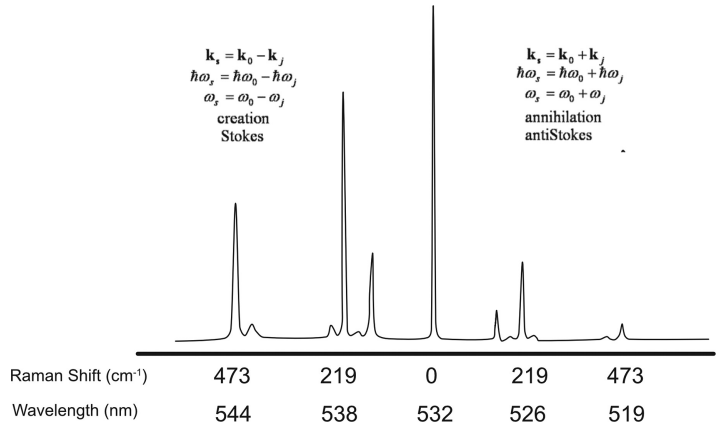

Figure 6.23. Raman spectrum of sulphur.

regimes, respectively). In Raman scattering, the optic modes are found symmetrically on either side of the incident-beam frequency (figure 6.23). Note that the intensity is higher on the Stokes side than on the anti-Stokes side. This is because, according to the Boltzmann distribution, there will be many more vibrating atoms in the ground state than those in the higher-energy state.

Therefore, the Raman spectrum consists of a central, very strong elastic peak (actually, it does have some width in frequency and so is quasi-elastic), and on either side, peaks corresponding to the optic mode frequencies close to $k_j \to 0$. Suppose now the frequency scale is stretched out. In that case, it is seen that the central peak becomes broader and, in practice, shows some extra features. These are due to the low-frequency acoustic modes, and this type of scattering is usually known as Brillouin scattering. This is useful for studying the elastic properties of a crystal, since the acoustic modes are connected with unit-cell distortions, affecting the whole crystal. Note that one can use polarisers placed in the incident and scattered beam paths to cut out or allow through different phonon peaks, thus helping one to identify the types of phonons found in the spectrum.

The third term in (6.65), which is generally weaker than the previous two, involves changes in wave-vector and light frequency of the form

$$\begin{aligned} \mathbf{k}_s &= \mathbf{k}_0 \pm \mathbf{k}_j \pm \mathbf{k}_{j'} \\ \omega_s &= \omega_0 \pm \omega_j \pm \omega_{j'} \end{aligned} \tag{6.69}$$

This is, therefore, a two-phonon interaction with the light. Because terms such as $\mathbf{k}_j \pm \mathbf{k}_{j'}$ can now be comparable with $\mathbf{k}_0$, the wave-vector for the incident light, the response signal covers phonon information from the whole of the Brillouin zone. It is usually seen as a background to the first-order scattering and provides some information on the phonon density of states rather than on individual phonons.

The matrix selection rule for Raman scattering is determined by

$$\left\langle \phi_f | \hat{\mathcal{H}}' | \phi_i \right\rangle = \left\langle \phi_f | \alpha(t) | \phi_i \right\rangle \mathbf{E}_0(t) \mathbf{E}_s(t) \tag{6.70}$$

where $\alpha(t)$ is the time-dependent polarisability due to the atomic vibrations, and whose symmetry is equivalent to the symmetry of quadratic coordinates. $\mathbf{E}_0(t)$ and $\mathbf{E}_s(t)$ are the incident and scattered light fields, respectively. As $\alpha(t)|\phi_i\rangle$ is an even function, so therefore must be $\langle\phi_f|$. Thus, for Raman scattering, the product of the states before and after transition must have the same symmetry as products of axes, e.g., x^2, xy, etc.

6.4.3 Inelastic scattering of neutrons

The most general method for obtaining phonon dispersion diagrams is by using the inelastic scattering of thermal neutrons [10]. As with the optical method, a monochromatic beam is often used, and a measure of the change in energy is obtained. To do this, use is made of a triple-axis diffractometer (figure 6.24). In this system, a beam of thermal neutrons from, say, a nuclear reactor is first monochromatized by a (111) cut crystal of germanium. This beam is incident on the crystal to be studied. The scattered neutrons are then energy-analyzed by a second crystal and a detector. By a combination of rotations of the sample, analyzer crystal and the detector, different regions of the Brillouin zone can be explored. Figure 6.25 shows an example in which an incident beam with wave-vector $\mathbf{k}_i$ is incident at some direction with respect to the reciprocal lattice, and the wave-vector $\mathbf{k}_f$ is of the correct length and orientation to measure data *between* the Γ- and X-points of a cubic Brillouin zone. In this example, note that we do not have to measure the X-point at the closest position to the origin of reciprocal space (e.g., at (0, ½, 0)), but, instead we can choose the X-point in a neighbouring Brillouin zone, in this case at the reciprocal-lattice coordinate (1, ½, 0). Indeed, it may not be possible to

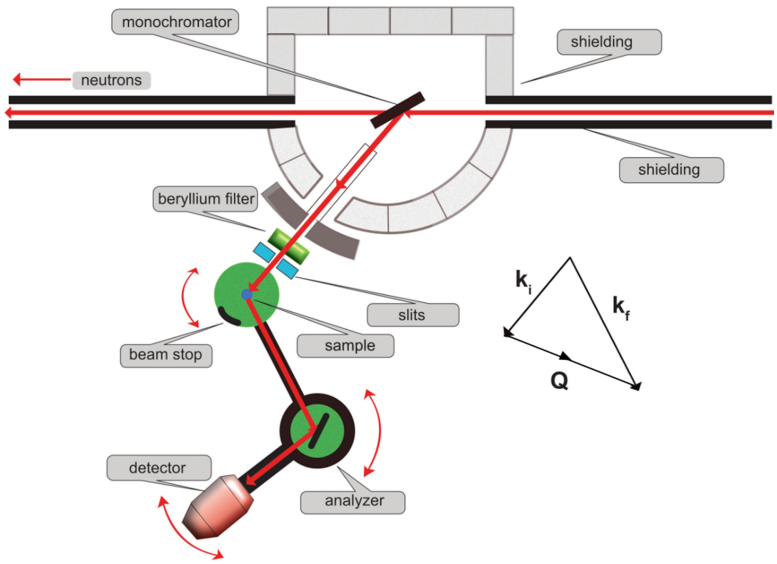

Figure 6.24. The triple-axis spectrometer.

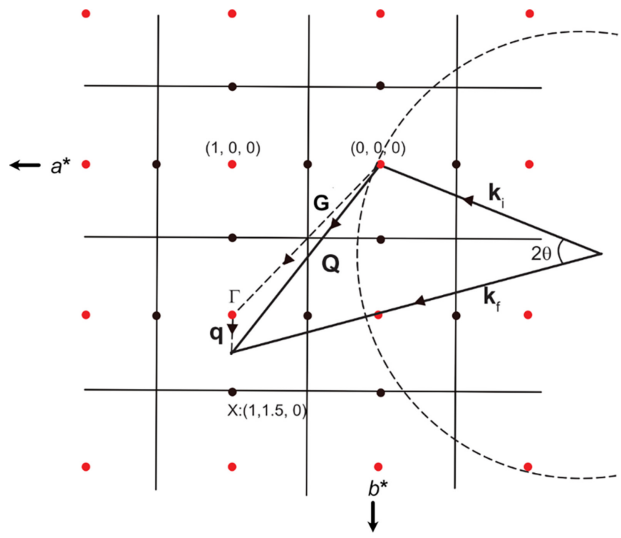

Figure 6.25. Measurement of phonons along Γ–X-direction of the Brillouin zone. Red: reciprocal lattice. Black dot: X-points. The dashed circle is the Ewald sphere for the incident wave-vector.

measure at the nearest X-point, as this depends on the initial neutron energy and the phonon energy.

In this example, the final wave-vector is greater than the initial wave-vector:

$$\mathbf{k}_f - \mathbf{k}_i = \mathbf{Q} = \mathbf{q} + \mathbf{G} \tag{6.71}$$

$$Q^2 = k_i^2 + k_f^2 - 2k_i k_f \cos 2\theta \tag{6.72}$$

The vector **q** is the phonon wave-vector measured from the Γ point at (1, 1, 0) towards the X-point at (1, 1.5, 0). Here, the initial neutron energy has been increased by destroying a phonon. The initial and final wave-vectors are given by

$$\begin{aligned} k_i &= \sqrt{E_i \frac{2m}{\hbar^2}} \\ k_f &= \sqrt{(E_i + E_{\text{phonon}}) \frac{2m}{\hbar^2}} \end{aligned} \tag{6.73}$$

where m is the neutron mass. With a different orientation of the crystal it is possible for the neutron to lose energy, thus creating a phonon. In this way, it is possible to trace out the phonon dispersion along any line in the Brillouin zone (as seen, for example, in figure 6.21)

6.5 Free electrons in a metal

One shouldn't work on semiconductors, that is a filthy mess; who knows whether any semiconductors exist.

(Wolfgang Pauli)

The theories on electrons in crystalline solids can be found in the many standard solid-state physics textbooks. Here, I shall give just a brief introduction to the electronic properties of metals, insulators and semiconductors and how they are related to reciprocal-space concepts.

The flow of electrons governs the conductivity of electricity in metals. To a good approximation, the important electrons are the valence electrons supplied by the metal atoms which are free to move without interactions with the inner electrons around the nuclei. The energy of these free electrons is given by

$$E = \frac{\hbar^2 k^2}{2m} \tag{6.74}$$

So, the energy curve follows a parabola (figure 6.26). Since electrons are fermions, they do not occupy the same energy states at the same time. This means that the conducting electrons occupy levels from a baseline (set at 0 here) up to a maximum value of energy E_F, the *Fermi energy*.

Note. *The Fermi energy is the energy of the maximum occupied state at* ***absolute zero of temperature***.

The Fermi wave-vector is given by (see equation (5.16))

$$k_F = \left(\frac{3\pi^2 N_{\text{states}}}{V_{\text{crystal}}}\right)^{1/3} \tag{6.75}$$

A factor of 2 has been included to deal with the fact that electrons occur in two spin states.

In many books, N_{states}, the number of occupied states, is often replaced by N_e, the total number of electrons in the metal. However, as we shall see later, this can result in a misunderstanding of the Brillouin zone. The Fermi energy is

$$E_F = \frac{\hbar^2}{2m}\left(\frac{3\pi^2 N_{\text{states}}}{V_{\text{crystal}}}\right)^{2/3} \tag{6.76}$$

The Fermi energy describes a shape in **k**-space, which is known as the *Fermi surface*. For a monovalent metal, where there is one valence electron per primitive unit cell,

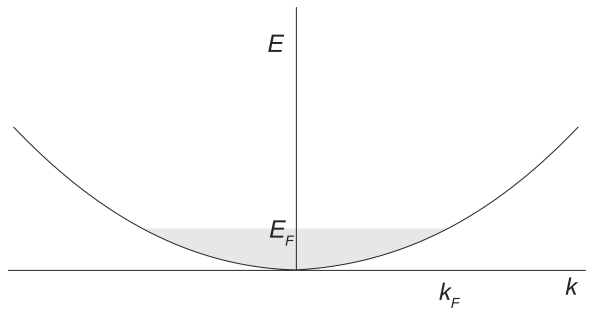

Figure 6.26. Energy versus wave-vector for free electrons.

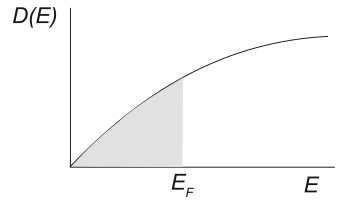

Figure 6.27. Density of states versus energy for free electrons.

this is a sphere, while more complex shapes can be found in other metals. Now, the Fermi–Dirac function is given by

$$f = \frac{1}{e^{(E-\mu)/k_BT} + 1} \tag{6.77}$$

where μ is the chemical potential. At a temperature of 0 K, this is equal to the Fermi energy. Now, it turns out that the Fermi energy for a typical metal is in the few eV range (e.g., 7 eV for metallic copper), amounting to Fermi temperatures of tens of thousands of degrees Kelvin. At room temperature, therefore, we are well below the Fermi temperature, and so the chemical potential can effectively be replaced by the Fermi energy:

$$f \simeq \frac{1}{e^{(E-E_F)/k_BT} + 1} \tag{6.78}$$

The density of states for a three-dimensional metal is given by

$$D(E) = \frac{V_{\text{crystal}}}{2\pi^2}\left(\frac{2m}{\hbar}\right)^{3/2} E^{\frac{1}{2}} \tag{6.79}$$

We see that $D(E)$ is parabolic in E (figure 6.27).

We now introduce translational symmetry into the discussion. Figure 6.28 (top) introduces Wigner–Seitz unit cells to form conventional extended Brillouin zones. In the bottom diagram, the vertical dashed lines mark the repeating unit cells, and within each unit cell, the E–k curves are folded in to create a repeating pattern.

From this, it can be seen that the reduced zone $0 \leqslant k \leqslant \pi/a$ can be used instead, showing an energy-level diagram at any value of k.

6.6 Tight-binding and nearly-free electrons

The free electron theory is only capable of explaining the existence of metals, and, on its own, cannot explain insulators and semiconductors. Instead, one has to include interactions, such as electron–electron and electron–nuclear couplings. There are many different theories that do this, the two most common approaches in solid-state texts are the tight-binding and nearly-free electron theories. The *tight-binding* model starts from atomic states that include the nuclear potential and then adds the kinetic energy due to the delocalization of the electrons when the solid is formed. The *nearly-free electron* model starts from the other end with completely free electrons

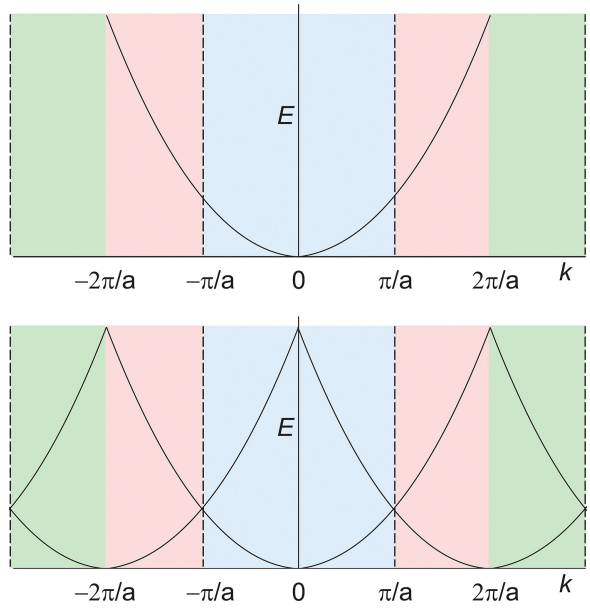

Figure 6.28. Effect of translational periodicity on free electron energy plots.

and then adds the effect of the nuclear potential. These theories naturally lead to electron energy bands and energy gaps.

6.6.1 Tight-binding

To illustrate the principle of the tight-binding approach, consider a simple arrangement of N single atoms forming a linear chain with unit-cell repeat a. Consider a linear combination of atomic orbitals (LCAO):

$$\psi = c_1\phi_1 + c_2\phi_2 + c_3\phi_3 \ldots = \sum_n c_n\phi_n \tag{6.80}$$

with the coefficients c_n normalized

$$\sum_n |c_n|^2 = 1 \tag{6.81}$$

As we are dealing with atoms in a crystal, periodic boundary conditions and the Bloch Theorem apply, and so

$$c_n = \frac{1}{\sqrt{N}} e^{ikna} \tag{6.82}$$

The energy eigenvalue is given by the usual formula $\mathcal{H}$

$$E = \frac{\langle\psi|\hat{\mathcal{H}}|\psi\rangle}{\langle\psi|\psi\rangle} = \langle\psi|\hat{\mathcal{H}}|\psi\rangle \tag{6.83}$$

Therefore, we can write

$$E = \frac{1}{N}\int\left(\sum_n e^{-ikna}\phi_n^*\hat{\mathcal{H}}\sum_m e^{ikma}\phi_m\right)dx \tag{6.84}$$

Separating terms, we write

$$\begin{aligned}
&\langle\phi_n|\hat{\mathcal{H}}|\phi_n\rangle = \alpha \\
&\langle\phi_m|\hat{\mathcal{H}}|\phi_n\rangle = -t \quad m, n \text{ near neighbours} \\
&\langle\phi_m|\hat{\mathcal{H}}|\phi_n\rangle = 0 \quad \text{otherwise}
\end{aligned} \tag{6.85}$$

t is known as a hopping, transfer or overlap integral. Therefore, for nearest-neighbour interactions, the total energy is given by

$$\begin{aligned}
E &= \alpha - t(e^{ika} + e^{-ika}) \\
&= \alpha - 2t\cos ka
\end{aligned} \tag{6.86}$$

creating bands of width $4t$ (figure 6.29). In the figure, the energy of the lower band derived from s orbitals is given by $t = t_1$ positive, and the upper band is with $t = t_2$ negative (corresponding, for example, to changing from symmetric s orbitals to antisymmetric p orbitals). If we pull the atoms apart to larger distances, the values of t decrease, since the inter-orbital potential interaction becomes smaller, and so the widths of the bands decrease too.

6.6.2 Nearly-free electron

In the *nearly-free electron theory*, the conduction electrons, responsible for current flow, experience forces exerted on them by their surroundings, mainly the atomic

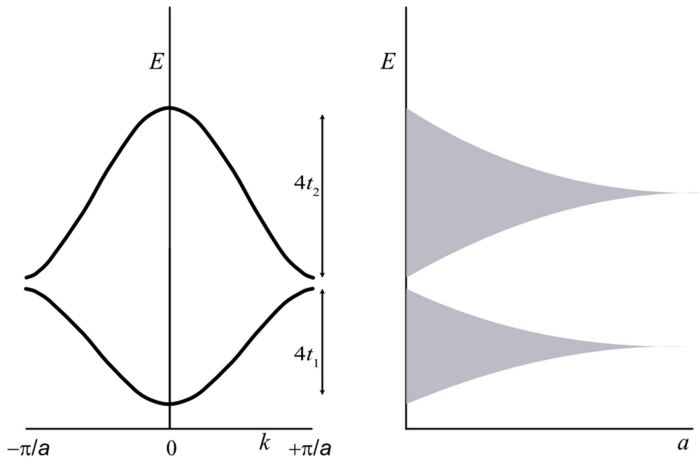

Figure 6.29. (a) Band structure for a one-dimensional array of atoms spacing a in the tight-binding approximation. (b) Effect on the width of the bands with increasing distance a between the atoms.

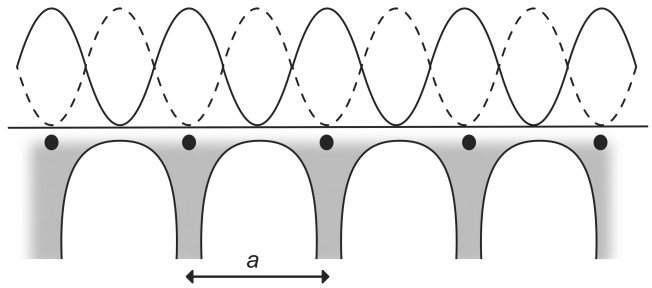

Figure 6.30. Periodic potential (bottom) and probability density waves (top). Full line $\Psi(+)^2$, dashed line $\Psi(-)^2$.

nuclei and inner electrons. Therefore, they are subject to a periodic potential (figure 6.30) analogous to how thermal waves are influenced by the periodic array of force constants in the crystal. For simplicity, we shall consider this in one dimension.

Consider the wave function at the Brillouin zone boundary. The periodic potential can be expressed in one dimension via a Fourier series.

$$V(x) = \sum_G V_G e^{iGx} \tag{6.87}$$

We now use the following wave function for any general value of k

$$|\psi\rangle = A|k_0\rangle + B|k_0 + G\rangle \tag{6.88}$$

The plane-wave states are $|k_0\rangle$ and $|k\rangle = |k_0 + G\rangle$ with approximately the same energy, i.e., k_0 and k on, or close to, the zone boundary. Using degenerate perturbation theory at the zone boundary,

$$\begin{aligned} \langle k_0|\hat{\mathcal{H}}|k_0\rangle &= \hbar^2(\pi/a)^2/2m + V_0 \\ \langle k|\hat{\mathcal{H}}|k\rangle &= \hbar^2(\pi/a)^2/2m + V_0 \\ \langle k_0|\hat{\mathcal{H}}|k\rangle &= V_G \\ \langle k|\hat{\mathcal{H}}|k_0\rangle &= V_{-G} \end{aligned} \tag{6.89}$$

Therefore,

$$\begin{vmatrix} \hbar^2(\pi/a)^2/2m + V_0 & V_G \\ V_{-G} & \hbar^2(\pi/a)^2/2m + V_0 \end{vmatrix} = 0 \tag{6.90}$$

and so the eigenvalues are

$$E = \hbar^2(\pi/a)^2/2m + V_0 \pm |V_G| \tag{6.91}$$

V_0 can be ignored for our purposes, as it merely acts as a base value for the energy. The first term is just the solution for the free electron case at the zone boundary. However, the third term represents a perturbation to the free electron solution by

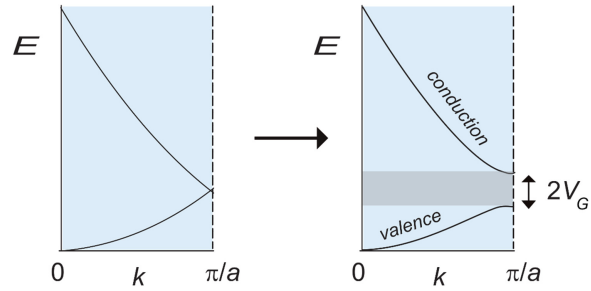

Figure 6.31. Reduced zone. Creation of an energy band gap (grey) by a first-order perturbation due to the periodic potential.

causing the 2-fold degeneracy to split into two separate energies separated by $2|V_G|$ (figure 6.31). The eigenstates are then correspondingly

$$|\psi_{\pm}\rangle = \frac{1}{\sqrt{2}}(|k_0\rangle \pm |k_0 + G\rangle) \tag{6.92}$$

The direct-space versions of the $|k\rangle$ wave functions are given by

$$\begin{aligned} |k\rangle &\propto \quad e^{ik_0x} = e^{i\pi x/a} \\ |k+G\rangle &\propto \quad e^{i(k_0+G)x} = e^{-i\pi x/a} \end{aligned} \tag{6.93}$$

We can, therefore, write for the two solutions in one dimension

$$\begin{aligned} \psi_+ &\propto (e^{i\pi x/a} + e^{-i\pi x/a}) = \cos \pi x/a \\ \psi_- &\propto (e^{i\pi x/a} - e^{-i\pi x/a}) = \sin \pi x/a \end{aligned} \tag{6.94}$$

The probability densities are then given by

$$\begin{aligned} \psi_+\psi_+^* &\propto \cos^2 \pi x/a \\ \psi_-\psi_-^* &\propto \sin^2 \pi x/a \end{aligned} \tag{6.95}$$

The + probability wave peaks on the nuclei, while the – probability wave peaks halfway between (figure 6.30). This means that an electron occupying one solution is subject to a different part of the periodic potential than the other, thus lifting the 2-fold degeneracy, and hence creating an energy gap.

We see that the *E–k* plot is split into two bands: the upper one is called the *conduction band*, the lower is called the *valence band*. Between the two, there is a forbidden region for the electrons known as the *band gap*. It is the presence of this band gap that determines the electrical conduction properties of the solid. Figure 6.32 shows how the extended zone scheme translates into the reduced zone scheme, where the different bands are more obvious as a series of energy levels for different wave-vector values.

So, if the band gap is large, electrons are not easily promoted from the valence to the conduction band, in which case the solid acts as an electrical insulator. If the

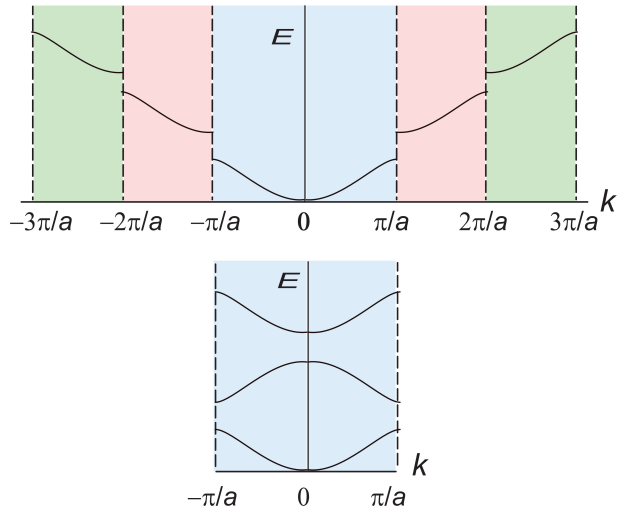

Figure 6.32. The extended zone scheme (top) and its associated reduced zone scheme.

band gap is smaller, then this becomes an intrinsic semiconductor, as then by Boltzmann statistics, thermal energy helps to promote the electrons across the gap. An intrinsic semiconductor, therefore, tends to increase its electrical conductivity as a function of temperature. If the band gap is negligible or even negative (band overlap), then metallic behaviour is expected.

Band-structure diagrams for real solids are more complicated than the simple picture given so far. The details of the bands and how the energy depends on wave-vector depend on the complexity of the actual periodic potential terms present in any particular case. These days, realistic model potential functions can now be computed, and the fit between experimental and theoretical band structures can be excellent. The complexity in real band structures also arises from the overlap between the various types of atomic orbitals of the atoms. The band structure for copper metal (figure 6.33) illustrates this, where we see various bands formed by the overlap of 3s, 3p and 3d orbitals. The Fermi surface for copper is found to be spherical but with extra projections pointing towards the L-points of the Brillouin zone boundary.

Definition. *The Fermi surface is the surface in reciprocal space which separates occupied from unoccupied electron states at zero temperature.*

6.7 Metal or insulator?

Relatively simple concepts can be used to determine if a particular solid should show metallic or insulator behaviour, by counting the number of electrons available within the different electronic bands. You may read that metallic behaviour occurs when an atom in an elemental solid has an odd number of electrons per atom. However, this statement needs a proper examination, as we need to be careful to

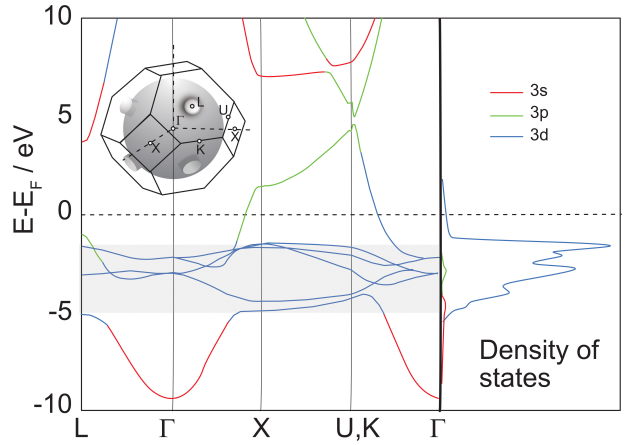

Figure 6.33. Band structure, density of states and Fermi surface for metallic copper. The grey band indicates s–d orbital hybridization.

compare unit cells in direct space with unit cells in reciprocal space in order to be able to count correctly the number of occupied states in an energy band.

Note that using the Wigner–Seitz construction to define the Brillouin zone as a primitive reciprocal-space unit cell means that for counting purposes we need to consider primitive unit cells in direct space. The number of independent states in the Brillouin zone is given by

$$N_{\text{states}} = \frac{V_{BZ}}{V_{\text{state}}} \tag{6.96}$$

where V_{BZ} is the volume of the Brillouin zone. For a cubic crystal with lattice spacing a

$$V_{BZ} = \left(\frac{2\pi}{a}\right)^3 = \frac{8\pi^3}{V_{\text{cell}}} \tag{6.97}$$

Here, V_{cell} is the volume of a primitive unit cell in direct space. V_{state} is the volume around any **k**-state.

$$\begin{aligned} \therefore V_{\text{state}} &= \left(\frac{2\pi}{L}\right)^3 = \frac{8\pi^3}{V_{\text{crystal}}} \\ \therefore N_{\text{states}} &= \frac{8\pi^3}{V_{\text{cell}}} \Big/ \frac{8\pi^3}{V_{\text{crystal}}} = \frac{V_{\text{crystal}}}{V_{\text{cell}}} \end{aligned} \tag{6.98}$$

Actually, this is true even for non-cubic lattices and so the number of states equals the number of primitive unit cells in the crystal. Since we are dealing with electrons the number of available states per band is equal to $2N_{\text{states}}$, taking account of the spin degeneracy of an electron. To illustrate this, consider some simple cases.

6.7.1 Sodium

Sodium is a metal that crystallizes in a body-centred cubic structure with two Na atoms per bcc unit cell. As the conventional choice of a Wigner–Seitz construction for the Brillouin zone gives us a primitive unit cell in reciprocal space, we need to consider the number of Na atoms in the direct space *primitive* unit cell too.

We know that in the Brillouin zone, there are $2N_{\text{states}}$ available states per band. In the primitive direct-space unit cell, there is one Na atom (the bcc cell volume is twice that of the primitive cell). Now each Na atom has electronic configuration $1s^2 2s^2 2p^6 3s^1$, and so for conductivity, we consider the outer $3s^1$ electrons. If there are $2N_{\text{states}}$ available, then only N_{states} are occupied at a temperature of absolute zero. This means that the $3s$ band is half-occupied, and so the Fermi energy lies well below the top of the band where a band gap can occur (see figure 6.34), where the Fermi surface is close to spherical and lies well inside the Brillouin zone). Note that, by the Pauli exclusion principle, only those electrons with energies close to the Fermi energy will be available to conduct electricity, thus making sodium a metal.

But suppose we invented a hypothetical sodium crystal structure with four Na atoms per bcc unit cell. We would then have two Na atoms per primitive cell, contributing two electrons per unit cell. We would then occupy all $2N_{\text{states}}$, and therefore have a Fermi energy just below the band gap. If this gap were large, then we would conclude that sodium is an insulator! Just because the atoms have an odd number of electrons, it does not follow that it must be a metal. What matters is whether there is an odd number of electrons per primitive unit cell rather than per atom!

6.7.2 Calcium

Calcium is also a metal, even though it has an even number of electrons. It crystallizes with four Ca atoms in a fcc unit cell. Therefore, there is one Ca atom per primitive unit cell. Calcium is divalent, and so each primitive unit cell contributes two electrons, thus filling $2N_{\text{states}}$ available states. This would be expected, therefore, to fill the energy band right up to the band gap. Yet calcium is a metal! The answer comes from the fact that the Fermi surface is three-dimensional (figure 6.34). Suppose we try to inscribe a sphere of the right size into the Brillouin zone shape. In that case, we discover that in certain directions (X and L) of the Brillouin zone, the radius of the sphere is larger than the maximum values of **k**, and this allows electrons

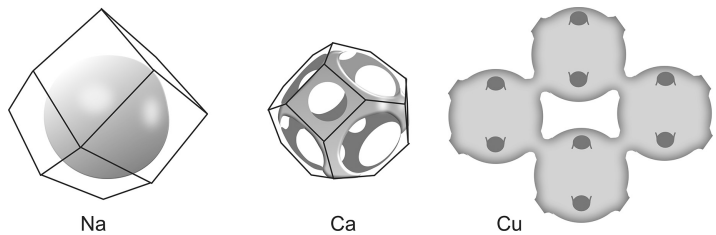

Figure 6.34. Fermi surfaces for sodium, calcium and copper.

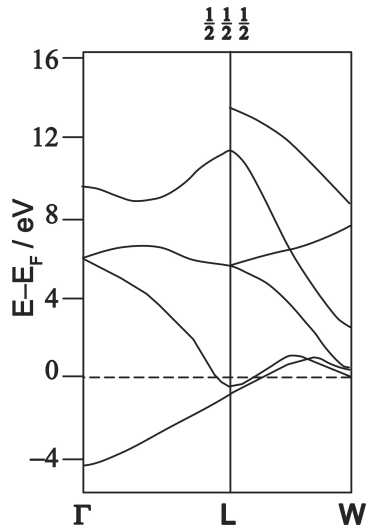

Figure 6.35. Computed band structure for calcium metal (adapted from [13]).

to occupy states in the conduction band. This can be seen in the computed band structure (figure 6.35), which shows that the Fermi energy lies just above the band gap at the L point, with a very small band gap at W.

6.7.3 Diamond, silicon, germanium

These crystals all have the same basic crystal-structural arrangement, yet diamond is an insulator, while silicon and germanium are semiconductors. So, let's do the counting. The crystal structure is fcc with eight atoms in the unit cell. Therefore, in a primitive cell, there must be only two atoms. Now, each atom contributes four valence electrons and so there are eight electrons per primitive cell. If we have N primitive unit cells in the crystal, then there are $2N_{\text{states}}$ in each band. Therefore, four bands are filled at 0 K. Now in diamond there are extremely strong covalent bonds between the carbon atoms. So the periodic potential is very deep at the atomic positions, thus making a very large band gap (approximately 5.5 eV). Diamond is, therefore, a good electrical insulator, even at room temperature, despite being an excellent thermal conductor. In silicon and germanium, the bonding is less strong with smaller band gaps (1.11 and 0.67 eV, respectively), as the periodic potential is flatter. In these cases, input of thermal energy is sufficient to drive some of the electrons near the Fermi surface across the band gap to allow electrical conduction. It is therefore obvious that the conductivity will increase with temperature, and, despite Pauli's view, these materials are *intrinsic semiconductors*.

References

[1] Ziman J M 1972 *Principles of the Theory of Solids* 2nd edn (Cambridge: Cambridge University Press)

[2] Glazer A M Monatomic and diatomic chains (https://www.amg122.com/programs/chains.html)

[3] Brillouin L 1946 *Wave Propagation in Periodic Structures* (New York: McGraw-Hill)
[4] Wannier G H 1959 *Elements of Solid State Theory* (Cambridge: Cambridge University Press)
[5] Dove M T 2003 *Structure and Dynamics. An Atomic View of Materials* (Oxford: Oxford Master Series in Condensed Matter Physics)
[6] Dove M T 1993 *Introduction to Lattice Dynamics* (Cambridge: Cambridge University Press)
[7] Bradley C J and Cracknell A P 1972 *The Mathematical Theory of Symmetry in Solids: Representation Theory for Point Groups and Space Groups* (Oxford: Oxford University Press)
[8] Cracknell A P 1975 *Group Theory in Solid-State Physics* (London: Taylor and Francis)
[9] Colthup N B, Daly L H and Wiberley S E 1990 *Introduction to infrared and Raman Spectroscopy* (New York: Academic)
[10] Furrer A, Strässle T and Mesot J 2009 *Neutron Scattering in Condensed Matter Physics* (Singapore: World Scientific)
[11] http://en.wikipedia.org/wiki/Debye_model
[12] Kresse G, Furthmüller J and Hafner J 1995 *Ab initio* force constant approach to phonon dispersion relations of diamond and graphite, *Eur. Lett.* **32** 729
[13] Chatterjee S and Chakraborti D K 1970 Energy-band structure and Fermi surface of calcium by the orthogonalized plane wave method, *J. Phys. C Met. Phys. Suppl.* **3** S120–6
[14] Tabor D 1991 *Gases, Liquids and Solids* (Cambridge: Cambridge University Press)

IOP Publishing

A Journey into Reciprocal Space (Second Edition)
A crystallographer's perspective
Anthony Michael Glazer

Chapter 7

Distortion modes

Distortion upon distortion: … the more one uses the mind, the more confused one becomes.

(Laozi 老子)

7.1 Introduction

In this final chapter, I shall give an introductory account of the topic of *distortion-mode analysis.* In recent years, there has been a lot of interest in phase transitions in materials, where the symmetries of the phases are group-subgroup related. To deal with this, the concept of *distortion modes* has been developed. This is based upon the idea of soft-mode phase transitions, in which, as temperature changes, the frequency of a normal mode of oscillation tends towards zero. At this point, the mode becomes unstable and condenses to become a static distortion of the crystal structure. The application of distortion-mode analysis to structural phase transitions nicely demonstrates the partnership between direct and reciprocal space. By condensation of modes at certain wave-vector positions (reciprocal space), one learns about changes in the crystal structure (direct space).

To illustrate how distortion modes can be determined, the perovskite structure acts as a useful example. First of all, we need to understand how this crystal structure can be distorted to form different structures. You will recall from figure 1.29 that the basic cubic structure (often called the *aristotype*) has the chemical formula ABX_3, where A and B are cations and X, is an anion, and the space group is $Pm\bar{3}m$. Such a structure is non-polar and is potentially the high-temperature phase of most perovskite materials. On cooling below a phase transition temperature, the structure undergoes small distortions, sometimes creating polar and antipolar structures. These can then exhibit diverse phenomena such as ferroelectricity, antiferroelectricity, pyroelectricity and piezoelectricity. In addition, distortions can occur in the arrangements of anion octahedra. These lower-temperature phases were called 'hettotypes' by Helen D Megaw

doi:10.1088/978-0-7503-3875-2ch7

(1907–2002). We now have to consider the types of distortions that are commonly found in perovskites.

7.2 Atomic displacements

Suppose the A and B cations are slightly displaced in a specific direction within the unit cell. If they all move in the same general direction, then the structure becomes polar, allowing for polar properties to be generated. The space groups must therefore be polar groups. In group-theoretical terms, these displacements can be treated as distortion modes condensing at the Brillouin zone centre, as they do not form superstructures. In general, the displacements are tiny, but at the same time, cause substantial changes in the polar properties. These properties are often temperature or pressure-dependent, as the atomic positions respond to the external environment. In some perovskites, such as in $CaTiO_3$, the displacements are antiparallel, making the crystal centrosymmetric, so that no net polarisation is obtained. Such compounds are termed antiferroelectrics. The antiparallel displacements result in a doubling or more of the basic aristotype unit cell, which can be seen in the appearance of superstructure peaks in diffraction patterns, due to condensation at the zone boundary.

The most well-known perovskite structure in which cation displacements have been studied is that of barium titanate, $BaTiO_3$. Barium titanate was the first of the ferroelectric perovskites to be explored. It was initially used as a piezoelectric transducer material during the Second World War as part of the British effort in submarine detection but was later superseded by another important perovskite, PZT (lead zirconate–titanate solid solutions). The crystal structure was first determined by Megaw in 1945 [1], who showed that it had tetragonal symmetry. Since then, there have been numerous other studies of the crystal structure [2], but almost all agree with her assignment of the crystal structure. To understand this structure, consider figure 7.1, adapted from information given by Megaw in 1973 [3].

Figure 7.1(a) shows the cubic aristotype structure, which is found above 135 °C in pure top-seeded crystals, or above 120 °C in flux-grown crystals. It is worth stating that almost all the research published on this material before around 1970 was conducted on flux-grown crystals, which contained Cl or F ions, and so were impure. These crystals were grown by the Remeika method [4], and had a slightly yellow appearance and formed plates. Later it became possible to grow top-seeded crystals, which formed blocks and were colourless. A comparison between the two types of crystal, pure and impure, was published using lattice-parameter measurements by Clarke [5]. This is shown in figure 7.2, where it can be seen that four different phases are found in both crystals. Phase I is the cubic aristotype; phase II is tetragonal, phase III orthorhombic and phase IV rhombohedral. Note how the phase transition temperatures are considerably higher in the pure material. The space group changes are

$$(I)Pm\bar{3}m \rightleftarrows (II)P4mm \rightleftarrows (III)Bmm2 \rightleftarrows (IV)R3m \tag{7.1}$$

Returning to the structure, figure 7.1(b) shows the essential features of the tetragonal structure schematically. This crystallizes in space group *P*4*mm*, which is a polar space

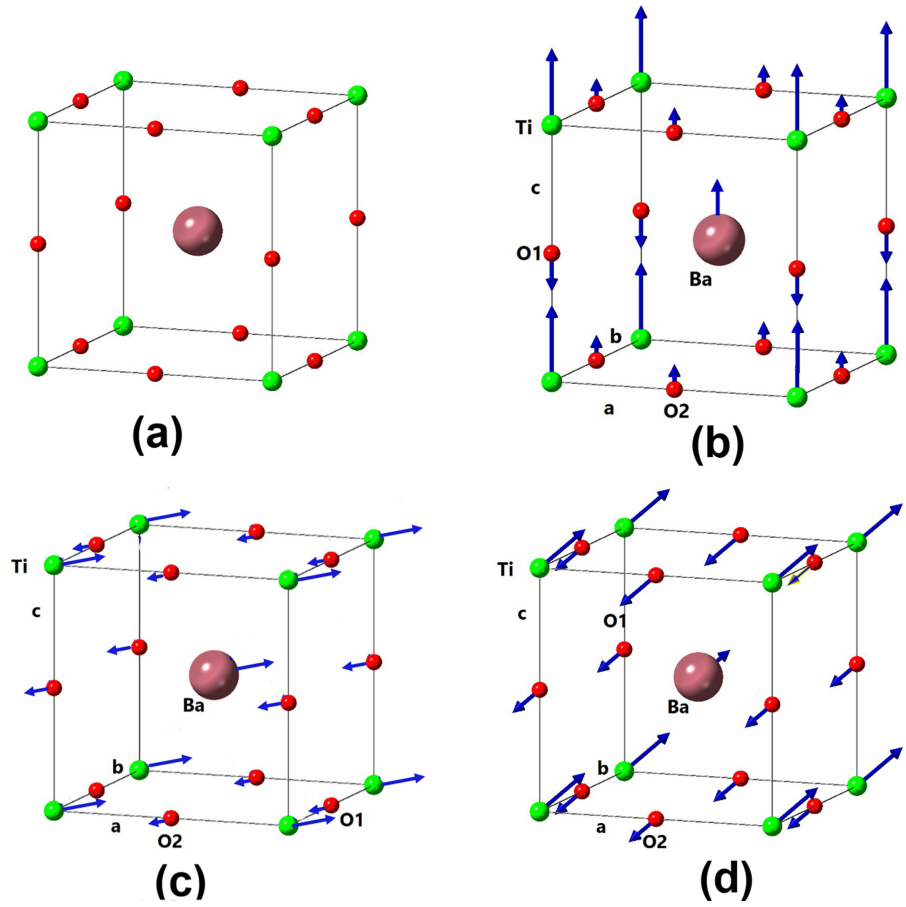

Figure 7.1. Crystal structures of barium titanate: (a) cubic, (b) tetragonal, (c) orthorhombic, (d) rhombohedral.

group, and the crystal is ferroelectric. This is the phase used in industrial applications, these days mainly as a dielectric material in electrical capacitors. The arrows in the figure indicate the displacement directions of the ions, with exaggerated magnitudes. In reality, they are tiny but sufficient to give rise to the polar properties.

It is not commonly appreciated that in polar structures such as this, the choice of origin to describe the structure is entirely arbitrary. We could decide to put the origin on the Ba atom, or on a Ti, or on an oxygen atom (or anywhere else for that matter). With each choice of unit-cell origin, the displacement directions would appear to be different. For example, with the origin chosen on a Ti atom, there would appear to be no Ti displacement! Megaw proposed that the most sensible choice of origin is at the centre of the oxygen octahedron, and this is used in figure 7.1(a). Using this choice, we see that in the tetragonal structure, the Ba, Ti and O2 atoms are displaced upwards along the direction of polarisation, whereas O1 is displaced downwards. The largest displacements are for the Ti ions.

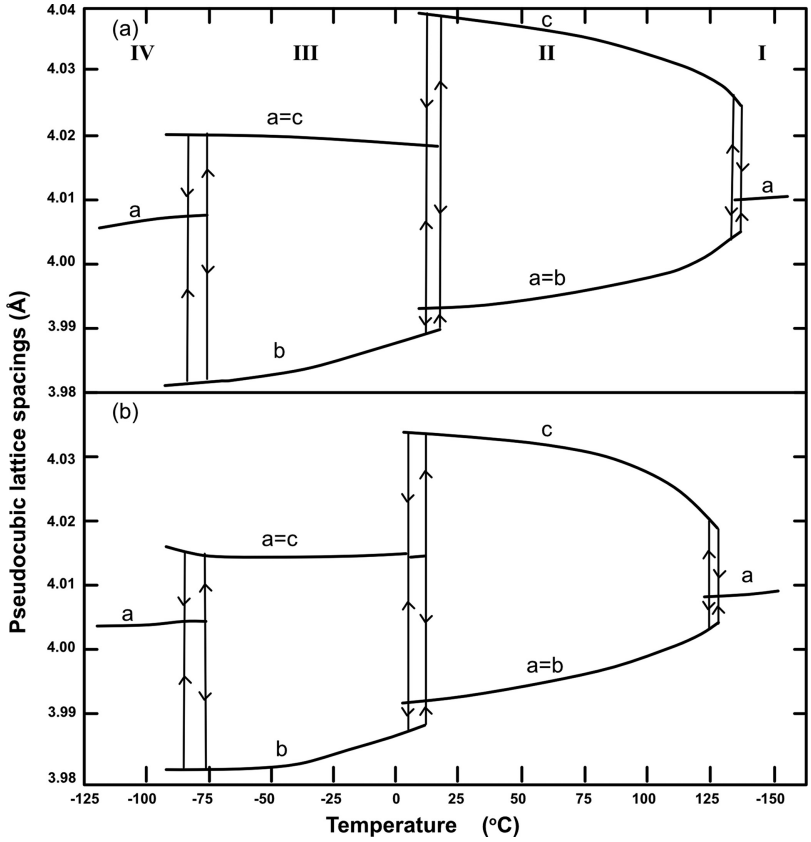

Figure 7.2. Plot of lattice parameters of $BaTiO_3$ as a function of temperature: (a) pure, (b) grown from KF flux. Reproduced from [6] by permission of the International Union of Crystallography.

Figure 7.3 gives schematic diagrams showing how the atomic displacements appear in the tetragonal structure using different origins (Ti and Ba at the unit-cell corners, respectively) and different choices of polar displacements. These are all equivalent descriptions of the structure.

In figure 7.1(c), the displacements in the orthorhombic phase III are shown. In this case, the displacements are directed along [110] directions instead of [001] as in the tetragonal phase II. Therefore, the polarisation vector must change dramatically at the phase transition temperature. The space group *Bmm*2 is not a subgroup of *P*4*mm*, and so the transition has to be of first order, as is observed. Note that *Bmm*2 is, however, a subgroup of $Pm\bar{3}m$. In figure 7.1(d), the displacements along [111] in the rhombohedral phase IV are shown. Here, again, there has to be a discrete change in the polar direction at the transition. The space group *R*3*m* is not a subgroup of *Bmm*2, although it is a subgroup of the aristotype space group $Pm\bar{3}m$. Therefore, again, this must be a first-order transition.

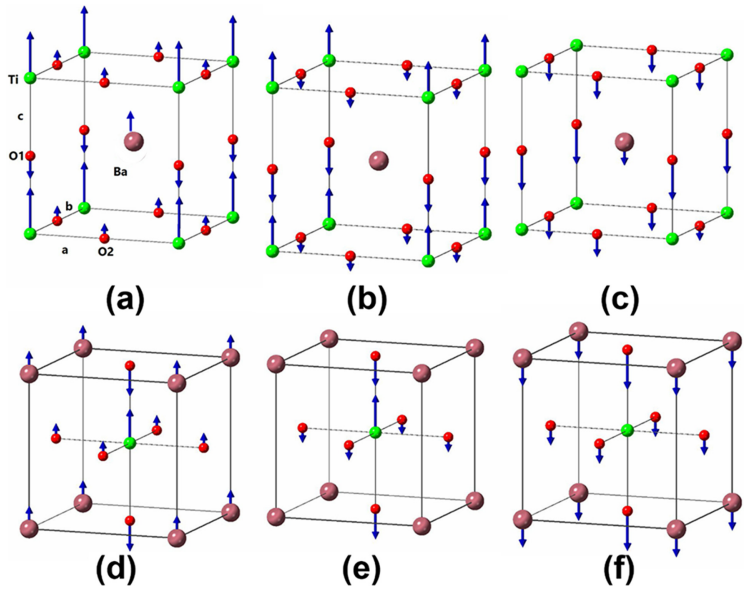

Figure 7.3. Tetragonal structure of $BaTiO_3$ showing the effect of different origin choices: (a) Megaw's choice with Ti at the corners of the unit cell, (b) Ba undisplaced, (c) Ti undisplaced, (d) Megaw's choice with Ba at the corners of the unit cell, (e) Ba undisplaced (f), Ti undisplaced.

While these structure determinations appear at first sight to be straightforward, the observation of x-ray diffuse scattering [8, 9] in both $BaTiO_3$ and in $KNbO_3$, which have a similar set of phase transitions, has suggested partial order in the local structure.

7.3 Octahedral tilting

The oxygen octahedra are all joined at their vertices to form an infinite framework of corner-linked polyhedra. A common feature of perovskites is that one finds many examples where the octahedra are tilted about different axes. Glazer made the first analysis of tilted structures in 1972 [10, 11], further expanded by Woodward [12]. The idea is quite simple. Consider the three pseudocubic axes, a_p, b_p and c_p. By *pseudocubic*, we mean that the unit cell has atomic positions, unit-cell axes and angles close to those in the aristotype phase, despite the crystal-symmetry change.

Suppose we now rotate an octahedron within an a_p–b_p layer through a small angle about the c_p-axis. Because it is connected by corner-linking to neighbouring octahedra within the a_p–b_p plane, the neighbouring octahedra must tilt in the opposite sense. This means that the a_p and b_p axes become doubled since the repeat between the octahedra goes from the first octahedron to another two places away. Now consider what happens to the layers of octahedra lying above and below the first layer. If the octahedra directly above c_p rotate in the same sense, we write this tilt system as $a^0a^0c^+$, the a^0a^0 terms signifying no tilting about the a_p and b_p axes. Alternatively, the octahedra may alternate their sense of rotation about the c_p-axis, and this is written as $a^0a^0c^-$. Both tilt systems create a tetragonal crystal structure,

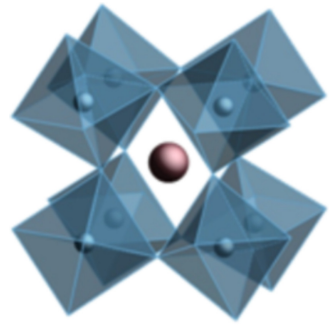

Figure 7.4. An example of a three-tilt system.

but $a^0a^0c^+$ produces a pseudocubic unit cell $a_p \times b_p \times 2c_p$, while $a^0a^0c^-$ creates $2a_p \times 2b_p \times 2c_p$. The tilting of the octahedra leads to superstructure reflections halfway between the main reflections.

It is then a simple matter to apply this idea about the other two axes to build two and three-tilt systems. Figure 7.4 shows an example of a three-tilt system labelled $a^+b^+c^+$, meaning that there are in-phase tilts about each axis with tilt angles of different magnitudes. Interestingly, the tilt system $a^+a^+a^+$, in which the three tilts are of equal magnitude, is another, but rare, cubic perovskite structure.

Initially, there were 23 different tilt systems, but the number was later reduced to 15 by Howard and Stokes based on group-theory arguments [13]. Table 7.1 shows a complete listing.

Howard and Stokes also produced a useful structure tree for possible phase transitions between all the structures with tilted octahedra (figure 7.5) with their tilt systems and space groups. Note that all the space groups are centrosymmetric. To create polar and antipolar structures, one has to add suitable atomic displacements, which will often change the space group assignment.

There are many examples of perovskites with tilted octahedra, sometimes combined with atomic displacements. Thus, $SrTiO_3$ has no tilts at room temperature, but on lowering to around 105 K, tilts appear with the tilt system $a^0a^0c^-$ in space group *I*4/*mcm*, due to condensation at the R-point on the Brillouin zone boundary. In $LaAlO_3$, the space group is $R\bar{3}c$, and the structure adopts the tilt system $a^-a^-a^-$, the three tilts being equal in magnitude. In the antiferroelectric compound, $NaNbO_3$, there are seven phases, with the room-temperature phase consisting of a mixture of different tilt systems plus antiparallel Na displacements. $NaNbO_3$ was the first perovskite in which the $a^0a^0c^+$ tilt system, space group *P*4/*mbm*, was discovered [14].

In addition to tilting of the octahedra, distortions of the octahedra often also occur. For instance, in the tetragonal phase of $BaTiO_3$, the oxygen octahedra become elongated along [001], as seen in figure 7.3, thus making the *c*/*a* ratio of the unit cell greater than 1. Another type of octahedral distortion occurs in Jahn–Teller structures, such as in tetragonal $KCuF_3$, space group *P*4/*mbm* (*C*4/*mmb* on pseudocubic axes), in which alternate octahedra are stretched or compressed. This causes a doubling of

Table 7.1. List of tilt systems and symmetries.

Serial no.	Tilt system	Space group	Sp. Gp. No.	Howard & Stokes
(1)	$a^+b^+c^+$	*Immm*	71	√
(2)	$a^+b^+b^+$	*Immm*	71	
(3)	$a^+a^+a^+$	$Im\bar{3}$	204	√
(4)	$a^+b^+c^-$	*Pmmn*	59	
(5)	$a^+a^+c^-$	$P4_2/nmc$	137	√
(6)	$a^+b^+b^-$	*Pmmn*	59	
(7)	$a^+a^+a^-$	$P4_2/nmc$	137	
(8)	$a^+b^-c^-$	$A2_1/m11$	11	√
(9)	$a^+a^-c^-$	$A2_1/m11$	11	
(10)	$a^+b^-b^-$	*Pnma*	62	√
(11)	$a^+a^-a^-$	*Pnma*	62	
(12)	$a^-b^-c^-$	$F\bar{1}$	2	√
(13)	$a^-b^-b^-$	*I2/a*	15	√
(14)	$a^-a^-a^-$	$R\bar{3}c$	167	√
(15)	$a^0b^+c^+$	*Immm*	71	
(16)	$a^0b^+b^+$	*I4/mmm*	139	√
(17)	$a^0b^+c^-$	*Bmmb*	63	√
(18)	$a^0b^+b^-$	*Bmmb*	63	
(19)	$a^0b^-c^-$	*F2/m11*	12	√
(20)	$a^0b^-b^-$	*Imcm*	74	√
(21)	$a^0a^0c^+$	*C4/mmb*	127	√
(22)	$a^0a^0c^-$	*F4/mmc*	140	√
(23)	$a^0a^0a^0$	$Pm\bar{3}m$	221	√

the pseudocubic unit-cell axes and gives rise to superstructure peaks half-way between the main reflections (figure 7.6).

7.4 Group representations

In group theory, the normal modes are classified by group *representations*. Representations describe abstract groups in terms of linear transformations under the operations of the group. In particular, they represent group elements as invertible matrices so that the group operation can be described by matrix multiplication. We saw earlier in section 1.3 how the symmetry operations could be written in matrix form. A full discussion on group representations can be found in the many group-theory books currently available, for example, [15, 16]. Here, I shall just give a brief résumé of sufficient detail for the discussion that follows in this chapter.

Let's start by considering the point group 2/*m* with the 2-fold axis along **c**. We can write down all the matrices representing the operations in this group (table 7.2):

The set of four matrices is said to form a *reducible* representation Γ_{red}. The traces of the matrices form a list of *characters* $\chi(R)$.

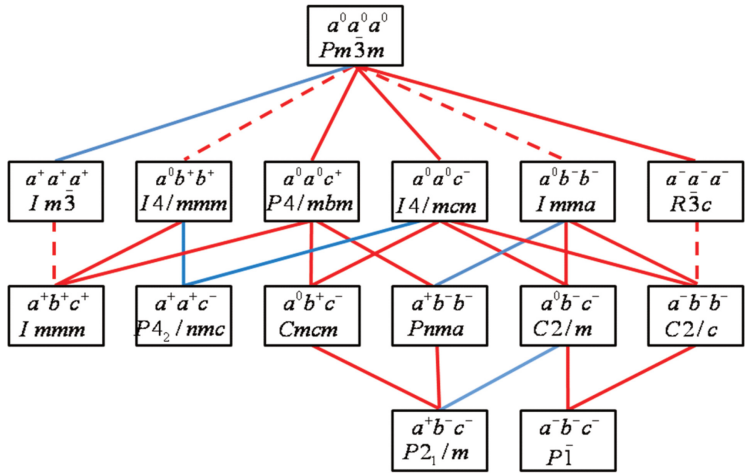

Figure 7.5. Schematic diagram for structures found by Howard and Stokes [13]. The full lines joining tilt systems denote phase transitions that may be continuous, while dashed lines indicate first-order transitions. Red lines are those for which the crystal system changes, while blue lines connect phases in the same crystal system. The space groups are given in the standard ITA form. Reproduced from [13] by permission of the International Union of Crystallography.

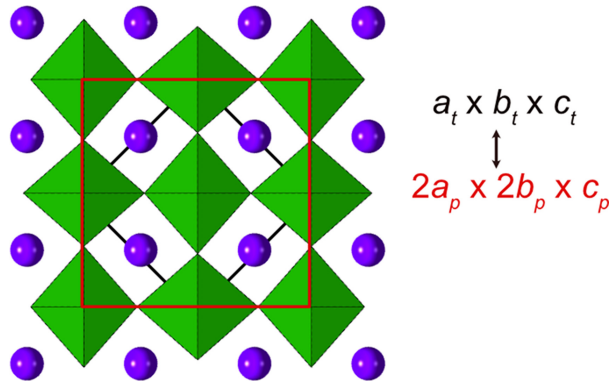

Figure 7.6. The $KCuF_3$ structure type in space group *P*4/*mbm*. The red cell is the doubled pseudocubic perovskite unit cell (space group *C*4/*mmb*), and the black cell is the tetragonal cell corresponding to the space group symbol, *P*4/*mbm*.

Table 7.2. Reducible representation in point group 2/*m*.

	1	2_{001}	$\bar{1}$	m_{001}
Γ_{red}	$\begin{bmatrix}1&0&0\\0&1&0\\0&0&1\end{bmatrix}$	$\begin{bmatrix}\bar{1}&0&0\\0&\bar{1}&0\\0&0&1\end{bmatrix}$	$\begin{bmatrix}\bar{1}&0&0\\0&\bar{1}&0\\0&0&\bar{1}\end{bmatrix}$	$\begin{bmatrix}1&0&0\\0&1&0\\0&0&\bar{1}\end{bmatrix}$
Characters $\chi(R)$	3	−1	−3	1

Consider matrices A, B, C and D, as a representation of a group. Suppose, now, we make a similarity transform with a matrix X

$$A' = X^{-1}AX$$
$$B' = X^{-1}BX$$
$$C' = X^{-1}CX$$
$$D' = X^{-1}DX$$

and then we find

$$A'B' = X^{-1}AXX^{-1}BX = X^{-1}ABX = X^{-1}DX = D' \tag{7.2}$$

Therefore, the set of matrices A', B', C' and D' also form a representation of the same group. Suppose now that we can find the matrix X that transforms A, B, C and D to A', B', C' and D', where the new matrices are block-diagonal in form. This is symbolized in figure 7.7, where a 6 × 6 matrix of a reducible representation is reduced to a set of smaller block-diagonal matrices. These matrix blocks are orthogonal to each other and define *irreducible representations* or *irreps* for short (orthogonality implies that eigenvectors are physically distinct in any single experiment). In this way, the reducible representation can be replaced by a sum over irreps. The irreps, so formed, act independently of each other, and can be used to represent the normal modes of vibration of the atoms.

In this example, the 2 × 2 and 3 × 3 matrices are two and three-dimensional, meaning that the modes that correspond to these irreps are 2 or 3-fold degenerate. This degeneracy applies to any functions described by the particular irreps. For example, if two phonon modes with the same value of k have the symmetry properties of a two-dimensional irrep, they will both have the same frequency. In other words, in an ω-k dispersion plot, the two phonon branches will coalesce at that value of k.

In general, this reduction may be difficult to do with matrices, but fortunately, one can easily reduce Γ_{red} using characters. For point groups, tables of characters are available in most group-theory books. The following is an example of the character table for point group 2/m (table 7.3).

In this case, there are four irreps, each of which carries a label. By convention, these are called A_g, B_g, A_u and B_u (Mulliken notation). These can be used to define

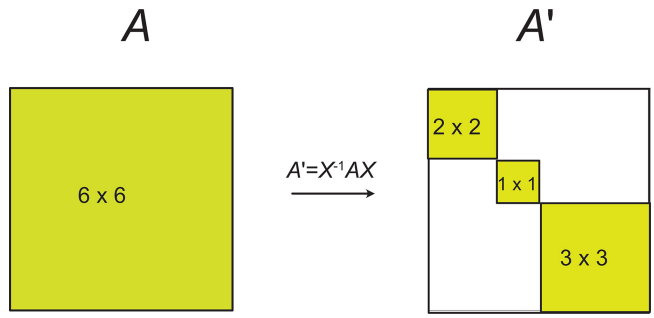

Figure 7.7. Reduction of a reducible representation to a sum of irreducible representations.

Table 7.3. Character table for point group 2/m.

$2/m$	1	2_{001}	$\bar{1}$	m_{001}		
A_g	1	1	1	1	R_z	x^2, y^2, z^2, xy
B_g	1	−1	1	−1	R_x, R_y	xz, yz
A_u	1	1	−1	−1	z	
B_u	1	−1	−1	1	x, y	

the symmetry of any chosen basis function. The last two columns show functions (R is rotation about an axis) and under which irreps they are invariant. For example, suppose we take the basis function xz. Applying each of this group's symmetry operations, we find that this function changes sign only under the operations 2_{001} and m_{001}. We can then say that the function xz has the symmetry property described by a B_g irrep under this group. By the way, the squared terms determine the selection rules for Raman scattering, while the linear terms denote possible IR optical absorptions. Also, the reducible representation in table 7.2 can be shown to be reduced to the sum $\Gamma_{red} = A_u + 2B_u$, which you can check for yourself by adding the relevant characters for each irrep.

Group theory applied to point groups is relatively straightforward. However, when applied to space groups, where one wants to describe the normal modes condensing out at some point in the Brillouin zone, the process becomes more complicated. Additional phase factors have to be applied to the characters. For details, see, for example, Bradley and Cracknell [15] or Dresselhaus, Dresselhaus and Jorio [16]. It turns out that for symmorphic space groups, the characters used are the same as in the point-group tables. However, in the non-symmorphic space groups, at some special points on the surface of the Brillouin zone, the irreps become two or three-dimensional, indicating degeneracy in the particular modes condensing at those points. Fortunately, the irreps for all the critical points in the Brillouin zones have been evaluated for all symmetries, with labels that are currently widely accepted, based on the tables produced by Miller and Love [17].

In short, therefore, the irreps are a way to describe the symmetry properties of basis functions for any abstract group. We are interested here in distortion modes, potentially arising from condensed vibrational normal modes.

7.5 Distortion modes

The various crystal structures adopted by perovskites are *pseudosymmetric*, meaning that they are formed by small distortions of the parent aristotype structure. As we have seen above, these mainly involve atomic displacements, tilted octahedra and distorted octahedra. These distortions can be thought of as arising from phase transitions from the aristotype structure through condensation of low-frequency modes of oscillation (phonons). The distorted structure adopts a space group that is a subgroup of the original space group. This subgroup is known as an *isotropy subgroup*. I shall only give a brief introduction here to the software tools available at [18] and [19]. We shall look at two useful software applications that enable one to

decide through symmetry arguments which modes are responsible for a particular structure, ISODISTORT [20] and the routine AMPLIMODES in the Bilbao Crystallographic Server [21]. In order to learn more in detail about these superb on-line facilities, see the tutorials at [22] and [23].

Generally speaking, ferroelectric structures arise from condensation at the Brillouin zone centre, while tilting and antiferroelectric structures come from condensation at the zone boundaries. Let me illustrate the concept with some examples. I shall start with a particular application using the on-line software ISODISTORT. On opening the initial webpage, you can enter details of the structure to be analyzed. However, we find the message:

Get started quickly with a cubic perovskite parent.

The default is the cubic perovskite structure, and so we can select this. On the next page, it can be seen that the chosen cations are Sr and Ti, and the anion is O, with the Ti atom placed at the unit-cell origin. We can change the Sr to Ba if we wish. Actually, for a symmetry argument, the atom types are irrelevant, and we can equally well call them something else. Five different methods are available for the next stage. Let us try method 2 (figure 7.8) in which we can choose a specific point of the Brillouin zone:

Now select GM, k12,(0,0,0): this refers to modes with wave-vectors at the Brillouin zone centre. The symbol k12 refers to tables of representations produced by Kovalev [7]. On clicking OK, the next page offers the irreducible representations for this point (figure 7.9).

The pull-down menu gives a series of different labels for the different representations. Let's choose the one labelled GM4−, k12t10. On the next page, we find

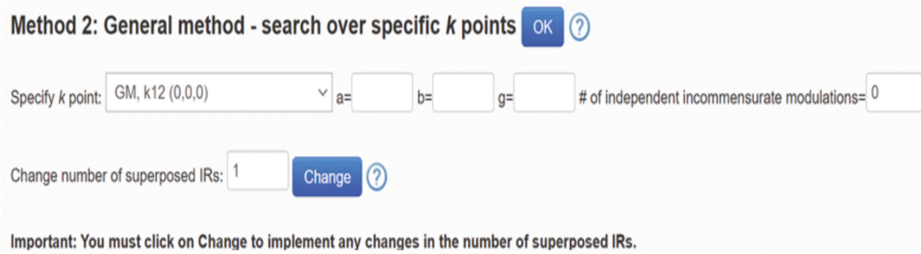

Figure 7.8. Method 2 in ISODISTORT. Reprinted from [20].

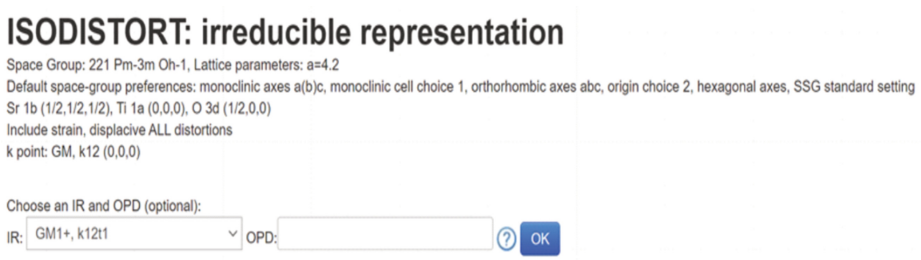

Figure 7.9. Selection of irreducible representations. Reprinted from [20].

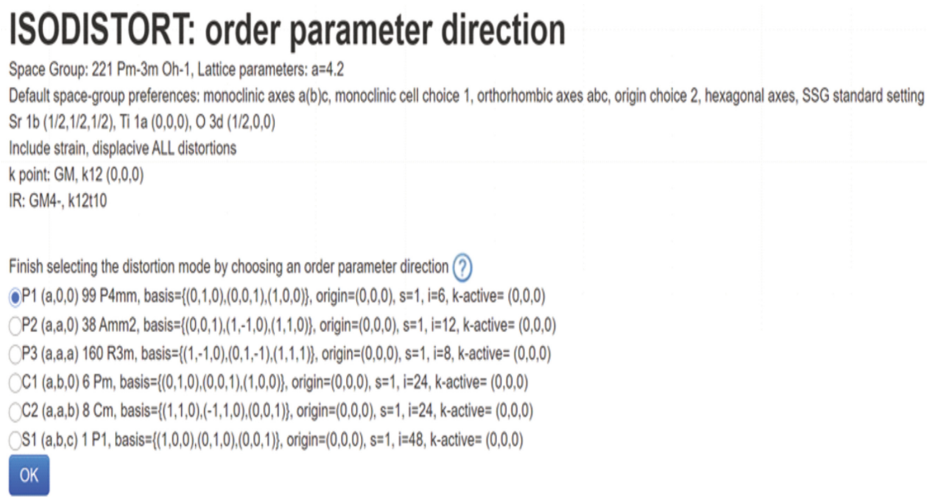

Figure 7.10. Selection of distortion modes via their order parameter directions for GM4−. Reprinted from [20].

(figure 7.10). The term *order parameter* comes from the Landau theory of phase transitions. It refers to some parameter that is zero in the high-temperature phase but has a growing value below the phase transition temperature. In this case, the order parameter may be taken to be the atomic displacement along the unique tetragonal axis. In the case of tilted octahedra, it can be taken to be the angle of tilt.

This means that starting with the cubic space group $Pm\bar{3}m$, the distortion mode labelled GM4− leads to several possible space groups that can be formed, including the isotropy subgroup P1 - *P*4*mm* (no 99). The order parameter (which is given by the atomic displacements along the tetragonal axis) has a single component symbolized by (a, 0,0). In this case, the axes are chosen in the order *bca* with the unit-cell origin at (0,0,0). The structure is ferroelectric with a mode at wave-vector $\mathbf{k} = (0,0,0)$, i.e., at the Γ point. $s = 1$ is the size of the primitive unit cell of the isotropy subgroup relative to the parent space group, and i is the index of the isotropy subgroup relative to the parent space group. Note that P2 gives space group *Amm*2, the space group of the orthorhombic phase of $BaTiO_3$: the order parameter is given by (a, a, 0), meaning that it has two equal components with a resultant along one of the <110> directions. P3 gives *R*3*m*, the lowest-temperature phase of $BaTiO_3$, and (a, a, a) means that the order parameter consists of three equal components with a resultant along the rhombohedral axis. We can see that ISODISTORT also suggests three other possible phases of lower symmetry descending from the cubic phase: space groups *Pm*, *Cm* and *P*1. It may be that experiments could be planned to see if these other possibilities exist (there was recently a controversy about whether the tetragonal phase was really monoclinic, for example). Let's choose *P*4*mm*, and click OK to take us to a page with several selections. The default is to save a file containing the details of the distortion for input into the program ISOVIZ (which can be downloaded from the ISODISTORT website). With this, you can make a helpful interactive image of the distortion mode.

In figure 7.11, we see a sketch of the structure. Using the sliders for the different atoms, we see that all atoms can move independently along the unique axis under the representation GM4−. Notice that this is consistent with the structure of tetragonal $BaTiO_3$, except that the unique axis has been unconventionally chosen by the software to be along [010] (this is just an arbitrary choice of axes and does not affect the interpretation). Irreducible representations at the Γ point, GM1+ and GM3+, are also listed as strain modes, which cause the unit cell to distort, corresponding to the effect of the acoustic modes. Note too that the motion of the atoms can be animated.

If you repeat this process by choosing the R point in the Brillouin zone, you obtain under R4+, figure 7.12.

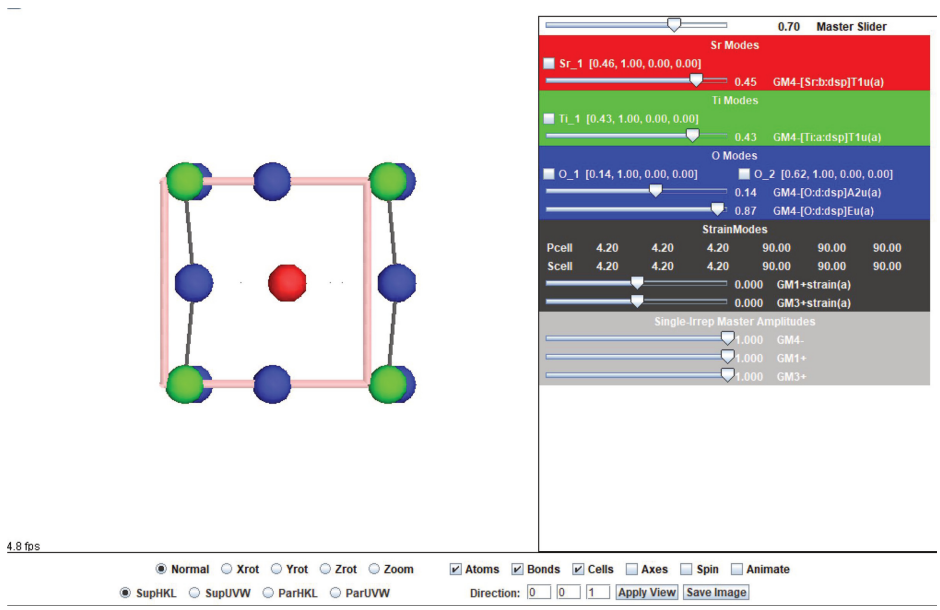

Figure 7.11. Interactive application in ISOVIZ for the irrep GM4−, space group *P*4*mm*. Reprinted from [20].

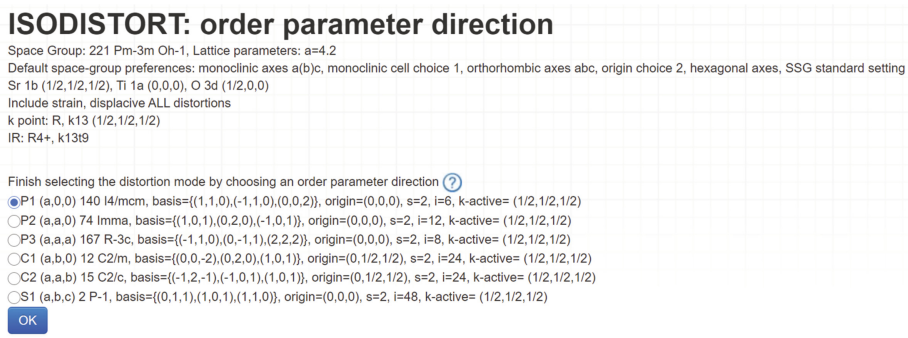

Figure 7.12. Selection of order parameters for R4+. Reprinted from [20].

The space group *I*4/*mcm* corresponds to the known low-temperature structure of $SrTiO_3$, in which only the octahedra are tilted as $a^0a^0c^-$. The orientation of the unit-cell axes is given by the matrix

$$\begin{bmatrix} 1 & 1 & 0 \\ 1 & \bar{1} & 0 \\ 0 & 0 & 2 \end{bmatrix}$$

This corresponds to a unit cell given by $\sqrt{2}\,a_p \times \sqrt{2}\,a_p \times 2c_p$.

On viewing the distortion, we now see (figure 7.13) that the distortion mode does correspond to the $a^0a^0c^-$ tilting system. Apart from the strain modes, the sliders only allow the oxygens to move, thus changing the tilt angle, with Sr and Ti fixed. If we choose in figure 7.12 the entry for space group $R\,\bar{3}\,c$, we obtain the distortions corresponding, for example, to the crystal structure of $LaAlO_3$, in which the octahedra have $a^-a^-a^-$ tilts.

Another way of carrying out distortion-mode analysis is to input both the aristotype and hettotype structures and then find the symmetry modes. While this can be done in ISODISTORT, consider, as an alternative, the use of the AMPLIMODES program in the Bilbao Crystallographic Server [21] (for a good tutorial on the use of the Bilbao Server in distortion-mode analysis, see [22]). Note that to load the structural information, the input file can be in the form of a CIF (Crystallographic Input File) or else entered manually. CIFs are text files that are usually published along with crystal-structure reports.

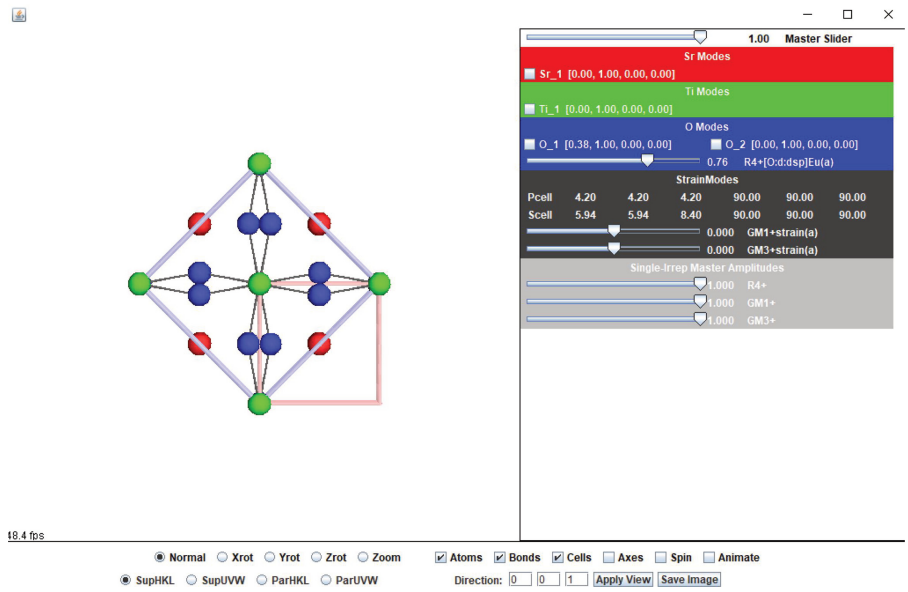

Figure 7.13. ISOVIZ sketch for the irrep R4+. Reprinted from [20].

For example, suppose we load the structure file for the $BaTiO_3$ tetragonal structure as the hettotype. First, we have to make sure that the transformation matrix is given as

$$\begin{bmatrix} 1 & 0 & 0 \\ 0 & 1 & 0 \\ 0 & 0 & 1 \end{bmatrix}$$

Then following the procedure, you finally discover a great deal of information after the symmetry-mode analysis (atomic shifts, global shift, etc), including the table:

Atoms	WP	Modes
O1	3c	GM4−(2)
Ti1	1b	GM4−(1)
Ba1	1a	GM4−(1)

where WP are the Wyckoff positions of each atom type in the aristotype structure. We see that the program has automatically found that the distortion mode relating the aristotype to the hettotype is GM4−.

Similarly, suppose we enter the following as the hettotype for the structure with tilt system $a^0a^0c^-$

```
# Space Group ITA number
140
# Lattice parameters
5.8 5.8 8.4 90 90 90
# Number of independent atoms in the asymmetric unit
4
# [atom type] [number] [WP] [x] [y] [z]
Sr 1 4b 0.5 0.0 0.25
Ti 1 4c 0.0 0.0 0.0
O 1 4a 0.0 0.0 0.25
O 2 8h 0.22 0.28 0.0
```

and the transformation matrices

$$\begin{bmatrix} 1 & -1 & 0 \\ 1 & 1 & 0 \\ 0 & 0 & 2 \end{bmatrix} + \begin{bmatrix} ½ \\ ½ \\ ½ \end{bmatrix}$$

Pressing the Show button, we get figure 7.14. In this case, the irrep is labelled R5-. The program also computes the atomic displacements relating the upper and lower structures: here, we see that only the O1 on a Wyckoff 8h site is displaced by 0.2404Å.

WP		Atom	Atomic Displacements			
			u_x	u_y	u_z	|u|
4b	(0,1/2,1/4)	Sr1	0.0000	0.0000	0.0000	0.0000
4c	(0,0,0)	Ti1	0.0000	0.0000	0.0000	0.0000
8h	(x,x+1/2,0)	O1	0.0300	-0.0300	0.0000	0.2404
4a	(0,0,1/4)	O1_2	0.0000	0.0000	0.0000	0.0000

NOTE: u_x, u_y and u_z are given in relative units. |u| is the absolute distance given in Å
Maximum atomic displacement in the distortion, Δ: 0.2404 Å
Total distortion amplitude: 0.4808 Å

Symmetry Modes Summary

Atoms	WP	Modes
O1	3*c*	**R5-(1)**

Note: The primary mode is written in bold letters

Figure 7.14. Part of the output from AMPLIMODES. Reprinted from [21].

Table 7.4. Tilt modes for the aristotype perovskite structure.

Critical point	Origin on B cation	Origin on A cation
M (½, ½, 0)	M3+	M2+
R (½, ½, ½)	R4+	R5−

You may wonder why this time, the irrep appears to be different from that found using ISODISTORT (R4+). The reason for this is subtle and is generally unappreciated. When dealing with symmetry modes with $\mathbf{k} \neq 0$, the actual irreducible representation and its label depend on the choice of origin. In our ISODISTORT example, the origin of the aristotype unit cell was on the Ti atom, whereas in our AMPLIMODES example, it is on the Sr atom. If the origin in the aristotype section is changed so that the Ti atom is at the origin, AMPLIMODES gives the same result as ISODISTORT. So, anyone publishing irreducible representation symbols for distortion modes should always state the origin choice at the same time. Unfortunately, I often see many papers in which the origin of the cubic perovskite structure is set on the A cation. Yet, the distortion-mode irrep for $a^0a^0c^-$ is stated incorrectly as R4+, because that is the irrep label that most working in this field are familiar with. Table 7.4 lists the tilt mode irreps for the A or B cation at the unit-cell origin. Generally speaking, + tilts correspond to M modes and − tilts to R modes.

Finally, returning to ISODISTORT, figure 7.15 shows that you can superpose more than one irrep, in this case, at the M and R points of the Brillouin zone. Choosing R4+ and M3+ then leads to space group *Pnma*, in which the tilt system becomes $a^-b^+a^-$ (equivalent to $a^+b^-b^-$ in table 7.1 and figure 7.5, with the

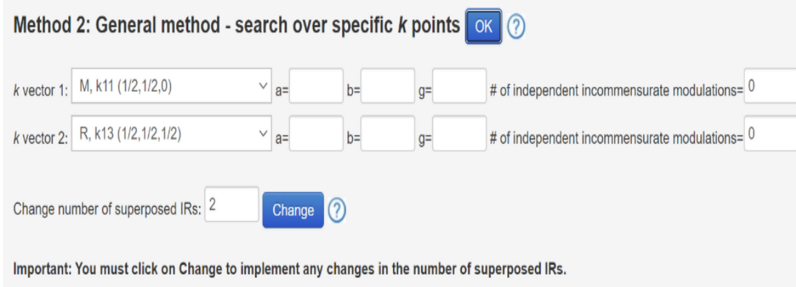

Figure 7.15. ISODISTORT: Superposing two irreps. Reprinted from [20].

transformation of axes). This tilt system is the most common one found in perovskites. At the same time, the A cations can be displaced in antiparallel arrangements to form potentially antiferroelectric structures.

You can see that distortion-mode analysis is a handy way of exploring new possible structures. A good example is a study of the high-temperature phases of $NaNbO_3$ [7], where ISODISTORT was used to determine the possible tilt systems that existed. The authors discovered a complex system in which the magnitudes of the tilts varied along a particular direction so that the repeat distance was increased beyond the simple unit-cell doubling. These software tools, ISODISTORT and AMPLIMODES, are well worth learning to use, especially if one is trying to find possible structures derived from a parent structure.

References

[1] Megaw H D 1945 Crystal structure of barium titanate *Nature* 484
[2] Kwei G H, Lawson A C, Billinge S J L and Cheong S W 1993 Structures of the ferroelectric phases of barium titanate *J. Phys. Chem.* **97** 2368–77
[3] Megaw H D 1973 *Crystal Structures: A Working Approach* (London: Saunders)
[4] Remeika J P 1954 A method for growing barium titanate single crystals *J. Am. Chem. Soc.* **76** 940–1
[5] Clarke R 1976 Phase transition studies of pure and flux-grown barium titanate crystals *J. Appl. Crystallogr.* **9** 335–8
[6] Kovalev O V 1993 *Space Groups: Irreducible Representations; Induced Representations and Corepresentations* 2nd edn (London: Gordon and Breach)
[7] Peel M D, Thompson S P, Daoud-Aladine A, Ashbrook S E and Lightfoot P 2012 New twists on the perovskite theme: crystal structures of the elusive phases R and S of $NaNbO_3$ *Inorg. Chem.* **51** 6876–89
[8] Lambert M and Comes R 1969 The chain structure and phase transition of $BaTiO_3$ and $KNbO_3$ *Solid State Commun.* **7** 305–8
[9] Comes R, Lambert M and Guinier A 1968 The chain structure of $BaTiO_3$ and $KNbO_3$ *Solid State Commun.* **6** 715–9
[10] Glazer A M 1972 The classification of tilted octahedra in perovskites *Acta Crystallogr.* B **28** 3384–92
[11] Glazer A M 2011 A brief history of tilts *Phase Trans.* **84** 405–20

[12] Woodward P M and IUCr 1997 Octahedral tilting in perovskites. I. Geometrical considerations *Acta Crystallogr.* B **53** 32–43
[13] Howard C J and Stokes H T 1998 Group-theoretical analysis of octahedral tilting in perovskites *Acta Crystallogr.* B **54** 782–9
[14] Glazer A M and Megaw H D 1972 The structure of sodium niobate (T_2) at 600 °C, and the cubic-tetragonal transition in relation to soft-phonon modes *Phil. Mag.* **25** 1119–35
[15] Bradley C J and Cracknell A P 1972 *The Mathematical Theory of Symmetry in Solids: Representation Theory for Point Groups and Space Groups* (Oxford: Oxford University Press)
[16] Dresselhaus M S, Dresselhaus G and Jorio A 2008 *Group Theory* (Berlin: Springer)
[17] Miller S C and Love W F 1967 *Tables of Irreducible Representations of Space Groups and Co-representations of Magnetic Space Groups* (Boulder, CO: Pruett)
[18] Bilbao Crystallographic Server (https://www.cryst.ehu.es/)
[19] Stokes H T, Hatch D M and Campbell B J ISOTROPY Software Suite (https://stokes.byu.edu/iso/isotropy.php)
[20] Stokes H T, Campbell B J and Hatch D M ISODISTORT (https://stokes.byu.edu/iso/isodistort.php)
[21] Orobengoa D, Capillas C, Aroyo M I and Perez-Mato J M 2009 AMPLIMODES: symmetry-mode analysis on the Bilbao Crystallographic Server *J. Appl. Crystallogr.* **42** 820–33
[22] Perez-Mato J M and Aroyo M I Tutorial on the application of the tools of the Bilbao Crystallographic Server in the study of group-subgroup phase transitions (https://www.cryst.ehu.es/html/cryst/tutorials/Tutorial_SPT_abr2010.pdf)
[23] Campbell B J and Stokes H T ISODISTORT tutorial exercises (https://conference.sns.gov/event/182/attachments/349/1938/Instructions_isodistort.pdf)

IOP Publishing

A Journey into Reciprocal Space (Second Edition)

A crystallographer's perspective

Anthony Michael Glazer

Appendix A

Stereographic projections

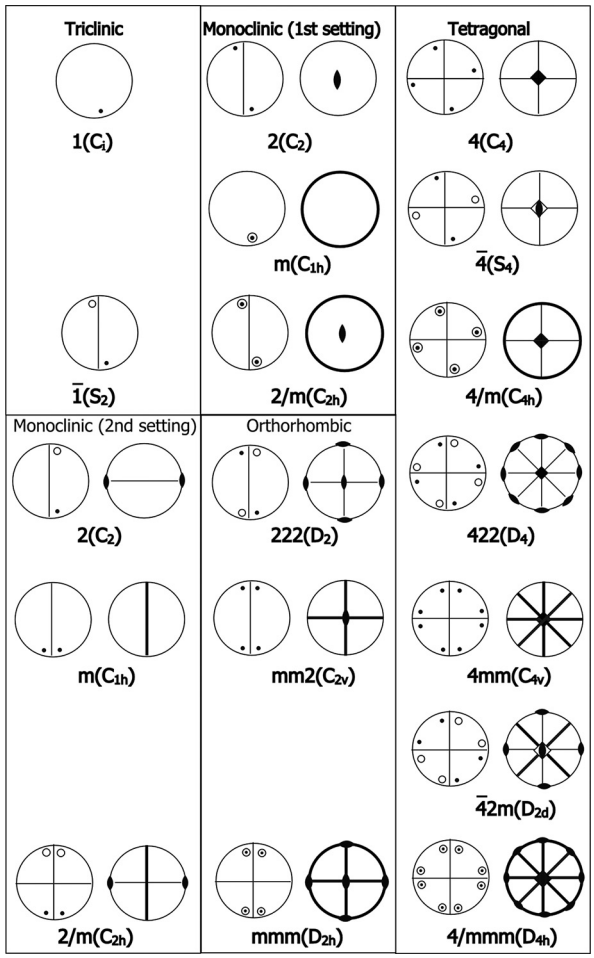

doi:10.1088/978-0-7503-3875-2ch8

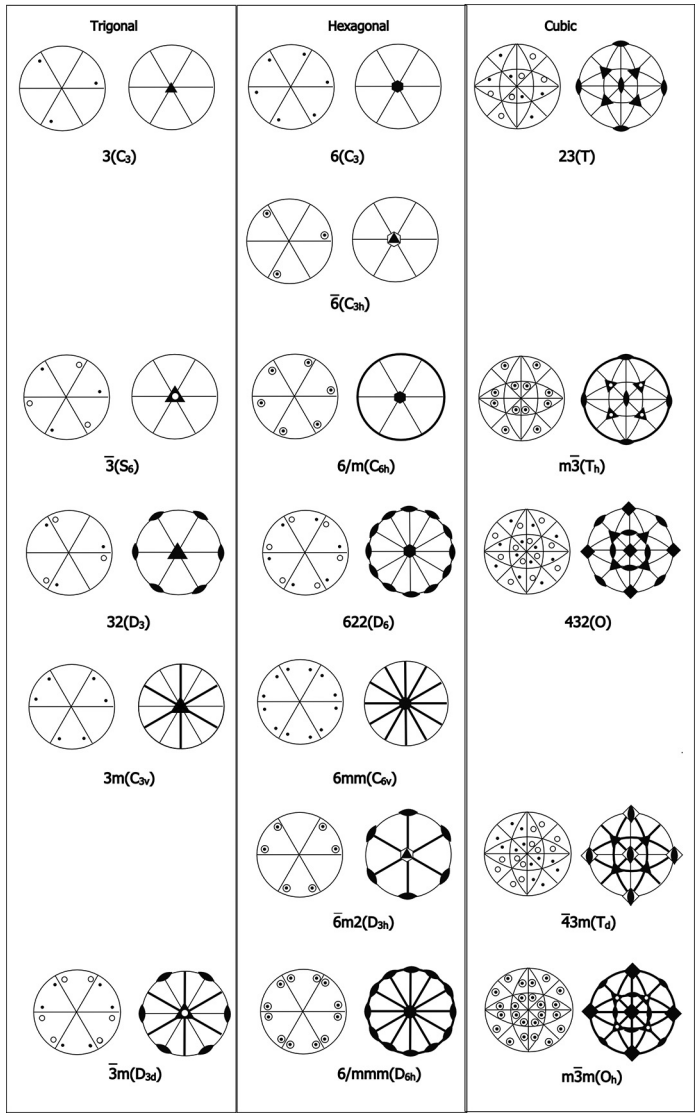
Trigonal
Hexagonal
Cubic
3(C3)
6(C3)
23(T)
$\bar{6}$(C3h)
$\bar{3}$(S6)
6/m(C6h)
m$\bar{3}$(Th)
32(D3)
622(D6)
432(O)
3m(C3v)
6mm(C6v)
$\bar{6}$m2(D3h)
$\bar{4}$3m(Td)
$\bar{3}$m(D3d)
6/mmm(D6h)
m$\bar{3}$m(Oh)

IOP Publishing

Appendix B

Symbols

Symbols of symmetry planes

(a) Symmetry planes normal to the plane of projection (three dimensions) and symmetry lines in the plane of the figure (two dimensions).

Symmetry plane or symmetry line	Graphical symbol	Glide vector in units of lattice translation vectors parallel and normal to projection plane	Printed symbol
Reflection plane, mirror plane Reflection line, mirror line (two dimensions)	———	None	*m*
'Axial' glide plane	– – – – – – –	½ along line parallel to projection plane	*a, b, or c*
Glide line (two dimensions)		½ along line in plane	*g*
'Axial' glide plane	·····	½ normal to projection plane	*a, b, or c*
'Diagonal' glide plane	▬▬▬▬▬	½ along line parallel to projection plane, combined with ½ normal to projection plane	*n*
'Diamond' glide plane (pair of planes; in centred cells only)	▬·▬·◄·▬ ▬·►·▬·▬	¼ along line parallel to projection plane, combined with ¼ normal to projection plane (arrow indicates direction parallel to the projection plane for which the normal component is positive)	*d*
'Double' glide plane	··▬··▬··▬··	Two glide vectors ½ along line parallel to projection plane ½ normal to projection plane	*e*

doi:10.1088/978-0-7503-3875-2ch9

For symbols used in cubic space groups see the ITA (tables 1.4.3, 1.4.6 and 1.4.7).

(b) Symmetry planes parallel to the plane of projection.

Symmetry plane	Graphical symbol	Glide vector in units of lattice translation vectors parallel to the projection plane	Printed symbol
Reflection plane, mirror plane	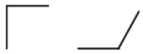	None	*m*
'Axial' glide plane		½ in the direction of the arrow	*a, b, or c*
'Double' glide plane		½ in either of the directions of the two arrows	*e*
'Diagonal' glide plane		½ in the direction of the arrow	*n*
'Diamond' glide plane (pair of planes; in centred cells only)	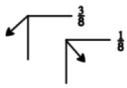	½ in the direction of the arrow; the glide vector is always half of a centring vector, i.e., one quarter of a diagonal of the conventional cell	*d*

Symbols of symmetry axes

Symmetry axes normal to the plane of projection (three dimensions)

Symmetry axis or symmetry point	Graphical symbol	Screw vector of a right-handed screw rotation in units of the shortest lattice translation vector parallel to the axis	Printed symbol
Identity	None	None	1
2-fold rotation axis. 2-fold rotation point (two dimensions)		None	2
2-fold screw axis: '2 sub 1'		$\frac{1}{2}$	2_1
3-fold rotation axis. 3-fold rotation point (two dimensions)		None	3
3-fold screw axis: '3 sub 1'		$\frac{1}{3}$	3_1
3-fold screw axis: '3 sub 2'		$\frac{2}{3}$	3_2

4-fold rotation axis. 4-fold rotation point (two dimensions)		None	4
4-fold screw axis: ‘4 sub 1’		$\frac{1}{4}$	4_1
4-fold screw axis: ‘4 sub 2’		$\frac{1}{2}$	4_2
4-fold screw axis: ‘4 sub 3’		$\frac{3}{4}$	4_3
6-fold rotation axis. 6-fold rotation point (two dimensions)		None	6
6-fold screw axis: ‘6 sub 1’		$\frac{1}{6}$	6_1
6-fold screw axis: ‘6 sub 2’		$\frac{1}{3}$	6_2
6-fold screw axis: ‘6 sub 3’		$\frac{1}{2}$	6_3
6-fold screw axis: ‘6 sub 4’		$\frac{2}{3}$	6_4
6-fold screw axis: ‘6 sub 5’		$\frac{5}{6}$	6_5
Centre of symmetry, inversion centre: ‘1 bar’ reflection point, mirror point (one dimension)		None	$\bar{1}$
Inversion axis: ‘3 bar’		None	$\bar{3}$
Inversion axis: ‘4 bar’		None	$\bar{4}$
Inversion axis: ‘6 bar’		None	$\bar{6}$
2-fold rotation axis with centre of symmetry		None	*2/m*

(*Continued*)

(*Continued*)

Symmetry axis or symmetry point	Graphical symbol	Screw vector of a right-handed screw rotation in units of the shortest lattice translation vector parallel to the axis	Printed symbol
2-fold screw axis with centre of symmetry		$\frac{1}{2}$	$2_1/m$
4-fold rotation axis with centre of symmetry		None	$4/m$
'4 sub 2' screw axis with centre of symmetry		$\frac{1}{2}$	$4_2/m$
6-fold rotation axis with centre of symmetry		None	$6/m$
'6 sub 3' screw axis with centre of symmetry		$\frac{1}{2}$	$6_3/m$

Order of symbols

This table summarizes the order of positions in the three-dimensional space group or point group symbols. Thus, for example, in the orthorhombic system, *mm*2 refers to mirror planes *perpendicular* to **a** and **b**, and a 2-fold axis *along* **c**. Similarly, in the hexagonal system $\bar{6}$ m2 means a $\bar{6}$ axis along **c**, mirror planes *perpendicular* to **a**, **b** and **a+b** ([110]), and 2-fold axes *perpendicular* to **a**, **b** and **a+b**. Finally, in the cubic system, $\bar{4}3m$ means $\bar{4}$ axes *along* the three cube axes, **a**, **b** and **c**, four 3-fold axes *along* the body diagonals <111> and diagonal mirror planes *perpendicular* to <110>. In $m\bar{3}$, the first position tells us that there are mirror planes *perpendicular* to the cube axes and the second position that there are 3-fold axes *along* the body diagonals. There is nothing in the third position, as in this case there is no symmetry operation acting about the <110> directions, except, of course, for the trivial identity operation.

Three-dimensional lattices

Lattice	Position in International Symbol		
	1	2	3
Triclinic		Only one symbol used	
Monoclinic		first setting: **c**-axis unique second setting: **b**-axis unique	
Orthorhombic	2 or $\bar{2}$ along **a**	2 or $\bar{2}$ along **b**	2 or $\bar{2}$ along **c**

Tetragonal	4 or $\bar{4}$ along **c**	2 or $\bar{2}$ along **a** and **b**	2 or $\bar{2}$ along [110] and [1$\bar{1}$0]
Trigonal	3 or $\bar{3}$ along **c**	2 or $\bar{2}$ along **a**, **b** and [110]	2 and $\bar{2}$ perpendicular to **a**, **b** and [110]
Hexagonal	6 or $\bar{6}$ along **c**	2 or $\bar{2}$ along **a**, **b** and [110]	2 or $\bar{2}$ perpendicular to **a**, **b** and [110]
Cubic	4, $\bar{4}$, 2 or $\bar{2}$ along **a**, **b** and **c**	3 or $\bar{3}$ along <111>	2 or $\bar{2}$ along <110>

Remember: $\bar{2}$ is equivalent to a mirror plane *m* perpendicular to the $\bar{2}$ axis.

Two-dimensional lattices

Lattice	Position in International Symbol		
	1	2	3
Oblique	Rotation point in plane		
Rectangular		[10]	[01]
Square		[10]	[1 $\bar{1}$]
		[01]	[11]
Hexagonal		[10]	[1 $\bar{1}$]
		[01]	[12]
		[$\bar{1}$ $\bar{1}$]	[$\bar{2}\bar{1}$]

IOP Publishing

Appendix C

Crystal families and systems

Crystal family	Symbol	Crystal system	Point groups*	Unit-cell restrictions	Bravais lattices
One dimension					
—	—	—	1, ***m***	None	*p*
Two dimensions					
Oblique (monoclinic)	*m*	Oblique	1, **2**	None	*mp*
Rectangular (orthorhombic)	*o*	Rectangular	*m*, ***2mm***	$\gamma = 90°$	*op* *oc*
Square (tetragonal)	*t*	Square	**4**, ***4mm***	$a = b$ $\gamma = 90°$	*tp*
Hexagonal	*h*	Hexagonal	3, **6** 3*m*, ***6mm***	$a = b$ $\gamma = 120°$	*hp*
Three dimensions					
Triclinic (anorthic)	*a*	Triclinic	1, $\bar{\mathbf{1}}$	None	*aP*

(*Continued*)

doi:10.1088/978-0-7503-3875-2ch10

(*Continued*)

Crystal family	Symbol	Crystal system	Point groups*	Unit-cell restrictions	Bravais lattices
Monoclinic	*m*	Monoclinic	2, *m*, ***2/m***	first setting	*mP*
				$\alpha = \beta = 90°$	*mS* (*mA, mB,mI*)
				second setting	*mP*
				$\alpha = \gamma = 90°$	*mS (mA, mB,mI)*
Orthorhombic	*o*	Orthorhombic	222, *mm*2, ***mmm***	$\alpha = \beta = \gamma = 90°$	*oP*
					oS(*oC, oA, oB)*
					oI
					oF
Tetragonal	*t*	Tetragonal	4, $\bar{4}$, ***4/m***	$a = b$	*tP*
			422, 4*mm*, $\bar{4}$2m, ***4/mmm***	$\alpha = \beta = \gamma = 90°$	*tI*
Hexagonal	*h*	Trigonal	3, $\bar{3}$	$a = b$	*hP*
			32, 3*m*, $\bar{3}$***m***	$\alpha = \beta = 90°$, $\gamma = 120°$	
				$a = b = c$ $\alpha = \beta = \gamma$	*hR*
				(Rhombohedral axes, primitive cell)	
				$a = b$	
				$\alpha = \beta = 90°$, $\gamma = 120°$ (hexagonal axes, triple obverse cell)	

		Hexagonal	6, $\overline{6}$, **6/*m*** 622, 6*mm*, $\overline{6}$2*m*, **6/mmm**	$a = b$ $\alpha = \beta = 90°$, $\gamma = 120°$	*hP*
Cubic	*c*	Cubic	23, ***m*$\overline{3}$** 432, $\overline{4}$3*m*, ***m*$\overline{3}$*m***	$a = b = c$ $\alpha = \beta = \gamma = 90°$	*cP* *cI* *cF*

*Symbols in bold are centrosymmetric.

IOP Publishing

A Journey into Reciprocal Space (Second Edition)

A crystallographer's perspective

Anthony Michael Glazer

Appendix D

Seitz symbols

(Reproduced by permission of the International Union of Crystallography, https://it.iucr.org.)

Table D1. Linear parts $\boldsymbol{R}$ of the Seitz symbols $\{\boldsymbol{R}|\mathbf{v}\}$ for space-group symmetry operations of cubic, tetragonal, orthorhombic, monoclinic and triclinic crystal systems. Each symmetry operation is specified by the shorthand description of the rotation part of its matrix-column presentation, the type of symmetry operation, and its characteristic direction.

ITA description				
No.	Coord. triplet	Type	Orientation	Setiz symbol
(1)	x, y, z	1		1
(2)	$\bar{x}, \bar{y}, z$	2	$0, 0, z$	2_{001}
(3)	$\bar{x}, y, \bar{z}$	2	$0,y,0$	2_{010}
(4)	$x, \bar{y}, \bar{z}$	2	$x, 0, 0$	2_{100}
(5)	z, x, y	3^+	x, x, x	3^+_{111}
(6)	$z, \bar{x}, \bar{y}$	3^+	$\bar{x}, x, \bar{x}$	$3^+_{\bar{1}1\bar{1}}$
(7)	$\bar{z}, \bar{x}, y$	3^+	$x, \bar{x}, \bar{x}$	$3^+_{1\bar{1}\bar{1}}$
(8)	$\bar{z}, x, \bar{y}$	3^+	$\bar{x}, \bar{x}, x$	$3^+_{\bar{1}\bar{1}1}$
(9)	y, z, x	3^-	x, x, x	3^-_{111}
(10)	$\bar{y}, z, \bar{x}$	3^-	$x, \bar{x}, \bar{x}$	$3^-_{1\bar{1}\bar{1}}$
(11)	$y, \bar{z}, \bar{x}$	3^-	$\bar{x}, \bar{x}, x$	$3^-_{\bar{1}\bar{1}1}$
(12)	$\bar{y}, \bar{z}, x$	2^-	$\bar{x}, x, \bar{x}$	$3^-_{\bar{1}1\bar{1}}$
(13)	$y, x, \bar{z}$	2	$x, x, 0$	2_{110}
(14)	$\bar{y}, \bar{x}, \bar{z}$	2	$x, \bar{x}, 0$	$2_{1\bar{1}0}$
(15)	$y, \bar{x}, z$	4^-	$0, 0, z$	4^-_{001}
(16)	$\bar{y}, x, z$	4^+	$0, 0, z$	4^+_{001}
(17)	$x, z, \bar{y}$	4^-	$x, 0, 0$	4^-_{100}

(*Continued*)

doi:10.1088/978-0-7503-3875-2ch11

Table D1. (*Continued*)

	ITA description			
No.	Coord. triplet	Type	Orientation	Setiz symbol
(18)	$\bar{x}, z, y$	2	$0, y, y$	2_{011}
(19)	$\bar{x}, \bar{z}, \bar{y}$	2	$0, y, \bar{y}$	$2_{01\bar{1}}$
(20)	$x, \bar{z}, y$	4^+	$x, 0, 0$	4^+_{100}
(21)	$z, y, \bar{x}$	4^+	$0, y, 0$	4^+_{010}
(22)	$z, \bar{y}, x$	2	$x, 0, x$	2_{101}
(23)	$\bar{z}, y, x$	4^-	$0, y, 0$	4^-_{010}
(24)	$\bar{z}, \bar{y}, \bar{x}$	2	$\bar{x}, 0, x$	$2_{\bar{1}01}$
(25)	$\bar{x}, \bar{y}, \bar{z}$	$\bar{1}$		$\bar{1}$
(26)	$x, y, \bar{z}$	m	$x, y, 0$	m_{001}
(27)	$x, \bar{y}, z$	m	$x, 0, z$	m_{010}
(28)	$\bar{x}, y, z$	m	$0, y, z$	m_{100}
(29)	$\bar{z}, \bar{x}, \bar{y}$	$\bar{3}^+$	x, x, x	$\bar{3}^+_{111}$
(30)	$\bar{z}, x, y$	$\bar{3}^+$	$\bar{x}, x, \bar{x}$	$\bar{3}^+_{\bar{1}1\bar{1}}$
(31)	$z, x, \bar{y}$	$\bar{3}^+$	$x, \bar{x}, \bar{x}$	$\bar{3}^+_{1\bar{1}\bar{1}}$
(32)	$z, \bar{x}, y$	$\bar{3}^+$	$\bar{x}, \bar{x}, x$	$\bar{3}^+_{\bar{1}\bar{1}1}$
(33)	$\bar{y}, \bar{z}, \bar{x}$	$\bar{3}^-$	x, x, x	$\bar{3}^-_{111}$
(34)	$y, \bar{z}, x$	$\bar{3}^-$	$x, \bar{x}, \bar{x}$	$\bar{3}^-_{1\bar{1}\bar{1}}$
(35)	$\bar{y}, z, x$	$\bar{3}^-$	$\bar{x}, \bar{x}, x$	$\bar{3}^-_{\bar{1}\bar{1}1}$
(36)	$y, z, \bar{x}$	$\bar{3}^-$	$\bar{x}, x, \bar{x}$	$\bar{3}^-_{\bar{1}1\bar{1}}$
(37)	$\bar{y}, \bar{x}, z$	m	$x, \bar{x}, z$	m_{110}
(38)	y, x, z	m	x, x, z	$m_{1\bar{1}0}$
(39)	$\bar{y}, x, \bar{z}$	$\bar{4}^-$	$0, 0, z$	$\bar{4}^-_{001}$
(40)	$y, \bar{x}, \bar{z}$	$\bar{4}^+$	$0, 0, z$	$\bar{4}^+_{001}$
(41)	$\bar{x}, \bar{z}, y$	$\bar{4}^-$	$x, 0, 0$	$\bar{4}^-_{100}$
(42)	$x, \bar{z}, \bar{y}$	m	$x, y, \bar{y}$	m_{011}
(43)	x, z, y	m	x, y, y	$m_{01\bar{1}}$
(44)	$\bar{x}, z, \bar{y}$	$\bar{4}^+$	$x, 0, 0$	$\bar{4}^+_{100}$
(45)	$\bar{z}, \bar{y}, x$	$\bar{4}^+$	$0, y, 0$	$\bar{4}^+_{010}$
(46)	$\bar{z}, y, \bar{x}$	m	$\bar{x}, y, x$	m_{101}
(47)	$z, \bar{y}, \bar{x}$	$\bar{4}^-$	$0, y, 0$	$\bar{4}^-_{010}$
(48)	z, y, x	m	x, y, x	$m_{\bar{1}01}$

Table D2. Linear parts $\boldsymbol{R}$ of the Seitz symbols $\{\boldsymbol{R}|\mathbf{v}\}$ for space-group symmetry operations of hexagonal and trigonal crystal systems. Each symmetry operation is specified by the shorthand description of the rotation part of its matrix-column presentation, the type of symmetry operation, and its characteristic direction.

ITA description				
No.	Coord. triplet	Type	Orientation	Seitz symbol
(1)	x,y,z	1		1
(2)	$\overline{y},x–y,\ z$	3+	0,0,z	3^{+}_{001}
(3)	$\overline{x}+y,\ \overline{x},\ z$	3−	0,0,z	3^{-}_{001}
(4)	$\overline{x},\ \overline{y},\ z$	2	0,0,z	2_{001}
(5)	$y,\ \overline{x}+y,\ z$	6−	0,0,z	6^{-}_{001}
(6)	$x-y,\ x,\ z$	6+	0,0,z	6^{+}_{001}
(7)	$y,\ x,\ \overline{z}$	2	x,x,0	2_{110}
(8)	$x-y,\ \overline{y},\ \overline{z}$	2	x,0,0	2_{100}
(9)	$\overline{x},\ \overline{x}+y,\ \overline{z}$	2	0,y,0	2_{010}
(10)	$\overline{y},\ \overline{x},\ \overline{z}$	2	$x,\ \overline{x},\ 0$	$2_{1\bar{1}0}$
(11)	$\overline{x}+y,\ y,\ \overline{z}$	2	x,2x,0	2_{120}
(12)	$x,\ x-y,\ \overline{z}$	2	2x,x,0	2_{210}
(13)	$\overline{x},\ \overline{y},\ \overline{z}$	$\overline{1}$		$\overline{1}$
(14)	$y,\ \overline{x}+y,\ \overline{z}$	$\overline{3}^{+}$	0,0,z	$\overline{3}^{+}_{001}$
(15)	$x-y,\ x,\ \overline{z}$	$\overline{3}^{-}$	0,0,z	$\overline{3}^{-}_{001}$
(16)	$x,\ y,\ \overline{z}$	m	x,y,z	m_{001}
(17)	$\overline{y},\ x-y,\ \overline{z}$	$\overline{6}^{-}$	0,0,z	$\overline{6}^{-}_{001}$
(18)	$\overline{x}+y,\ \overline{x},\ \overline{z}$	$\overline{6}^{+}$	0,0,z	$\overline{6}^{+}_{001}$
(19)	$\overline{y},\ \overline{x},\ z$	m	$x,\ \overline{x},\ z$	m_{110}
(20)	$\overline{x}+y,\ y,\ z$	m	x,2x,z	m_{100}
(21)	$x,\ x-y,\ z$	m	2x,x,z	m_{010}
(22)	$y,\ x,\ z$	m	x,x,z	$m_{1\bar{1}0}$
(23)	$x-y,\ \overline{y},\ z$	m	x,0,z	m_{120}
(24)	$\overline{x},\ \overline{x}+y,\ z$	m	0,y,z	m_{210}

IOP Publishing

Appendix E

Fourier transforms

As Gregor Samsa awoke one morning from uneasy dreams, he found himself transformed in his bed into a gigantic insect.

(Franz Kafka, The Metamorphosis)

Fourier transformation is the most important concept in the theory of diffraction. For instance, light from a diffracting object passing through a standard convex optical lens leads to the diffraction pattern located on the back-focal plane. This is described by the function $F(u,v)$, the Fourier transform of the diffracting object in two dimensions. The lens, therefore, acts as a Fourier transforming device. Furthermore, the lens's action is then to Fourier transform this diffraction information to produce an image on the image plane. Thus, we have

$$\text{Object plane} \xrightarrow{FT} \text{Back-focal plane} \xrightarrow{FT} \text{Image plane}$$

Even in the absence of a lens, the diffraction pattern, such as that formed by light passing through or reflected by a diffraction grating, is calculated using Fourier transforms. The Fourier transform relates one vector space to another, in our case direct and reciprocal space. Linear operations performed in one domain (time or frequency) have corresponding operations in the other domain. So, let us take a look at what this means, with a few examples. We shall confine the discussion to transformations in spatial domains, although time and frequency domains can easily be treated in a similar way.

The one-dimensional Fourier transform of a function $f(x)$ is given by

$$f(Q) = \int_{-\infty}^{\infty} f(x) e^{iQx} dx$$

and its inverse is given by

$$f(x) = \frac{1}{2\pi} \int_{-\infty}^{\infty} f(Q) e^{-iQx} dQ$$

doi:10.1088/978-0-7503-3875-2ch12

In three dimensions, we have

$$f(\mathbf{Q}) = \int_{-\infty}^{\infty} f(\mathbf{r}) e^{i\mathbf{Q}\cdot\mathbf{r}} d^3\mathbf{r}$$

$$f(\mathbf{r}) = \left(\frac{1}{2\pi}\right)^3 \int_{-\infty}^{\infty} f(\mathbf{Q}) e^{-i\mathbf{Q}\cdot\mathbf{r}} d^3\mathbf{Q}$$

Be aware that the normalisation factor is, to some extent, a matter of choice, as there are many different conventions in the literature. Notice that the sign in the exponential term changes between the Fourier transform equation and its inverse. Also, note that some authors use a negative sign in the exponent in $f(Q)$, and a positive sign in $f(\mathbf{r})$.

The Fourier transform has the following properties:

1. Parity is preserved, i.e., if $f(x)$ is even/odd then $f(Q)$ is even/odd. If $f(x)$ is real-valued, then $f(Q)$ is complex and has the symmetry $f(-Q) = f(Q)^*$, where $f(Q)^*$ is the complex conjugate of $f(Q)$.
2. The *power spectrum* (in our case, the intensity distribution) is given by
$$P(Q) = f(Q)f(Q)^* = |f(Q)|^2$$
3. The *similarity theorem* states that if $f(Q) = \tilde{f}(x)$, where the squiggle means Fourier transform
$$\tilde{f}(ax) = \frac{1}{|a|} f\left(\frac{Q}{a}\right)$$
i.e., stretching of the coordinate in x-space leads to a contraction in the Fourier space and a change by a factor of $1/|a|$.
4. The *shift theorem* states that
$$\tilde{f}(x - a) = f(Q)e^{2\pi i Q a}$$
i.e., a translation of a function leads to a linear phase shift in Fourier space.
5. Parsval's theorem states that
$$\int_{-\infty}^{\infty} |f(x)|^2 dx = \int_{-\infty}^{\infty} |f(Q)|^2 dQ$$
6. The *convolution theorem* states that the Fourier transform of the convolution of two functions is equal to the product of their individual Fourier transforms. Conversely, the Fourier transform of the product of two functions is equal to the convolution of their individual Fourier transforms.

The convolution theorem can be proved as follows. We start by considering the Fourier transform applied to a convolution of two functions, $f(x)$ and $g(x)$:

$$h(x) = f(x) * g(x) = \int_{-\infty}^{\infty} f(x)g(u - x)dx$$

The Fourier transform $h(k)$ of $h(x)$ is given by

$$h(k) = \int_{-\infty}^{\infty} e^{iku} \left[\int_{-\infty}^{\infty} f(x)g(u-x)dx \right] du$$

Now, let $u-x = w$, and $dw = du$

$$h(k) = \int_{-\infty}^{\infty} e^{ik(x+w)} \left[\int_{-\infty}^{\infty} f(x)g(w)dx \right] dw$$

Changing the order of the integration

$$h(k) = \int_{-\infty}^{\infty} f(x)e^{ikx}dx \int_{-\infty}^{\infty} e^{ikw}g(w)dw$$

The variables of integration can have any names we please, so we can now replace w with x

$$h(k) = \int_{-\infty}^{\infty} f(x)e^{ikx}dx \int_{-\infty}^{\infty} g(x)e^{ikx}dx$$

In other words,

$$f(x) * g(x) \overset{FT}{\longleftrightarrow} f(k) \times g(k)$$

where f (k) and $g(k)$ are the Fourier transforms of the functions $f(x)$ and $g(x)$, respectively. Conversely

$$f(x) \times g(x) \overset{FT}{\longleftrightarrow} f(k) * g(k)$$

This is a statement of the *convolution theorem*, one of the most important and useful theorems for calculating Fourier transforms. Let us take a few simple examples of Fourier transforms. For illustration purposes, we shall consider Fourier transforms in one dimension.

Delta function

Suppose we have a single spike (infinitesimally narrow and infinitely high) at position x_o on the x-axis (figure E1(a)). This is denoted by the Dirac delta function

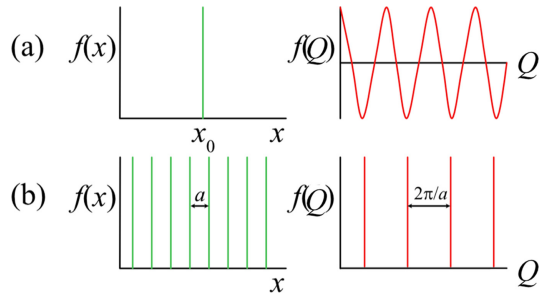

Figure E1.

$$\begin{aligned}\delta(x - x_0) &= 1 \quad \text{for } x = x_0 \\ &= 0 \quad \text{for x} \neq \text{x}_0\end{aligned}$$

The Fourier transform is then given by

$$f(Q) = \int_{-\infty}^{\infty} \delta(x - x_0) e^{iQx} dx = e^{iQx_0}$$

In other words, the delta function picks out from the exponential function the value only at x_0. Plotting the real part, we get an infinite cosinusoidal function (figure E1(a)). Conversely, if we had started, instead, with a monochromatic wave, the inverse Fourier transform would give a delta function.

Infinite periodic array of delta functions

We can express this by the formula

$$f(x) = \sum_{n=-\infty}^{n=\infty} \delta(x - na)$$

Here, n is an infinite set of integers, and a is the repeat distance between the spikes (figure E1(b)). The Fourier transform is now given by

$$f(Q) = \int_{-\infty}^{\infty} \sum_{n=-\infty}^{n=\infty} \delta(x - na) e^{iQx} dx = \sum_{n=-\infty}^{n=\infty} e^{iQna}$$

Again, the delta function has picked out the values of $x = na$. This can be written as

$$f(Q) = \sum_{n=0}^{n=\infty} (e^{iQa})^n + \sum_{n=-\infty}^{n=0} (e^{-iQa})^n - 1$$

The two sums are for terms forming a geometric series

$$\begin{aligned}f(Q) &= (1 - e^{iQa})^{-1} + (1 - e^{-iQa})^{-1} - 1 \\ &= 0\end{aligned}$$

except that $f(Q) = \infty$ for the particular case $e^{iQa} = 1$. If we take $Qa = 2\pi h$, where h is an integer, then

$$f(Q) = 2\pi a^{-1} \sum_h \delta(Q - 2\pi h/a)$$

In other words, the Fourier transform of the periodic array of delta functions along x of spacing a is a periodic array of delta functions along Q of spacing $2\pi/a$ (figure E1(b)).

Diffraction from a grating of very thin slits

To a first approximation, we can think of this as a finite periodic array of delta functions. Start with the infinite array of delta functions again, but this time multiplied by a function $W(x)$, effectively a slit function of width Na

$$W(x) = \begin{cases} 0 & \text{if } |x| > Na/2 \\ 1 & \text{if } |x| \leqslant Na/2 \end{cases}$$

which limits the number of delta functions:

$$f(x) = \left[\sum_n \delta(x - na)\right] \times W(x)$$

To find the Fourier transform, we now appeal to the convolution theorem. Thus, we have

$$f(Q) = \left[2\pi a^{-1} \sum_h \delta(Q - 2\pi h/a)\right] * W(Q)$$

where $W(Q)$ is the Fourier transform of $W(x)$. $W(Q)$ is given by

$$W(Q) = \int_{-½Na}^{½Na} e^{iQx} dx = \frac{2 \sin ½QNa}{Q}$$

This is the well-known *sinc* function for diffraction from a single slit. Figure E2 shows the $sinc^2$ function. The width of the central maximum to the first zero is given by $2\pi/N\alpha$.

Figure E3 shows a sketch of what the power spectrum looks like along Q. We see a series of sharp peaks of spacing $2\pi/a$ and widths measured from the maximum to

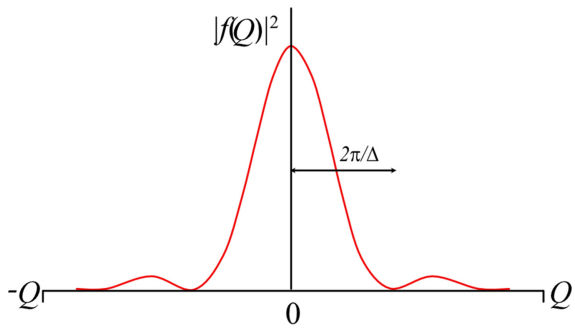

Figure E2.

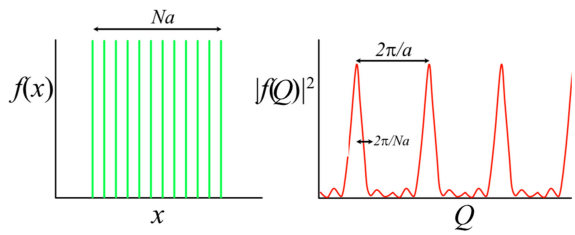

Figure E3.

the first zero of $2\pi/Na$. This demonstrates that as the number N of delta functions increases, the widths of the diffraction peaks decrease, while the spacing between the peaks remains constant.

Another way to calculate the spectrum is to start with the lattice term

$$f(x) = \sum_{n=-p}^{n=p} \delta(x - na)$$

where $N = 2p + 1$. The Fourier transform is given by

$$f(Q) = \sum_{n=-p}^{n=p} e^{iQna} = \sum_{n=-p}^{n=p} \cos Qna$$

as the positive and negative sine terms cancel out. We now can write this as

$$\begin{aligned} f(Q) &= \frac{1}{2\sin Qa/2} \sum_{n=-p}^{n=p} 2\cos Qna \sin Qa/2 \\ &= \frac{1}{2\sin Qa/2} \sum_{n=-p}^{n=p} \sin Qa[n + \tfrac{1}{2}] - \sin Qa[n - \tfrac{1}{2}] \\ &= \frac{1}{2\sin Qa/2} \left\{ \begin{matrix} \sin Qa[p + 1/2] - \sin Qa[p - 1/2] + \sin Qa[p - 1/2] - \sin Qa[p - 3/2] ..... \\ ..... + \sin Qa[-p + 1/2] - \sin Qa[-p - 1/2] \end{matrix} \right\} \\ &= \frac{\sin Qa[p + 1/2]}{\sin Qa/2} \\ &= \frac{\sin QNa/2}{\sin Qa/2} \end{aligned}$$

Although it is not immediately obvious, this formula gives the same result as in figure E3.

Diffraction from a grating of thicker slits

Suppose the grating consists N parallel slits each of width $\Delta \ll a$. Then we can write

$$f(x) = \left[\sum_n \delta(x - na) \right] \times W(x) \Big\} * S(x)$$

where

$$S(x) = \begin{cases} 0 & \text{if } |x| > \Delta/2 \\ 1 & \text{if } |x| \leqslant \Delta/2 \end{cases}$$

and then by the convolution theorem

$$f(Q) = \left[2\pi a^{-1} \sum_h \delta(Q - 2\pi h/a) \right] * W(Q) \times S(Q)$$

In other words, the result is the Fourier transform of the grating consisting of very thin slits of width $\Delta \ll a$ *multiplied* by the Fourier transform of the slit-width function. The power spectrum $|f(Q)|^2$ before and after applying this narrow slit function is shown in figures E4(a) and (b).

Fourier transform of cosinusoidal/sinusoidal wave

Let $f(x) = \cos(sx)$. The Fourier transform is then

$$\begin{aligned} f(Q) &= \int_{-\infty}^{\infty} (\cos sx) e^{iQx} dx \\ &= \frac{1}{2}\int_{-\infty}^{\infty} (e^{isx} + s^{-isx}) e^{iQx} dx \\ &= \frac{1}{2}\int_{-\infty}^{\infty} e^{i(Q+s)x} dx + \frac{1}{2}\int_{-\infty}^{\infty} e^{i(Q-s)x} dx \\ &= \pi\delta(Q+s) + \pi\delta(Q-s) \end{aligned}$$

The result (figure E5) is two delta functions at $Q = \pm s$, height π, either side of $Q = 0$. For the case $f(x) = \sin(sx)$ the result is again two delta functions at $Q = \pm s$ of height $\pm i\pi$.

Inverse Fourier transform and filters

In figure E6, an example is shown of the use of the inverse Fourier transform, in this case applied to the diffraction pattern created from a photograph of Max von Laue. The middle section shows the effect of inserting a mask into the diffraction pattern such that only the central area is allowed in the transformation. This means that only low-frequency information is passed. This is equivalent to reducing resolution, as for example in crystal diffraction at high temperature. The bottom section shows what happens when only the high-frequency information is passed

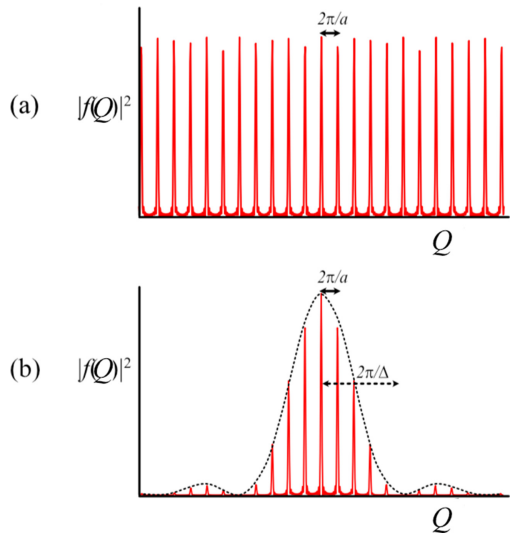

Figure E4.

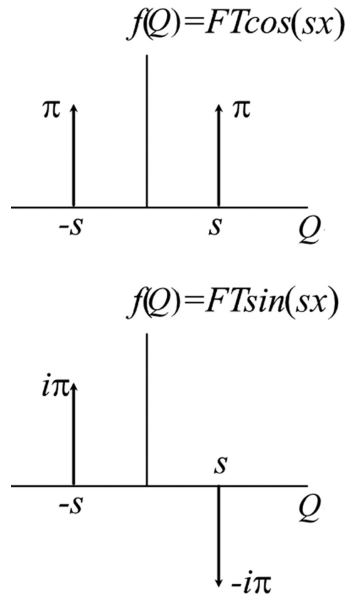

Figure E5.

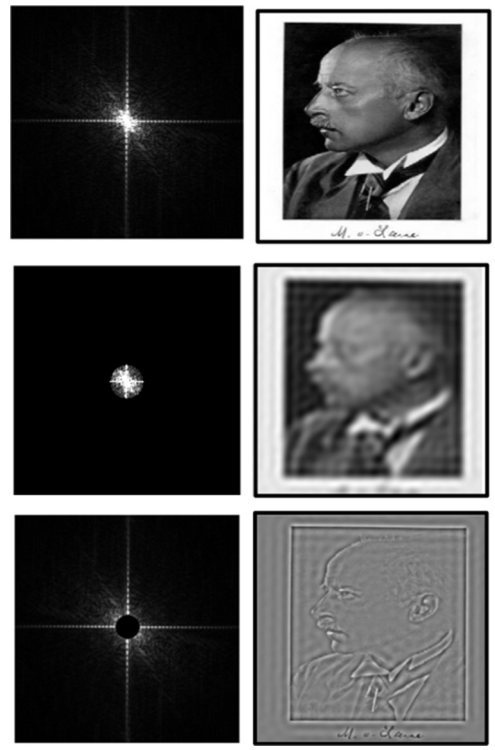

Figure E6. Inverse Fourier transform of Max von Laue. Images on the right reconstructed from the diffraction images on the left. Top: No filter; Middle: low-pass filter; bottom: high-pass filter.

(the sharp edges in the original image are formed by high-frequency waves). In structure solution from crystal diffraction patterns, the high-angle reflections are needed to achieve high resolution of the atomic positions. It is for this reason that crystal diffraction patterns are often measured when the crystal is cooled to low temperatures.

IOP Publishing

Appendix F

The Patterson function

Consider a one-dimensional electron density at two positions $\rho(x)$ and $\rho(x + u)$. The average product (or autocorrelation) in a repeat of length a is then given by the formula

$$A(u) = \int_0^1 \rho(x)\rho(x + u)dx$$

Therefore,

$$A(u) = \int_0^a \frac{1}{a^2}\sum_h F(h)e^{-2\pi ihx}\sum_{h'} F(h')e^{-2\pi ih'(x+u)}dx$$
$$= \frac{1}{a^2}\sum_h F(h)\sum_{h'} F(h')e^{-2\pi ih'u}\int_0^a e^{-2\pi i(h+h')x}dx$$

But since h and h' are integers

$$\int_0^a e^{-2\pi i(h+h')x}dx = \left[\frac{e^{-2\pi i(h+h')x}}{-2\pi i(h + h')}\right]_0^a = a$$

when $h = -h'$, otherwise the value of the integral is 0. Therefore,

$$A(u) = \frac{1}{a}\sum_h\sum_{-h} F(h)F(-h)e^{2\pi ihu}$$

Now, we also know that from Friedel's Law

$$F(-h) = F(h)*$$

and so

$$A(u) = \frac{1}{a}\sum_h |F(h)|^2 e^{2\pi ihu}$$

doi:10.1088/978-0-7503-3875-2ch13

This can be rewritten as

$$A(u) = \frac{1}{a}\sum_{h>0}\left(|F(h)|^2 e^{2\pi ihu} + |F(h)|^2 e^{-2\pi ihu}\right)$$

and using Friedel's Law

$$A(u) = \frac{2}{a^2}\sum_{h>0}|F(h)|^2 \cos 2\pi hu$$

For convenience, we now define the Patterson function $P(u)$ by

$$P(u) = \frac{2}{a}\sum_{h>0}|F(h)|^2 \cos 2\pi hu$$

In three dimensions, this becomes

$$P(uvw) = \frac{2}{V}\sum_{h>0}\sum_{k}\sum_{l}|F(hkl)|^2 \cos 2\pi(hu + kv + lw).$$

IOP Publishing

Appendix G

Definition of crystal

In 2021, the Nomenclature Commission of the International Union of Crystallography has been debating the definition of a crystal. After much discussion, a form of words was arrived at, and this new definition has been entered into the IUCr Crystallographic Dictionary. The following is the new wording.

(The following applies to solids that, when illuminated by radiation having a wavelength on the order of Å, generate a three-dimensional diffraction pattern primarily characterized by discrete peaks. The entry for *subperiodic crystal* discusses crystals for which the diffraction pattern is instead primarily characterized by intensity maxima that are layers or rods.)

Historically, crystals were first defined in terms of their external morphologies, with the angular and symmetry relationships between their faces leading, in *ca*. 1800, to the *Law of Rational Indices*. Over a century later the information from *X*-ray diffraction resulted in a definition based on the three-dimensional translational periodicity inferred from the periodicity of the array of Bragg peaks in the diffraction patterns of most crystals. More recently crystals have been discovered for which the array of Bragg peaks is not periodic in three dimensions so that the repeating atomic arrangement lacks translational periodicity in at least one direction. Currently there are two alternative (but theoretically equivalent) definitions of a crystal; both are based on the central idea of spatial order. One focusses on direct (or real) space, the other on reciprocal (or diffraction) space. The latter is more compact and elegant; the former can be easier to visualize.

Direct-space definition: A solid is a crystal if its atoms, ions and/or molecules form, on average, a long-range **ordered** arrangement.

> In most crystals the arrangement is a periodic array that is governed by the rules of translational symmetry. In aperiodic crystals (incommensurate and quasicrystals) the arrangement is not periodic in three dimensions but is nevertheless still fully ordered, where the ordering follows particular mathematical rules.

doi:10.1088/978-0-7503-3875-2ch14

Reciprocal-space definition: A material is a crystal if it has **essentially** a sharp diffraction pattern.

A solid is a crystal if it has **essentially** a sharp diffraction pattern. The word **essentially** means that most of the intensity of the diffraction is concentrated in relatively sharp **Bragg peaks**, besides the always present diffuse scattering. In all known cases, the positions of the diffraction peaks can be expressed by

$$\mathbf{H} = \sum h_i \, \mathbf{a}_i^* \, (n \geqslant 3)$$

Here $\mathbf{a}_i^*$ and h_i are the basis vectors of the reciprocal lattice and integer coefficients, respectively, and the number n is the minimum for which the positions of the peaks can be described with integer coefficient h_i.

The conventional crystals are a special class, though very large, for which $n = 3$.

[The adjective 'known' reflects the fact that it is possible to envisage mathematically-based models that lie outside these definitions. See, *e.g.*, Grimm U 2015 *Acta Cryst.* **B71** 258–74.]

See also

- *Acta Cryst.* 1992 A**48** 928 where the definition of a *crystal* appears in the **Terms of reference** of the IUCr Commission on Aperiodic Crystals.

IOP Publishing

A Journey into Reciprocal Space (Second Edition)
A crystallographer's perspective
Anthony Michael Glazer

Appendix H

Debye heat capacity at low temperature

In this case, we are well below the Debye temperature, and so the integral can be taken from 0 to ∞.

$$E = 3N_{\text{states}}k_BT\left(\frac{T}{\Theta_D}\right)^3\int_0^\infty \frac{x^3}{e^x-1}dx$$

The integral can be evaluated as follows

$$\begin{aligned}\int_0^\infty \frac{x^3}{e^x-1}dx &= \int_0^\infty\left(\sum_{n=1}^\infty x^3e^{-nx}\right)dx\\ &= \sum_{n=1}^\infty\left(\int_0^\infty x^3e^{-nx}dx\right)\\ &= \sum_{n=1}^\infty I_n\end{aligned}$$

Integrating by parts we get

doi:10.1088/978-0-7503-3875-2ch15

$$
\begin{aligned}
I_n &= \int_0^\infty x^3 e^{-nx} dx \\
&= \left[-x^3 \frac{e^{-nx}}{n} \right]_0^\infty + \int_0^\infty 3x^2 \frac{e^{-nx}}{n} dx \\
&= 0 + \frac{3}{n} \int_0^\infty x^2 \frac{e^{-nx}}{n} dx \\
&= \frac{3}{n} \left[-x^2 \frac{e^{-nx}}{n} \right]_0^\infty + \frac{3}{n} \int_0^\infty 2x \frac{e^{-nx}}{n} dx \\
&= 0 + \frac{6}{n^2} \int_0^\infty x \frac{e^{-nx}}{n} dx \\
&= \frac{6}{n^2} \left[-x \frac{e^{-nx}}{n} \right]_0^\infty + \frac{6}{n^2} \int_0^\infty \frac{e^{-nx}}{n} dx \\
&= 0 + \frac{6}{n^3} \int_0^\infty \frac{e^{-nx}}{n} dx \\
&= \frac{6}{n^3} \left[-\frac{e^{-nx}}{n} \right]_0^\infty \\
&= \frac{6}{n^4}
\end{aligned}
$$

Therefore,

$$
\int_0^\infty \frac{x^3}{e^x - 1} dx = 6 \sum_{n=1}^{\infty} \frac{1}{n^4} = \frac{6\pi^4}{90}
$$

using the Riemann Zeta function evaluated at $\zeta(4)$. Thus,

$$
\begin{aligned}
E &= 3 N_{\text{states}} k_B T \left(\frac{T}{\Theta_D} \right)^3 \frac{6\pi^4}{90} \\
&= \frac{3\pi^4}{15} N_{\text{states}} k_B T \left(\frac{T}{\Theta_D} \right)^3
\end{aligned}
$$

The heat capacity is then given by

$$
C_V = \frac{12\pi^4}{15} N_{\text{states}} k_B \left(\frac{T}{\Theta_D} \right)^3
$$

correctly showing that $C_V \propto T^3$ in line with experiment.

Index: With reference to Section Headings

acentric 1.4.2
acoustic branch 6.2.2
acoustic mode 6.4.2
adiabatic approximation 6.2.3
affine group 1.7.1
$Al_{63}Cu_{24}Fe_{13}$ 3.14
Ammann, Robert 3.14
AMPLIMODES 7.5
anisotropic displacement parameter 3.9
anomalous dispersion 3.12, 3.13.1
anomalous transmission effect 4.3
anorthic 1.5.6.1
antiferroelectric 7.2
AntiStokes regime 6.4.2
aperiodic 3.14
aristotype 7.1, 7.5
Armstrong Henry Edward
  Letter to Nature 3.5.1
asymmetric unit 1.7, 1.7.1.
atomic scattering factor 3.7.1, 3.7.2
$AuTe_2$ 3.14
Avogadro's number 6.1
axial glide 1.7.2.2

back-focal plane 3.6
band gap 6.6.2, 6.7.2
band structure 6.6.1, 6.7.2
barium titanate 7.2
basis convoluted with a lattice 1.6.3
basis function 4.4
$BaTiO_3$ 3.5.5, 7.2
benzil 3.15
Bieberbach, Ludwig Georg Elias Moses
  1.7.2.1
Bieberbach group 1.7.2.1
Bijvoet, Johannes Martin 3.12
Bilbao Crystallographic server 1.7.4.2,
  5.4, 7.5
Bloch function 4.4
Bloch's theorem 4.4, 6.6.1
body-centred unit cell 1.5.2
Boltzmann's constant 6.1
Borrmann effect 4.3, 4.5
Borrmann, Gerhard 4.3
Bragg geometry 4.3
Bragg, William Henry 3.13.2, 3.5.1
Bragg, William Lawrence 3.13.2, 3.3
Bragg's Law 3.3
brass 1.6.3.4
Bravais lattice 1.5.6
Bravais, Auguste 1.5.6
bright-field image 3.6
Brillouin scattering 6.4.2
Brillouin Zone 5.3, 5.4. 5.5, 5.6, 6.2.1,
  6.3.1, 6.4, 6.4.3, 6.5, 6.7.1, 6.7.2,
  7.2, 7.4.
Brillouin Zone boundary 4.5, 6.2.1,
  6.2.2, 6.6.2
Brockhouse, Bertram 3.7.2

calaverite 1.2, 3.14.
calcium 6.7.2
centre of inversion 1.4.2
centred unit cell 1.5.2
centric 1.4.2
centrosymmetric 1.4.2
cesium chloride 1.6.3.4
Chapman, Henry 3.13.7
character 7.4
charge flipping 3.13.4
chemical potential 6.5
chirality 1.1, 1.4.2, 1.7.2.1
condensed mode 7.1
conduction band 6.6.2
convolution 1.6.1
convolution theorem 3.6.2, 3.9,
  Appendix E
coordinate triplet 1.7.1

copper 1.5.1, 1.6.3.1
copper band structure 6.6.2
critical point 5.4
crystal class 1.4.3
crystal family 1.5.6.1
crystal momentum 4.4
crystal structure 1.6.3, 1.7.2.2.
crystal system 1.5.4
crystal, new definition 3.14, appendix G
crystallographic basis 1.6.2
Crystallographic Input File (CIF) 7.5
crystal family 1.6.6.1, Appendix C
crystals 1.1
crystal, definition 3.14
crystallographic order 3.14, 3.15
CsC l 1.6.3.4.
cubic 1.5.4, 1.5.6.
$CuS0_4.5H_20$ 3.5.1
CuZn 1.6.3.4

dark-field image 3.6
Darwin width 4.3
Darwin, Charles Galton 4.3
Davisson, Clinton 3.7.3
De Bruijn, Nicolaas 3.14
Debye heat capacity 6.1.2
Debye temperature 6.1.2, 6.3.2
Debye, Peter Joseph William 6.1.2
Debye-Waller factor 3.9
degenerate perturbation theory 6.6.2
Density of States 5.6, 6.1.2, 6.5.
diagonal glide *n* 1.7.2.2
diamond 1.5.1, 1.6.3.5, 1.7, 6.2.3, 6.7.3
diamond crystal structure 3.10
diamond glide *d* 1.7.2.2
diatomic chain 6.2.2
diatomic molecule 6.1, 6.2.3.
diffraction 3.1
diffraction pattern 3.6.2
diffuse scattering 3.15, 3.9.
Dirac delta function Appendix E
direct methods 3.13.1
direction 1.5.3
Dirichlet domain 5.4
disorder 3.15
dispersion curve 6.2.1, 6.2.3
dispersion surface 4.5
distortion-mode analysis 7.1
double glide *e* 1.7.2.2
Dulong and Petit Law 6.1, 6.1.1
Dulong, Pierre Louis 6.1
dynamical diffraction 4.1
dynamical matrix 6.2.3
dynamical theory 4.3, 4.5

Einstein's heat capacity 6.1.1
elastic scattering 5.1
electron density 3.6.1, 3.13.1
electron diffraction 3.7.3, 4.5
element set 1.3
enantiomorphic space-group 1.7.2.1
energy-dispersive diffraction 3.5.5
equi-class subgroup 1.7.4.1
equi-translational subgroup 1.7.4.1
Ewald sphere 3.3, 3.6.2, 3.7.3, 4.5
Ewald, Paul Peter Ewald 2.1
Extended Zone Scheme 5.5, 6.2.2, 6.6.2
extinction 4.1
extinction distance 4.1, 4.5

Fermi energy 6.5,6.7.2
Fermi temperature 6.5
Fibonacci 3.14
First Born Approximation 3.6.3, 3.7.3, 4.1, 4.5
force constant 6.2.1, 6.2.2, 6.2.3
form 1.2
form factor 3.7.1
Fourier map 3.13.2
Fourier synthesis 3.13.2
Fourier Transform 3.6, 3.6.1, 3.10, 3.13.4, Appendix E
Frankenheim, Moritz Ludwig 1.5.6
free electrons 6.5
free-electron laser 3.13.7
Friedel's Law 3.11, 3.12, Appendix F
Friedrich, Walter 3.1
full symbol 1.7.1
function space operator 4.4
fundamental domain 1.7

gas constant 6.1
Gauss, Carl Friedrich Gauss 2.4.2
general position 1.4.1, 1.7.1
generator 1.7.1
geometric crystal class 1.4.3
geometric element 1.3
germanium 1.6.3.5, 6.7.3.
Gibbs, Josiah Willard 2.1
Glazer tilt notation 7.3
glide operation 1.7.2.2
Gonen, Tamir 3.13.7
graphite 6.2.3
Grimm, Uwe 3.14
group 1.3, 1.7.1

habit 1.1
Hajdu, Janos 3.13.7
Han Ying 1.1
Hauptmann, Herman Aaron 3.13.1
Häuy, René Just 1.2
heat capacity 6.1
heavy atom method 3.13.1
Hermann, Carl 1.4.1
Hermitian 6.2.3
hettotype 7.1, 7.5
hexagonal 1.5.4, 1.5.6.1
hexagonal centring 1.5.6.1
high-energy electron diffraction 3.7.3
holohedry 1.5.6
Homo Erectus 1.1
homometric 3.14

icosahedrite 3.14
ideal crystal 1.6
identity operation 1.7.2.1
incoherent scattering 3.7.2, 92
incommensurate crystal 3.14
irreducible representation 7.4
index 1.7.3
inelastic neutron scattering 6.4, 6.4.3
infrared absorption 6.4, 6.4.1.
insulator 6.7.1, 6.7.3.
intensity 3.11
International Notation 1.4.1
International symbol 1.7.1
International Tables for Crystallography, Vol. A 1.7
International Union of Crystallography 1.4.1
intrinsic semiconductor 6.6.2, 6.7.3
inversion 1.4.2
irreducible representation 7.4
ISODISTORT 7.5
isomorphic space group 1.7.4.1
isomorphous replacement 3.13.1
isotropy subgroup 7.5

Josiah Willard Gibbs, 2.1

Karle, Jerome 3.13.1
KCl 3.7.2, 3.10
$KCuF_3$ 7.3
Kepler, Johannes 1.1, 3.14
Kinematic approximation 4.1
kinematic theory 3.6.3
klassengleiche subgroup 1.7.4.1
klassengleiche supergroup 1.7.4.2
Knipping, Paul 3.1
k-space 5.1

$LaAlO_3$ 7.3
Landau theory of phase transitions 7.5
lattice 1.5.1, 1.6.2
lattice basis 1.6.2
lattice diffraction 3.6.3
Lattice Dynamics 6.2.3
lattice function 3.6.2
lattice system 1.5.6.1
lattice type 1.7.3, 3.10
Laue class 3.11
Laue cone 3.2
Laue condition 3.3, 3.8, 4.4
Laue diffraction 3.5.4
Laue Equations 3.2
Laue geometry 4.3
Laue photograph 3.5.4
Laue zone 3.7.3
Laue, Max Theodor Felix 3.1
Law of Rational Indices 1.2
lead zirconate 1.5.4

Legendre, Adrien-Marie 2.4.2
limiting sphere 3.5.2
$LiNbO_3$ 4.2
linear combination of atomic orbitals (LCAO) 6.6.1
Lonsdale, Kathleen 3.5.4
low-energy electron diffraction 3.7.3

magnetic neutron scattering 3.7.2
Mauguin, Charles-Victor 1.4.1
maximal subgroup 1.7.4.1
Maxwell's equipartition theorem 6.1
medium-energy electron diffraction 3.7.3
Megaw, Helen D. 7.1, 7.2
metric tensor 2.4.1
MicroED 3.13.7
Miller index 1.2
Miller, William Hallowes 1.2
minimal supergroup 1.7.4.2
mirror operation 1.4.2
modulated crystal 3.14
molecular transform 3.6.2
molybedenum 1.6.3.2
momentum operator 4.4
momentum space 5.1
monatomic chain 6.2.1
monoclinic 1.5.4, 1.7.1
morphology 1.1
mosaicity 4.1
Mott-Bethe formula 3.7.3
Mulliken notation 7.4
multiple scattering 4.1, 4.2.

Na_2CO_3 3.14
NaCl 1.6.3.3, 3.5.6.
$NaNbO_3$ 3.5.6, 7.3
nearly-free electron theory 6.6.2
neutron scattering 3.5.5, 3.7.2
neutron time of flight 3.5.5
non-symmorphic 1.7.2
normal coordinate 6.2.3
normal mode 6.2.3
Normal Process 6.3.1

obverse setting 1.5.6.1
octahedra 7.3
operation 1.2
operator 1.2
optic branch 6.2.2
optic mode 6.4.2
optical transform 3.6.2
order of diffraction 3.3
order of group 1.4.3, 12
order parameter 7.5
orthorhombic 1.5.4
Oszlányi, Gabor 3.13.4

pair correlation function 3.13.6
Pair Distribution Function 3.13.6
Parsval's theorem Appendix E
Pasteur, Louis 1
Patterson, Arthur Lindo Patterson 3.13.3
Patterson function 3.13.3, Appendix F
Patterson map 3.13.3
Patterson symmetry 1.7.1
Pauling, Linus 3.14
$PbZr_{1-x}Ti_xO_3$ 3.13.6
Pendellösung 4.6, 150
Penrose, Roger 3.14
Periodic Boundary Condition 5.2, 6.6.1
periodic potential 4.4, 4.5, 6.6.2
perovskite 1.6.3.7, 7.1
Petit, Alexis Therese 6.1
phase problem 3.6, 3.13.1
phonon 6.1.2, 6.3
phonon dispersion 6.4
phonon-phonon collision 6.3
piezoelectric 7.2
plane group 1.7.1
planes 1.5.3
plane-wave 4.5
point group 1.3, 1.4.3, 7.4
point symmetry 1.4
polar lattice 2.1
polarisability 6.2.3, 6.4.2
polymorphism 1.1, 1.6.3.8
powder diffraction 3.5.3, 3.10, 3.13.5
power spectrum Appendix E

preferred orientation 3.5.3
primary extinction 4.1
primitive cell 5.4
primitive translation 1.5.1
primitive unit cell 1.5.2, 6.1.2, 6.2.2, 6.7.1
proper subgroup 1.7.4.1
proximity cell 5.4
pseudocubic 7.3
pseudosymmetry 7.5

quartz 1.1, 1.4.2, 1.7.3, 3.9
quasicrystal 3.14
quasiperiodic 3.14

radial distribution function 3.13.6
Raman scattering 6.4, 6.4.2
reciprocal lattice 2.2
reciprocal space 2.3, 5.1
reciprocal unit cell 3.10
reciprocal-lattice vector 2.3, 4.4
Reduced Zone Scheme 5.5, 6.2.2, 6.6.2
reducible representation 7.4
reflection 1.4.2
reflection condition 3.10
reflectivity 4.3
Remeika method 7.2
Renninger reflection 4.2
representation 7.4
resonant scattering 3.12
restriction theorem 1.5.5
Reverse Monte Carlo 3.13.6
reverse setting 1.5.6.1
rhombohedral 1.5.6.1
Rietveld refinement 3.13.5
Rietveld, Hugo M. 3.13.5
rock crystals 1.1
rotation 1.4.1
rotoinversion 1.4.2
rotoreflection 1.4.2

scattering cross-section 3.7.2
scattering length 3.7.2
scattering vector 3.3, 3.6.3.
Schoenflies symbol 1.7.1
Schoenflies, Artur Moritz 1.4.1
Schrödinger equation 4.5
screw axis 3.10
screw rotation 1.7.2.1
Secondary extinction 4.1
Seitz operation 1.7.2
Seitz operator 4.4
Seitz symbol 1.7.1
semiconductor 6.7.3
Shechtman, Daniel 3.14
shell model 6.2.3
shift theorem Appendix E
short symbol 1.7.1
Shull, Clifford 3.7.2
silicon 1.6.3.5, 6.7.3
similarity theorem Appendix E
sinc function Appendix E
sodium 6.7.1
sodium chloride 1.6.3.3
Sohncke group 1.7.2.1
Sohnke, Leonhard 1.7.2.1
space group 1.7, 7.3
space-group type 1.7.3
spallation source 3.13.7
special position 1.7.1
Spence, John 3.13.7
$SrTiO_3$ 1.6.3.7, 3.5.4, 3.9
stereographic projection 1.4.1, 1.4.2, Appendix A
Stokes regime 6.4.2
Straumanis method 3.5.3
strontium titanate 1.6.3.7
structure amplitude 3.8
structure factor 3.8, 3.10, 3.11
subgroup 1.7.3, 1.7.4.1, 3.5.6
sublattice 3.5.6
subsidiary maxima 3.6.2
sulphur 6.4.2
supergroup 1.7.4.2
superlattice 3.5.6
superspace group 3.14
superstructure 3.5.6
Sütő, András 3.13.4
symmetry element 1.3, 1.7.1, 1.7.2.2
symmetry operation 1.3, 1.4.1
symmetry operator 1.4.1, 1.7.1

symmorphic space-group 1.7.1
synchrotron radiation 3.5.4
systematic absence 3.10

tetragonal 1.5.4, 1.5.6, 1.7.1
thermal conduction 6.3
thermal diffuse scattering 3.9
thermal neutrons 6.4.3
thermal scattering 3.9
thickness fringes 4.6
Thomson, George Paget 3.7.3
Thomson, Joseph John 3.7.3
tight-binding theory 6.6.1
tilted octahedra 7.3
Total Scattering 3.13.6
translation group 1.5.1, 4.4.
translational symmetry 1.5
translationengleiche subgroup 1.7.4.1
translationengleiche supergroup 1.7.4.2
Transmission Electron Microscope 3.6
triclinic 1.5.4
trigonal 1.5.4, 1.5.6.1
triple-axis spectrometer 6.4.3
two-beam approximation 4.5
type 1.7.3

Umklapp Process 6.3.2
unit cell 1.5.2
urea 3.13.2

valence band 6.6.2
vibrational modes 6.1
Voronoi cell 5.4

wave field 4.5
wave state 5.2
wave-vector 4.5, 5.2
Wigner-Seitz cell 5.4
Wigner-Seitz construction 6.3.2
Wilson, Arthur James Cochran 3.15
wurtzite 1.6.3.8
Wyckoff symbol 1.7.1

zinc blende 1.6.3.6
zinc sulfide 1.6.3.6, 1.6.3.8
ZnS 1.6.3.6, 1.6.3.8